Department of Spatial Sciences

Quasi-Continuous GPS Steep Slope Monitoring: A Multi-Antenna Array Approach

Troy Andrew Forward

"This thesis is presented as part of the requirements for the award of the Degree of Doctor of Philosophy of Curtin University of Technology"

April 2002

Declaration

This thesis contains no material which has been accepted for the award of any other degree or diploma in any university.

To the best of my knowledge and belief this thesis contains no material previously published by any other person except where due acknowledgment has been made.

Signature: …….

Date: ……...

ABSTRACT

This thesis investigates the design, implementation and validation of a multi-antenna GPS system to monitor the displacement of deforming slopes. The system utilises a switched antenna array design allowing data from multiple antennas to be sampled sequentially by one GPS receiver. The system provides quasi-continuous GPS observations that can produce a precise and reliable coordinate time-series of the movement of the slope under consideration.

GPS observations in general, and particularly those concerned with the monitoring of steep slopes, are subject to systematic errors that can significantly degrade the quality of the processed position solutions. As such, this research characterises the data in terms of multipath effects, the spectrum of the coordinate time-series, and the carrier to noise power density ratio of the raw GPS observations. Various GPS processing parameters are then investigated to determine optimal processing parameters to improve the precision of the resulting coordinate time-series.

Results from data stacking techniques that rely on the daily correlation of the repeating multipath signature find that the GPS data actually decorrelates somewhat from day to day. This can reduce the effectiveness of stacking techniques for the high precision monitoring of steep slopes. Finally, advanced stochastic models such as elevation angle and carrier-to-noise weighting are investigated to optimise the precision of the coordinate time-series data. A new in-line stochastic model is developed based on weighting GPS observations with respect to the level of systematic error present within the data. By using these advanced types of stochastic models, reductions to the noise level of the coordinate time-series of approximately 20 and 25 percent are possible in the horizontal and height components respectively.

Results from an extensive field trial of this system on a deforming high-wall of an open-pit mine indicate that approximately 135mm of displacement occurred over the 16-week field trial. The precision of the coordinate time-series for surface stations approaches ±4.0mm and ±5.4mm in the horizontal and height components respectively. For sub-surface stations next to the mine wall, coordinate precision has been determined as ±4.9mm in the horizontal component and ±7.6mm in the height component respectively.

ACKNOWLEDGMENTS

I would like to express my gratitude to my supervisor, Associate Professor Mike Stewart, and to my associate supervisor Dr. Derek Lichti for their help and support in the course of my research. Thanks are also extended to Dr. Nigel Penna, and Dr. Maria Tsakiri for their guidance and help during much of this research.

Thanks are also extended to Minghai Jia for his assistance in the software design process.

This project was partially funded by the Australian Research Council with further funding from a Curtin University Postgraduate Scholarship.

In-kind support was also received from Western Mining Corporation with particular thanks to Peter Taylor and the Mount Keith survey team for their assistance during the field testing phase of this research. Thanks also to William Sarunic formerly of Western Mining Corporation for his help during the initial development phase of this project.

Finally, I would like to thank my family, for their continued support, and especially to my wife Jenny, for all of her love, help and support that has helped make this possible.

TABLE OF CONTENTS

LIST OF FIGURES

LIST OF TABLES

1. INTRODUCTION

1.1 Introduction

Maintaining the stability of steep slopes is an important aspect of any geotechnical engineering exercise. Monitoring the surface displacement of a slope can provide valuable information about the dynamics of any movements or changes within the structure. The magnitude, velocity and acceleration of displacements can then provide an indication of the stability of the slope. These movements, if detected early enough, can also indicate impending catastrophic failure of a slope mass. One such instance of catastrophic slope failure in recent Australian history is the landslide that occurred at Thredbo Village in the Kosciusko National Park in New South Wales on 30 July 1997. This monumental landslide resulted in the deaths of 18 people and was considered by the coroner as "the worst natural disaster in Australian history" (Hand, 2000). Figure 1.1 presents an aerial view of the post-collapse area around Thredbo Village.

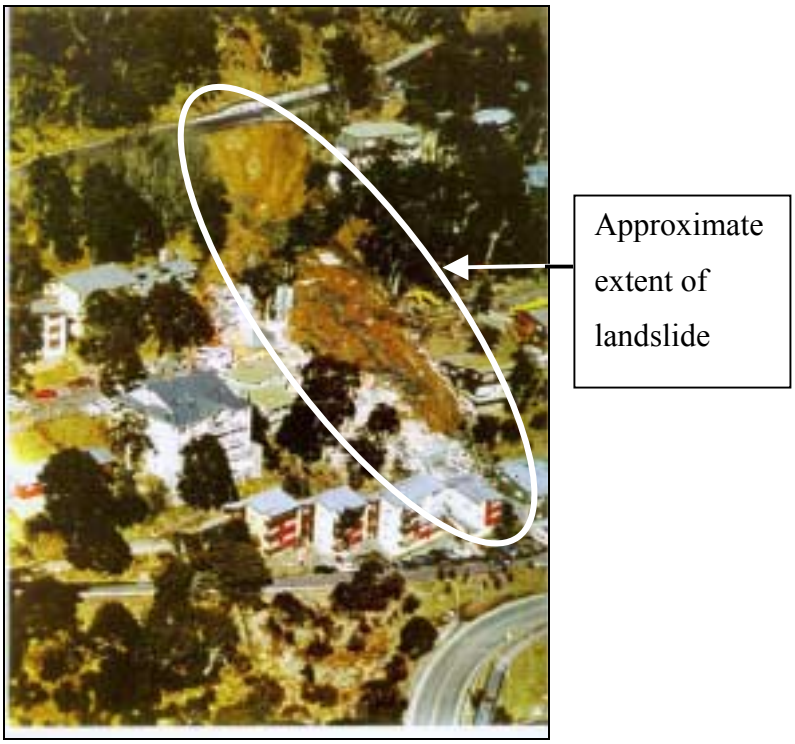

Figure 1.1 Aerial view of Thredbo landslide (after: LawLink, 2001)

The history and development of this landslide stems back some 40 years. The long-term nature of such events highlights the need for vigilant geotechnical monitoring and appraisal regimes to detect movement for stability analysis over the lifetime of a slope.

Another area requiring geotechnical monitoring of slopes is the open-pit mining industry. During 1999 and 2000, 251 wall failure incidents were recorded in Western Australian mining operations. Of these, 250 occurred in surface mining operations with four involving injury to personnel (Department of Minerals and Energy, 2000). The safety of surface mining operations is of paramount concern for mining companies. Often mine walls are constructed with steep slope angles to minimise the amount of waste material excavated. Deformation of a mine wall can then occur which requires that the wall be monitored to ensure that the stability of the wall is maintained. The timely detection of these movements is paramount in the monitoring process. Figure 1.2 illustrates a partial slip on the south-eastern wall at the Western Mining Corporation Mount Keith mine site in December 2001.

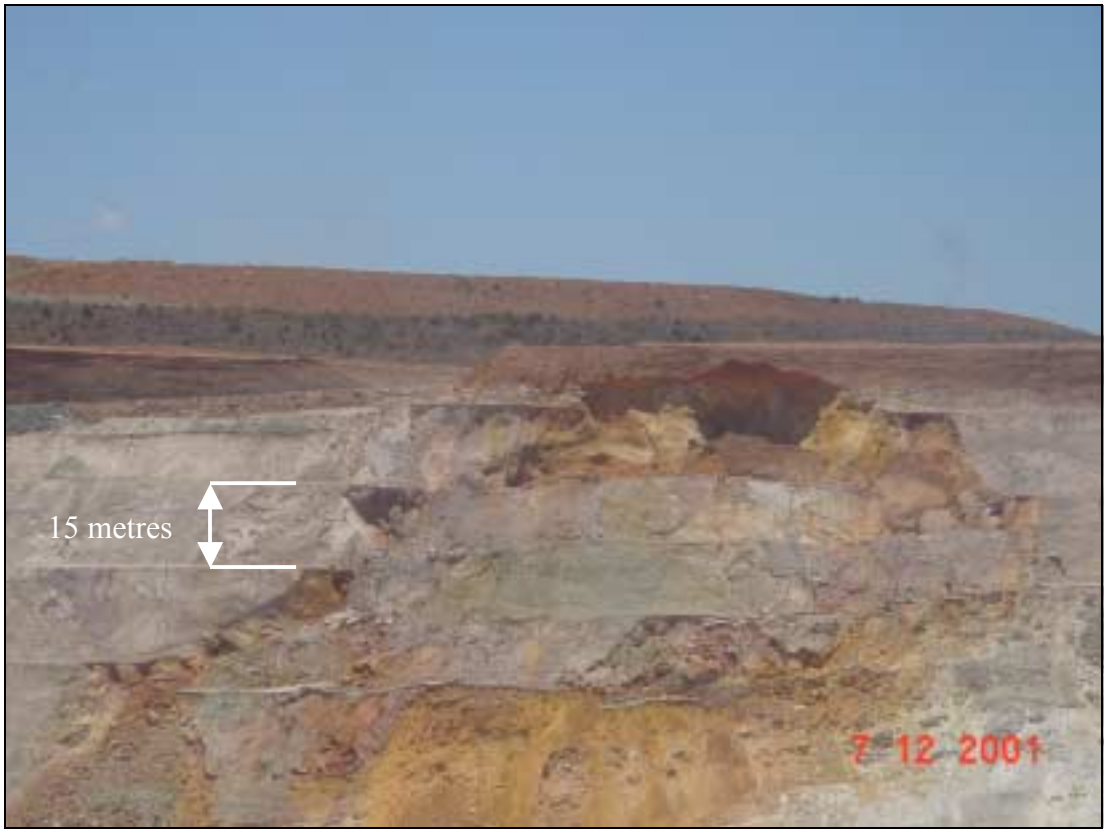

Figure 1.2 Mine wall failure at Mount Keith nickel mine – December 2001

Each horizontal bench that can be seen in Figure 1.2 above is separated by 15m in height, illustrating the magnitude of such slope failures.

The primary surveying technique for monitoring slopes and mine walls uses total station instruments to measure angles and distances to prisms located on the slope surface. As with any observational technique, total station systems have both advantages and disadvantages associated with their use. The main advantage of using total station instruments is that they provide three-dimensional (3D) coordinate information of the points that are measured. One of the disadvantages is the requirement to have an unobstructed line-of-sight between the instrument and the targeting prism. Another disadvantage is that vertical refraction errors can reduce the precision of the height information that may be obtained from the total station measurements.

The Global Positioning System (GPS) can be used as an alternative surveying tool to assist in geotechnical evaluations of steep slopes by providing 3D coordinate time-series of slope displacements at discrete locations on the slope surface. In this research, a multi-antenna GPS deformation monitoring system is developed to measure surface displacements of deforming slopes. This system provides high precision GPS-derived coordinate solutions of multiple monitoring points using only one GPS receiver. This is achieved by sampling data from a number of GPS antennas using a coaxial switching device. This innovative approach to GPS deformation monitoring reduces the amount of hardware required to monitor multiple locations on the slope surface. This in turn reduces the implementation costs associated with establishing such a monitoring system. The data collection strategy adopted results in the generation of periodic coordinate solutions from the continuous GPS data for each station that is monitored (hence the term quasi-continuous monitoring).

1.2 Technical Issues for GPS Slope Deformation Monitoring System Design

The use of GPS as a monitoring tool offers an alternative to conventional surveying techniques. GPS-based measurements offer a 3D time-series of discrete positions without the line-of-sight requirement of total station techniques. However, the use of

GPS for high precision positioning also has deficiencies, firstly in terms of the capabilities of GPS positioning in steep slope environments, and secondly in the strategies that are often employed to obtain monitoring results.

Current GPS positioning techniques for monitoring applications typically include the use of either episodic techniques for small-scale projects or continuous monitoring for regional scale projects. Each of these techniques has associated trade-offs between system installation and maintenance costs, and the quality of the resulting coordinate time-series. GPS results are also often contaminated by unmodelled systematic errors such as signal multipath and residual atmospheric delays. Furthermore, safety issues must be considered with respect to the requirement of personnel visiting the site to conduct the GPS survey in the episodic monitoring case.

This research is concerned with the development of a dedicated GPS-based monitoring system that can be used to detect movements of discrete points on a slope surface. The development of a dedicated system is aimed at bridging the gap between the episodic and continuous GPS monitoring techniques introduced above. Some of the design objectives of such a system include:

- High precision coordinate time-series;
- Robust system components;
- Low implementation cost;
- Advanced systematic error mitigation capabilities;
- Reduced need for personnel entering site.

Obviously, cost is an important factor in the development of any monitoring technique. Often, the cost of installing and maintaining a network of GPS receivers that operate continuously prohibits the use of such systems. Episodic GPS monitoring systems, while cheaper to deploy, require personnel costs throughout the lifetime of the monitoring regime. Dedicated systems can be designed to operate autonomously, at a reduced implementation cost to continuous systems.

1.3 GPS Data Analysis Issues for Steep Slope Monitoring

There are a number of data processing and analysis issues associated with GPS monitoring of steep slopes. Reducing the impact of unmodelled systematic errors such as signal multipath, residual atmospheric delays, and antenna phase centre variations, can improve the precision of the GPS-derived positioning results. This can involve the use of advanced stochastic modelling techniques to reduce the impact that poor quality observations have on the GPS coordinate solutions. Data stacking approaches can also be used to reduce the impact of satellite geometry dependent errors that repeat on a daily basis.

The issue of ambiguity resolution should also be considered for GPS slope deformation monitoring, especially when observation spans are relatively short and the monitoring stations experience conditions of systematic error such as signal multipath and diffraction. Simplified ambiguity resolution techniques can be employed to instantaneously resolve the GPS ambiguities when the *a priori* coordinates are well known.

To further optimise the positioning results of the deformation monitoring system, the optimal choice of data processing options should also be considered. Simple issues such as careful selection of the data collection and processing interval, the length of data observed at each monitoring station, and the best elevation–masking angle can have an impact on the precision of the final coordinate solutions. The frequency of repeat observations at each station within the monitoring network is a further issue that requires consideration. The resulting temporal density of the coordinate time-series may have an impact on the ability of the system to extract or estimate the actual surface motion.

Finally, the generation of realistic quality estimators from the GPS least squares estimation process is another issue that requires consideration. Internal quality indicators are required to assess the precision of the coordinate results that are computed. If the quality estimators do not represent the actual precision of the GPS solutions, the user may be falsely informed about the precision of the positioning results. This can have negative implications if safety-based decisions rely on these precision estimators.

While some of these issues may seem trivial, they can have a considerable impact on the precision of the resulting coordinate time-series. Each of these issues is discussed in an effort to ensure that the effectiveness of the deformation monitoring system developed in this thesis is optimised.

1.4 Research Objectives

The key objectives of this research may be defined as follows:

- Design and build a GPS-based deformation monitoring system utilising a multi-antenna array design;
- Install and operate the GPS antenna array monitoring system under 'real-life' operating conditions;
- Determine the optimal GPS processing parameters that maximise the precision of the resulting coordinate time-series;
- Evaluate the ability of data stacking techniques to reduce multipath that is correlated on a daily basis;
- Evaluate the impact of implementing different stochastic models on the precision of the coordinate time-series;
- Evaluate the correlation between the internal least squares quality indicators and the actual precision of the resulting coordinate solution.

1.5 Outline of Thesis

This thesis is divided into eight chapters. Chapter 2 introduces the concept of deformation monitoring of steep slopes including geotechnical issues and the existing techniques that can be employed to monitor such slopes. Chapter 3 summarises the necessary GPS positioning theory as related to high-precision GPS positioning for deformation monitoring. Chapter 4 details the multi-antenna monitoring system developed for this research. This includes a description of the various hardware and software components that have been developed to enable the quasi-continuous monitoring of multiple stations with only GPS receiver and related peripheral hardware. The test site used to validate the multi-antenna monitoring system is also introduced in this chapter. Initial test results are presented in chapter 5 with the establishment of a set of benchmark processing parameters. Optimisation of

these benchmark processing parameters is then introduced in chapter 6 to maximise the precision of the resulting coordinate time-series. Data stacking techniques and stochastic modelling approaches for GPS deformation monitoring of steep slopes are introduced as advanced GPS positioning techniques in chapter 7. GPS quality indicators are also investigated by considering the correlation present between the internal quality indicators of GPS processing software and the associated coordinate precision. Finally, chapter 8 concludes with a summary of the major findings of this research and includes suggestions for future work that may further enhance the use of the multi-antenna GPS approach for slope deformation monitoring.

2. DEFORMATION MONITORING OF STEEP SLOPES

The measurement of displacements at a slope surface is often the simplest way to observe the evolution of slope failure. These measurements provide the geotechnical engineer with the ability to observe and analyse the kinematics of the deformation, the response of the triggering conditions, and possibly the effectiveness of any corrective measures that are employed to reduce the rate at which the slope deforms.

It is also beneficial to understand the underlying modes and mechanisms affecting the stability of steep slopes and how various monitoring techniques can be used to best model slope dynamics. These modes of deformation will be discussed in more detail below, as will some of the major types of instruments and techniques that have traditionally been employed to monitor the deforming environment.

2.1 Modes of Deformation and Failure

There are many different modes of deformation and failure that can exist within a steep slope. The different failure mechanisms need to be understood in order to assist in the design process of any monitoring scheme that is implemented for monitoring of a particular slope. As the field testing phase of this research is conducted in the open-pit mining environment, emphasis in this section is placed on the process of mining and excavation for the formation of the slope structure. However, the general principles can be applied to both natural and man-made slopes.

The stress states within a rock mass undergo changes as the surrounding ground is mined or excavated. Excavation causes a change from a virgin stress state (that before any excavation) to an induced stress state, resulting in the surrounding areas deforming in response to the changing stress fields. The deformation experienced is an expected phenomenon, and should be factored into the slope design process. Unfortunately, such changes in the associated stress fields, and the effect of these changes on the stability of the slope, cannot be modelled exactly. Empirical or

historical information may be used in conjunction with discontinuity mapping and mechanical testing of the rock properties to assist in the design process. After excavation, slope monitoring can be a useful tool to evaluate the performance of the slope with respect to the design criteria.

The groundwater conditions in and around a slope have a considerable influence on the stress states within the rock mass. Factors influencing the state of the water table include seasonal rainfall, the mechanical properties of the rock mass within the surrounding area, and the mining process itself.

Failure of slopes, and open-pit mine walls in particular, can occur in various forms which are typically determined by different failure modes. Most of these failures occur in relation to structural discontinuities of the rock mass. The main failure modes include plane shear, wedge, circular shear and toppling as discussed below.

2.1.1 Plane and Wedge Shear Failures

These classes of failure mode occur where combinations of discontinuities in the rock mass form blocks or wedges within the rock which are (or become) free to move. The pattern of the discontinuities may be comprised of a single discontinuity, two discontinuities that intersect each other, or a combination of multiple discontinuities that are linked together to form a failure mode set, for example step path and step wedge failures (Sjöberg, 1999).

Figure 2.1 illustrates schematically some of the types of plane (Figure 2.1a) and wedge shear (Figure 2.1b) failure modes. These also include the slab and the step path failure (Figure 2.1c and Figure 2.1d respectively).

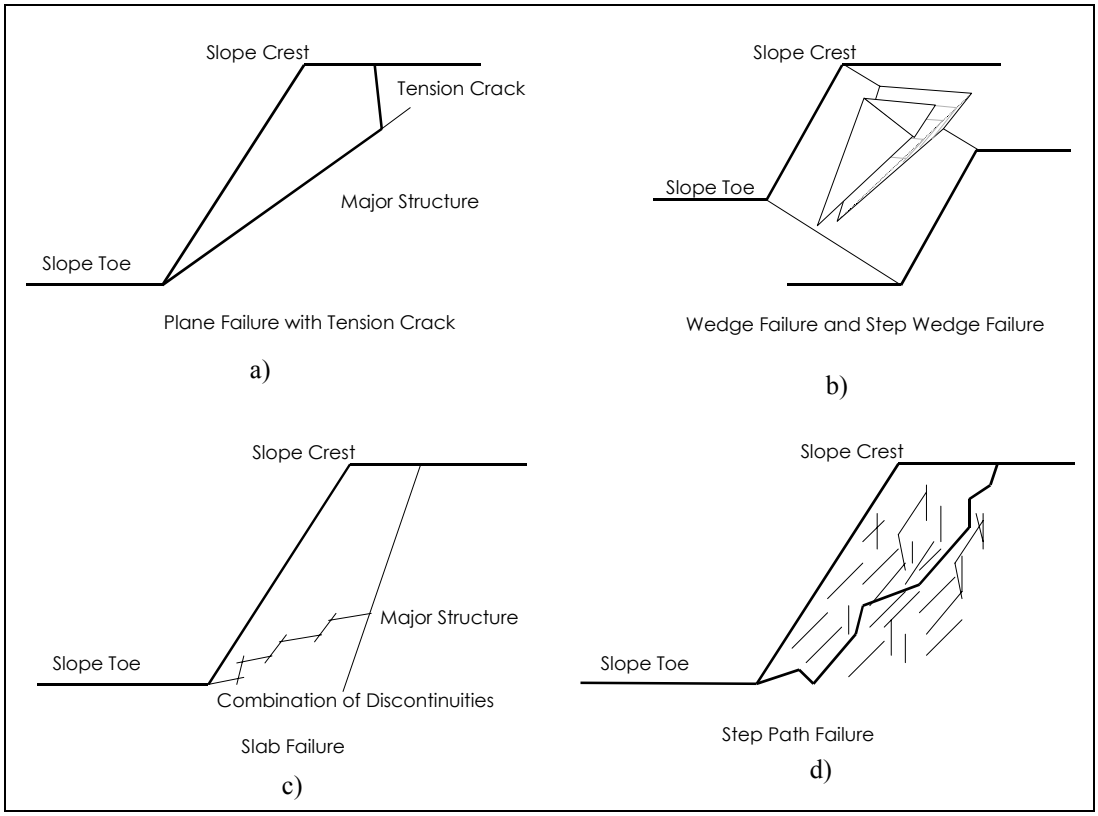

Figure 2.1 Combinations of discontinuities (adapted from Sjöberg, 1999)

As is evident in Figure 2.1, plane shear and wedge failures can be comprised of many different and complex failure patterns. One common feature, however, is that these failure modes are typically associated with the formation of tension cracks at the crest of the slope. This can be a precursory indicator that deformation is present within the slope structure.

2.1.2 Circular Shear Failures

Circular shear failures are closely related to step path failures. While failures of this type do not necessarily occur along a purely circular arc, some form of curved failure surface is normally apparent. This failure mode can occur in rock structures that exhibit no planes of weakness, and may not be associated with any underlying critical discontinuity. Circular shear failures are influenced by the size and mechanical properties of the particles in the soil or rock mass. Figure 2.2 illustrates some of the circular shear failure modes. These are only two of the many failure types that may involve complex combinations of different failure modes.

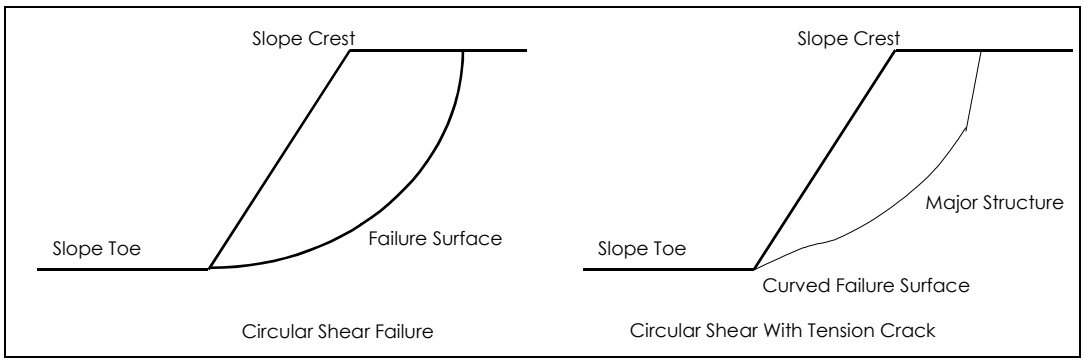

Figure 2.2 Circular shear failure modes (adapted from Sjöberg, 1999)

2.1.3 Toppling Failures

Toppling failures occur when columns of rock, formed by steeply dipping discontinuities in the rock structure, experience an overturning type of motion. This failure type is illustrated in Figure 2.3.

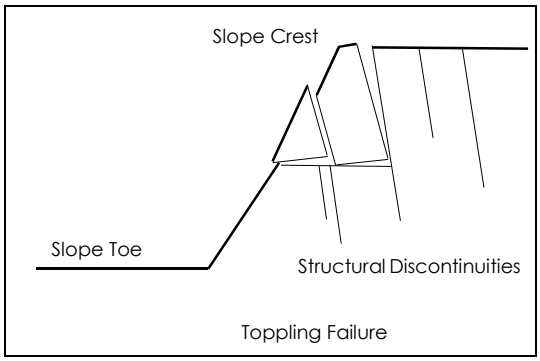

Figure 2.3 Toppling failure mode

The removal of overburden and confining rock, as is the case in mining excavations, can result in a partial relief of the constraining stresses within the rock structure, resulting in a toppling failure as indicated above (Selby, 1987). This type of failure mode may be further categorised as flexural toppling, block toppling, or block flexural toppling, all of which exhibit similar characteristics. For further details, the reader is referred to Turner and Schuster (1996).

2.2 Factors Influencing Slope Stability

Some of the major factors that influence slope stability include the mechanical properties of the rock, the geological structure of the rock mass, groundwater and rainfall. These are discussed below.

2.2.1 Geological Structure of the Rock Mass

The geological structure of the rock mass is one of the most important factors affecting slope stability. The size, type, location, and orientation of discontinuities (or defects) within the structure all have an impact on the way the rock mass deforms. These discontinuities include bedding planes, fractures and faults, folds, and cavities. Most slope deformations, and many failures, are correlated with discontinuities such as these within the rock mass.

Bedding planes are interruptions in the course of sedimentary type rock grains as the rock is being deposited. These interruptions create laterally extensive breaks between discrete layers of deposit "beds" or strata within the rock mass (Giani, 1992). Bedding planes form lateral planes of weakness in the rock structure which are susceptible to shear type failures. These are influenced by the morphology of the bedding plane surfaces, the mineralogy, and the distribution of the grain size within the bedding plane.

Faults are fractures or fractured zones in the rock mass where there has been a sizeable shear displacement. The magnitude of these fault zones can vary greatly (from centimetres to kilometres along the fault zone). In the case of faults, the dip and direction of the fault correspond to the stress states within the rock mass at the time that the fault was formed. The bending process of the strata in a layered rock mass typically causes folds.

Cavities within the rock mass may be natural or man-made features, both of which require caution in slope stability assessment. Man-made cavities are of particular concern in the mining environment due to their potentially hazardous impact on both mining operations and the safety of personnel operating in and around these areas.

2.2.2 Mechanical Properties of the Rock Mass

Rock mass strength is the primary mechanical property of consideration in slope stability analysis. Furthermore, factors such as the spacing, orientation, continuity, roughness and width of joints, together with the effects of weathering of the rock mass, also have an impact on overall slope stability.

Testing of intact rock may be undertaken to evaluate the strength of the rock mass. The uniaxial compressive strength of the rock is of particular interest to the geotechnical engineer. While testing intact rock may give an insight into the theoretical mechanical properties of rock, the presence and influence of any discontinuities is much more complex than can be modelled adequately.

2.2.3 Groundwater and Rainfall

The stress state within a slope is highly correlated with the groundwater conditions and pressures within the rock mass. The effect of groundwater on the slope is related to the surrounding precipitation levels, topography, nearby water masses, and the geo-hydrological characteristics of the rock mass (Sjöberg, 1999). Changes within the water table around the slope will occur as a function of time and of the mining process itself.

The influence of groundwater on the rock mass, and hence the stability of the slope, is one factor that can be modified to alter the stress states within the rock mass. Draining of the local groundwater can be achieved through the use of horizontal drains, vertical bores, or more complex drainage galleries to alter the state of the pressure resulting from local groundwater. The process of de-watering can be undertaken to alter the stress state within the rock mass to improve the stability of the slope.

2.3 Techniques and Instrumentation for Monitoring Deformation

The monitoring of steep slopes can be accomplished using many different types of sensors. It is the role of the geotechnical engineer to determine which sensors will allow the deformation to be best described. Table 2.1 (adapted from Gili *et al.,*

2000) presents an overview of various methods used in measuring surface displacements, together with the associated precision level that may be expected for each system.

Method	**Displacement Parameter**	**Typical Measurement Range**	**Typical Precision**
Precision tape	Δdistance	< 30m	0.5mm/30m
Fixed wire extensometer	Δdistance	< 10 – 80m	0.3mm/30m
Crack meter	Δdistance	< 5m	5mm
Offsets from baseline	ΔH,ΔV	< 100m	0.5–3mm
Surveying triangulation	ΔE,ΔN,ΔH	< 300 – 1000m	5–10mm
Surveying traverses	ΔE,ΔN,ΔH	Variable	5–10mm
Geometrical levelling	ΔH	Variable	2–5mm/km
Precise geometrical levelling	ΔH	Variable	0.2–1mm/km
Electromagnetic distance measurement	Δdistance	Variable (usual 1- 14km)	1–5mm + 1–5ppm
Terrestrial photogrammetry	ΔE, ΔN, ΔH	Ideally < 100m	20mm from 100m
Aerial photogrammetry	ΔE, ΔN, ΔH	H_{flight} < 5 00m	100mm
Clinometer	Δelevation angle	± 10°	5–10mm + 1–2ppm
GPS	ΔX, ΔY, ΔZ	Variable (usual < 20km)	5-10mm + 5ppm

Table 2.1 Overview of surface displacement measurement techniques

Different modes of deformation will affect the choice of stability analysis undertaken by the geotechnical engineer and consequently the type of deformation monitoring strategy employed.

The techniques that are commonly used to monitor the deformation of steep slopes can be broadly classified as *instrumentation techniques* and *observational techniques* (Windsor, 1993). These are discussed below with particular emphasis on those techniques that monitor surface displacements.

2.3.1 Monitoring by Instrumentation Techniques

Instrumentation techniques include the use of movement indicators, convergence meters, strain meters, joint meters, fixed and portable borehole extensometers, fixed and portable inclinometers, deflectometers and piezometers. Of these, the principal techniques/instrumentation will be discussed. For a more extensive discussion of these types of instruments, the reader is referred to Dunnicliff (1988), Windsor and Worotnicki (1986), and Gili *et al*. (2000).

2.3.1.1 Extensometers

One of the principal instruments used to measure rock deformation is the extensometer. Extensometers measure the axial displacement between a number of reference points in the same measurement axis. The wire extensometer is widely used and may be installed on the slope surface (Bonnard and Steinmann, 1990), or within a borehole (Angeli *et al.,* 1988, 1989). One such instrument is illustrated in Figure 2.4.

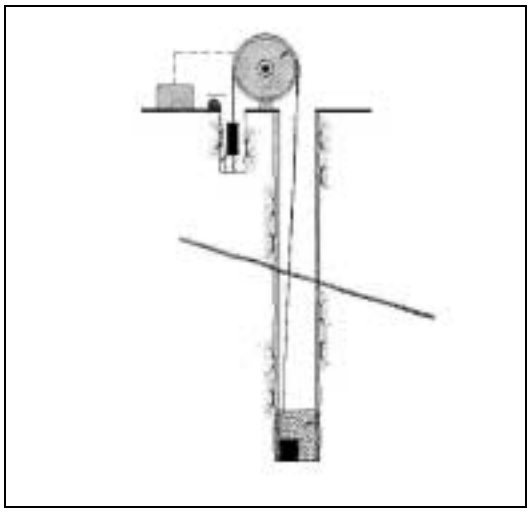

Figure 2.4 Wire Extensometer (after: Corominas *et al*., 2000)

Wire extensometers typically measure baselines of up to 80m in length with a precision of ±0.3mm per 30m of baseline length (Gili *et al.*, 2000). The advantage of the wire extensometer is the high level of precision attainable in the line of the measurement axis. The obvious disadvantage, however, is that the one-dimensional displacement vector does not measure out-of-line displacements. The main sources

of error in extensometers result from friction in the reference head and between the linkages (the wire or rod used as the physical medium to be measured), temperature induced sag, and the stress/strain characteristics between the linkages. All of these can have a significant impact on their use in the harsh Australian mining environment. The extensometer must also be anchored outside the zone of deformation, which can be an issue if the deformation area is large.

2.3.1.2 Piezometers

Piezometers measure the pore pressure of the groundwater within a geological structure. These instruments give an indication of the build-up of stresses and strains within the rock mass. Differential pore pressure measurements allow the changing structural and rainfall conditions to be mapped. Common types of borehole piezometers are the vibrating wire, pneumatic and standpipe piezometers. The type of piezometer used varies depending on the level of permeability of the surrounding rock mass. The level of permeability is not just related to the type of rock, but may also depend on any discontinuities within the rock which will increase the mass permeability. The use of some of these instruments (for example pneumatic standpipe piezometers) can be limited by the need to manually measure the pore pressure. This can be subject to human reading accuracy and site re-visitation constraints. Vibrating wire piezometers should be protected from electrical transients and must also compensate for local barometric pressure when used in wells that are open to the atmosphere.

2.3.1.3 Crack Meters

Crack meters can be very useful tools in the early detection of deforming mass movements. These devices measure the displacement between two points on the surface that are exhibiting signs of separation. They are often used due to their low cost and ease of implementation. One such configuration is illustrated in Figure 2.5 where a pin crack arrangement was used to assist in the measurement of wall displacement at Mount Keith nickel mine in Western Australia operated by Western Mining Corporation (WMC).

Figure 2.5 Pin crack meter measuring crack displacement

The distance between the pins is measured regularly to establish a time-series of the wall movements. Velocity and acceleration indicators can then be established for the time-series. The main disadvantage of this type of monitoring device is the risk involved with personnel making measurements on unstable ground. This issue is of concern for any technique that requires manual collection of the deformation data from within the slope failure zone.

2.3.1.4 Inclinometers

Inclinometers measure the curvature of initially straight boreholes. This is typically accomplished through the use of a gravity operated tilt sensor. Multiple servo-accelerometers can also be used to measure vertical deviations in horizontal boreholes. Sensors can be placed orthogonally, allowing for measurement in perpendicular planes to be made.

There are many different configurations of borehole inclinometers available. These are usually distinguished by the measurement sensors used, such as vibrating wire transducers, differential wire transducers, servo accelerometers and gravity activated

electrolyte cells. The type and spacing of these sensors within the system to be measured determines the precision attainable. This can typically be of the order of ±0.02mm over a baseline length of 3m (Windsor, 1993). The main disadvantage of this type of instrument is that curvature is only observed in one axis (one dimension).

2.3.2 Monitoring by Observational Techniques

Observation techniques are those which are quantitative and observe the deformation at the exposed rock mass boundary (Windsor, 1993). These techniques include geodetic and terrestrial surveying, imaging techniques such as photogrammetry, and the use of satellite-based positioning techniques such as GPS. Other techniques include ground-based radar interferometry (for example, Reeves *et al*., 1997), satellite-based radar interferometry (for example Ohkura, 1998), microseismic rockburst emissions (Srinivasan *et al.,* 1999), laser scanning (Baltsavias, 1999), and other satellite-related positioning systems such as GLONASS (Global Navigation Satellite System) and pseudolites (for example Dai *et al*., 2000). The main techniques commonly used are discussed in the following sections.

2.3.2.1 Total Station

Total station instruments consist of a device to measure horizontal and vertical angles, and some form of Electromagnetic Distance Measurement (EDM) capability to measure distances. These instruments allow the surveyor to measure 3D coordinates of points remotely (typically targeted by the placement of reflective prisms). They also permit the recording of the data in a digital format to be later downloaded or transmitted to a central processing site.

The latest total station instruments are equipped with servo-motors and automatic target recognition algorithms that reduce the need for personnel to physically record the observations. Additionally, due to the introduction of reflectorless instruments, survey prisms are no longer required at the slope surface. This, however, may result in a loss of coordinate precision due to imprecision in the repeatability of the reflecting surface.

One advantage of using total stations to monitor surface deformation is that the measurements can provide 3D position solutions of the point of interest. Coordinate precision in the vertical domain, however, is typically worse than in the horizontal domain and may not provide the precision required for the monitoring of deformations. Observations may also be subject to systematic errors that cannot always be mitigated or removed completely. The main error source is vertical refraction, which can significantly degrade the vertical component of total station observations. For example, deformation monitoring tests at the Diamond Valley Lake in California, USA, found that approximately 40mm of unmodelled vertical refraction error remains in some total station measurements (Duffy *et al.*, 2001). Deficiencies in the pointing accuracy of automated total station instruments have also been noted. These issues are discussed briefly in section 5.3.6 for results collected at an open-pit nickel mine in Western Australia.

Often, slope distance measurements alone are used as the primary indicator for deformation monitoring due to the precision attainable in a range observation. This provides adequate precision when the displacements occur along the line-of-sight of the instrument. However, when this is not the case, the resulting precision with which the deformation may be detected may be compromised. Line-of-sight must also be maintained between the instrument and the monitoring point, which may be difficult to achieve with some slopes. To overcome this problem, and that of the slope distance measurement issue discussed above, multiple total station instruments may be required to monitor complete structures. Strict field practices must also be maintained, especially in the case of non-automated measurement procedures.

2.3.2.2 Levelling

The most precise method of monitoring local vertical deformations is the use of precise levelling techniques. These techniques can provide a vertical component precision of 0.2 to 1 parts per million (ppm) of the level run length (Gili *et al.,* 2000). While this is extremely useful in determining vertical deformations such as subsidence monitoring, the downfall is the provision of information in only one ordinate (height), and that the survey crew must traverse directly to the deformation point, increasing the risk to personnel in unstable environments. Levelling must also

be initiated from a stable monument situated outside the zone of deformation. This may require that the level run start some distance away (up to a few kilometres) which makes the task of levelling laborious, often slow, and subject to the propagation of levelling errors. This reduces the overall effectiveness of this technique.

2.4 Monitoring by Satellite-Based GPS Techniques

As shown above, monitoring of steep slopes by conventional survey methods (such as the use of total stations and levelling) can be slow, and labour intensive. The successful application of satellite-based deformation monitoring techniques can provide a solution to these problems by providing a continuous, or quasi-continuous 3D time-series, while also maintaining a high level of precision, and operating with minimal user intervention.

GPS is the primary system of interest, with other systems, for example GLONASS, currently failing to provide the level of operational capability needed for high-precision deformation monitoring. A new civil system named Galileo is scheduled for future development by the European Union.

For deformation monitoring, the use of GPS techniques can normally be divided into two broad areas. The first area involves high precision static methods such as Continuously Operating Reference Systems (CORS) that are used to (typically) monitor regional scale deformations such as crustal dynamics, subsidence and geotechnical movements (for example, Koivula *et al*., 1998; de Heus, 1997). These continuous systems are normally combined to form permanent networks. The second class of GPS technique is the use of *episodic* GPS data (for example, Stewart *et al*., 1999), commonly used for monitoring on a smaller scale (with baselines up to a few kilometres). The use of the episodic technique commonly includes the monitoring of dams, open-pit mine walls and landslides.

The primary technical differences between the two GPS monitoring classes are the permanency of the GPS receiver locations and the processing strategies employed to

obtain deformation solutions. Both of these monitoring techniques are discussed below.

In this research a new class of monitoring technique is defined as *dedicated GPS monitoring systems* whereby hardware and software systems are designed specifically for the monitoring application at hand. This technique is discussed in more detail in section 2.4.3.

2.4.1 Continuously Operating Reference Systems

Typically used for regional scale monitoring, CORS are comprised of many high precision GPS receivers established in a permanent network configuration. These dual frequency receivers are normally coupled to high quality antennas mounted atop specifically designed survey pillars that are anchored into the local bedrock structure. For example, the Southern California Integrated GPS Network (SCIGN) consisted of 239 such stations as of March 2001 (Hudnut *et al*., 2001) situated across the western corridor of the United States of America. The Japanese Geographical Survey Institute (GSI) crustal monitoring project is another example where networks of CORS are used to monitor over 1000 stations spread across Japan (El-Fiky *et al*., 1999).

These types of monitoring systems have the benefits of:

- Continuous solutions enabling the generation of time-series of high temporal resolution, from which deformation motions may be estimated from a shorter data time span and with more confidence than episodic sampling of the deformation signal;
- Mitigation of systematic errors (for example the removal of multipath and atmospheric delays in the received GPS signal, time decorrelation of the data, removal of antenna set-up error);
- Reduction in the likelihood of gross errors and data outliers (due to, for example, use of forced centring, elimination of set-up errors);
- Lower manpower costs as CORS operate automatically.

Smaller scale projects are now beginning to use CORS for the high precision monitoring of engineering structures, for instance the monitoring of Pacoima Dam (Behr *et al.*, 1998) and Diamond Valley Lake in California, USA (Bock *et al*., 2001). At the Diamond Valley Lake six points are monitored continuously by a local GPS network. Horizontal coordinate precision is stated as ±10mm over the network spanning some 8-10km (at the 68 percent confidence level). This may be reduced to the ±4mm level for sub-networks of this system with baselines less than one kilometre (Bock *et al*., 2001).

The main advantage of a CORS monitoring system is the high level of coordinate precision that can be achieved to enable small deformations (in the order of a few millimetres or centimetres) to be detected over long periods of time (months to years). This is essentially made possible because of the stability of the station monuments that are used and the high temporal density of the resulting coordinate time-series. Solutions are often computed daily, for example, for crustal motion and geophysical applications. CORS operate autonomously which offers safety advantages when monitoring in hazardous environments (for example near catastrophic failure zones associated with steep slopes).

The biggest disadvantage of CORS monitoring systems is the high implementation cost that is associated with establishing such systems. As a result, smaller-scale operations with limited resources may only be able to install a minimum of continuous monitoring points. Episodic GPS monitoring (discussed below) may be the viable alternative in these cases, where many points can be monitored with one set of GPS equipment. The high costs associated with installing continuous systems often preclude their use for all but large-scale monitoring exercises such as those mentioned previously.

2.4.2 Episodic GPS Monitoring

Episodic monitoring offers a more cost-effective alternative to CORS networks. Here, a survey team will revisit the deformation site at regular intervals (for example every few weeks or months) using static, rapid static or real-time kinematic GPS surveying techniques to construct a time-series of the deformation observed at unique

survey points. The main advantage of this type of system is the lower establishment cost associated with the purchase of an episodic monitoring system. The one set of GPS equipment (and associated communications hardware and software) can then be used to monitor multiple locations on the slope. The GPS equipment can also be used for other surveying tasks when not used for deformation monitoring.

Unfortunately, there are many disadvantages to the use of the episodic technique for the monitoring of centimetre level deformation. The main disadvantage is the lower precision that is obtained from this type of survey and the poorly sampled time-series of coordinate solutions. This is primarily related to the monumentation type used (ground marks), the use of (normally) only one GPS reference station, and shorter observation times that are used to collect the episodic data (for example, between 2 and 15 minutes of data may be recorded for rapid static surveys). Set-up errors can also add to the overall error budget of episodic monitoring systems. From a practical viewpoint, survey teams are often required to observe many points in a short period of time. The coordinate precision then suffers as a result of the short observation times and systematic errors may propagate through to the final station solutions. This phenomenon has been observed by Featherstone *et al*. (2001) where stop-and-go style surveys conducted by survey contractors over GPS testing facilities have resulted in erroneous coordinate solutions. This issue is also discussed in section 6.5. Another disadvantage is the discontinuous time-series that is obtained from the episodic nature of the monitoring. The frequency of the observations is often not high enough to ensure that the time-series modelling can adequately extract the trend of the deformation from the noise existing within the observations. This may be illustrated by episodic monitoring results from North Dandalup Dam in Western Australia (Stewart and Tsakiri, 2001). The results, shown in Figure 2.6, illustrate the height component computed at two locations on the North Dandalup Dam in Western Australia. Results from the height observations of rapid static GPS positioning (dashed line) and spirit levelling (solid line) are presented.

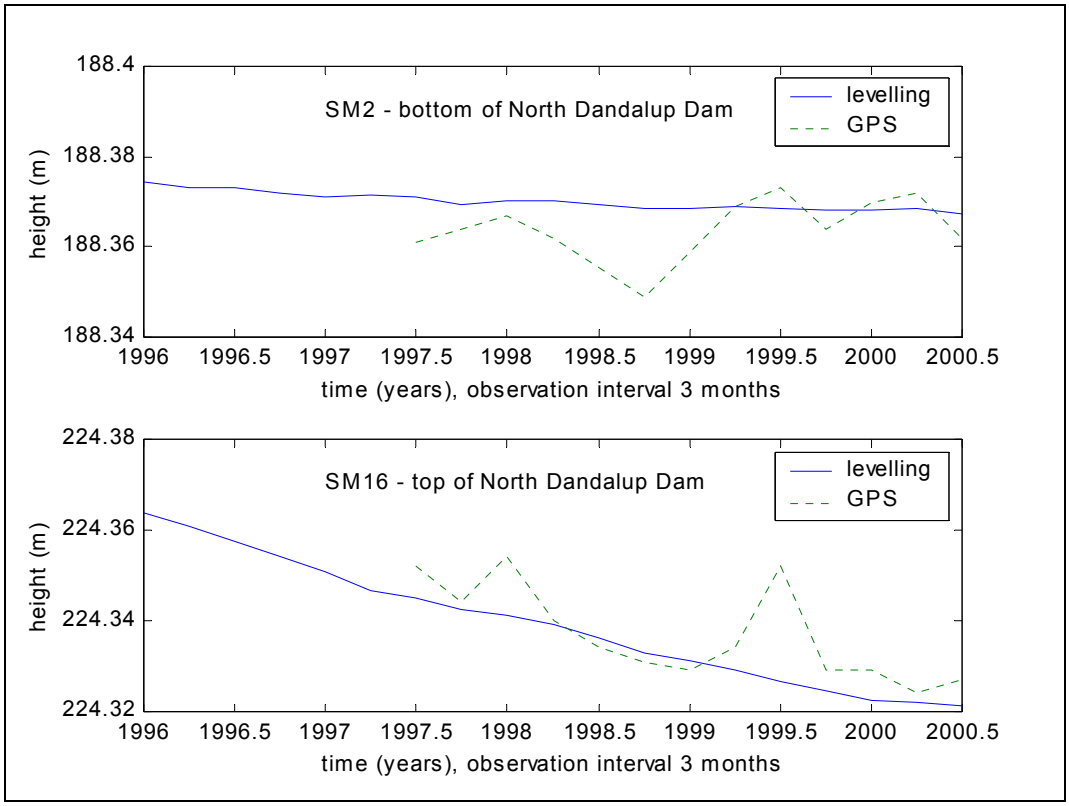

Figure 2.6 Comparison of height differences from precise levelling and GPS at North Dandalup Dam, Western Australia (after: Stewart and Tsakiri, 2001)

It can be seen that the level of noise present within the GPS observations precludes the realistic definition of the deforming movements of the dam wall. This is an artefact of the precision of the GPS observations themselves and the temporal density of the GPS observation campaign (in this case points are surveyed every three months).

Safety is one further issue that requires consideration for these types of systems. Episodic monitoring with GPS techniques can pose a risk to the survey personnel every time they revisit the deformation zone. While in many instances this poses minimal risk, it should nevertheless be considered in the design of any deformation monitoring system. Manual observation of each monitoring point should also be considered in the ongoing cost of this type of GPS monitoring technique. Costs associated with the various GPS monitoring techniques are discussed in section 4.3.6.

The dedicated GPS monitoring system presented in this research has been designed to bridge the gap between the CORS networks, and the episodic monitoring type of GPS systems. These types of dedicated systems are discussed in section 2.4.3.

2.4.3 Dedicated GPS Monitoring Systems

Dedicated GPS systems can provide an intermediate solution to CORS networks and the episodic GPS monitoring techniques presented in the previous sections. These systems are typically designed on a case-by-case basis to target smaller-scale permanent operations that require a high level of solution precision and density at a cost more closely aligned with episodic monitoring techniques. Dedicated GPS monitoring systems can be designed to optimise the advantages of both aforementioned systems while reducing the various disadvantages that are associated with each. Specifically, the system objectives may be defined as:

- High precision positioning results;
- Low establishment and running costs;
- The use of multiple GPS reference stations;
- The generation of a dense and continuous time-series;
- Advanced systematic error modelling capabilities afforded by the continuous time-series analysis;
- Minimal user interaction, which will reduce ongoing costs while also reducing safety concerns.

The surface monitoring of volcanic activity is one such application that has seen the development of dedicated GPS monitoring systems. For example, in the work presented by Rizos *et al*. (2000), a continuously operating GPS monitoring system comprised of low-cost L1-frequency GPS receivers and dedicated processing software was used to monitor the deformation of a volcano at Papandayan, Indonesia. The complete monitoring system also required the development of robust and secure (from vandalism) peripherals such as specialised radio communications hardware and solar power.

Other concept-level systems have included multi-antenna array approaches similar to the research presented in this thesis (Ding *et al.,* 2000; Petrovski *et al*., 2000) although these systems are as yet (as of April 2002) somewhat untested in slope monitoring environments.

Some GPS equipment manufacturers have also identified the benefits of developing a modular approach to monitoring system design and are beginning to work more closely with individual clients to create dedicated monitoring systems. An example of note is the Leica Geosystems Geodetic Monitoring System (GeoMoS) (Sippel, 2001). In this case, clients interact with the development teams to produce specialised applications to integrate hardware and software modules for individual applications.

In this research, a dedicated GPS monitoring system has been developed for the small-scale monitoring of steep slopes using dedicated hardware and software systems to provide quasi-continuous positioning results with high temporal frequency and precision. This system is described in detail in chapter 4.

2.5 Summary

There are many different modes and mechanisms that can lead to slope failure. The geotechnical engineer must record, model and analyse any movements within the slope structure in order to ensure safe operation within and around the slope.

Many geotechnical- and survey-based techniques can be used to aid the monitoring of steep slopes in a deforming environment. Of the techniques available, few provide a true 3D indication of the displacement vectors of points of interest at the surface of the slope. GPS is an emerging technology that can be used to provide a dense 3D time-series that can be used to map the position and velocity of the deforming mass. There is a gap, however, in the GPS-based positioning technologies available in the marketplace at the present time. Regional scale CORS networks, such as those used for the monitoring of tectonic motion, can provide a temporally dense and precise time-series of 3D deformation data. These systems, however, suffer from high installation costs. Episodic GPS monitoring techniques can provide

the user with a cheaper alternative, with the possibility of higher spatial density (per unit cost), but result in a poorer solution precision and reduced temporal density of the coordinate time-series. Dedicated GPS monitoring systems can bridge the gap between the continuous style of permanent GPS networks and the episodic monitoring techniques by offering a high level of coordinate precision at a reduced implementation cost. In subsequent chapters, one such dedicated monitoring system, is proposed, based on a multi-antenna approach to permanent positioning. In this configuration, data from multiple permanent antennas are sampled sequentially by one GPS receiver. This system reduces the implementation cost of monitoring multiple points, while providing a precise quasi-continuous coordinate time-series of the slope deformation.

3. GPS BACKGROUND

This chapter presents a condensed overview of the background and theory required for high precision relative positioning using GPS carrier-phase measurements over baselines a few kilometres long (<5km). The theory and background presented here focuses on the specific GPS positioning problem at hand, that of high precision positioning for deformation monitoring. For further details and background on GPS, the reader is referred to the many textbooks available on GPS (for example Leick, 1995; Hofmann-Wellenhof *et al*., 1997).

3.1 GPS Phase Observables

The carrier-phase observable is a measure of the difference between the satellite generated carrier signal and a similar signal generated within the receiver. The phase pseudorange represents the distance between the satellite and receiver antennas, plus the clock biases. As only the phase is measured by the receiver, the so-called integer ambiguity must be determined as part of the precise positioning process. When the integer ambiguity (N) and clock biases have been successfully determined, the phase measurement, when added to this bias, can be considered to represent a precise range measurement between the satellite and receiver antennas. However, the range measurement is contaminated by other error components which must also be considered. In GPS positioning, this carrier-phase measurement can be denoted by (Wells *et al.,* 1997; Leick, 1995):

$$\Phi = \rho + d\rho + c\left(dt - dT\right) + \lambda N - d_{ion} + d_{trop} + d_{hw} + \varepsilon_{Mp} + \varepsilon_{\varphi} \qquad (3.1)$$

where:

- Φ is the measured carrier phase (metres);
- ρ is the geometric range between the satellite and receiver antennas (metres);
- $d\rho$ is the orbital error (metres);
- c is the speed of light (metres per second);
- dt is the satellite clock error with respect to GPS time (seconds);

dT is the receiver clock error with respect to GPS time (seconds);
λ is the carrier wavelength (metres);
N is the integer cycle ambiguity (cycles);
d_{ion} is the ionospheric delay error (metres);
d_{trop} is the tropospheric delay error (metres);
d_{hw} is the hardware delay in both the satellite and receiver components (metres);
ε_{Mp} is the carrier-phase multipath error (metres);
ε_{φ} is the receiver carrier-phase noise (metres).

This observable is sometimes referred to as the zero-difference carrier phase observable.

3.2 Differenced Observables

Many of the errors existing within the carrier-phase observable can be reduced, and in some cases removed completely, by considering the correlations between observations from different satellites and receivers. The differencing of observables is used to accomplish this task.

3.2.1 Single Difference Observable

Errors that are correlated by simultaneous observations at two receivers can be reduced by the so-called between-receiver single differencing approach. This concept is shown in Figure 3.1.

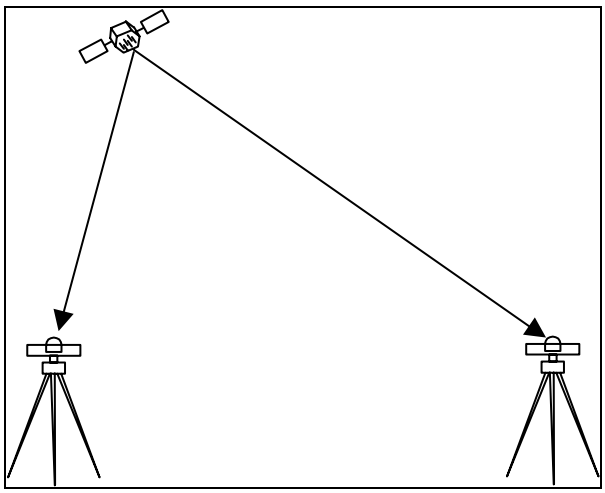

Figure 3.1 Schematic of between-receiver single differencing of GPS observations

The between-receiver single difference (SD) observable is thus formed:

$$\Delta\Phi = \Delta\rho + c\Delta dT + \lambda\Delta N - \Delta d_{ion} + \Delta d_{trop} + \Delta d_{hw} + \Delta\varepsilon_{Mp} + \Delta\varepsilon_{\Phi} \qquad (3.2)$$

where:

Δ represents the between-receiver single difference operator.

The satellite clock term has been removed in the formation of the single difference observable. Moreover, orbital error, ionospheric delay error, and tropospheric delay error are now significantly reduced for short baselines and the ambiguity parameters remain integer.

3.2.2 Double Difference Observable

To further remove the remaining systematic error components, it is often useful to difference the single difference observable between satellites. This concept is shown in Figure 3.2.

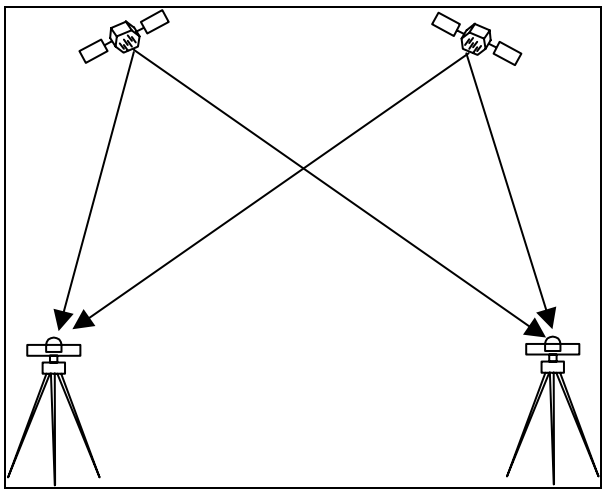

Figure 3.2 Schematic of double differencing of GPS observations

The so-called double difference (DD) observable is therefore presented as:

$$\Delta\nabla\Phi = \Delta\nabla\rho + \Delta\nabla d\rho + \lambda\Delta\nabla N - \Delta\nabla d_{ion} + \Delta\nabla d_{trop} + \Delta\nabla\varepsilon_{Mp} + \Delta\nabla\varepsilon_{\Phi} \qquad (3.3)$$

where:

$\Delta\nabla$ represents the double difference operator.

Both the receiver and satellite clock errors are removed completely by double differencing, as are the hardware delay errors. Accordingly, the ambiguities remain of an integer nature after the double differencing process. For short baselines, the residual orbital error, and ionospheric delay errors are generally considered to be very small. The dominant error source remaining, therefore, is the double differenced phase multipath error. The other main error source that can have an impact on solution quality is the residual tropospheric delay error. These two components will be discussed in more detail below. For further detailed information on the other remaining error sources, the reader is referred to the many comprehensive GPS texts available (for example Hofmann-Wellenhof *et al*., 1997; Leick, 1995).

3.3 Dominant Error Sources in the Double Difference Observable

As mentioned previously, signal multipath error is the dominant error source remaining after the double differencing process for short baselines.

3.3.1 Signal Multipath

Multipath is the phenomenon that occurs as an incoming signal is reflected by objects within the surrounding antenna environment before reaching the antenna measurement centre. While the causes of signal multipath are numerous, the overall effect is a delay of the incoming signal due to the increased path length that the signal must take to reach the antenna. This effect is illustrated in Figure 3.3.

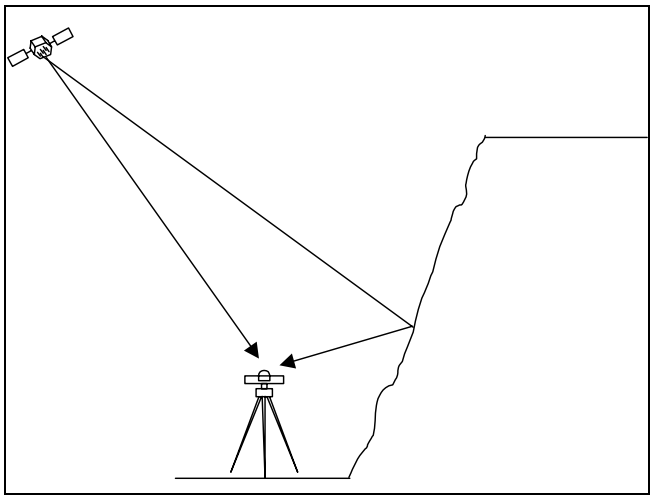

Figure 3.3 Signal multipath

The complete signal as measured by the antenna is comprised, therefore, of a combination of the direct line-of-sight signal (free from multipath), and a multipath delayed component. The theoretical maximum carrier phase multipath error to a single reflected signal can reach a maximum of $\pm\lambda/4$ (Julg, 1996; Wanninger and May, 2000), where λ is the wavelength of the carrier signal. This research is primarily concerned with the effects of carrier-phase multipath effects for high-precision GPS deformation monitoring techniques.

Multipath mitigation strategies can generally be grouped into one of three classes (or combinations thereof). These are broadly classified as hardware mitigation, firmware mitigation and software mitigation strategies.

3.3.1.1 Hardware Methods for Multipath Mitigation

The first class of multipath removal or mitigation strategy uses specialised antenna designs to attenuate spurious (or multipath delayed) signals at low elevation angles. These designs include ground plane antennas and Dorne-Margolin type choke-ring antennas. Other antenna designs include the use of multiple closely spaced antenna array configurations to estimate and remove the multipath signature using the geometrical relationships of the antenna array system (Brown, 2000; Ray, 2000).

3.3.1.2 Firmware Methods for Multipath Mitigation

The second class of multipath removal/mitigation technique is the design of receiver correlators that increase the probability of correctly extracting the uncorrupted GPS signal. Some of these correlator types include the narrow correlator design (Fenton *et al*., 1991), the edge correlator (Garin *et al*., 1996) and the strobe and enhanced strobe correlator (Garin and Rousseau, 1997). However, Ray (1999) indicates that none of these techniques effectively reduces low frequency multipath induced by nearby structures.

3.3.1.3 Software Methods for Multipath Mitigation

The third technique is based on software methods that remove or mitigate the presence of any residual multipath from the GPS data themselves. These techniques vary from the use of adaptive Kalman filters (Ge *et al.*, 2000) and finite impulse response filters (Han and Rizos, 2000), to the use of semi-parametric modelling and penalised least squares techniques (Jia *et al*., 2000). Multipath calibration techniques for permanent GPS sites are also under investigation including techniques to estimate carrier phase multipath corrections to reduce the impact of this type of signal delay (Wanninger and May, 2000).

Data stacking techniques can also be used to mitigate the effects of repeating signal multipath effects. These techniques can include observable stacking, whereby the double difference observations are stacked across the sidereal day (for example, Ding *et al*., 2000; Ma *et al.,* 2001; Radovanovic, 2000), or solution stacking techniques in which the coordinate solutions are stacked on a day-to-day basis (for example, Bock

et al., 2000). The theoretical difference in the length between the solar and sidereal day is approximately 236 seconds. If this difference is considered when designing a GPS monitoring system (see section 4.1.6) the data may be easily correlated to perform such stacking techniques. Both stacking approaches operate on the assumption that the multipath (and signal diffraction) experienced at a site will be replicated each sidereal day as the satellite geometry repeats. The use of data stacking techniques to remove the effect of signal multipath on GPS observations in the deformation monitoring case is discussed in section 7.1.

Stochastic modelling can also be used to limit the contribution of poorer quality observations affected by signal multipath to the position solution. This commonly takes the form of elevation weighting (Han, 1997; Gerdan, 1995) or carrier-to-noise power density ratio weighting (Brunner *et al.*, 1999). The different stochastic models tested within this thesis are discussed in detail in section 3.4.2 and are used in this research to reduce the impact of multipath delayed signals on the final solution precision. Test results using these stochastic models to reduce the impact of signal multipath, and other systematic errors, are presented in section 7.2.

3.3.2 Atmospheric Delay Errors

As satellite signals propagate through the atmosphere, they experience a delay (or advance) that is associated with signal refraction through the differing atmospheric media. The ionosphere is the part of the atmosphere that extends from approximately 50km to 1000km above the Earth's surface. In this part of the atmosphere electron loss occurs as gas molecules are ionised by the sun’s ultraviolet radiation. The free electrons then contaminate the propagation of microwave signals as they pass through this atmospheric layer (Rizos, 1997). The propagation of the carrier-phase is advanced by this effect, whereas the Pseudo-Random Noise (PRN) code is delayed by the same amount (Parkinson, 1996). For GPS observations, the ionospheric delay error decorrelates over longer distances, requiring the use of ionosphere-free observables to mitigate the effect of the delay over longer baselines (Hofmann-Wellenhof *et al*., 1997). As this research is only concerned with the use of GPS positioning techniques for short baselines (<5km), the ionospheric delay error is considered to be correlated over short baselines and for short observation

periods. As such, the double differencing process (section 4.2.2) is assumed to completely remove this systematic error source.

The troposphere should be considered because it decorrelates over much shorter distances than the ionosphere. The electrically neutral portion of the atmosphere comprises the troposphere, extending to approximately 8km above the earth's surface, and the stratosphere, extending upwards from the troposphere to the base of the ionosphere. This neutral atmosphere is commonly referred to collectively as the troposphere in GPS positioning. Differentiation, however, is made between the way that different constituents affect a GPS signal. These are typically defined for GPS positioning as the 'wet' and 'dry' portions of the troposphere.

The 'dry', or hydrostatic component of the tropospheric delay is dependent on the dry air gasses within the atmosphere, and contributes to approximately 90 percent of the overall tropospheric delay. The 'wet' component depends on the moisture content of the atmosphere, and makes up the final 10 percent of the tropospheric delay. Empirical models are often used to remove the effect of the troposphere on GPS observations (for example, Saastamoinen, 1973; Black, 1978). Such models typically provide an estimate of the zenith delay and are then mapped down to other elevation angles by the inclusion of any one of many mapping functions that have been proposed. Some of the more widely used mapping functions include those developed by Marini (1972), Goad and Goodman (1974) and Niell (1996).

One further consideration is the tropospheric delay error induced by vertical separation between GPS receivers. The refined Saastamoinen model (after Hofmann-Wellenhof *et al*., 1997) may be used to estimate the contribution of the differential tropospheric path delay for vertically separated observation stations. As an example, the residual (single difference) contribution of the tropospheric delay is computed at the millimetre level for two stations separated by 50m in height. This is not considered to be significant for the data presented in this research.

3.4 Least Squares Estimation

Modern optimal estimation theories as applied to satellite geodesy include the least squares method and the Kalman filtering method. These methods are based on the application of *Gauss-Markov* models which make use of both a functional model and a stochastic model (Cross, 1994; Mikhail, 1976; Gelb, 1996). Appropriate definition of both of these models is imperative for successful, high-precision GPS positioning.

The standard linear observation model for the generalised least squares process applied to GPS positioning may be represented in matrix-vector notation as:

$$\underline{l} + \underline{v} = \underline{A}\underline{x}_{xyz} + \underline{B}\underline{x}_N \tag{3.4}$$

where:

$\underline{l}$	is the vector of observations;
$\underline{v}$	is the vector of residuals;
$\underline{A}, \underline{B}$	are design matrices;
$\underline{x}_{xyz}$	is the vector of unknown coordinate parameters;
$\underline{x}_N$	is the vector of unknown integer ambiguity parameters.

Both the functional and stochastic models are discussed below.

3.4.1 Functional Model

The functional model, also known as the mathematical model, describes the mathematical relationships between the measurements and the unknown parameters to be estimated.

Here, the double differencing procedure is formed to create the mathematical model as denoted by Equation 3.3. While attempts are made to appropriately describe the functional relationship between the observations and the unknown parameters to be estimated, complex relationships, such as the atmospheric effects, signal multipath and other unmodelled errors often result in the development of a less than optimal functional model. Any errors not included in the functional model need to be described in the associated stochastic model (Barnes and Cross, 1998).

3.4.2 Stochastic Model

The stochastic model describes the statistical properties of the mathematical models. These are primarily represented by the covariance matrices of the measurement errors which are associated with the functional model (Wang, 1999). The stochastic model can be used to improve the quality of the least squares solution by assigning appropriate weights to each observation. This in turn helps to improve the quality of the least squares solution. When the stochastic model has been adequately defined, realistic quality measures can also be computed (see section 7.3). The functional and stochastic models can also be considered equivalent (Blewitt, 1998). It is this property that allows the stochastic model to be used to partially compensate for deficiencies in the functional model. The appropriate modelling of the statistical properties of the observations is both a difficult and controversial task to accomplish (Wang, 1999; Cross *et al*., 1994).

Four types of stochastic models are presented here and tested in later chapters throughout this research. The first and simplest form of stochastic model considers the time invariant mathematical correlations between the double difference observations. The second and third of these models are a sine-based elevation angle model and an exponentially weighted elevation model respectively. The fourth model is the SIGMA-Δ stochastic model which considers the carrier-to-noise power density ratio of the observed GPS data. A new stochastic model based on the level of the systematic error within the double difference observations is also introduced and discussed in section 7.2.

3.4.2.1 Mathematical Stochastic Model

The simplest approach to stochastic modelling that is often used considers only the mathematical correlations between the double difference observations. This type of stochastic model assumes a time invariant correlation between double difference measurements which is set at +0.5 (Remondi, 1984; Bock *et al*., 1986). In practice, this model is often implemented by the correlation matrices as shown below. Considering a single baseline between two stations that observe four satellites

resulting in three double difference observations, the weight matrix P can be constructed:

$$P = \left(\sigma^2 CC^T\right)^{-1} \tag{3.5}$$

where :

P is the $(n \times n)$ weight matrix where n is the number of double difference observations;

σ^2 is the double difference variance factor;

C is the $(n \times m)$ correlation matrix where m is the number of single difference observations multiplied by the number of stations such that:

$$C = \begin{bmatrix} 1 & -1 & 0 & 0 & -1 & 1 & 0 & 0 \\ 1 & 0 & -1 & 0 & -1 & 0 & 1 & 0 \\ 1 & 0 & 0 & -1 & -1 & 0 & 0 & 1 \end{bmatrix} \tag{3.6}$$

The correlation matrix presented here is constructed using the base satellite concept, and also sometimes referred to as the double difference operator matrix.

Fast and efficient computations of P have been presented by Beutler *et al*. (1986). This weighting strategy is termed the Math model in this thesis. It should be noted, however, that this simple type of stochastic model does not consider the spatial or temporal correlations that may exist within the data.

3.4.2.2 Sine Function Elevation Dependent Stochastic Model

The simplest of the elevation-based stochastic models is formed by a sine-based weighting function which may be introduced as (Gerdan, 1995):

$$\sigma = \frac{1}{\sin a} \tag{3.7}$$

where:

σ is the standard deviation of a zero-difference GPS observation;

a is the elevation angle of satellite.

This model will be referred to as the Sine stochastic model in subsequent chapters. The standard deviation of a zero-differenced GPS observation using the Sine model for varying elevation angles is illustrated in Figure 3.4.

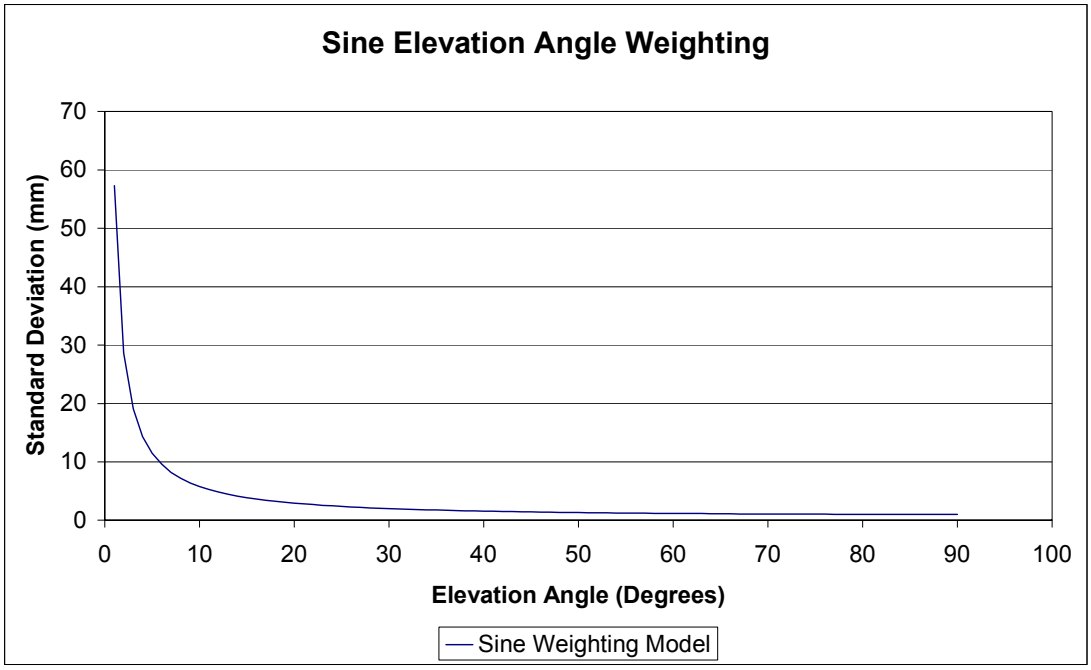

Figure 3.4 Standard deviation of zero-differenced GPS observations using the Sine elevation weighting function.

The relatively simple sine weighting function shows the reduction in the predicted standard deviation of a GPS observation as elevation angle increases. At an elevation angle of 10°, for example, the standard deviation of a GPS observation is estimated to be approximately ±5.76mm. At 15° elevation, this standard deviation is computed as ±3.86mm, further reducing to ±1mm at an elevation angle of 90°.

While a standard deviation of 1mm may be overly optimistic for GPS observations (Rizos, 1997), the relative weighting ratio between satellite observations in the double differencing process will be maintained.

3.4.2.3 Exponential Function Elevation Dependent Stochastic Model

Exponentially-based elevation dependent stochastic models of the following form have been proposed, for example, by Jin (1996) and Han (1997):

$$\sigma = s \cdot \left(a_0 + a_1 \cdot \exp\left(-E / E_0 \right) \right) \tag{3.8}$$

where:

σ	is the standard deviation of a zero-difference L1 GPS observation;
s	is a scaling factor;
a_0	is an experimentally determined constant term;
a_1	is an experimentally determined constant term;
E	is the elevation angle of the satellite in degrees;
E_0	is an experimentally determined constant term.

Here, the scale factor s is determined from real data under the assumption that it is the same for all observations (both carrier phase and pseudorange) over a short period. From the data presented in Han (1997), the constant terms of Equation 3.8 were computed as:

	a_0 (mm)	**a_1 (mm)**	**E_0 (degrees)**
Carrier Phase Observations	3	26	20
Pseudorange Observations	70	600	20

Table 3.1 Exponential stochastic model constant terms (Han, 1997)

The implementation of this stochastic model will adopt the constant terms of Han (1997) presented in Table 3.1 and will be referred to as the Han stochastic model in subsequent chapters. The estimated standard deviation of a zero-differenced GPS observation using this model is illustrated in Figure 3.5.

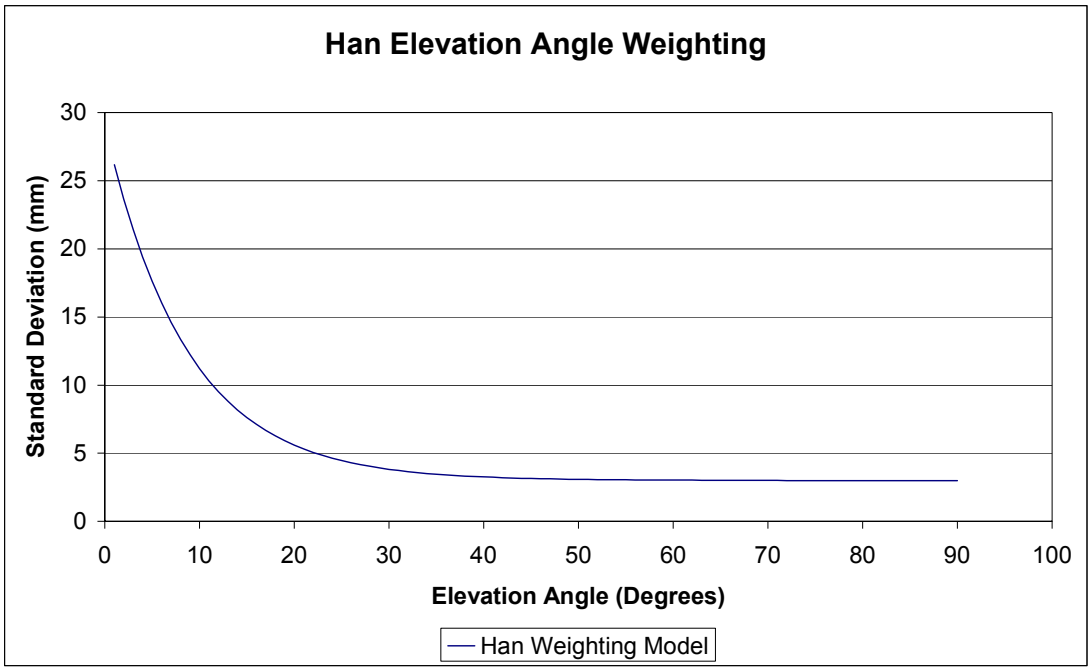

Figure 3.5 Standard deviation of zero-differenced GPS observations using the Han elevation weighting function

The standard deviation of a zero-differenced GPS observation, as illustrated in Figure 3.5, indicates that the Han model results in a slower decay rate for low elevation satellites than for the Sine model presented in the previous section. At an elevation angle of 10°, the Han model estimates that a zero-differenced GPS observation will have a standard deviation of approximately ±11.22mm. This reduces to approximately ±7.62mm at 15° elevation and ±3.00mm at 90° elevation. Elevation-based stochastic models such as this and the Sine model assume azimuthal symmetry. Under certain conditions of signal multipath and diffraction, for example when positioning next to a steep slope, these types of elevation dependent stochastic model may not completely describe the stochastic properties of the resulting observations.

3.4.2.4 SIGMA Stochastic Model

The development of the SIGMA family of stochastic models originates from the work initially presented by Hartinger and Brunner (1999) which investigated the variance of phase measurements using the carrier-to-noise power density ratio. The first SIGMA model developed was the SIGMA-ε model (Hartinger and Brunner,

1999) which was subsequently developed into the SIGMA-Δ model with the inclusion of a template design (Brunner *et al*., 1999). Here, a template is constructed for a particular GPS receiver and antenna combination that represents the maximum C/N0 level recorded for each particular elevation angle. The zero-difference variance is then calculated by considering the difference between a recorded observation that may be contaminated by diffraction and one that is assumed to be free from such effects. For further information on the development of using the C/N0 level to estimate GPS phase variances, the reader is referred to Ward (1996) and Langley (1997).

The SIGMA-Δ model is presented as:

$$\Delta = C/N0_{template} - C/N0_{measured} \tag{3.9}$$

where:

Δ is the indicator for the diffraction noise which yields a larger variance than σ_i^2 in Equation 3.9 (Brunner *et al*., 1999; Hartinger and Wieser, 2000).

The SIGMA-Δ model is then presented for a zero-difference observable as:

$$\sigma_\Delta^2 = C_i \cdot 10^{-\left(C/N0_{measured} - \alpha \cdot \Delta\right)/10} \tag{3.10}$$

In Brunner *et al*. (1999), values of C_1 and α were calculated as C_1=1.61 × 10^4mm^2 and α=2 respectively.

It should be noted that the C_i-term may be considered an *a priori* variance factor for L1-only (or L2-only) processing. This means that for an experimental implementation, the C_i term need not be determined empirically, as is the case in Brunner *et al*. (1999). This *a priori* variance factor will not affect the coordinate solution but will have an impact on the calculation of the *a posteriori* variance factor. The α-term is important, however, as it determines the decay of the SIGMA-Δ function with respect to changes in the noise level, and thus the relative weights that

are applied. Results of implementing this technique in the open-pit mining environment are discussed in detail in section 7.2.1.

Furthermore, a recent paper by Wieser and Brunner (2000) proposed a change to the SIGMA-Δ model presented above. The new SIGMA-Δ model is represented by:

$$\sigma^2_{\Delta new} = V_i + C_i \cdot 10^{-\left(C/N0_{measured} - \alpha \cdot |\Delta|\right)/10} \tag{3.11}$$

where:

V_i are model parameters (0.0 for L1, $0.88 \cdot 10^{-6} m^2$ for L2);

C_i is equal to $0.244 \cdot 10^{-3} m^2$ for L1 and $0.77 \cdot 10^{-3} m^2$ for L2.

The parameters V_i and C_i will have no impact on the solution quality for the L1-only observations used in this research.

The $|\Delta|$ term, however, has been changed to consider increases in the C/N0 value of a received signal that is reported to be induced by signal distortion (Allnutt, 1989).

It is expected that this implementation of the SIGMA-Δ model would require a much more involved process for generation of the template model, due to the inseparability of a signal experiencing distortion and one that is not, with respect to determination of the template model itself. As such, the original implementation of the SIGMA-Δ model is used in this research.

The SIGMA-Δ model provides an enhanced stochastic modelling approach by considering the distortion effects such as diffraction that reduce the quality of the GPS signal. This is an important issue for steep slope deformation monitoring where the received GPS signals are expected to be more affected by distortion (by the closeness of the GPS antenna to the slope surface) than for most typical GPS positioning applications.

3.5 Ambiguity Resolution

Successful ambiguity resolution is fundamental to the success of relative GPS techniques for high precision positioning at the centimetre level. Much research has

revolved around robust and efficient methods of ambiguity resolution. The principal technique in use today is the Least Squares Ambiguity Decorrelation Adjustment (LAMBDA) technique (Teunissen, 1993, 1995; Tiberius and de Jonge, 1995). This technique uses a transformation to decorrelate the ambiguity parameters and provide the best statistical estimate of the correct ambiguity set.

There are a number of steps that are typically associated with the ambiguity resolution process. These steps, as summarised by Rizos (1997) include:

- Define an estimate of the *a priori* ambiguity parameter values;
- Conduct a search of the possible ambiguity set;
- Perform a discrimination test to determine the most probable ambiguity set;
- Re-compute the ambiguity-fixed solution.

Usually, within the least squares positioning process, the formulation of the linear positioning model is based on the fact there are (usually) two unknown parameter sets to be resolved (Equation 3.4). The first of these are the coordinate values (x_{xyz} in Equation 3.4), while the second are the double difference integer ambiguity parameters (x_N in Equation 3.4). In many GPS positioning applications, the user is only provided with a very coarse indication of the coordinate parameters prior to the data being collected. This is not the case for many deformation monitoring applications, however, as the user often has high precision coordinates available from previous epochs of the monitoring campaign. Based on this assumption, step one of the above ambiguity resolution process leads to the following mathematical formulation, after Equation 3.4 above:

$$\underline{v} = \underline{\underline{B}}\underline{x}_N - \underline{l} \tag{3.12}$$

As can be seen from Equation 3.12, the coordinate parameters may be removed from the linear estimation model if (and only if) the *a priori* coordinate values are known to a sufficient level of precision.

The ambiguity resolution process is further simplified by the definition that the double difference ambiguity parameters will necessarily be integer (for the simple L1 or L2 only double difference observable). The next step is to choose an appropriate integer estimation strategy that can adequately determine the most appropriate ambiguity set.

Without any other constraints on the least squares estimation process, one would typically choose the most robust ambiguity estimation technique to ensure that the correct ambiguities are most likely resolved. The LAMBDA technique is one such example (de Jonge and Tiberius, 1996; Teunissen *et al.*, 1997). This technique is often used as it endeavours to decorrelate the ambiguity parameters, providing a higher chance of resolving the correct ambiguity set.

A simpler method of ambiguity resolution is the integer rounding technique (Teunissen, 1998). This technique involves the componentwise rounding of the estimated ambiguity parameters (x_N) to their nearest integer values. This method can be used as a viable alternative to the LAMBDA method when the *a priori* coordinates are well known, as is the case of deformation monitoring when there is relatively small motion (at the centimetre level) between measurement epochs.

Both this technique and that of integer bootstrapping (*ibid.*) can be applied to the final accumulated least squares ambiguity parameter set. This research, however, uses a subset of the integer rounding technique described above, whereby each double difference ambiguity is rounded every epoch, rather than in the final stage of the accumulated adjustment. This is highly dependent on the precision of the *a priori* coordinate estimates, which do not present a particular problem for this research, considering that high-precision estimates are available approximately every hour (see chapter 4). The advantage of this technique is the computational efficiency that is achieved by such a simple mathematical process. The disadvantage, however, is that the ambiguity set has not been decorrelated, resulting in a (theoretically) poorer ability to resolve and distinguish the correct ambiguity set, as is the case in integer least squares techniques such as the LAMBDA. The technique of integer rounding may not be appropriate for conventional GPS positioning applications.

However, it can be extremely useful in the case of deformation monitoring of slowly moving points.

One other advantage not immediately apparent, is the application of this ambiguity resolution technique in an epoch-by-epoch approach to GPS static positioning. By applying this technique to the raw double difference vector of observations ($\underline{l}$), or more appropriately the observed value minus the computed value (hereafter denoted as DDOmC), this technique absolutely removes the effect that double difference cycle slips have on the final positioning solution. When ambiguity parameters are resolved at every epoch, the magnitude of a cycle slip will be included in the following ambiguity estimation. This is particularly important when automated processing of data is required as no cycle slip detection step is required for data processing.

The necessary requirement for successful integer rounding and cycle slip removal, however, is a high level of relative accuracy of the *a priori* coordinate estimates on each baseline. When positioning in a deforming environment, this can be difficult to achieve. As the *a priori* coordinates diverge from the actual location, the data become less normally distributed. This is illustrated in Figure 3.6 where DDOmC values are plotted for three different days during GPS week 1081 at the Mount Keith nickel mine in central Western Australia (see chapter 4 for site description). These data represent a deforming environment where the *a priori* coordinate estimates are not updated from day-to-day. The deformation between day 1 and day 7 was estimated as approximately 37mm.

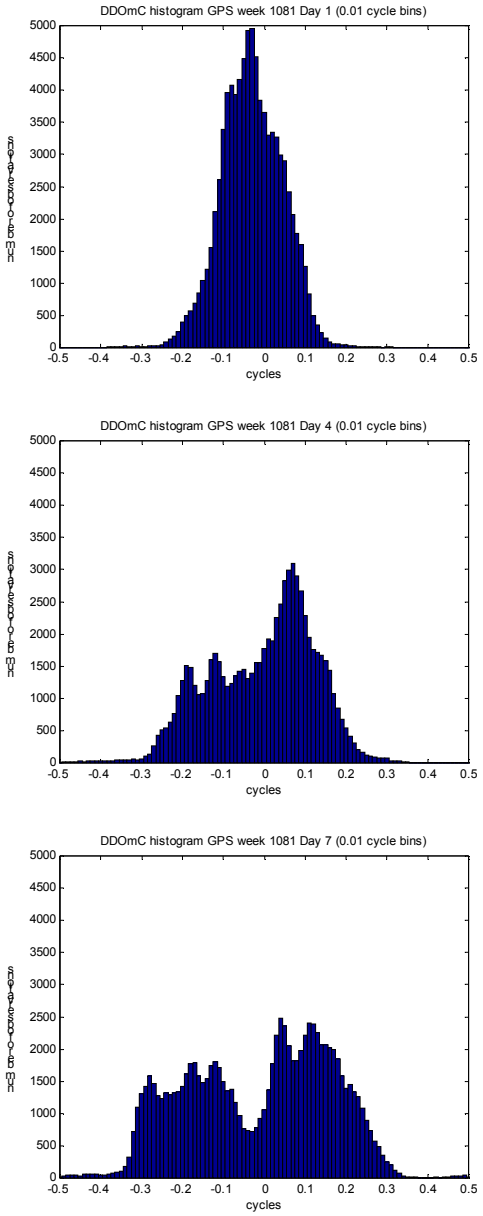

Figure 3.6 DDOmC values for three days of data in a deforming environment indicating divergence of the *apriori* coordinate estimates from the initial value

By visual inspection of Figure 3.6, the initial *a priori* coordinate estimate results in a relatively normal DDOmC distribution (day 1). For day 4, when the station location has moved, the resulting DDOmC distribution is less normal. By day 7, the distribution appears to be bimodal as the *a priori* coordinates deviate further from those that represent the actual antenna location.

When using the integer rounding technique introduced above in the deforming environment, it is necessary to update the *a priori* coordinate estimates to ensure that

the rounding pull-in region is sufficiently small. In some instances, depending on the dynamics of the deforming movement, this will require regular updates of the *a priori* coordinate estimates. This issue is further discussed in sections 5.3.4 and 6.2.

Data snooping functions are also required to remove poor quality observations and reduce the probability of mis-resolution of the ambiguity parameter.

3.6 Data Snooping

Data snooping is the process of screening the GPS data to identify poor quality observations. This is often completed at the pre-processing stage and may include:

- Data comparisons to establish common observation times between receivers;
- Removal of observations based on elevation cut-off angles;
- Removal of observations from unhealthy satellites;
- Detection and repair of cycle slips;
- Removal of poor quality data.

The repair of cycle slips and the removal of poor quality observations are simplified with the formulation of the GPS least squares estimation process presented in previous sections. Cycle slips are automatically removed when the integer ambiguities are resolved (rounded) at every measurement epoch. Individual GPS observations after integer rounding can also be removed if they exceed a predetermined threshold. This rejection level should consider the contribution of both the various systematic errors and the normal noise level of each double difference observation. Empirical tests are presented in section 6.3 to establish data rejection levels for the double difference observations when using the in-line ambiguity rounding technique discussed in section 3.5.

3.7 Summary

In this chapter, the various GPS positioning models required for high precision deformation monitoring have been presented. The error sources of concern for this type of positioning task were reviewed, together with the least squares estimation process to be used throughout the remainder of this research. Both the functional and

stochastic models pertaining to this estimation process have been discussed, and in particular those stochastic models to be tested in forthcoming chapters. These stochastic models include two elevation dependent models and the SIGMA-Δ model, in addition to the correlation-only stochastic modelling process.

The issue of ambiguity resolution has also been introduced. While much of the recent published research is concerned with the use of the LAMBDA technique, there are alternatives to this technique that can be customised to provide a robust estimate of the integer double difference ambiguity set. An in-line integer rounding technique can be used to estimate the correct ambiguity parameters. This type of integer rounding technique, however, relies on precise knowledge of the *a priori* positional information. This can be the case in the presence of quasi-continuous ambiguity-fixed deformation monitoring when the dynamics of surface points allow the deforming movements to be adequately tracked. The use of this type of ambiguity resolution technique has also been discussed in terms of the simplified data snooping capabilities that are afforded within the context of GPS positioning for high precision slope deformation monitoring. The development of a multi-antenna array GPS monitoring system that uses these positioning techniques is introduced in the next chapter.

4. DESIGN AND IMPLEMENTATION OF A MULTI-ANTENNA ARRAY GPS DEFORMATION MONITORING SYSTEM

Techniques used to monitor the stresses and deforming movements in and around steep slopes have been discussed in chapter 2. GPS-based positioning for deformation monitoring was discussed with respect to the positioning types commonly in use, namely that of CORS networks and episodic monitoring techniques. The gap between these technologies was also discussed in terms of the level of precision attainable, the density of the time-series obtained from such methods, and the associated cost advantages and disadvantages of each type of positioning technology. This research aims to bridge the gap between these two classes of GPS positioning systems for deformation monitoring by creating a dedicated GPS system for monitoring steep slopes.

This chapter discusses the hardware and software components of a prototype system designed for the specific task of GPS-based positioning for deformation monitoring in small-scale applications. The system concept is based around the design of a multiple switched antenna array that allows the system to monitor multiple points quasi-continuously with only one GPS receiver. The specific aims of the multi-antenna array design are to provide positioning capabilities similar to CORS networks, in terms of coordinate precision and the frequency at which coordinate updates are available, at a lower implementation cost. The primary cost saving offered by the multi-antenna array approach is the reduction in the number of hardware components that are required to monitor multiple locations continuously and the autonomy of the system which does not require manual collection of the GPS data.

Similar hardware designs have been reported in the literature by researchers in Hong Kong (Ding *et al.*, 2000; Chen *et al*., 2000; Ma *et al*., 2001) and in Japan (Petrovski *et al*., 2000). These are only concept level systems, however, and have not been used extensively in field trials. Furthermore, some of these systems offer the specialised

hardware necessary for multi-antenna positioning, but lack the software processing capabilities also required to optimise the deformation monitoring results.

The monitoring system hardware has been chosen to provide the most precise positioning possible. Where the required components were not available, they have been designed and manufactured as dedicated products for the specific application of deformation monitoring. All software used has either been developed in-house as part of this research, such as the GPS processing software called *Multibas*, or commissioned as task specific applications, as is the case with the communications software used. This has allowed the whole system to be designed and built with the purpose of monitoring the deformation experienced around steep slopes and in particular for open-pit mining operations.

4.1 Hardware

Historically, the prohibitive cost of installing CORS monitoring systems has been because of the need to establish one complete system at each monitoring station. This 'system' typically includes a GPS receiver, GPS antenna, and data communications equipment controlling hardware and software to appropriately *store and forward* the data back to the office, and some type of power source. Any reduction in hardware requirements can significantly reduce the overall cost of the complete system. System costs are discussed in section 4.3.6.

The system developed in this research utilises a GPS antenna array design whereby multiple GPS antennas are connected to one, geodetic quality GPS receiver. Data are sampled from one antenna and transmitted back to a base station, before the antenna switch moves on to sample data from the next antenna, and so on. The concept of this system is illustrated in Figure 4.1.

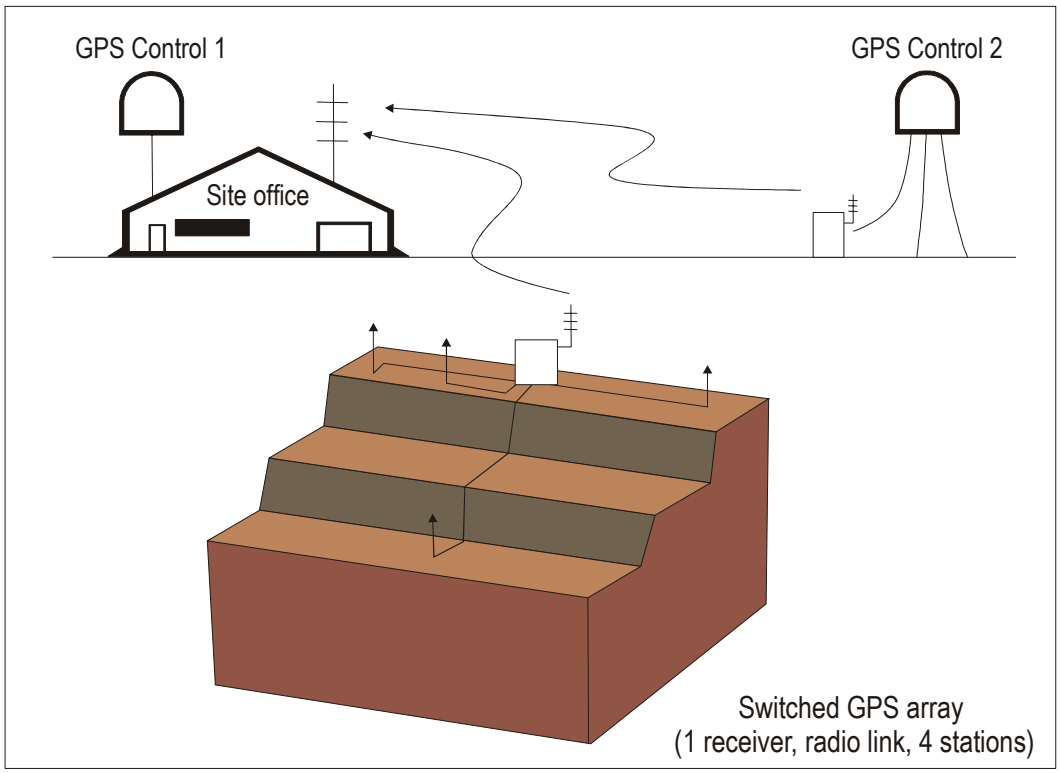

Figure 4.1 Multi-antenna GPS deformation monitoring system

This design reduces the need for multiple sets of the aforementioned hardware, software and communication components at each monitoring station. Only one receiver, and the associated communications system, is required using this approach for the monitoring of multiple locations. The number of ports on the switching device is the only restriction to the number of stations that can be monitored using this approach. In the system developed the switcher featured six ports.

A schematic diagram of the system components is depicted in Figure 4.2.

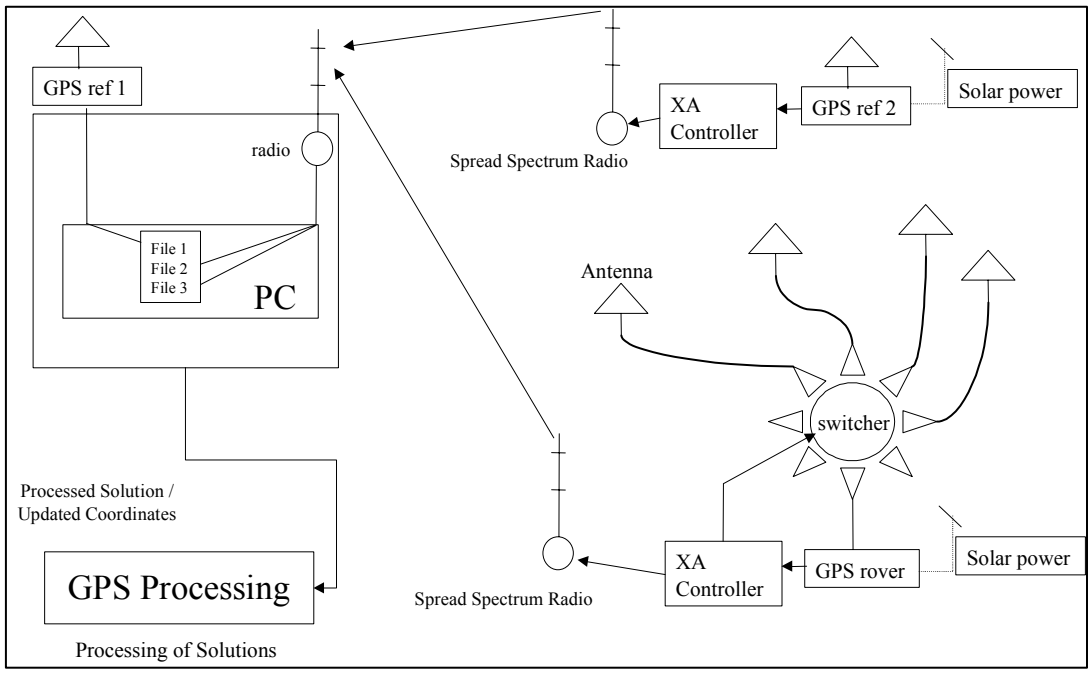

Figure 4.2 Schematic of switched antenna array design

Figure 4.2 illustrates the primary hardware components of the GPS monitoring system. Each major component is described in detail below.

4.1.1 GPS Receivers

Leica CRS1000 geodetic receivers have been used for the prototype phase of this research. These particular receivers, as shown in Figure 4.3, offer the robustness required for continuous operation, combined with the ability to log raw GPS data in real time, through one or both of the RS232 serial data ports available.

Figure 4.3 Leica CRS1000 receiver

Standard features of the Leica CRS1000 GPS Sensor used in this project include (Leica, 1999):

- Twelve channels for both L1 and L2;
- Continuous, all-in-view tracking capabilities;
- Less than 50ms measurement latency;
- Oven Controlled Crystal Oscillator (OCXO) stable to one part in 10^{-11} seconds;
- 486-80MHz CPU on board computer;
- 60 Megabytes of internal memory;
- Full wavelength carrier-phase on L1 and L2;
- Real-time kinematic (RTK) operational capabilities;
- Military specification connectors;
- Military specification pressurised, shock mounted housing.

Furthermore, the CRS1000 can also output data at up to 10Hz, and is also capable of producing 1 pulse per second output for precise timing applications.

While the CRS1000 receiver represents state of the art geodetic quality positioning capabilities, it is also expensive (approximately $A30000 for each unit). This research, however, is aimed at simulating a more cost-effective L1-only system that could be deployed in the future at a further reduced cost. As such, only L1 observations were used for data processing to simulate the results that may be expected from cheaper single frequency receivers. It is possible, however, that the use of lower cost single-frequency receivers might result in poorer quality GPS data than was collected for this research. The impact of this on the quality of the resulting coordinate time-series is not investigated in this project. The CRS1000 receivers were used in this research due to their availability for this project.

4.1.2 GPS Antennas

Leica AT504 L1/L2 choke ring antennas (Figure 4.4) were used at all survey stations. The close proximity of the slope was expected to induce signal multipath

and diffraction effects on the GPS observations. The use of the choke ring antenna helps to mitigate signal multipath effects that might be expected in GPS deformation monitoring (see section 3.3.1.1).

Figure 4.4 Leica choke ring antenna with radome

These antennas comprise a single piece, gold anodised NASA/JPL choke ring design (Leica, 1999) and provide approximately +25dB gain in the L-band. Hemispherical radomes were also used with each antenna to minimise contamination of the antenna choke ring channels.

4.1.3 Coaxial Switch

Fundamental to the monitoring system is a coaxial switching device, enabling data from multiple antennas to be sampled sequentially. The switching device used was a RADIALL® SPnT (Single-Pole, n-Throw) switcher offering up to six coaxial cable inputs, as pictured in Figure 4.5.

Figure 4.5 RADIALL® coaxial switcher

A transistor to transistor logic (TTL) compatible driver was used to operate the switching operations via a standard RS232 data connection. The switching cycle was controlled via the XA-board and is discussed in section 4.1.5. Specifications of the RADIALL® switcher used are included in Appendix 1.

4.1.4 Radio Communications

Radio communications are required to transmit the raw GPS data from the remote stations to the central processing site. The design of a radio communications network is site specific and should consider the following issues:

- Distance between radio receivers/transmitters;
- Terrain over which the data is to be transmitted;
- Amount of data transmitted;
- Radio frequency to be used;
- Interference sources;
- Other radio communication networks operating in the same locality;
- Type and use of radio antennas (antenna gain patterns);
- Federal radio communication guidelines.

Each of these issues should be carefully considered. The distance and terrain over which the data is to be transmitted, together with the operating frequency of the radio modems may require that radio repeater be used to extend the operating range or to transmit data around obstructions. The radio modem network should also be designed to consider both governmental regulations and any other radio networks in the immediate area to minimise signal interference problems. The communication radios used in this research are discussed in section 4.3.2.1.

4.1.5 XA-Board

The Extended Architecture (XA) controller is a custom designed PC board that was programmed to maintain the data handling operations of the system remote sites.

Both the GPS antenna switching device and the communications radio were driven by the XA-board to ensure that all components were synchronised appropriately. Furthermore, the XA-board was configured to provide *store and forward* capability at the remote sites. This allows only one radio to be used at the base processing site. The raw code, carrier-phase data and satellite ephemerides were transferred to the main processing station via the spread spectrum radios.

The XA-board is a single board computer that is powered by an XA-G30 microcontroller operating at a clock speed of 30MHz. The XA-board also features 128Kbytes of low power static RAM and 32Kbytes of erasable programmable read only memory (EPROM). Dual RS232 serial ports allow data to be ported to and from the memory chip.

As mentioned previously, the XA-board controls the *store and forward* operations of the raw GPS binary data. On receiving the data, the XA-board completes an initial integrity scan, processes for GPS time synchronisation, and then stores the data in a circular buffer memory arrangement. When the station is next polled by the base station, the GPS data are then transmitted, or *forwarded*, over the radio network back to the base station for data storage and processing.

The circular buffer memory can store a minimum of approximately 3.5 minutes of GPS data comprising the raw dual frequency 1Hz GPS code and carrier phase data and any associated ephemeris messages that have also been recorded. Typically each remote station is polled at 30-second intervals. The more often each station is polled, the lower the risk of data loss. In this case, the power required for data transmission rises accordingly.

At the deformation station, the XA-board also controls the RADIALL® coaxial switcher through the TTL driver protocols mentioned in section 4.1.3.

The XA-board can also be expanded to include other digital sensors such as thermometers, hygrometers, and air pressure sensors. Subsequent prototype systems could include such sensors to record real-time environmental and weather conditions at each remote station.

4.1.6 Data Control and Communications Software

To schedule the execution of the GPS data processing module and to control all other hardware/software/communications operations, a specialised software suite, *Gather GPS*, was developed. A company based in Western Australia, Hascom International, was commissioned to write this software suite for this project.

Gather GPS is a 32-bit multi-tasking application designed to run on Microsoft Windows 95/98/NT4/2000 operating systems. This software schedules the data polling interval between each remote site, initialises and controls the antenna switching operations and performs initial data integrity scans to ensure that all data have been transmitted correctly. The raw binary data is then binned into appropriate sessions and archived if required. The naming convention adopted for the data files is:

wwwwssss.nnn

where:

wwww	identifies the four digit GPS week number;
ssss	identifies a four digit session number within the current week;
nnn	identifies a node (or GPS receiver) number.

One session is defined as the maximum number of antennas at the switching site, multiplied by the length of data collected at each of those antennas. For example, if the system is configured with three antennas at the switching site, and 15 minutes of data are required at each of those antenna locations, then one session will comprise 45 minutes of data. This would mean that there are approximately 224 sessions in each GPS week. The time between repeat observation time at each antenna would be 45 minutes.

For real-time operation, the *Gather GPS* application would also initiate the GPS processing software (section 4.2).

One of the primary design requirements of this software was to record data sessions in multiples of the sidereal day to allow daily correlation of data for the testing of data stacking techniques. Hence the software uses the theoretical length of a sidereal day, rather than the theoretical length of the solar day. The difference between the two is approximately 236 seconds. This approach enables daily repeatability of the satellite geometry to be realised in the sidereal time reference frame. This is significant because each repetitive daily session will be automatically correlated with similar satellite observations, rather than having to post-correlate similar overlapping data times.

In this project, data were recorded for approximately 15 minutes at each antenna within the switching array (actually 14 minutes, 57.54 seconds were used). If the data were to be based on a repeating solar day and post-correlated by a mean shift of 236 seconds, only 74 percent of the data could be used for daily cross-correlation investigations.

4.1.7 Antenna Cabling Considerations

The multi-antenna approach to GPS deformation monitoring may require that the GPS antennas be located some distance from the GPS receiver and coaxial switch. These distances will obviously vary from site to site, and should be carefully considered in the system design process. The loss of signal strength in long cables can result in a complete loss of positioning ability. However, low-loss antenna cables and in-line amplifiers can be used to ensure that sufficient signal remains at the GPS receiver. Lightning protection should also be used to reduce the probability of component loss from direct or indirect lightning strikes. The antenna cabling, in-line amplifiers, and lightning protectors used in this research are discussed in detail in section 4.3.2.2.

4.1.8 Pillars/Monumentation

Where feasible, stations should use stable monumentation to ensure that there is no movement of the physical antenna location with respect to the surrounding ground mass. One other consideration for the survey monuments used are toppling effects that could magnify (or possibly absorb) the apparent effect of any deforming movements. This problem is not unique to GPS techniques, and will be an issue for any monitoring practice that uses reference points above the ground (and not direct monitoring of a ground mark). In practice, this problem can be addressed by regular verticality checks on all monuments to separate monument toppling from actual displacement of the ground mark. The station monumentation used in this research is discussed in section 4.3.2.3.

4.1.9 Computing Requirements

A Pentium personal computer running Microsoft Windows 95 controls the data collection and storage facilities for this system. The specific computing facilities and data storage considerations for this research are discussed in section 4.3.2.4. In theory, the monitoring system was designed to operate in a real-time environment. This option was not implemented in this proof-of-concept research.

4.1.10 Equipment Housing

The GPS receivers, radio modems, XA board, and switching device were all housed in Stevenson Screens to reduce the effects of direct solar and terrestrial radiation (Macquarie University, 2001).

Figure 4.6 Equipment housing

Figure 4.6 illustrates the equipment housing based on the Stevenson Screen design commonly used throughout Australia for meteorological measurements. The design of the Stevenson Screen regulates the temperature within the housing to represent the ambient air temperature, without the conductive and inductive effects of solar radiation. This particular design is intended to regulate the temperature within the housing to within 0.1°C of the actual ambient temperature and is constructed from a louvred, laminated polycarbonate material. As shown in Figure 4.6, the housings are elevated from the ground (to reduce conductive heat transfer and to promote air circulation around the structure), and firmly anchored in place. The support frame also provides electrical grounding for the lightning charge arresters that are installed (see section 4.3.2.2). As the temperature variations in the Australian outback can range from approximately -5°C to +50°C, the housing reduces the need for internal extraction fans to remove the heated air generated by the electronic equipment within.

4.1.11 Power Supply

Power supply at remote sites is a vital consideration to ensure continuous deformation monitoring. In most instances, a solar power system will be required to operate the GPS receiver, coaxial switcher, radio modem and XA-board at the remote sites. The design of such a system should consider the power requirements of each of these components, together with the amount of sunlight received in the local area. The power supply considerations for the testing phase of this research are discussed in section 4.3.2.5

4.2 GPS Processing Software

The core GPS processing software, *Multibas*, written by the author for this research, receives the binned Leica binary data and computes an estimate of the antenna location. The location is based on the least squares estimation principle (section 3.4), giving a statistically rigorous estimation of the point location. *Multibas* uses the GPS double difference processing technique (section 3.2.2) to reduce the effect of satellite and receiver clock errors, and the atmospheric errors induced by the ionosphere and the troposphere (for short baselines). Moreover, *Multibas* offers a complete multi-baseline processing approach (hence the name *Multibas*) and was designed to have the capability to implement the stochastic models discussed in chapter 3. The raw binary data were used as input to *Multibas* because of the massive volume of data collected at a 1Hz continuous sampling rate by the multiple GPS receivers that were used in this research (see section 4.3.2 for operational details of the system installed). The software was developed as a 16-bit application developed under the Borland™ C++ Version 4.52 development suite. Figure 4.7 illustrates the structure of the program *Multibas*.

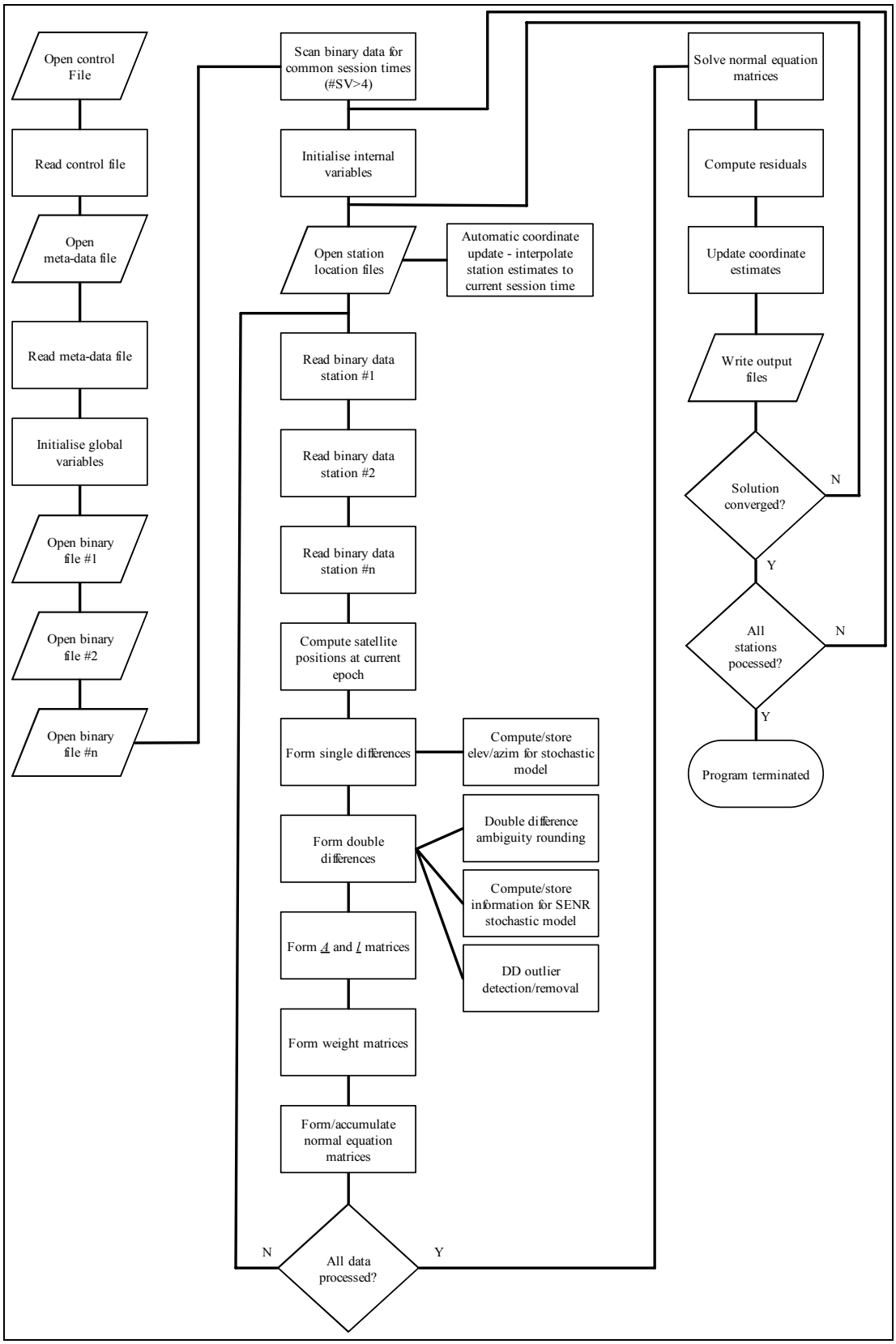

Figure 4.7 Data flow diagram of the software *Multibas* developed for high precision deformation monitoring of steep slopes

After reading in the control and meta-data files, *Multibas* then opens each binary data file containing the GPS observations and ephemeris data. The control file contains processing information such as the data processing interval, elevation-masking angle, stochastic model to be used, data snooping flags and output options that can be selected. The meta-data file is produced from the *GatherGPS* software (discussed in section 4.1.6) and lists the information pertaining to the binary data that were recorded. This includes the GPS week, session number within that week, the number of antennas at the monitoring site, and the session length. An initial scan is then performed on each data file to determine the common session times collected at each station. Next, the session times are adjusted so that at least four satellites are visible at each antenna within the session (as signal re-acquisition can take a few seconds after switching). The *a priori* station coordinates are then read in and interpolated to the current session time. This procedure is discussed further in section 6.2. Following this, the binary data files are rewound and coordinate estimates are computed for each antenna location within the session. Of note are the ambiguity rounding and stochastic modelling modules that are shown in Figure 4.7. These modules are also discussed in later chapters (sections 6.3 and 7.2).

For real-time operation of the system, batch processing of one complete cycle of the switching device would result in coordinate solutions for each station being available within a few minutes of the last observation in the current switching cycle. This would mean that under real-time operation, the deformation solutions would be updated approximately every hour. In more dynamic situations, where a slope slip or failure may be moving at an increased velocity, the individual station(s) monitoring the failure could be monitored more regularly, providing near to real-time deformation solutions (for example every few minutes).

4.3 The Test Site

Being application-based, research of this nature requires that the system, including the hardware, software and algorithms presented previously, be implemented and tested in the environment in which it would normally be deployed. The open-pit mining environment provides an excellent stage for the *real-world* testing phase of

this research. Open-pit mining operations in Western Australia present a particularly challenging environment for any satellite-based system. The steep mine walls that are in close proximity to the GPS antenna induce substantial multipath error. Also, the environment itself can be particularly harsh, with temperatures ranging from -5° to 60°+ Celsius at the bottom of the pit. Flyrock from blasting operations can also damage equipment or sever antenna cables, and the busy pit operations can provide a particularly challenging RF (radio frequency) environment for the data modems.

4.3.1 Western Mining Corporation Mount Keith Operations

The site used throughout this research was the Western Mining Corporation (WMC), Mount Keith Operations (MKO). This open-pit nickel mine is located approximately 700km north-east of Perth, Western Australia. The ore body at Mount Keith was discovered in 1968 by a local pastoralist and forms part of the Agnew-Wiluna greenstone belt. In 1993, WMC acquired full interest in Mount Keith, with production and shipment of nickel concentrate beginning in late 1994.

Nickel mineralisation occurs in disseminated nickel iron sulphide, called pentlandite. At Mount Keith, the pentlandite occurs as small disseminations (~1mm) throughout the deposit. The central portion of the deposit is measured as 1200m long. It is also up to 330m wide, with a continuous depth of at least 500m (Western Mining Corporation, 2000a).

The total nickel resources at the Mount Keith nickel deposit is projected as 477 million tonnes at a cut-off grade of 0.4 percent nickel (255 million tonnes measured, 130 million tonnes inferred and 92 million tonnes indicated). The size, shape and type of deposit offers a projected mine life of up to 20 years (Western Mining Corporation, 2000b).

Figure 4.8 illustrates the cross section schematic view of lithology, alteration and ore outline of the WMC MKO open-pit mine (after: Western Mining Corporation, 2000c).

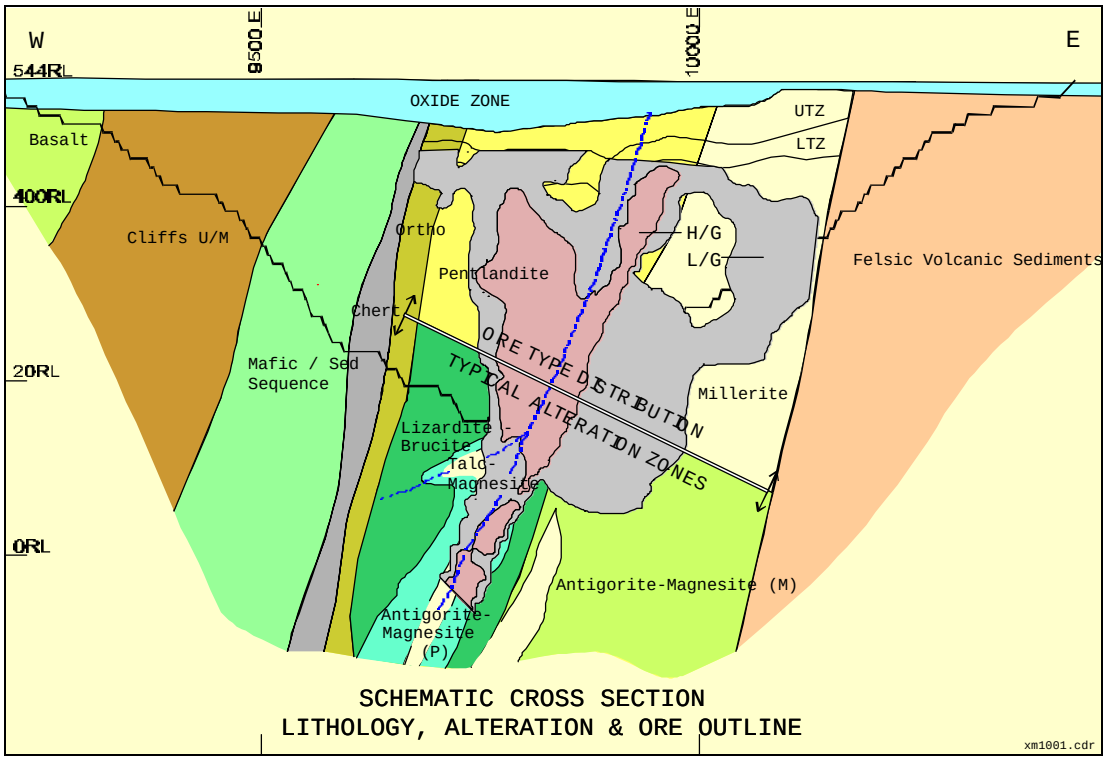

Figure 4.8 Schematic cross section of WMC MKO open-pit mine illustrating lithology, alteration and ore outline (after: Western Mining Corporation, 2000c)

Figure 4.9 below shows the design stages and annual face positions of a cross-section of the open-pit mine. This work is concerned with the cutback operations at stage E on the eastern pit wall. The cutback of this eastern wall (section 4.3.2) was expected to generate relaxation movement in response to the unloading of the wall mass.

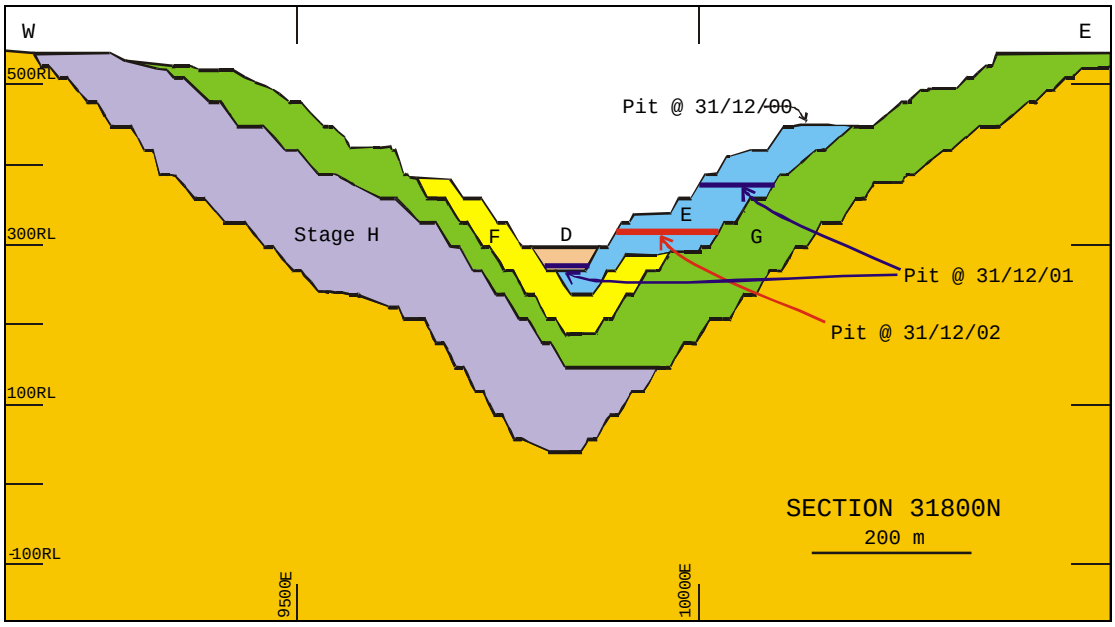

Figure 4.9 Design pit stages and annual face positions (after: Western Mining Corporation, 2000c)

Mapping the movement of stations on the wall face in a closely spaced time-series (hourly observation solutions) can provide important 3D information, not exclusively available through any other geotechnical monitoring scheme. An existing monitoring scheme at the mine site uses automatic total station instruments to monitor prisms placed on the eastern wall. Monitoring is usually conducted on a daily schedule. A sample of these results is presented in section 5.3.7.

4.3.2 Installed System

The network installed at WMC MKO was comprised of two reference stations, BASE and REF, and four monitoring stations numbered 0 through 3. A schematic diagram of the network of stations is illustrated in Figure 4.10.

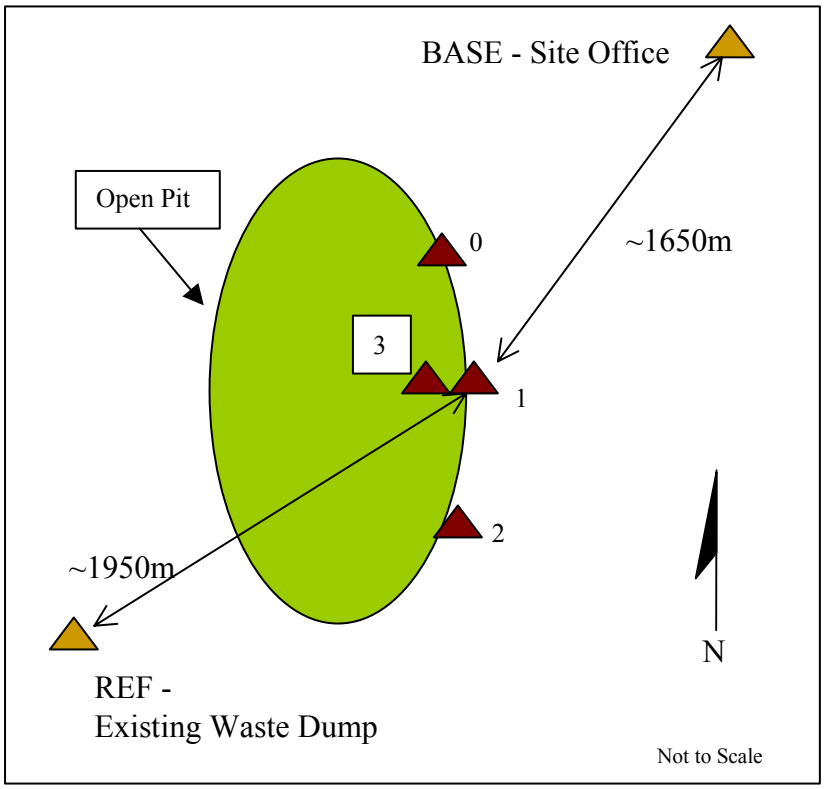

Figure 4.10 Schematic of site layout at Mount Keith open-pit mine

As indicated in Figure 4.10, the network was comprised of two reference stations, denoted hereafter as BASE and REF, and a network of four switched stations (numbered 0, 1, 2, 3). The locations of the monitoring points (Stations 0 through 3 in Figure 4.10) were selected by the WMC geotechnical engineer to monitor the wall stability. The first three stations are situated at the crest of the pit, while the fourth station is located below the natural ground level. By situating the stations in this manner, they can be used to provide the capability to monitor both plan and profile sections of the wall movement. The monitoring point situated below ground level is located 45m below the natural level of the surrounding surface. A profile view of the mine wall is illustrated in Figure 4.11

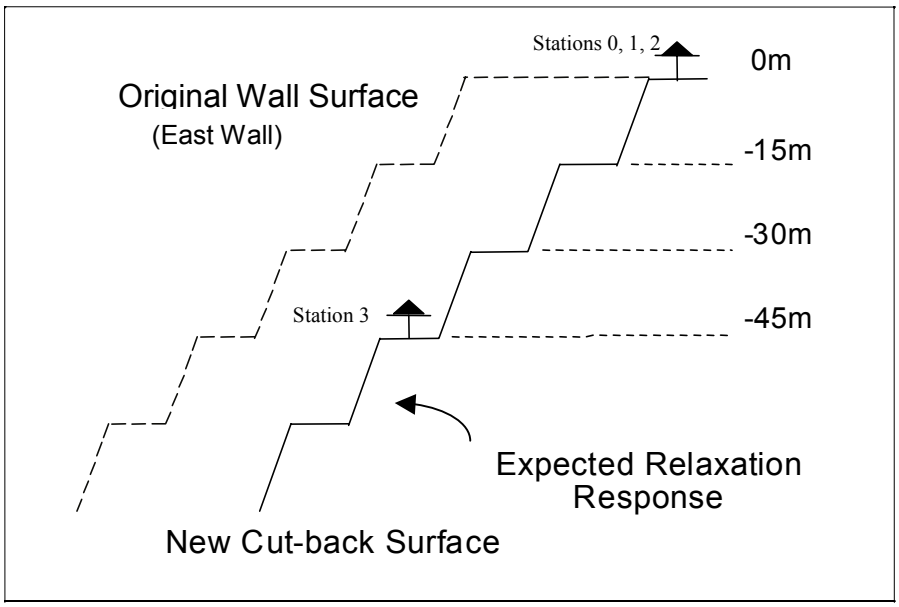

Figure 4.11 Profile view of the location of monitoring stations

The profile view featured in Figure 4.11 illustrates the vertical distribution of the GPS antennas. An indication of the expected relaxation response is also plotted (Sarunic, 2000). The relaxation response was expected to be primarily normal to the wall face (in a westerly direction) resulting from elastic rebound of the constraining mass. A smaller vertical shift (upwards) was also expected from the unloading of the mass where gravity is the constraining force.

The hardware components as installed at WMC MKO are discussed below.

4.3.2.1 Radio Communications

The communication radios used in this research were Radio Frequency Innovations RFI-9526 Data Strike Series 3 radio modems (Figure 4.12). These spread spectrum radio modems operate within the 915 – 928 MHz band and utilise pseudo-random code hopping to move through the allocated frequency band. This code hopping technique helps to minimise the effects of inter- and intra-band interference. These radios operate under a full duplex mode of data transfer, provide an over air data rate of 128Kb/second, and can be configured for point-to-point and point-to-multipoint connections, depending on the system requirements. Furthermore, these radio modems can also be configured as back-to-back repeaters, should the local

environment restrict direct line of sight between the slave and master radios (between the remote and base stations respectively). The maximum power radiated by these radio modems is 1W to meet spread spectrum standards (Radio Frequency Innovations, 1998).

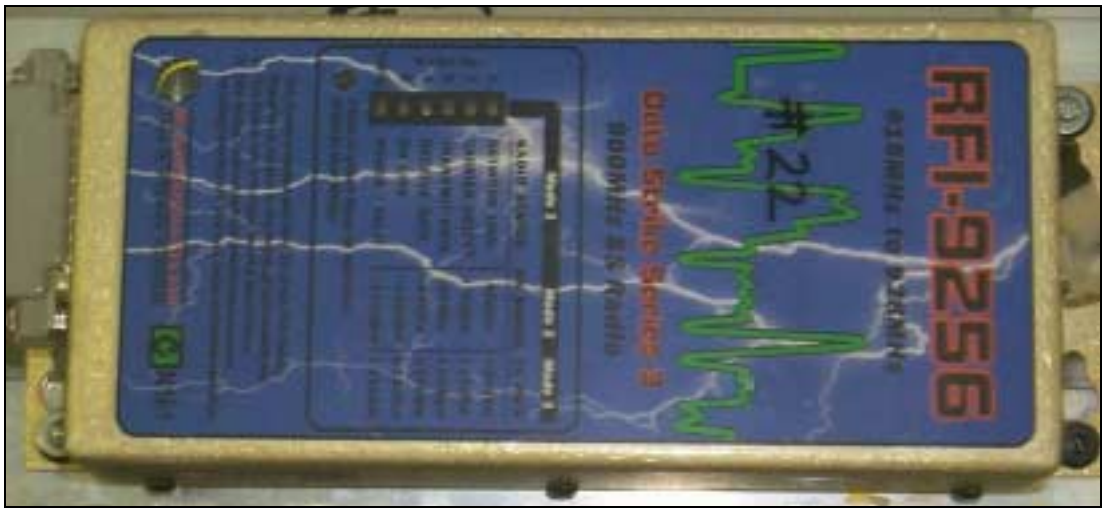

Figure 4.12 Radio Frequency Innovations spread spectrum communication radio

Directional Yagi antennas with 14dB gain (in the 900MHz band) were used at each site to transmit the data between radio modems (see Figure 4.14).

4.3.2.2 Antenna Cabling Considerations

The antenna array, at its furthest point, extends approximately 340m from the GPS receiver and antenna switching device. As such, the signal strength loss induced by the long antenna runs becomes significant. To reduce this effect, low-loss antenna cables were used throughout the system, supplemented by line amplifiers as required.

Three different types of antenna cables were used throughout the system (based on availability of equipment). Their types and specifications are listed in Table 4.1.

Cable	**Type**	**Nominal Attenuation dB/100 Metres**	
		@ 1000 MHz	@ 4000 MHz
Belden	9913	15.7	34.4
Belden	8214	23.0	70.5
Times Microwave	LMR-400	13.5	28.8

Table 4.1 Coaxial cable specifications

Ashtech dual frequency line amplifiers were also added in-line to boost the depleted satellite signal. These amplifiers (model # 700389) provide approximately +21dB gain at 1575.42MHz and +19dB gain at 1227.60MHz. The placement of amplifiers depended on the type and length of the cable segments used and the number of in-line connectors in place (each of which induces signal power loss).

The use of long antenna cables, such as those used in this system, is still a consideration, firstly in terms of maintaining sufficient signal strength, and secondly in terms of the quality of the signal itself after being transmitted such distances. Both of these issues were addressed by conducting simple C/N0 tests for both short and long antenna cables. The results of this test are illustrated in Figure 4.13 which show the repeat C/N0 values for satellite PRN19 over three days during GPS week 1084. Data from two stations are plotted where Station 1 has the shortest antenna cable length of 20m, and Station 2 has the longest antenna cable length of 340m.

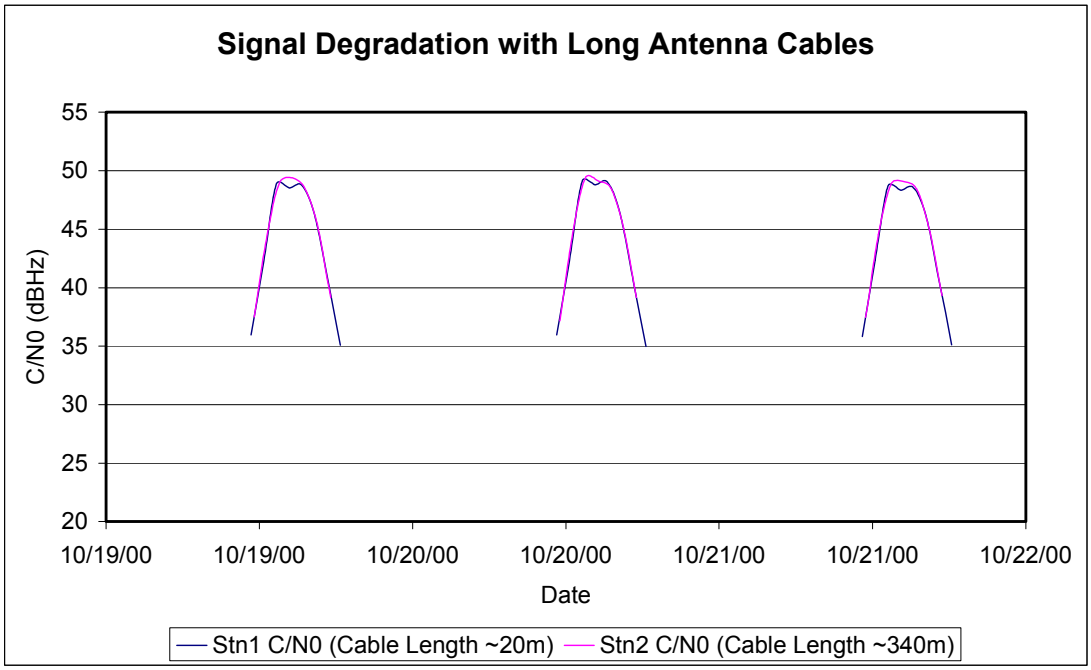

Figure 4.13 Effect of antenna cable length on carrier to noise ratio

The first point to note is that in both cases, sufficient signal strength remains after the GPS signal is propagated through the long antenna cable. This is verified simply by the fact that the receiver continues to track the satellites. For the receiver to search and track satellites must mean that there is sufficient signal strength remaining at the receiver. In every instance, the receiver is able to track the satellite in both the rising and setting case. The second point to note is that there is almost no difference in the C/N0 recorded between the station with a 20m long antenna cable and the station with a 340m long antenna cable. This implies that there is little loss in the quality of the signal observed at the receiver. If the quality of the signal were being degraded due to the length of the antenna cable being used, the observed C/N0 values would be consistently lower for the longer antenna cable than for the shorter one. This is not the case for the data collected to date.

Also of interest is the repetition of the structure of the C/N0 level that is recorded. In the case of the data collected at Station 1, similar deviations in the observed C/N0 values can be seen each day. This suggests that the power of the received signal is related to the satellite geometry that repeats every sidereal day.

Protection from lightning strikes is another issue to be considered for a permanently deployed GPS system. The probability of a direct equipment strike resulting in loss or damage of any particular component within the whole system is very small. The probability of component loss is increased, however, with the induction effects of nearby strikes, either at surrounding equipment locations or by local ground strikes. This occurs as a result of the power of the lightning strike being discharged into surrounding structures, or into the ground itself, which can create an induction effect on nearby equipment, destroying sensitive electronic components.

To minimise component loss, all components were fitted with lightning protection using gas surge arrester capsules. All arresters were fitted at the electronic equipment end of the signal run, near to the GPS receiver and radio modems, to reduce the impact of both direct and indirect (ground) strikes.

4.3.2.3 Pillars/Monumentation

Where feasible, stations featured concrete filled steel pillars for monumentation. Each pillar was capped with a steel plate and featured a $5/8^{th}$-inch thread commonly used in surveying for the forced centering of equipment. The pillars were drilled into the surrounding ground structure and cemented in place to ensure station stability. Survey tribrachs were also used to ensure that the antennas were levelled appropriately.

The only point not utilising this steel pillar configuration was the base station, where logistical considerations (having to drill under nearby roads to lay the antenna cables) restricted the use of such a survey monument. As such, this site featured a 60mm diameter steel pole, fixed to an office building (see Figure 4.14).

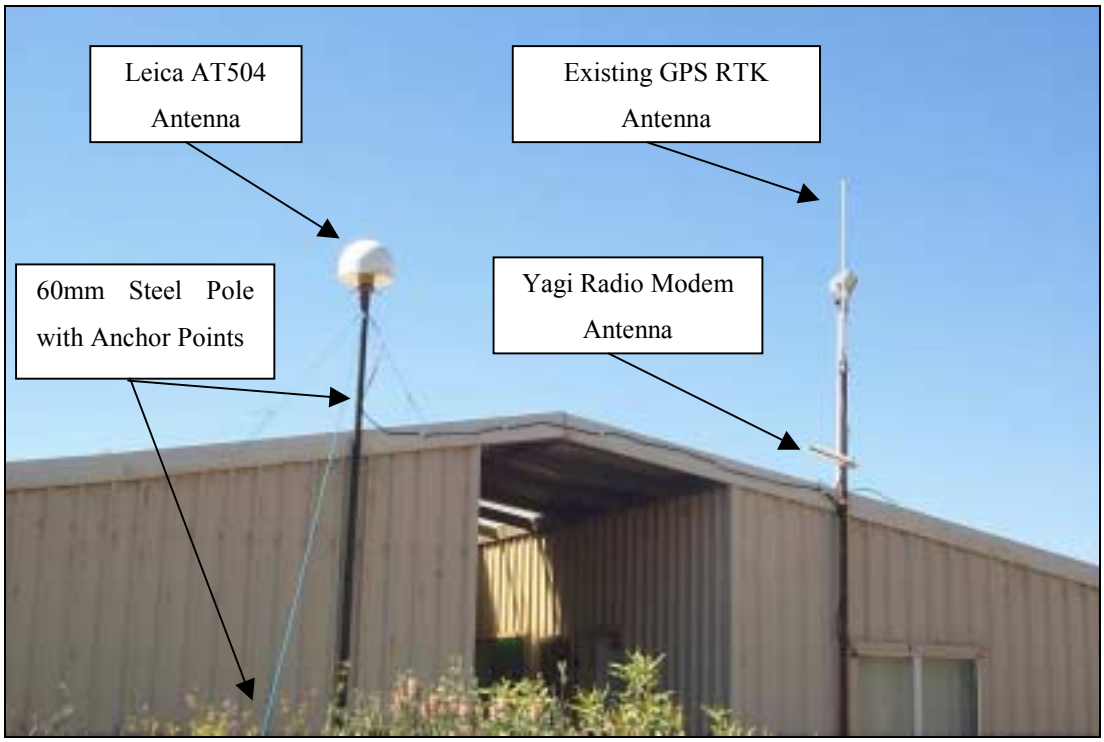

Figure 4.14 Survey station at the base site

Further to being fixed to the adjacent building, the monument was anchored to the rooftop and surrounding surface structure.

The thermal expansion of the monuments can affect the precision of the deformation solution achievable. As with many GPS-related positioning concepts, only the residual effect of differential thermal expansion needs to be considered between monuments. The linear thermal expansion of steel can be calculated by:

$$e = k \times l \times \Delta t \tag{4.1}$$

where:

e is the linear expansion;
k is the coefficient of expansion (in this case 12.0×10^{-6});
l is the length of material;
Δt is the temperature change (degrees Celcius).

The differential expansion between two stations of similar material is therefore calculated by:

$$\Delta e = k \times \Delta l \times \Delta t \qquad (4.2)$$

where:

Δe is the differential linear expansion between two stations of similar material.

As an example, a temperature difference between two stations of 10°C, and a difference in length of the monument installed of 3.5m (the maximum difference in the monument lengths between the steel pole used at the base site and the steeel pillars at all other stations), would result in differential expansion in the height between monuments of approximately 0.42mm. This is not considered to contribute significantly to the overall error budget of the deformation monitoring system presented in this research.

4.3.2.4 Computing Requirements

A Pentium personal computer running Microsoft Windows 95 controlled the data collection and storage facilities at the processing station. This computer, operating at a clock speed of 200MHz was fitted with 64Mb of RAM and also featured a CD writer for data archival. Once recorded to CD, the data were sent to Curtin University for post-processing. In theory, the monitoring system was designed to operate in a real-time environment. This option was not implemented in this proof-of-concept research.

4.3.2.5 Power Supply

Power at the base station was provided via a constant supply operating at a 240V alternating current.

As no power was provided at the remote sites, a solar power supply was installed. One remote site was powered by two 80-W Solarex™ solar panels connected to a 165 Amp-hour deep cycle storage battery via a 12V regulator. This system was designed

to maintain a full/floating power supply to maintain the GPS receiver, radio-modem and XA controller for at least five days without sunlight.

The mine site operator also provided a similar solar power supply for the second remote site.

Figure 4.15 Solar panel array

Figure 4.15 illustrates the solar power supply as installed for this research. The orientation of the solar panel structure was north facing, and inclined to account for the local latitude. The solar panel array was also located a sufficient distance (approximately 15m) from the GPS antenna to reduce any multipath effects that may be induced from the panel structure.

4.3.2.6 Station Descriptions

Figure 4.16 shows the site configuration at the station REF illustrating the monumentation, equipment housing and solar panel arrays.

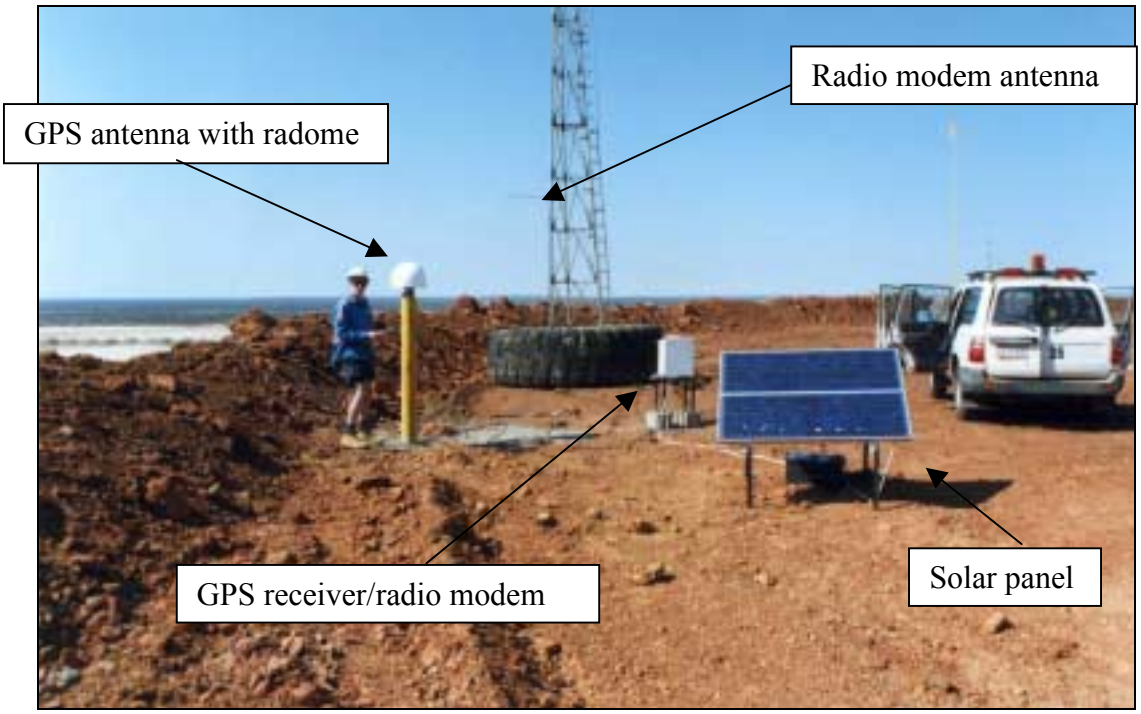

Figure 4.16 Reference station (REF) configuration at Mount Keith open-pit mine

The large communications tower illustrated in Figure 4.16 was removed, leaving a completely unrestricted sky view for the satellite observations. The REF station featured no sky obstructions or multipath reflectors. The other reference station BASE was illustrated in Figure 4.14. The data from this station, while not affected by sky obstructions, may contain signal multipath error from the surrounding rooftop. Most of the reflectors, however, were below 0° in elevation angle. Much of the remaining reflected signals would also be attenuated by the choke-ring design antennas (section 4.1.2) used at each station.

Figure 4.17 illustrates one of the stations at the surface (Station 1). This figure illustrates the concrete pillar used, together with the proximity of the Stevenson screen housing the GPS receiver, switching device and radio modem. The antenna cables coming from Stations 0 to 3 are all fed into the base of the Stevenson screen featured in Figure 4.17.

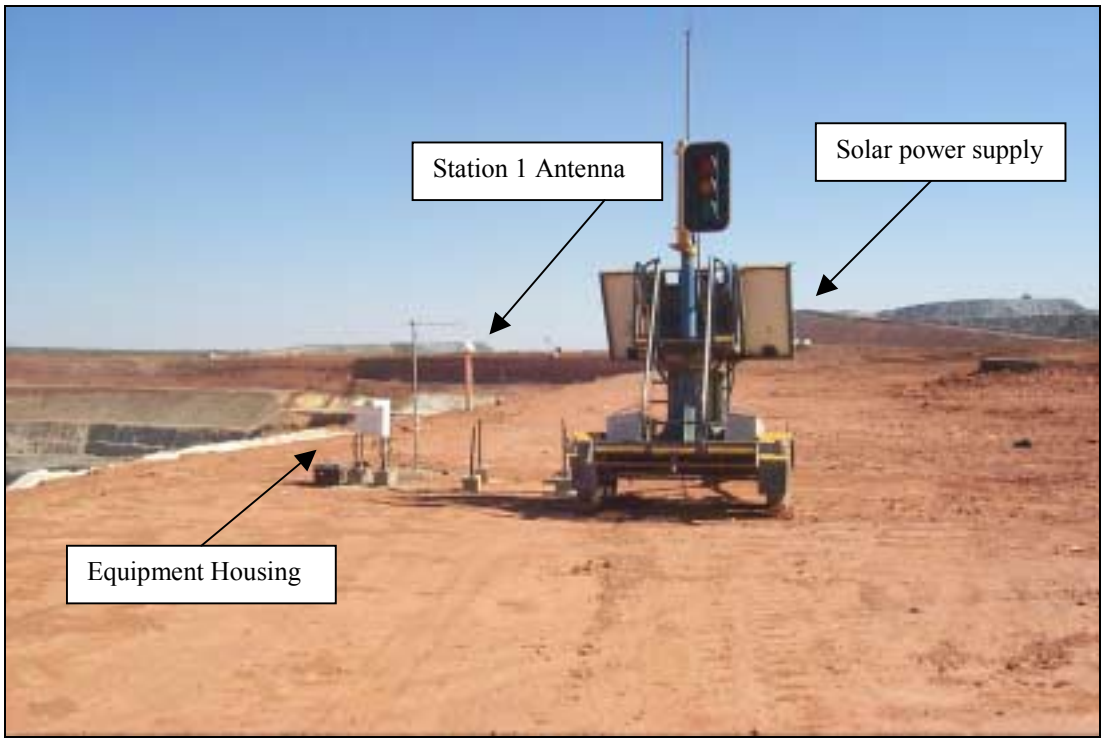

Figure 4.17 Deformation station at the surface level – Station 1

Minimal signal distortion is expected at Stations 0 to 2 with each station having no sky obstruction or nearby multipath reflectors.

Figure 4.18 shows the monitoring station as situated on the mine wall (Station 3).

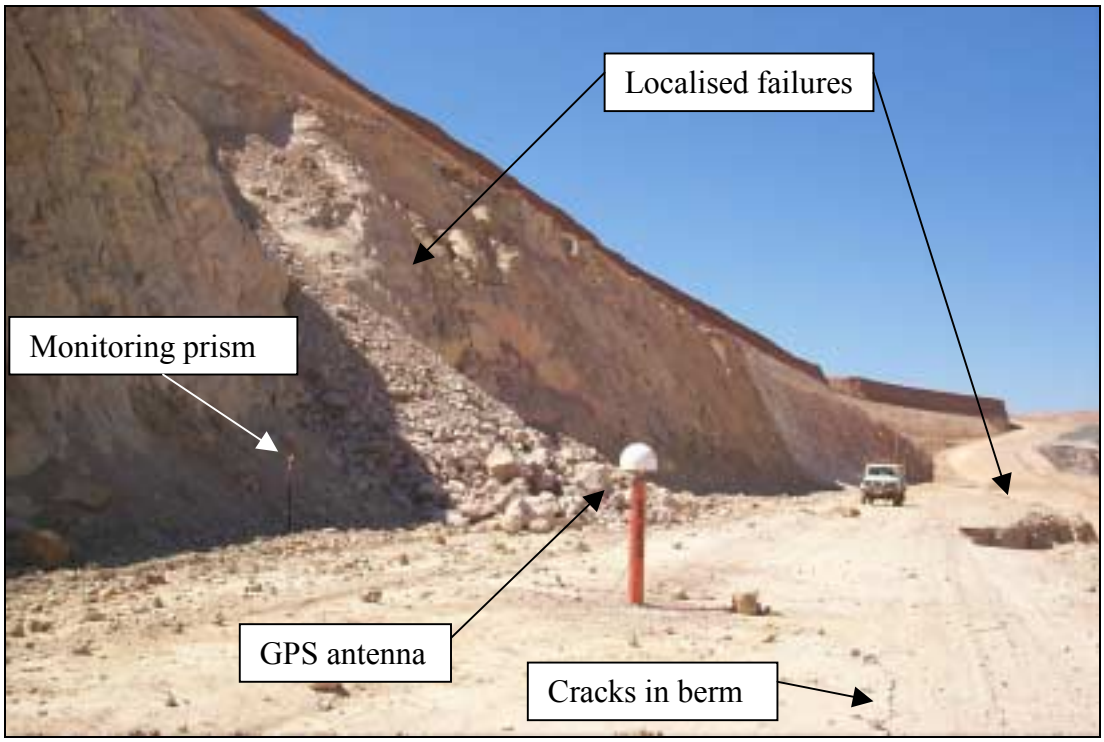

Figure 4.18 Deformation station situated near to the mine wall – Station 3

Station 3 is located in the middle of the berm to provide the best combination of geotechnical suitability and reduced signal multipath effects from the nearby wall. The most appropriate location for monitoring from a geotechnical perspective is at the toe of the wall, as indicated by the placement of the monitoring prism in Figure 4.18. This is the worst possible location from a satellite positioning viewpoint because more of the sky is obstructed by the nearby wall, and the close proximity of the wall itself leads to increased multipath delay error. The ideal location for GPS positioning in this situation would be at the crest of the berm to the right of the existing station in Figure 4.18. This is an undesirable location from both a geotechnical perspective and from a safety point of view, with localised failures generally occurring at the crest of the berm. A compromise was achieved by placing the monitoring station in the middle of the berm. As well as the localised slips that can be seen in the wall both above and below the berm, ground cracks are also present, which indicate localised separation, possibly delamination of the wall structure. Signal multipath from the nearby pit wall was expected to contaminate the GPS data at Station 3. The proximity of the mine wall to the GPS antenna may be seen in Figure 4.19.

Figure 4.19 Location of Station 3 near to the mine wall

4.3.3 Station Positions

The position of the reference station (REF) was calculated using the Australian Surveying and Land Information Group (AUSLIG) Online GPS Processing Service. This service utilises the MicroCosm® GPS processing software (AUSLIG, 2001), and produces precise positioning results based on a network solution of the nearest three International GPS Service (IGS) stations (in this case Karratha, Perth, and Yaragadee).

Twenty one days of data from GPS week 1084 to 1086 were decimated into daily files at a 30-second interval and processed using the on-line GPS processing service at AUSLIG to establish a precision estimate of the estimated coordinates. The position of REF is presented in Table 4.2.

Station	X (m)	Y (m)	Z (m)	Ant Height (m)
REF	-2883382.977	4888132.256	-2902324.594	0.110

Table 4.2 WGS84 adopted coordinates for the REF station

The associated coordinate precision of the solutions from the 21 days of GPS data is presented in Table 4.3 below.

Station	σ_X (m)	σ_Y (m)	σ_Z (m)
Ref	±0.0036	±0.0056	±0.0034

Table 4.3 Standard deviations of the reference station coordinates

To establish the precise coordinates of the other reference station (BASE) within the network, the relative baseline vector between REF and BASE was processed using 24 hours of 30-second data. By establishing the coordinates of the two reference stations in this manner, the absolute accuracy at the station REF could be maintained, while the precision of the ambiguity-fixed baseline vector propagates the precision into the station BASE.

Finally, initial approximate positions of the deformation stations relative to the REF were processed using between two and four hours of 30-second data. The station REF was chosen as the primary point of control due to the combination of a completely unmasked sky visibility, and the use of the concrete filled steel pillar for monumentation (section 4.1.7).

The initial estimated control positions were computed as:

Station	X (m)	Y (m)	Z (m)	Ant Height (m)
REF	-2883382.977	4888132.256	-2902324.594	0.110
BASE	-2885871.840	4888144.925	-2899746.933	0.092
0	-2884810.709	4888081.547	-2900895.242	0.0948
1	-2884804.695	4888022.557	-2900999.500	0.0935
2	-2884790.726	4887871.596	-2901265.854	0.0955
3	-2884736.188	4888001.678	-2901010.149	0.0945/0.1160

Table 4.4 Initial WGS84 coordinates for each station in the monitoring network

Table 4.4 indicates the initial starting coordinates in the six-station network. On the 12 October 2000, a faulty tribrach was replaced on Station 3. For the sake of completeness therefore, both antenna heights are presented.

4.3.4 Summary of System Settings

The system settings as installed and operated on Mount Keith open-pit mine may be summarised as follows:

Parameter	**Setting**
GPS data capture rate	1 second
Communication/data baud rate	19600
Type of GPS data	Binary - Leica LB2
GPS measurement data string	LB2 0x03 message
Satellite ephemeris data string	LB2 0x88 message
Number of deformation antennas	4
Time at each antenna	897.542604 seconds
Time between repeat	4*897.54 = 3590.17 seconds
Elevation masking angle for GPS data collection	0 degrees

Table 4.5 System settings used at Mount Keith open-pit mine

4.3.5 Operational Stability of Monitoring System

The switched antenna array system operated from the 19 September 2000 to 8 January 2001. The system operated almost without fault for the complete 16-week duration. The initial system consisted of one reference station (BASE) and the set of deforming points (Stations 0, 1, 2, 3). On 12 October 2000, the second reference station (REF) was brought on-line. This is shown graphically in Figure 4.20, which illustrates the availability of data from each receiver in the multi-antenna monitoring system.

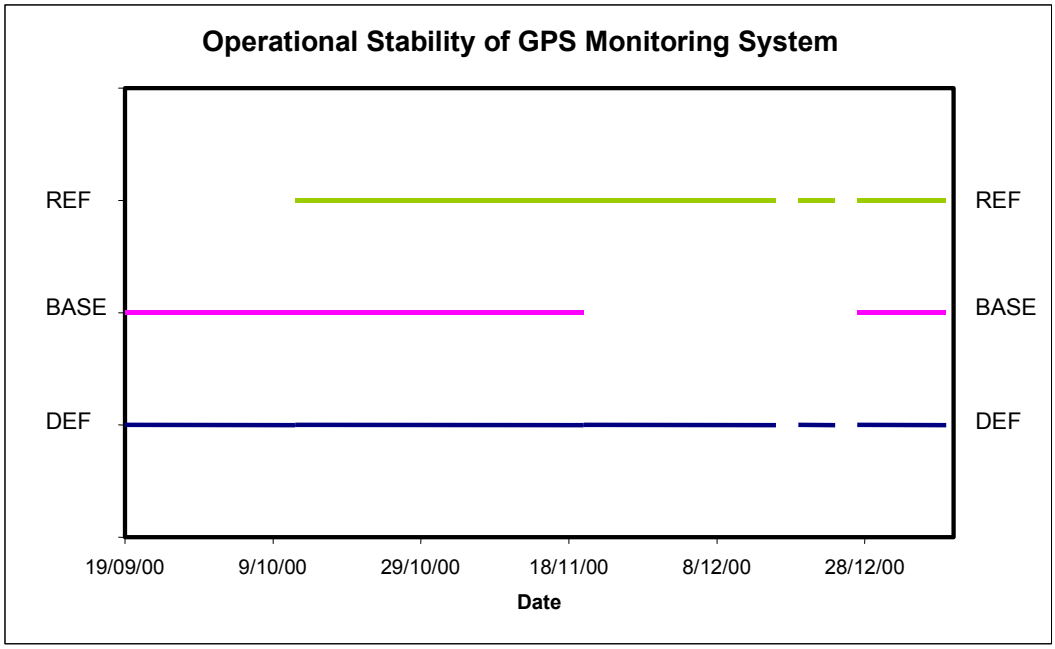

Figure 4.20 Operational stability of the GPS test system

The continuity of the data is shown for the GPS receivers REF, BASE, and the GPS receiver located at the pit surface (denoted as DEF). One major disruption to the data collection occurred on 20 November 2000 with the loss of the BASE receiver after a power outage at the WMC MKO site office. This power outage required a resetting of the internal GPS receiver settings. The receiver reset was effected on 27 December 2000. On-site support and/or constant monitoring of the system would have minimised the loss of data experienced but support was not available at the time.

A complete loss of data also exists as a result of the data backup procedures not being performed on-site. As a result, all data were lost between 16 to 19 December 2000 and 24 to 27 December 2000. While this does not detract from the operational capability of the system in terms of continued performance, it highlights the need for strict data storage and backup procedures in a production environment. This system outage highlights the importance of using multiple reference stations for a GPS-based deformation monitoring system. Not only does the use of multiple reference stations increase the precision of the coordinate solutions by up to 50 percent (see section 5.3.2) it also provides the necessary component redundancy to ensure that monitoring is still possible if data from one of the reference stations are unavailable.

4.3.6 GPS Deformation Monitoring System Costs

A simple costing is provided to evaluate the different costs of installing GPS monitoring systems. The figures provided are approximate costs in Australian dollars at the time of writing (April 2002). Only prices for the major equipment components are included for simplicity.

	Rapid Static	**Continuous**	**Switched**	**Low-cost Switched**
GPS Receiver	3*30000	8*30000	3*30000	3*10000
Antenna	3*1500	8*6000	8*6000	8*1500
Cables	0	0	6*750	6*750
Radios	0	8*2000	3*2000	3*2000
Switcher	0	0	1500	1500
Personnel	50000	0	0	0
Stations monitored	18	6	6	6
Total	94500	304000	150000	54000
Cost per point	**5250**	**50666**	**25000**	**9000**
Personnel per Year	50000	0	0	0
Personnel per Station per year	**2778**	**0**	**0**	**0**
Solutions per day	**1**	**user selected**	**24+**	**24+**

Table 4.6 Approximate system installation and running costs (Australian dollars) for GPS deformation monitoring

The system costs included above are very approximate. The costing for episodic rapid static monitoring include the annual cost of employing one surveyor. Based on an eight-hour day, it is estimated that a competent surveyor could monitor 18 stations. This would include mobilisation and de-mobilisation of the equipment each day, data processing time, and set-up and transit time between stations to be monitored. The low cost switched option is based on using L1-only GPS receivers and antennas.

The system costs for episodic monitoring are approximately $5250 for equipment purchase plus $2777 per point per year ($8750 in the first year plus nearly $3000 each year thereafter). The drawback of this type of monitoring is the frequency with which each point is monitored (only once per day). Sampling frequency is further discussed in section 6.7. For continuous and multi-antenna approaches, six points

were used in the costing calculation. This is the maximum number of antennas that can be connected using the switcher used in this research. Other switchers can be purchased that provide switching between more antenna locations. The installation cost for continuous monitoring exceeds $50000 per point, while the multi-antenna array approach proposed in this research costs approximately $25000 per point. Using lower cost L1-only components, this could be reduced to under $10000 per point. The sampling frequency of these final three systems could be user selected ranging from single-epoch solutions to one solution per day. The appropriate selection of session length for quasi-continuous monitoring is discussed in more detail in section 6.5.

4.4 Summary

This chapter has presented the hardware and software components that have been included in a system to monitor steep slopes using GPS positioning. The system developed used a switched antenna array design to sample data from multiple antennas using only one GPS receiver. This dedicated system is aimed at bridging the gap between continuously operating GPS systems and episodic monitoring campaigns by providing a quasi-continuous data time-series at a reduced implementation and operating cost.

The software *Multibas* was developed to process the continuous binary GPS data from the deformation monitoring stations established on the Mount Keith open-pit mine in Western Australia. The software was developed to implement the specific GPS processing algorithms presented in chapter 3 for high precision slope deformation monitoring using the multi-antenna array approach. By using the raw binary data it was also possible to extract the C/N0 information directly from the Leica CRS1000 GPS receivers.

The mining operations at Mount Keith have recently (2000) undergone cutback operations performed on the eastern wall of the mine. Relaxation of the wall face was expected in response to the unloading of the rock mass from the wall structure.

Two reference stations and four monitoring stations were installed at the mine site to measure and monitor any relaxation of the wall face. Reference station coordinates were determined by the use of the precise carrier-aided point solutions obtained through the AUSLIG Online GPS Processing Service with a coordinate repeatability in the order of approximately ±4mm.

Approximate system costs have also been detailed for episodic, continuous, and multi-antenna array monitoring systems. While the implementation costs of both continuous and multi-antenna array systems exceed those of episodic monitoring, there are no ongoing personnel costs that would be associated with the manual collection of the GPS data. Cheaper multi-antenna system components could also be used to further reduce the costs associated with installing a dedicated GPS monitoring such as the one proposed in this work.

Preliminary tests results are presented in the next chapter to illustrate the capability of the system developed.

5. TEST RESULTS USING BENCHMARK PROCESSING PARAMETERS

Initial test results are presented for the complete time-series of data collected at the WMC MKO open-pit mine from September 2000 to January 2001. These results represent a benchmark dataset that will be discussed in detail throughout the remainder of this research. It is intended that these results will form the basis from which optimisations and improvements to the processing strategy can be gauged.

5.1 Benchmark Processing Parameters

The processing parameters used for the benchmark processing strategy are listed in Table 5.1.

Processing Parameter	**Values Used**
Processing Interval	1 second
Session Length	~15 minutes
Elevation Cut-off	15 degrees
Tropospheric Model	Saastamoinen
Double Difference Outlier Detection	None
Coordinate Update	Manual
Stochastic Model	Math

Table 5.1 Benchmark processing parameters

Tables similar to this will be presented throughout the remainder of this thesis. They will enable the reader to easily identify the processing options that have been used in each relevant section.

5.1.1 Processing Interval

The basic processing strategy makes use of the 1Hz data that are recorded by the Leica CRS1000. No time correlation is assumed between the observations.

5.1.2 Session Length

All of the available data are used in the benchmark processing strategy. Section 6.5 discusses the sensitivity of the coordinate solution to the length of the session processed.

The mean session length for this dataset is calculated as 884 seconds from the 9004 sessions that were observed over the 16-week field trial. As the design session length was 897.54 seconds, approximately 13 seconds of data were lost due to the duty cycle of the coaxial switcher and GPS signal re-acquisition. This equates to a loss of approximately 1.5 percent of the total possible data at each session.

5.1.3 Elevation Cut-off

The initial elevation cut-off angle was set to 15°. An elevation-masking angle of 15° is often chosen to reduce the effects of residual atmospheric errors. Alternative elevation angles are discussed in chapter 6.

5.1.4 Tropospheric Model

The Saastamoinen tropospheric model (Saastamoinen, 1973) was used for all data processing strategies presented within this research. This model was chosen for its simplicity of implementation.

5.1.5 Double Difference Outlier Detection

No double difference outlier detection was applied to the in-line integer rounded ambiguity resolution process (chapter 3.6) for the benchmark processing strategy. Outlier detection schemes using an empirically based ambiguity bound are introduced in section 6.3.

5.1.6 Coordinate Update

Coordinates are updated manually in the initial benchmark processing strategy. These were updated as required, based on a visual inspection of the graphical results (section 5.3.4). Automation of this strategy is discussed in more detail in section 6.2.

5.1.7 Stochastic Model

The stochastic model implemented in the benchmark processing strategy only considers the mathematical correlations between the double difference observables (section 3.4.2). This mathematical model (Math) is implemented following the strategy suggested in Beutler *et al*. (1986). Stochastic modelling is discussed further in section 7.2.

5.2 Initial Test Results Using Benchmark Processing Parameters

The initial test results for the deformation of four points installed at MKO are presented overleaf. The graphs illustrate nearly 16 weeks of single frequency deformation solutions computed at each station approximately every hour. There are a number of data gaps that exist within the time-series that result from system outages. These have been discussed in section 4.3.5, with reference to the overall stability of the system.

Figures 5.1 through 5.4 illustrate the UTM projected northing and easting coordinate differences, and WGS84 ellipsoidal height difference, of Stations 0 to 3 respectively. These differences, and those presented throughout the remainder of this thesis, are computed with respect to a nominal coordinate at the beginning of the time-series. As stated in section 4.3.2, Stations 0 through 2 were situated on the surface surrounding the open-pit mine, while Station 3 was situated on the wall berm, approximately 45m below surface level.

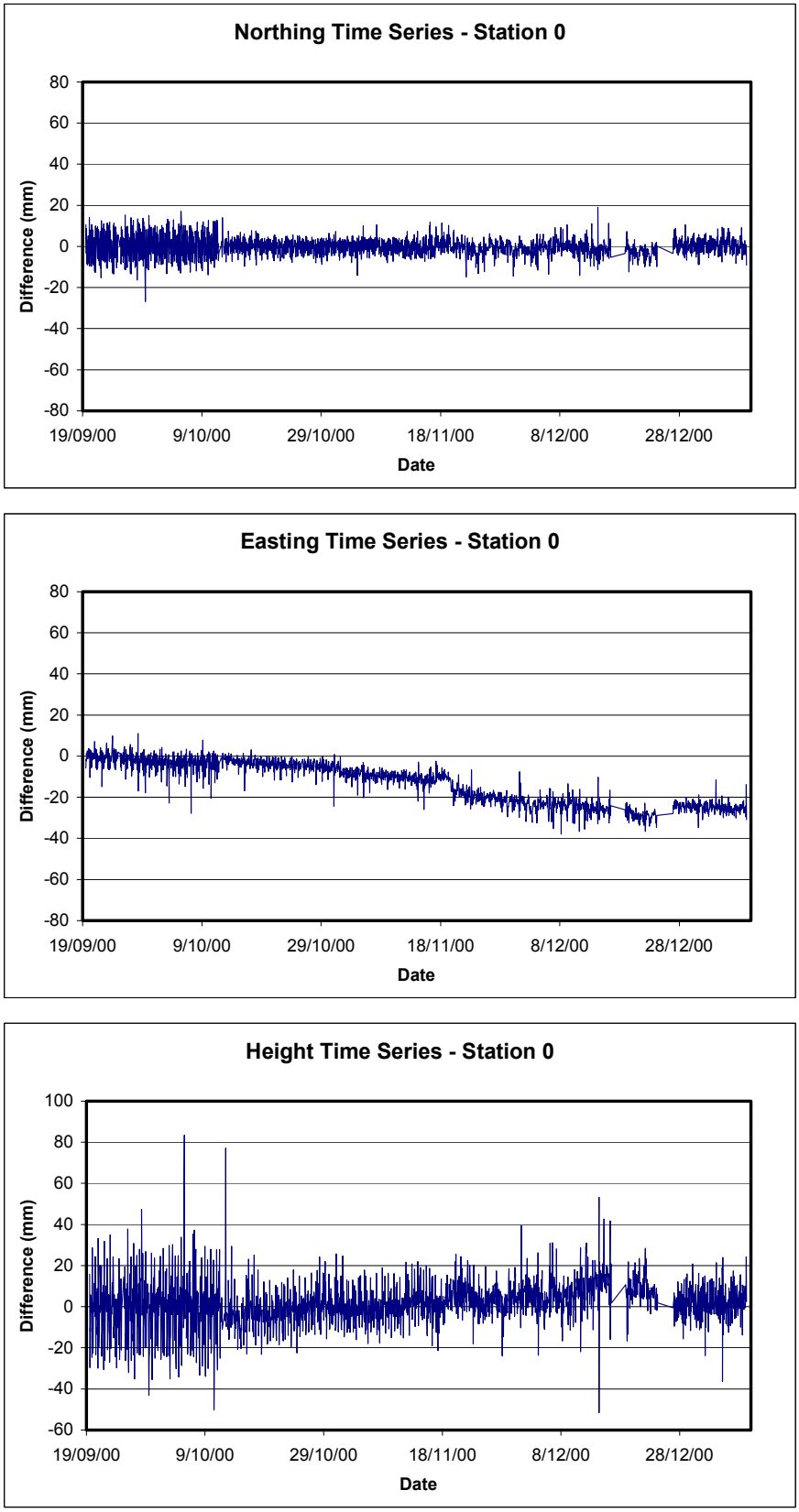

Figure 5.1 Northing, easting and height differences for Station 0 using benchmark processing parameters

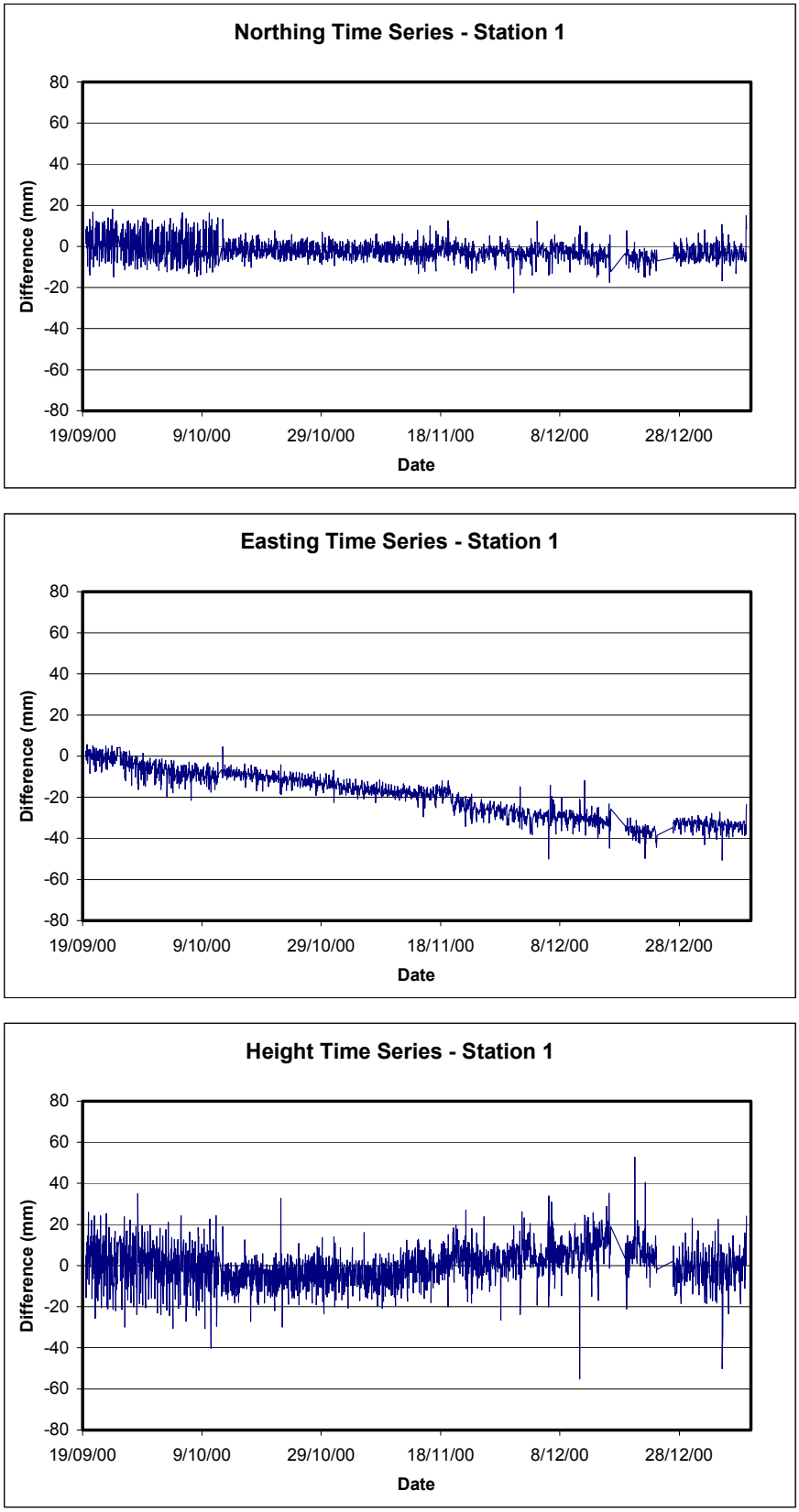

Figure 5.2 Northing, easting and height differences for Station 1 using benchmark processing parameters

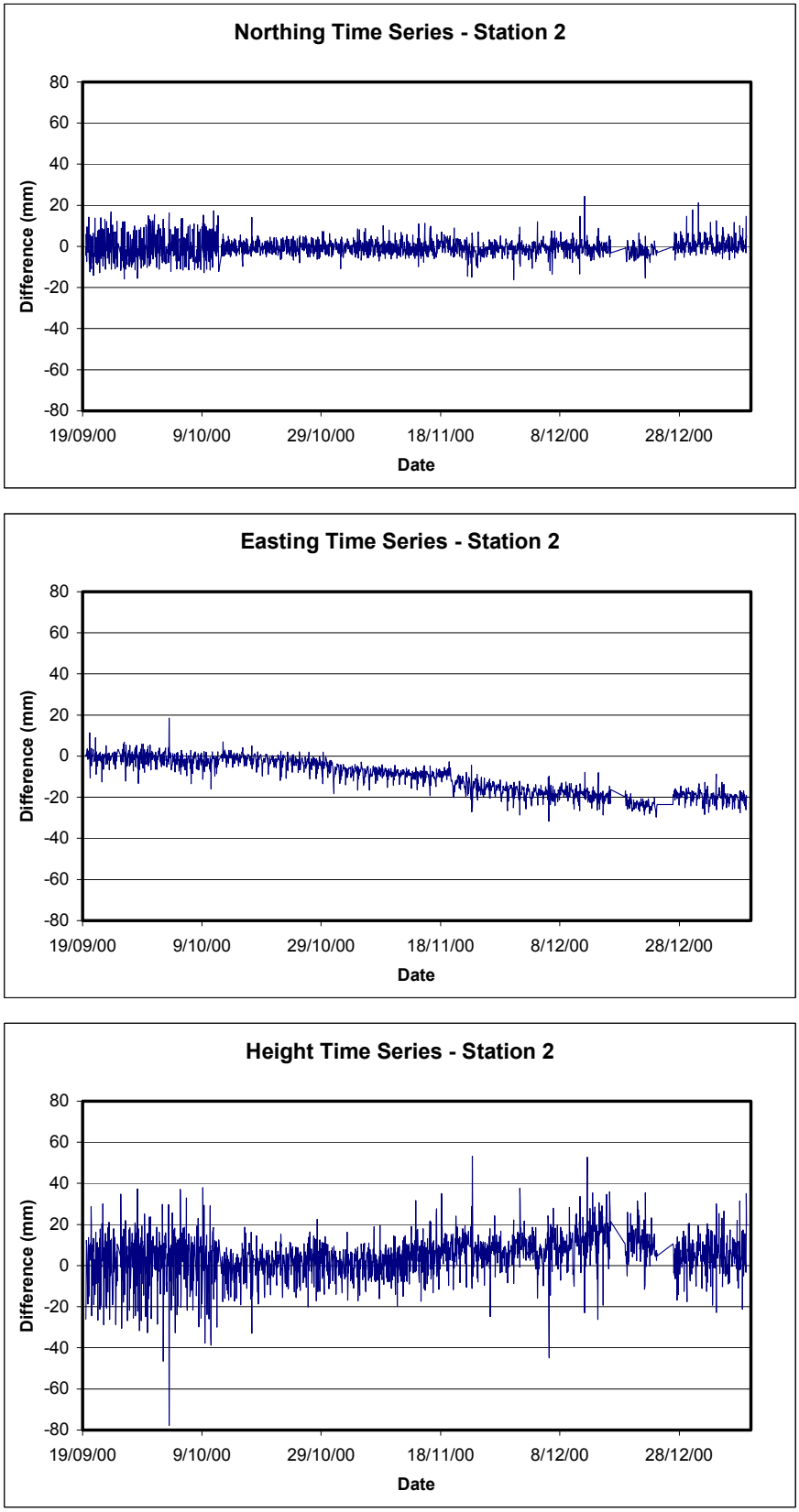

Figure 5.3 Northing, easting and height differences for Station 2 using benchmark processing parameters

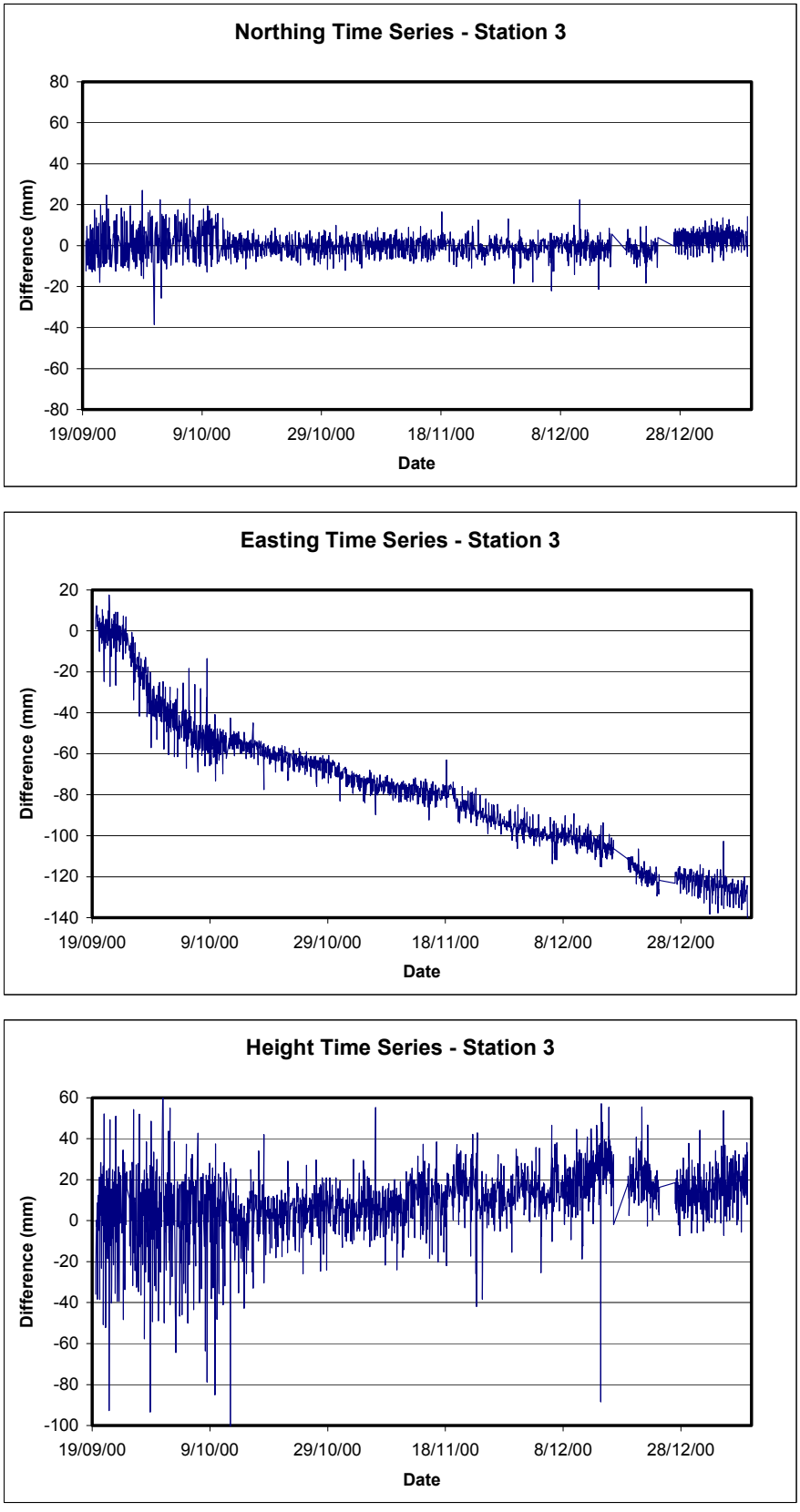

Figure 5.4 Northing, easting and height differences for Station 3 using benchmark processing parameters

Inspection of Figure 5.1 shows that small deformations may be detected in the northing and height components at Station 0. Approximately 25mm of deformation appears to have occurred in the easting component over the 16-week observation period. A trend extraction technique is introduced in the following section to quantify the magnitude of the movements detected. There is also a noticeable increase in the precision of the time-series after 12 October 2000 in all three coordinate components. This improvement is the result of the introduction of the second reference station to the monitoring strategy. This effect is discussed in more detail in section 5.3.2.

Figure 5.2 shows that minimal deformation can be detected in the northing and height components of Station 1. Approximately 35mm of deformation can be detected visually in the easting component.

Station 2, as shown in Figure 5.3, exhibits similar magnitudes of deformation as does Station 0. These two stations were not situated directly within the zone of maximum deformation, with Station 0 being positioned to the north of the deformation zone and Station 2 situated to the south.

Figure 5.4 illustrates the displacement observed at Station 3, 45m below ground level. Although minimal deformation appears to be present in the northing component, deformation appears in the height component, and significant movement can be seen in the coordinates computed for the easting component. It would appear by visual inspection that approximately 130mm of motion is present in this component. The increase in the ellipsoidal height at this station supports the expected relaxation response of the wall face proposed in section 4.3.2.

The actual magnitude of the deforming trend is difficult to quantify without the use of some form of trend extraction facility. This is introduced and discussed in more detail in section 5.3.1. Precision estimates of the GPS observations are also difficult to generate without an appropriate technique to remove the trend that exists within the coordinate time-series. This is also discussed in section 5.3.1.

5.3 Remarks on Initial Test Results

The deformation solutions presented above will now be discussed in more detail to characterise the data obtained from using GPS positioning in a deforming environment, such as the one presented within this thesis.

5.3.1 Trend Extraction from Raw GPS Position Data

Possibly the most important aspect of characterising the results from the multi-antenna deformation monitoring system is having the ability to extract the underlying trend of the deforming movements. By extracting this trend, it is then possible to make a qualitative assessment of the magnitude of the deforming movements, and the precision with which this deformation can be estimated.

A simple Moving Average Window (MAW) can be an effective tool for extracting trends. One such simple moving average window may be presented by:

$$MAW_2(t) = \sum_{t-\frac{w_l}{2}}^{t+\frac{w_l}{2}} x(t) \Big/ w_l \qquad (5.1)$$

where:

$MAW_2(t)$	is the value of the two-tailed simple moving average window at time *t*;
x(t)	is the current value of time-series at time *t*;
w_l	is the length of the moving average window.

Equation 5.1 defines a simple two-tailed moving average window with a length of w_l. This type of moving average window is noncausal and is used here for post-processing purposes as it considers data both before and after the current epoch.

The disadvantage of the MAW_2 is the transient period that is required at both the beginning and the end of the time-series. For real-time data acquisition systems, where trend prediction may be necessary, it may be appropriate to use a causal system (Oppenheim and Willsky, 1997) which is defined in this case as a one-tailed MAW. This may be represented by:

$$MAW_1(t) = \sum_{t-w_l}^{t} x(t) \Big/ w_l \tag{5.2}$$

where:

$MAW_1(t)$ is the value of the one-tailed simple moving average window at time *t*.

As all the data presented here are post-processed, the MAW_2 is used with a window length of 40 sessions (40 sidereal hours with one solution per hour). A window length of 40 sessions is chosen (based on both empirical testing and data simulation) as a reasonable trade-off between trend detection capability and smoothness. The choice of window length is discussed in more detail in section 6.1.4.

The following trends (Figures 5.5 to 5.9) were extracted from the individual deformation solutions at each monitoring station.

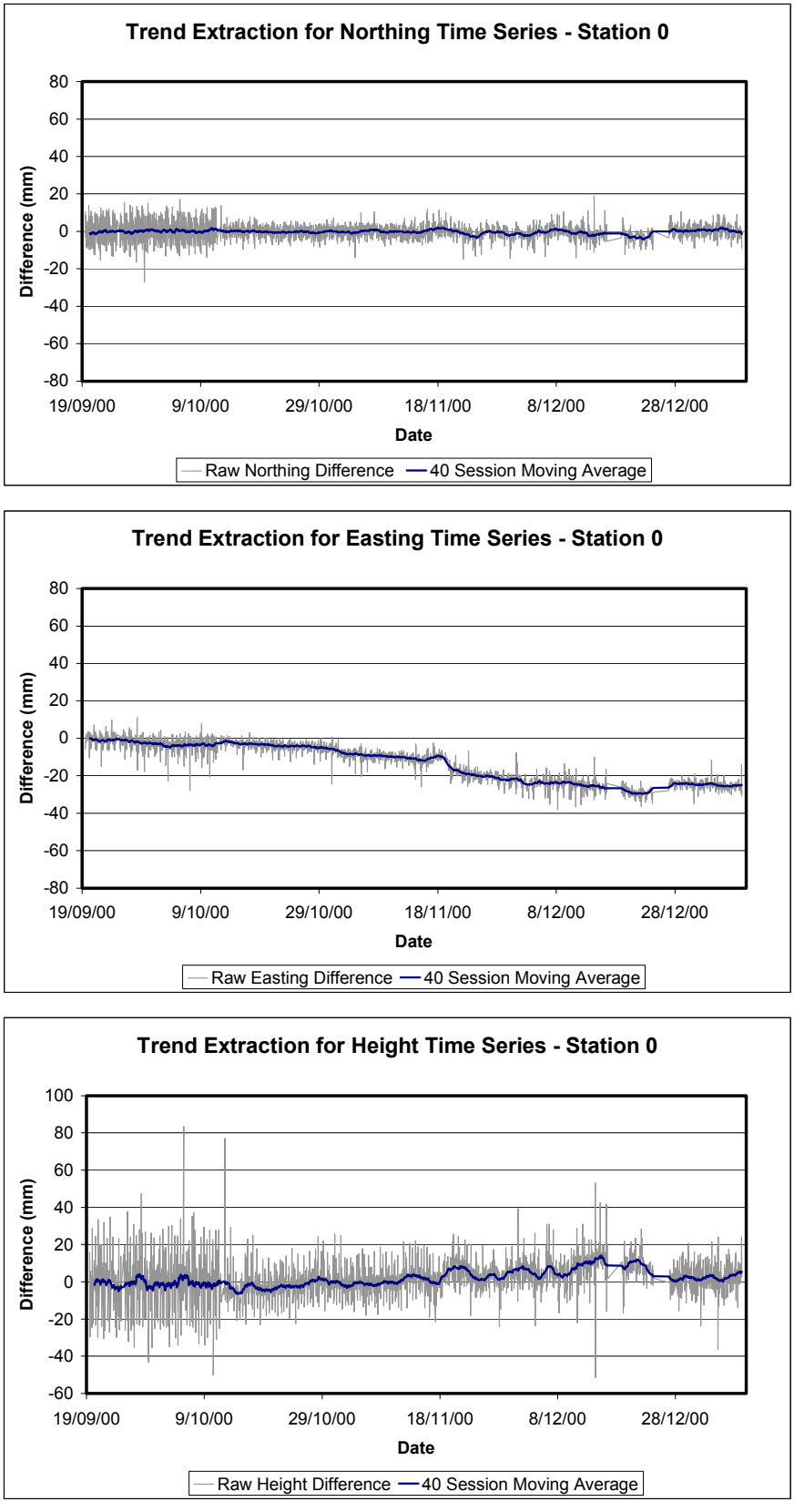

Figure 5.5 Northing, easting and height trends extracted via a 40 sidereal hour two-tailed moving average window at Station 0

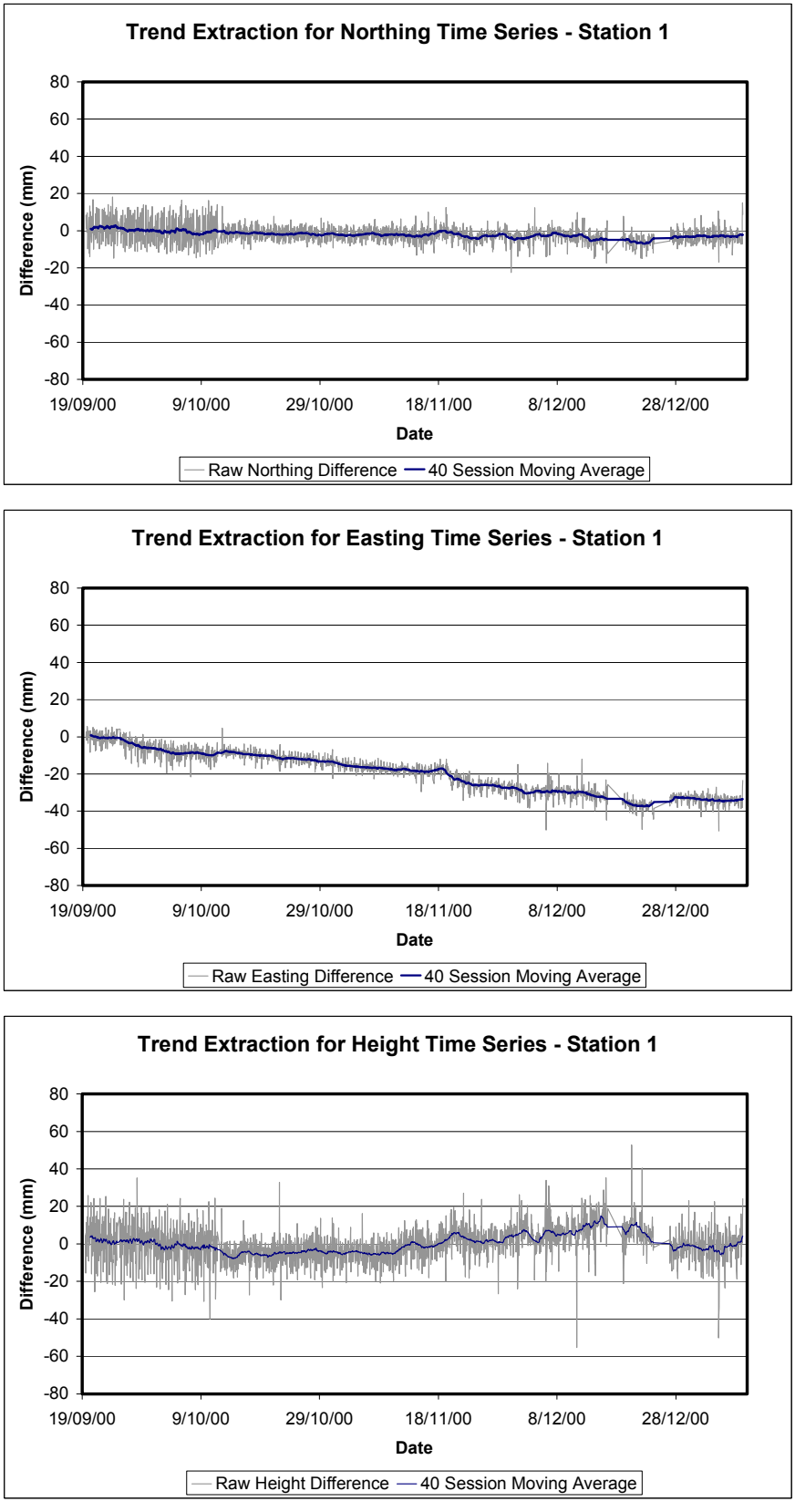

Figure 5.6 Northing, easting and height trends extracted via a 40 sidereal hour moving average window at Station 1

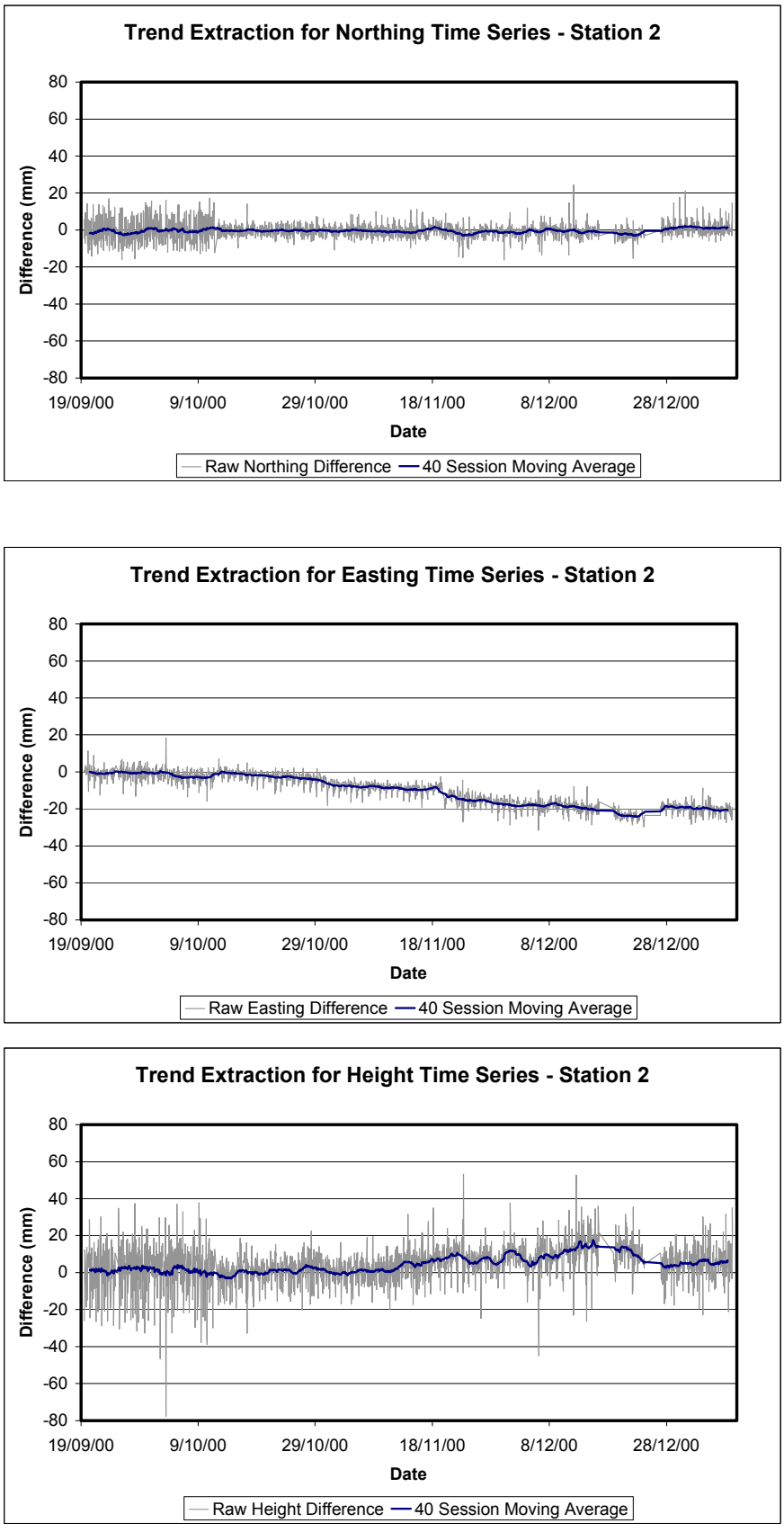

Figure 5.7 Northing, easting and height trends extracted via a 40 sidereal hour moving average window at Station 2

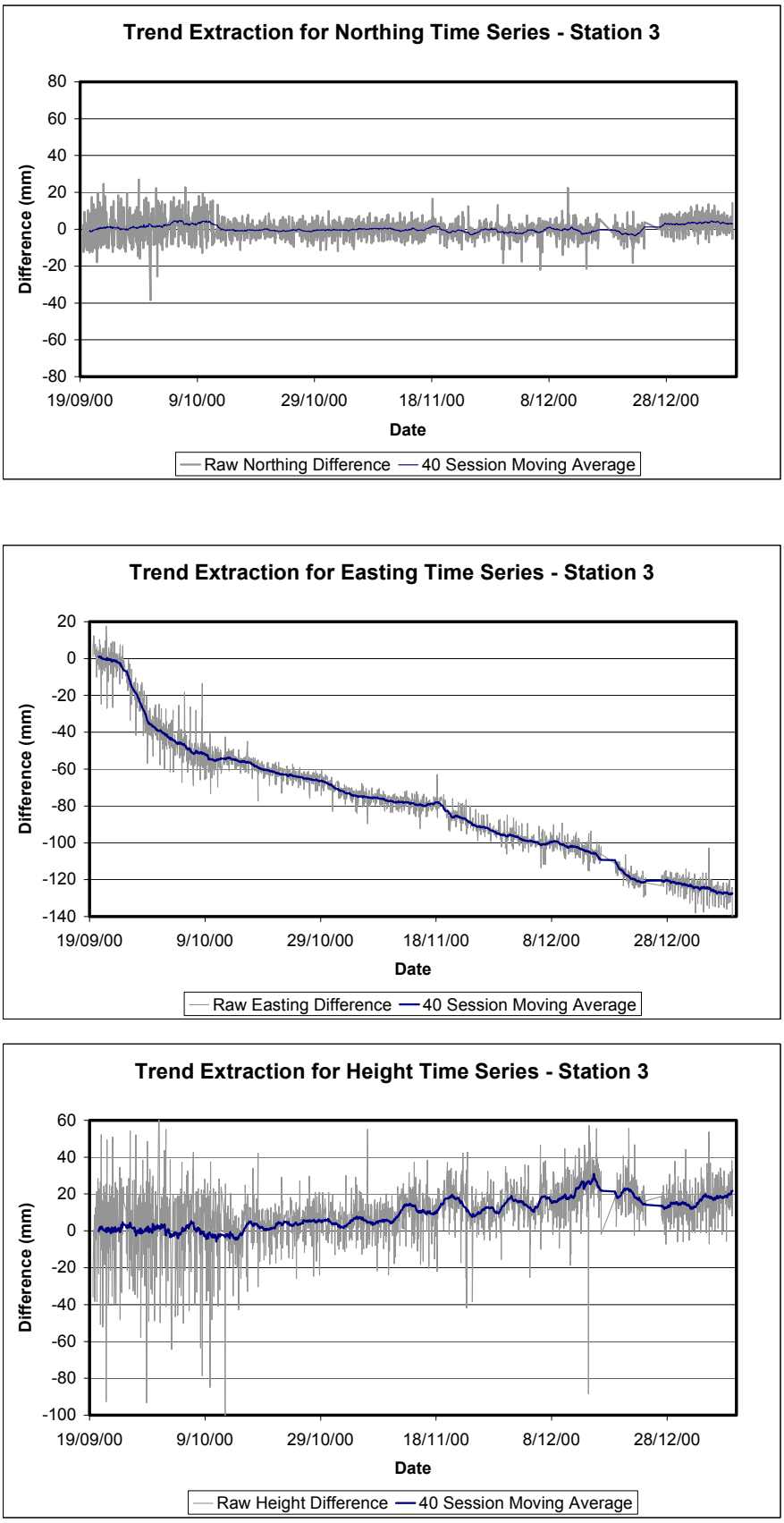

Figure 5.8 Northing, easting and height trends extracted via a 40 sidereal hour moving average window at Station 3

Visually extracting the trend from the raw difference data does not provide the user with viable information for deformation analysis. By using even a simple filter such as the MAW_2, it is possible to detect displacements relatively easily (although it may be difficult to separate deformation from system noise).

The magnitudes of the displacements detected at each of the four stations using the MAW_2 are summarised in Table 5.2.

Station	**Northing Displacement (mm)**	**Easting Displacement (mm)**	**Height Displacement (mm)**
0	6.2	29.7	20.7
1	9.7	38.2	22.8
2	5.4	24.6	20.8
3	8.4	129.2	36.8

Table 5.2 Maximum absolute displacements calculated at each deformation station using a two-tailed moving average window to extract wall displacement

Of interest is the deformation that is experienced at Station 3, situated approximately 45m below the surrounding surface level. The magnitude of the 3D displacement vector over the 16-week field trial was calculated as 134.6mm.

The increase in the height component experienced at Station 3 supports the relaxation response of the wall that may be expected when unloading of the wall mass results in such a rebound effect (Sarunic, 2000).

Small perturbations in the MAW_2 trend can also be seen in the height components for all stations presented. With the absence of external information (for example spirit levelling data), it is difficult to determine if this effect is caused by actual deformation, or system noise. While the overall trend in the height component over the length of the time-series appears to be real, the shorter period perturbations that are present require further testing in a controlled environment to determine if they represent real deformation or system noise.

5.3.2 Number of Reference Stations and Precision of the Coordinate Time-series

The number of reference stations used in the network was found to have a significant impact on the quality of the deformation solution attainable. On 12 October 2000 the second reference station (REF) was brought on-line. Between this date and 19 November 2000, the two reference stations were fully operational, after which, however, one of the reference stations became unusable (see section 4.3.5 on the operational stability of the multi-antenna monitoring system). On 27 December 2000 this fault was rectified, with the continuation of correct operation of both reference stations. Figure 5.9 shows both the raw northing solutions computed at Station 3 over this period, together with the number of base stations operating. It should be noted that each reference station is fully constrained within the network.

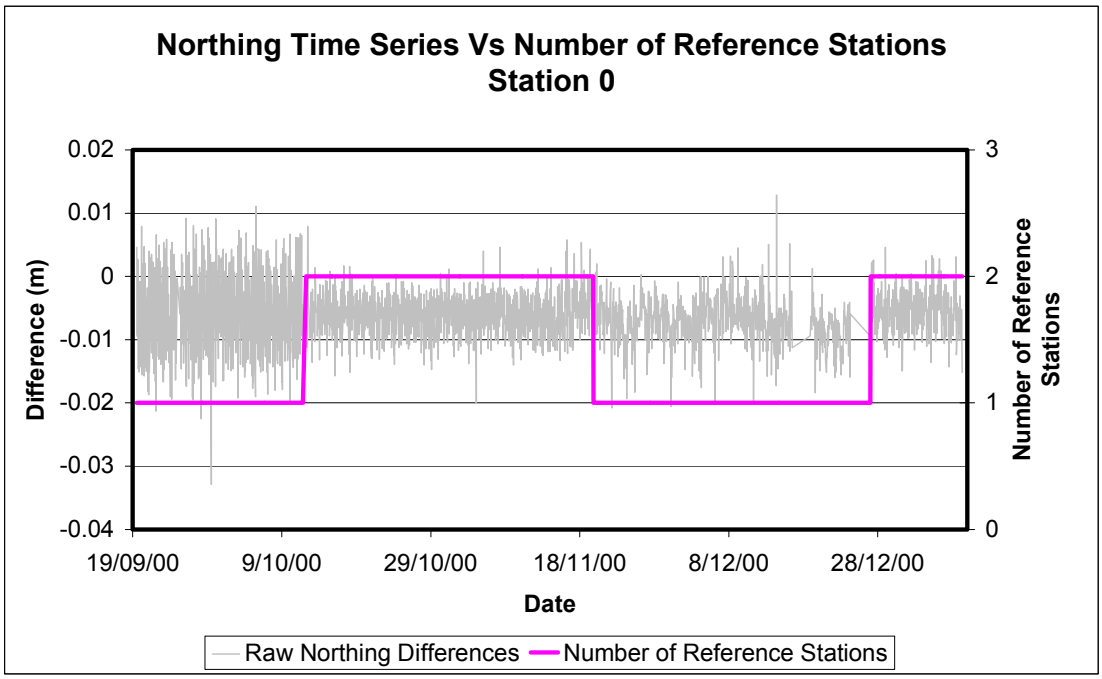

Figure 5.9 Coordinate precision with respect to number of reference stations used

It can be clearly seen that the number of reference stations in the deformation network has a substantial impact on coordinate quality. This may be illustrated statistically by considering the Root Mean Square (RMS) differences between the raw coordinate solutions and the trend extracted using the 40-session MAW_2 before and after the introduction of the second reference station.

Station	**No. Sessions**		**North RMS (mm)**		**East RMS (mm)**		**Height RMS (mm)**	
# Ref Stn	*1*	*2*	*1*	*2*	*1*	*2*	*1*	*2*
0	503	887	±6.8	±3.2	±4.1	±2.6	±15.6	±7.9
1	474	833	±6.7	±3.4	±3.3	±2.2	±11.4	±6.5
2	411	770	±6.8	±3.1	±3.3	±2.4	±14.3	±7.2
3	393	724	±8.1	±3.8	±7.5	±3.4	±22.8	±10.9

Table 5.3 Dependence of coordinate solution precision on the number of reference stations in monitoring network

Table 5.3 shows the statistical impact on the precision of the coordinate time-series when one and two reference stations are used in the deformation monitoring strategy between 19 September 2000 and 19 November 2000. An average improvement of approximately 47.3 percent in the horizontal and 47.7 percent in the height component is demonstrated for the surface stations (0, 1, and 2) when two reference stations are used. Similar improvements of 53.8 percent and 52.2 percent in the horizontal and height components are demonstrated at Station 3, the point located 45m below ground level, which experiences a degradation of satellite geometry by the surrounding pit-wall.

The number of reference stations is an important factor in reducing the noise level of GPS coordinate time-series for short-baseline deformation monitoring schemes. Other strategies to further improve the solution quality are discussed in chapter 6.

5.3.3 Quality Indicators

There are a number of quality indicators that may be used to assess the statistical quality of the data. The unscaled unit variance (a measure of the factor by which the *a priori* covariance matrix was on average incorrect in the least squares estimation process (Cross, 1994)), and the positional dilution of precision (PDOP) (Leick, 1995) are two examples of such quality indicators.

The average unit variances and PDOP values for the initial test results over the 16-week field trial are presented in Table 5.2 for each deformation station.

Station	Number of Samples	Average Unit Variance	Average PDOP per Session
0	2459	1.88	3.39
1	2313	1.87	4.52
2	2123	1.81	5.74
3	2109	2.04	7.17

Table 5.4 Internal Quality Indicators

It is common practice to use the unscaled *a posteriori* variance as a quality indicator. The results from Station 3 are typically poorer than those computed for the surface stations, which is to be expected considering the reduced geometrical strength and higher levels of signal multipath expected at this station. The poorer PDOP recorded at Station 3 also shows the effect of masking from the nearby pit wall.

In the case of quality indicators for the precision of the estimated coordinates, it is common to use the mean and standard deviation of the difference between the 'truth' and the parameters being tested. This technique is commonly based on the assumption that both the truth and the test parameters are stationary (in mean) over the sample domain. In the deforming environment, however, this is not the case, and these conventional quality indicators cannot be implemented to rigorously test the external quality of the results.

The RMS between the raw coordinates and the filtered data (using the MAW_2) at each measurement epoch is used here as a measure of variance (Koch, 1999) in order to evaluate the noise level of the data about the trend that can be extracted.

The overall RMS computed at each station using the benchmark processing strategy is presented in Table 5.5.

Station	North RMS (mm)	East RMS (mm)	Height RMS (mm)
0	±4.3	±3.0	±9.9
1	±4.4	±2.9	±8.4
2	±4.2	±2.7	±9.4
3	±5.0	±4.7	±13.7

Table 5.5 RMS precision estimates between the raw coordinate solutions and the trend extracted using a 40-session moving average window

The three stations situated at surface level show comparatively less error than the station below ground level. On average, the surface stations (Stations 0,1,2) maintain RMS levels of ±5.2mm in the horizontal component, and ±9.2mm in height, while the sub-surface station (Station 3) RMS is ±6.9mm and ±13.7mm in the horizontal and height components respectively. This equates to a loss of precision of approximately 32 percent in the horizontal, and 48 percent in height components when operating in an environment such as this experiencing restricted satellite geometry and possible increased signal multipath.

5.3.4 Coordinate Update

The use of the in-line integer rounding technique presented in chapter 3 relies completely on the quality of the *a priori* positional information. As the computed coordinate time-series drifts further from the initial approximate position, the probability of incorrectly rounding the integer ambiguities increases. As such, adjustments were made to the initial approximate positions of some of the data to ensure that the integer rounding technique performs adequately. Table 5.6 illustrates the update information that was applied manually to the GPS data in the easting component.

Station	GPS Time	Date	3D Magnitude of Adjustment (mm)
3	655370000	12/10/2000	56.2
3	660446850	10/12/2000	54.4
1	658244289	14/11/2000	38.3

Table 5.6 Manual Coordinate Updates applied to processing strategy

The larger deforming movements experienced at Station 3 required that the coordinates be updated twice from their initial approximate values. These adjustments totalled 100.6mm. Station 1 (also within the zone of maximum deformation) also experienced displacements requiring that the initial approximate coordinate be updated.

The manual adjustments were applied to the initial approximate position information based on the selection of appropriate coordinates prior to the solution quality degrading. This degradation in solution quality can be easily detected visually in the post-processing operation. Figure 5.10 illustrates this degradation in the solution quality in the height component at Station 3 both before and after the adjustment that was performed on the data after 10 December 2000.

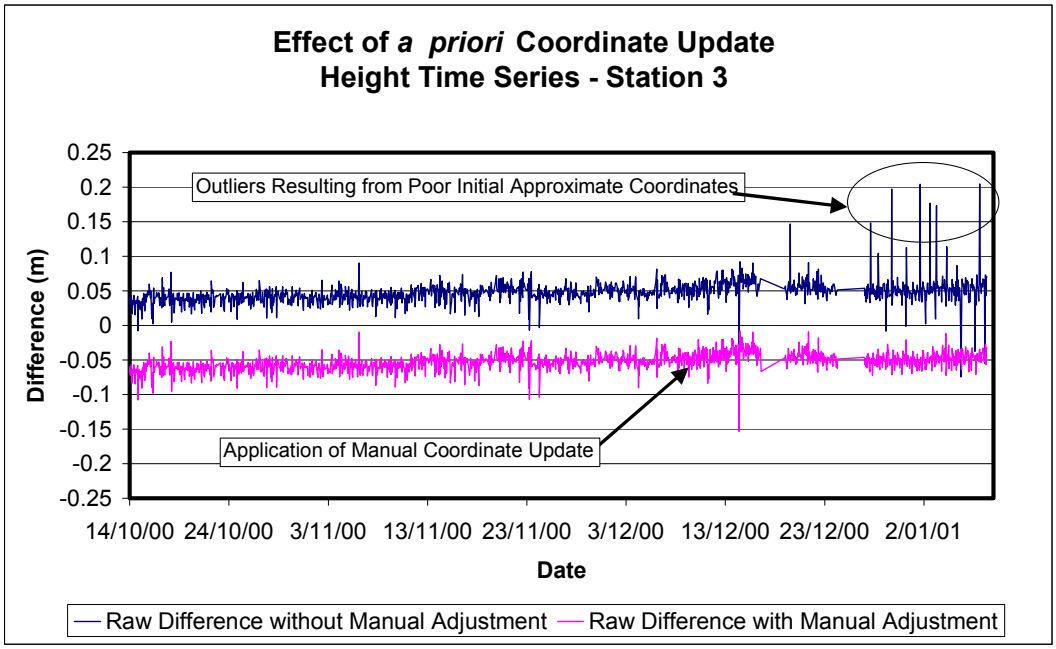

Figure 5.10 Effect of manual coordinate update on height time-series – Station 3

Figure 5.10 indicates the quality of the height component time-series for Station 3 with and without updating the *a priori* coordinates on 10 December 2000. The two time-series are offset by 0.1m for clarity.

The quality of the time-series degrades quite considerably when the coordinate update is not applied. This is evident from the higher number of data spikes present (represented by spikes in the time-series). These spikes result from the *a priori* coordinate estimates being too far away from the estimated position to adequately resolve (round) the integer ambiguities (the ambiguities for some observations are rounded to the wrong integer). Similar effects are also evident in the northing and easting components.

The system of manually updating the coordinates is not suitable for an autonomous, real-time system. As such, a more appropriate automatic strategy is introduced in section 6.2.

5.3.5 Spectral Analysis of Time-series Data

The spectral properties of the data can be analysed to evaluate periodicity within the coordinate solutions using the Discrete Fourier Transform (DFT) (for example Brigham, 1974).

Figure 5.11 illustrates the spectral response of the coordinate time-series for Station 0, for the northing, easting and height components.

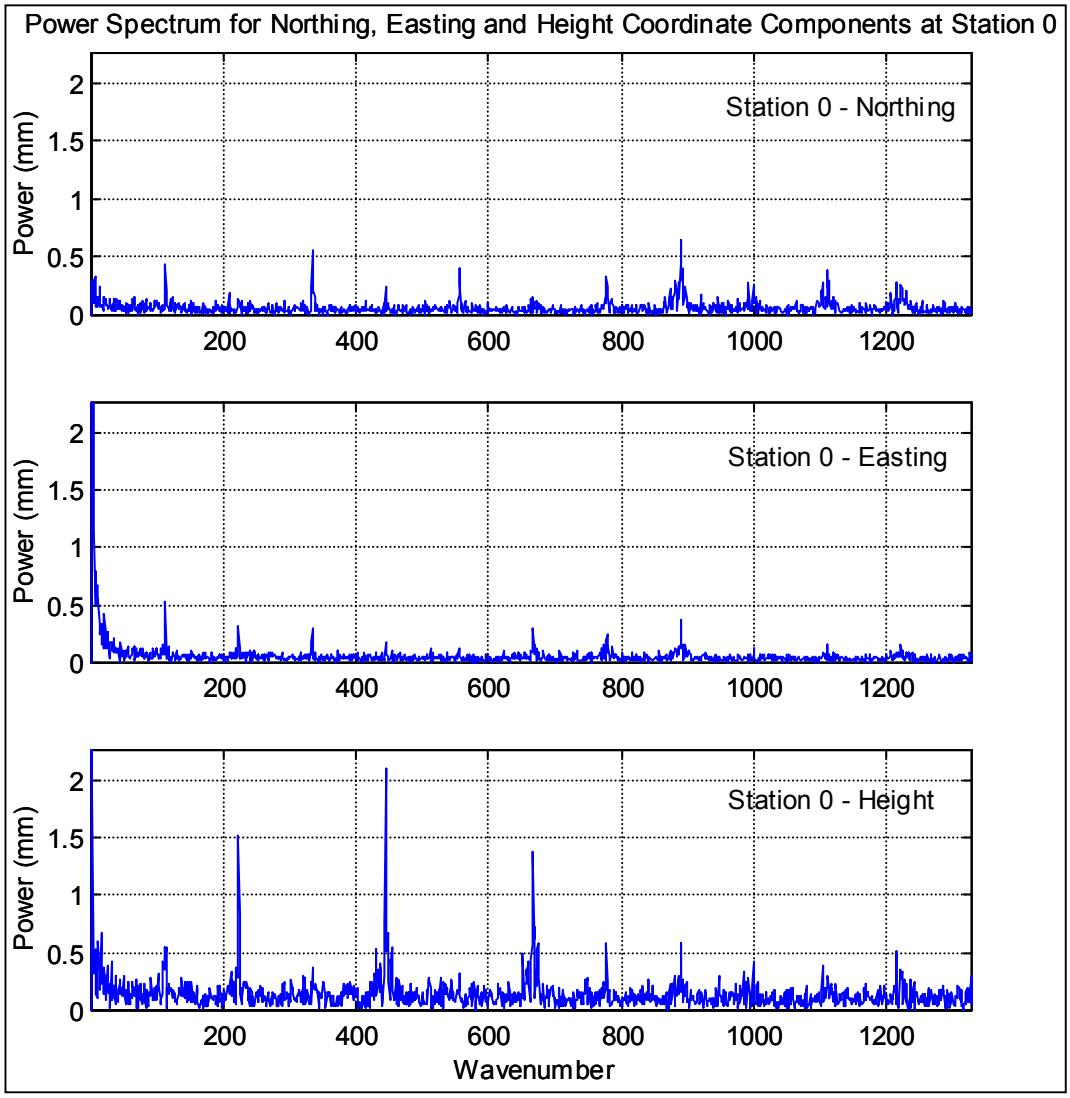

Figure 5.11 Spectral response of coordinate time-series – Station 0

Figure 5.11 represents the spectral response of the coordinate time-series for Station 0 over the 16-week field test. The frequency of the power spectrum presented in Figure 5.11 may be calculated by dividing the wavenumber by the length of the time-

series. Similarly, to obtain the period, the length of the time-series is divided by the associated wavenumber. As the ground track of each GPS satellite repeats every sidereal day, it would be expected that power would be visible in the spectrum at this frequency. In the time-series presented in Figure 5.11, this frequency equates to a respective wavenumber of 112. Indeed, power is visible in this portion of the spectrum, especially in the northing and easting components. What is unexpected, however, is the high level of power that appears to exist at regular intervals throughout the spectrum. These can be seen in the height component, for example at wavenumbers of 224, 336 and 448. These wavenumbers equate to power that repeats at periods of approximately 12 hours, 8 hours and 6 hours respectively. Clearly, in satellite positioning applications, and particularly the slope deformation monitoring situation presented within this research, there does not appear to be any physical interpretation of this repeating power signature. If this effect does not represent a physical process then it is likely to be a result of an artefact within the data. This phenomenon is discussed in more detail below.

Figure 5.12 below illustrates a spectral plot of the coordinate time-series at Station 3.

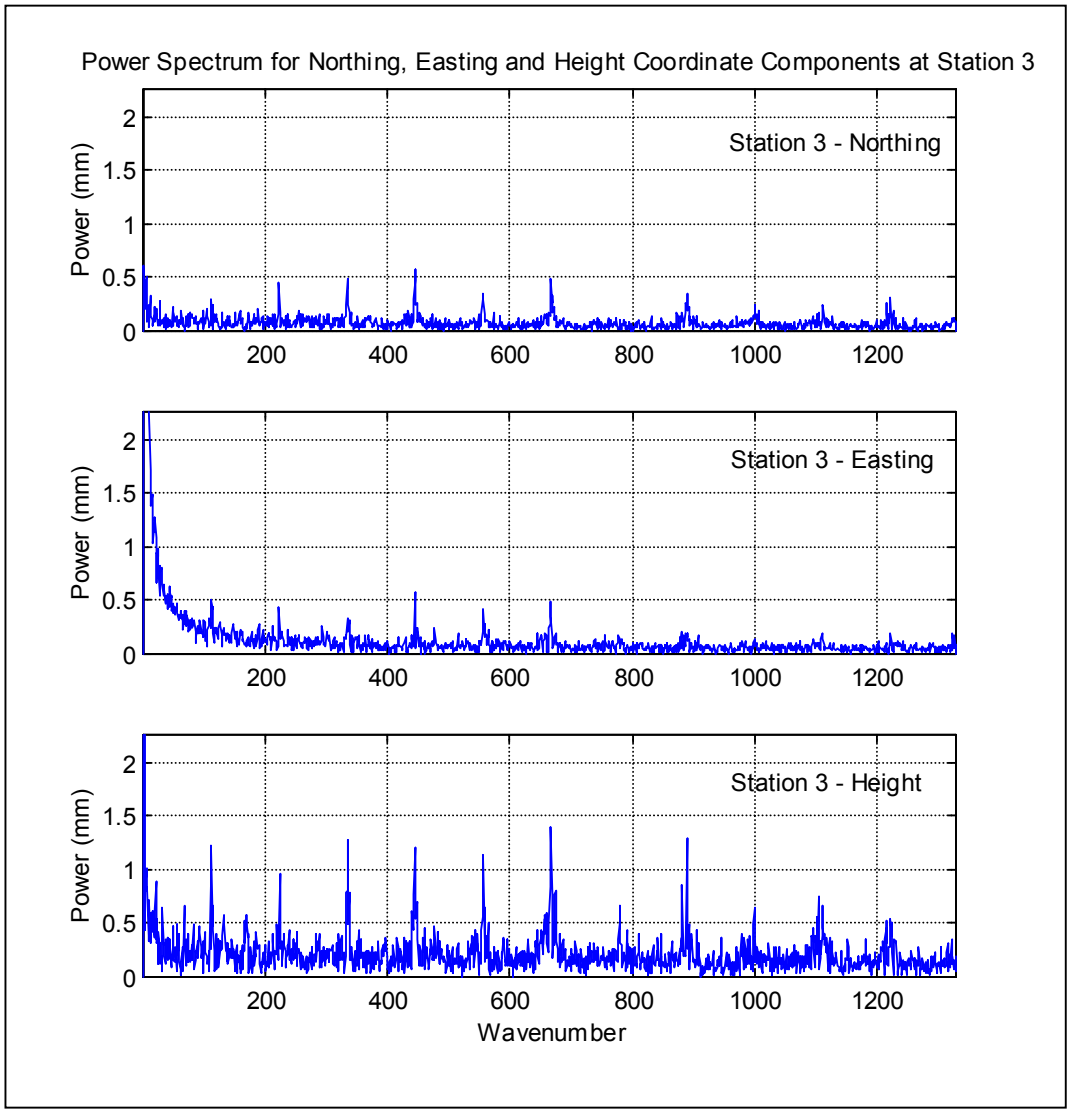

Figure 5.12 Spectral response of coordinate time-series – Station 3

Similar power characteristics to Station 0 can be seen at Station 3. Also of interest here is the signature of the deformation in the easting component that manifests itself as power in the lower frequencies (lower wavenumbers). Also of note is the spread of power in all three coordinate components that can be seen across the spectrum. This relatively flat power represents the presence of white noise in the time-series.

One possible explanation for the power that is repeating across the spectrum in Figure 5.11 and Figure 5.12, is that this feature is a result of the sampling interval of the GPS coordinate time-series that induces a sawtooth effect. This sawtooth pattern may be caused by the changes in satellite geometry by satellites rising and setting that can occur between the times that a station is sampled (in this case each hour).

To illustrate a simple sawtooth effect, data have been simulated to represent a linear repeating function represented by the following equation:

$$x(t)=2/24 \times t - 1 \qquad (5.3)$$

where:

$x(t)$ is the value of the discrete time-series at time t.

This function was then sampled for values of t ranging from 1 to 24 and replicated 10 times. The resulting discrete time-series is illustrated in the time and frequency domains in Figure 5.13.

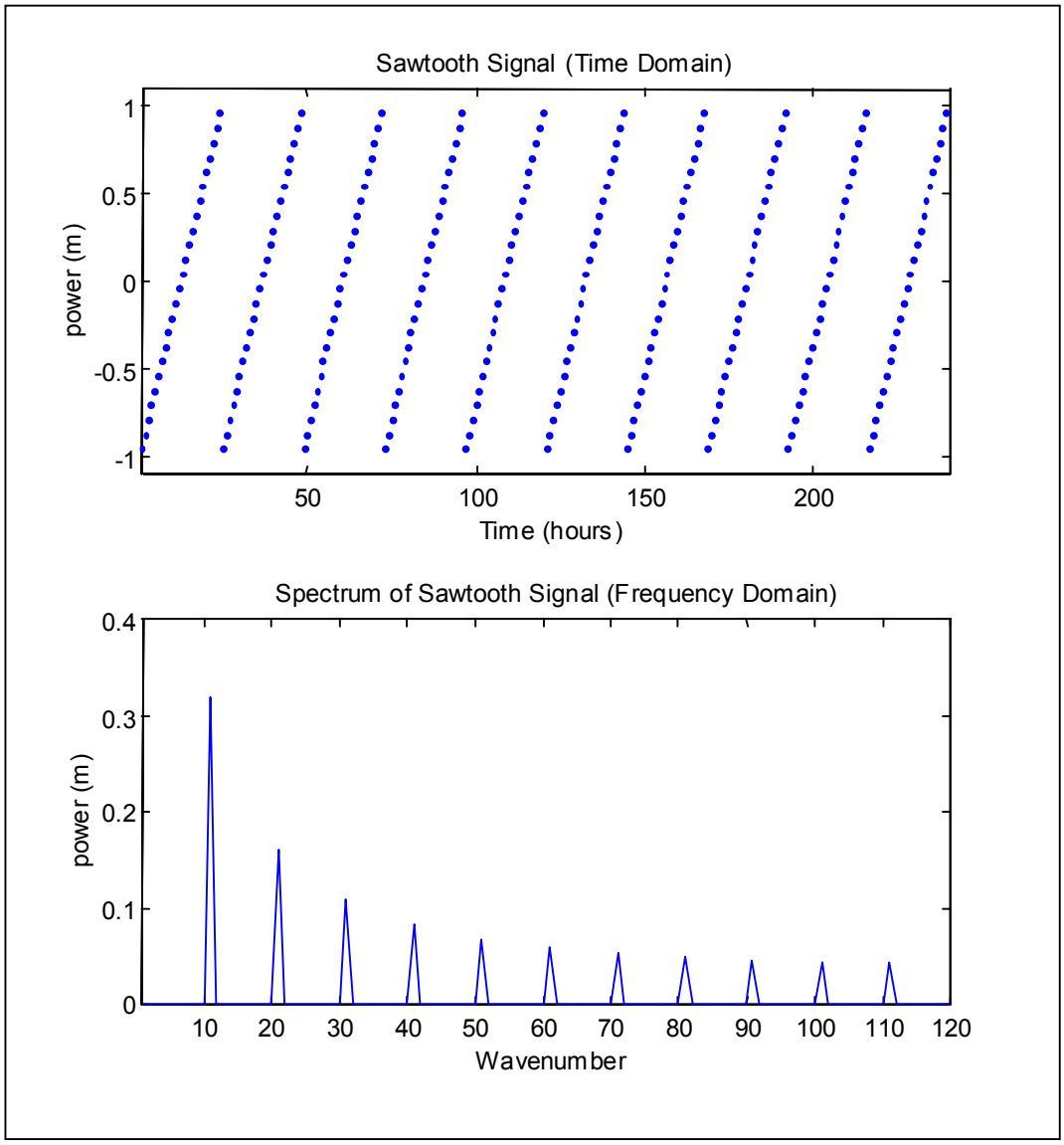

Figure 5.13 Simulated sawtooth function and associated power spectrum

Figure 5.13 illustrates the simulated sawtooth function in both the time domain (top of figure) and the frequency domain (bottom of figure). It can be seen that while the magnitude of the power spectrum differs from the coordinate time-series presented above, similar repetitions occur at regular intervals.

The simple sawtooth pattern illustrated above shows a deficiency in using a DFT when the data are discontinuous (in terms of the underlying function). This problem may be developed further by considering coordinate time-series data in place of the simulated sawtooth function. Twenty-four hours of coordinate data from Station 0 have been replicated ten times to create a new coordinate time-series. The resulting time-series and associated power spectrum are plotted in Figure 5.14.

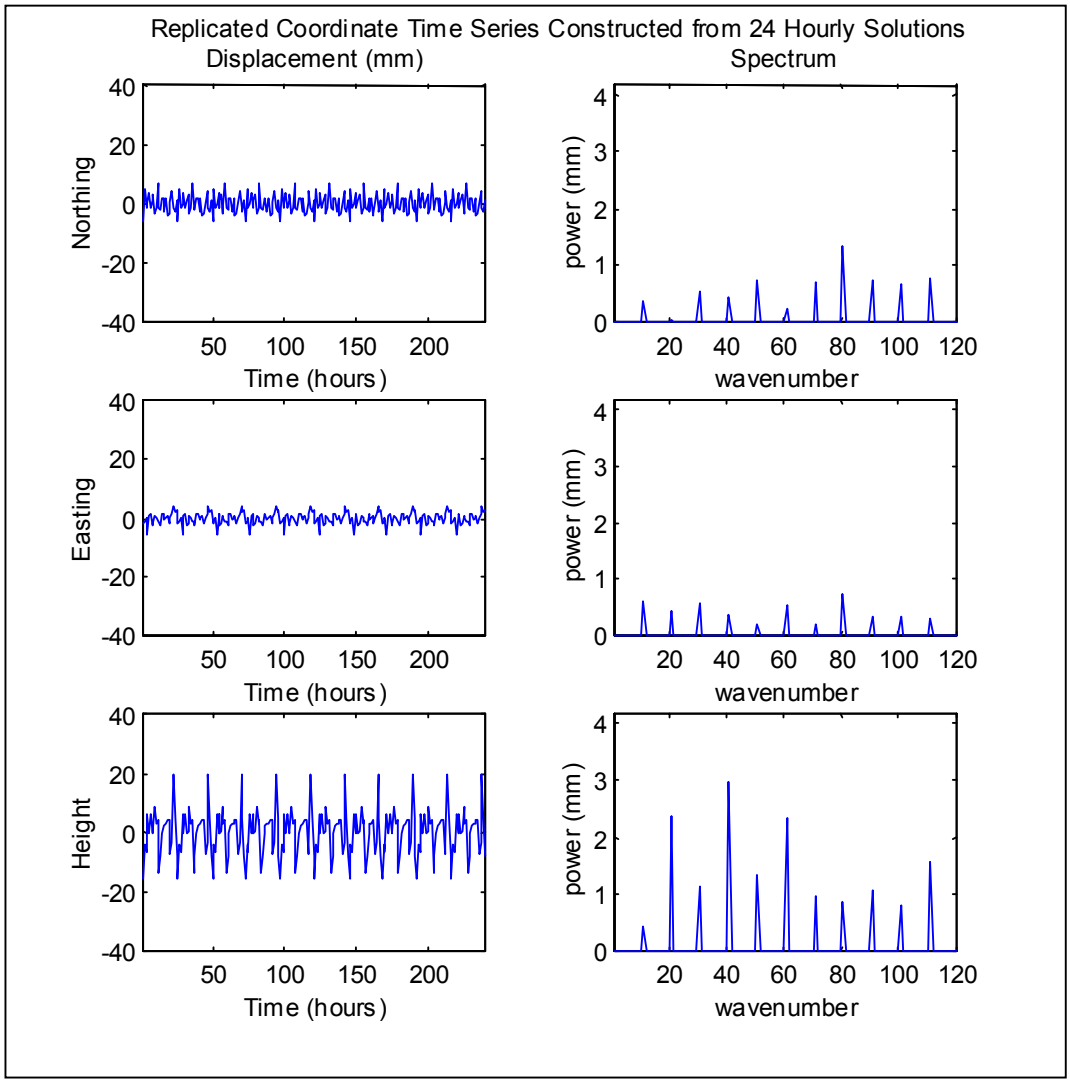

Figure 5.14 Replicated coordinate time-series using 24 hours of data at Station 0

It can be seen from Figure 5.14 that the spectrum of the coordinate time-series more closely follows the spectrum presented for the complete time-series (see Figure 5.11 and Figure 5.12). It is proposed that these power signatures occur as a result of the frequency at which the GPS solutions are observed (in this case every sidereal hour). The repeating satellite geometry is expected to bias the coordinate solution each sidereal day. If the repetition of this effect is not perfect, it will induce a small sawtooth effect into the coordinate time-series. The resulting power spectrum will, therefore, be comprised of the repetitive power signatures that have been presented above. This effect may also be magnified in the presence of movement of the station, and hence the coordinates.

Overall, this effect may simply be a data artefact from the system design, whereby the multi-antenna monitoring method adopted creates a segmented or discontinuous time-series of coordinate solutions. This, however, may have serious implications for the use of spectral analysis techniques for this type of GPS data.

5.3.6 Performance Comparison between GPS Positioning and Automatic Total Station Data

As part of the existing deformation monitoring scheme at the WMC MKO, an Automatic Total Station (ATS) system has been installed to monitor the progress of the deforming pit wall movements. The system is based on Geodimeter DR200+ series automated total stations. These instruments are servo-driven which reduces the need for an operator to be present during the observation regime. The ATS data are then transmitted over spread-spectrum radio links to the geotechnical monitoring office. Monitoring of each prism is conducted once per day.

At the time of this research, thirteen prisms were established over the eastern pit wall. Of these points, one prism, E11, was located near to Station 3 (see Figure 4.18).

Figure 5.15 illustrates the calculated coordinate differences observed at Station 3 using the multi-antenna GPS array design and the results from monitoring using total station survey procedures. It should be noted that Station 3 and point E11 are not coincident. It is instructive, however, to plot the results of both systems together to illustrate the respective noise levels of each.

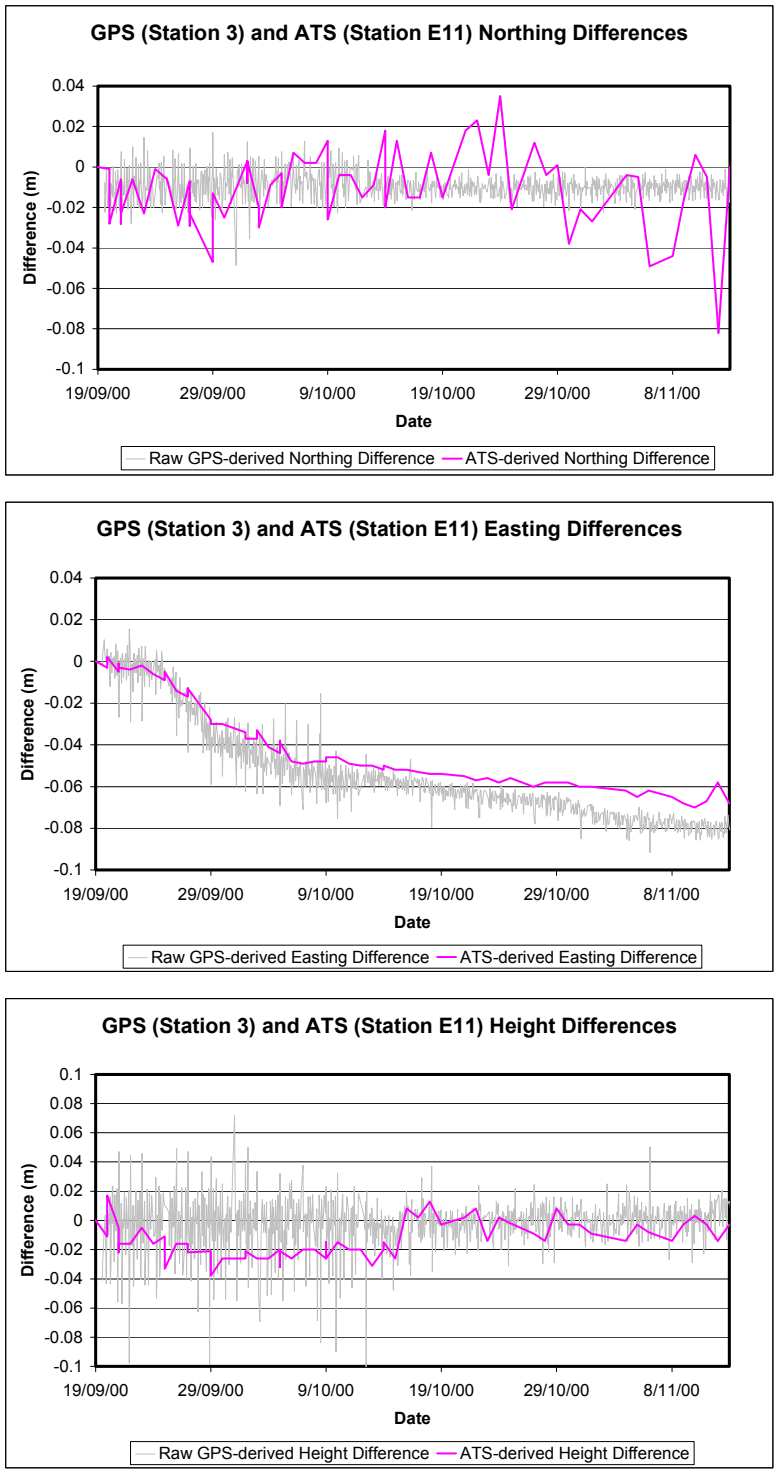

Figure 5.15 Raw GPS deformation results versus automatic total station data for Station 3

From Figure 5.15 it is evident that similar trends exist between the GPS-derived deformation and the ATS results. As the actual points are not coincident, it is difficult to speculate as to the relative accuracy of the two types of deformation monitoring systems. There is, however, an obvious disparity present in the level of

precision attainable in the northing component between the two monitoring systems. It can be clearly seen that the precision of the ATS coordinates in the northing component are worse than similar results from the multi-antenna GPS monitoring system developed for this research. The poorer precision is related to a deficiency in the targeting capabilities of the servo-driven ATS equipment. In this specific case, the ATS instrument was established on the western side of the WMC MKO pit. As such, any deficiency in the targeting capability of the ATS system would predominantly be mapped into the northing component for horizontal targeting, and the height component for vertical targeting.

The easting component of the ATS time-series is much more precise than the northing component. This is highly correlated with the placement of the ATS instrument. As the changes on the surface of the pit wall are predominantly along the line of sight of the ATS instrument, a high level of precision is attained due to the internal consistency of the EDM measured distances. Effectively, much of the measurement in the easting component may be mapped into the slope length observed by the EDM (rather than the azimuth/height domain observed by the theodolite components). As the ATS is much more precise in measuring ranges than angles, measurements that map into the range domain will be more precise than those that map into the angle domain.

The height component is primarily affected by vertical refraction errors. These exist in all types of total station measurements. This effect may be magnified when observing over an open-pit mine, where complex atmospheric conditions exist in and around the open-pit mine (due to complex thermal inversion layers and trapped atmospheric moisture). The poorer precision of the ATS height solutions can be seen in Figure 5.15.

5.3.7 Multipath Effects

The effect of signal multipath should also be considered in the analysis of GPS results, considering the specific environment under which positioning is undertaken.

Figure 5.16 illustrates the double difference residuals for satellite pair 20-11 for GPS week 1084, session number 108. The cyclic trends that can be seen commonly indicate the presence of multipath delay error remaining within the data.

Epochs ranging from 1 through to approximately 900 represent the double difference residuals computed at the surface, Station 2. Epochs from approximately 900 to 1800 represent similar residuals for Station 3, near to the pit wall, observed immediately after those at Station 2.

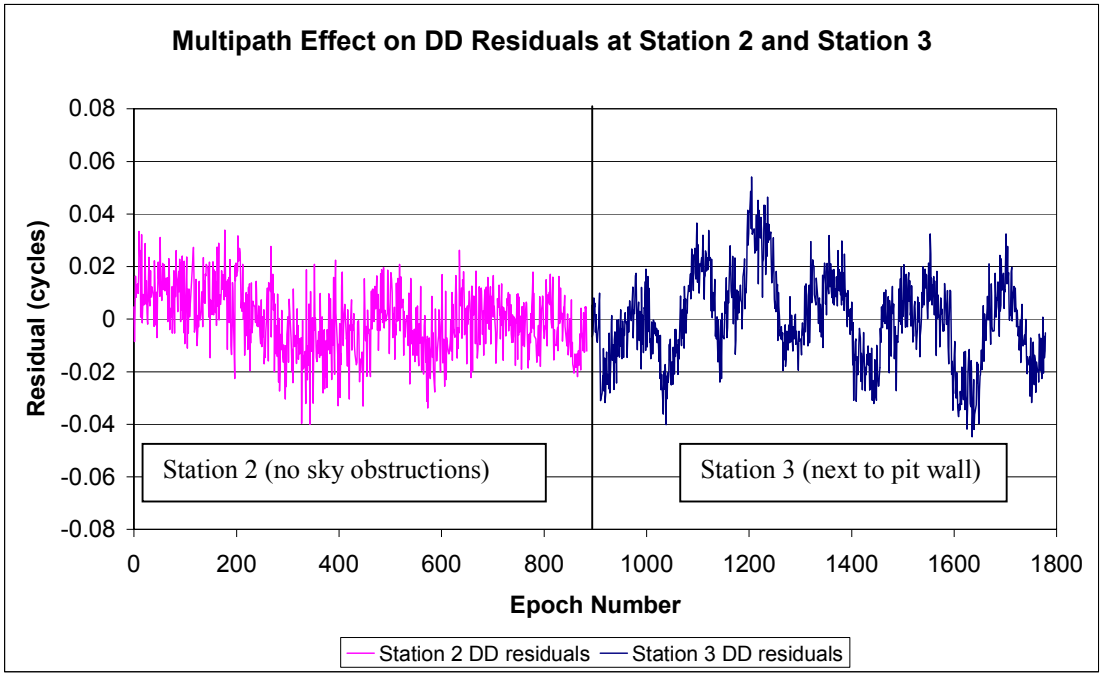

Figure 5.16 Effect of signal multipath on double difference residuals

The effect of multipath can be clearly seen in Figure 5.16 from the residuals obtained from Station 2 at the site surface and from Station 3 below ground level and next to the mine wall. The close proximity of the pit wall to Station 3 induces the cyclic-type trends that are evident. These effects signify the presence of unmodelled systematic error, typically multipath in this case. The average elevation angle for the reference satellite (satellite 11) was 75.4°, while the average elevation angle for satellite 20 was 34.9° for the two sessions. The RMS of the double difference residuals at Station 2 is ±0.013 cycles (±2.3mm), while the RMS for Station 3 is ±0.017 cycles (±3.2mm) indicating an increase of approximately 36 percent in the

noise level of the double difference residuals in this case. There may also be a small amount of multipath present in the double difference residuals from Station 2 due to the site conditions at the reference station.

The daily repeatability of the multipath effects further highlights the geometry dependent attributes of the multipath signatures. This phenomenon is illustrated in Figure 5.17.

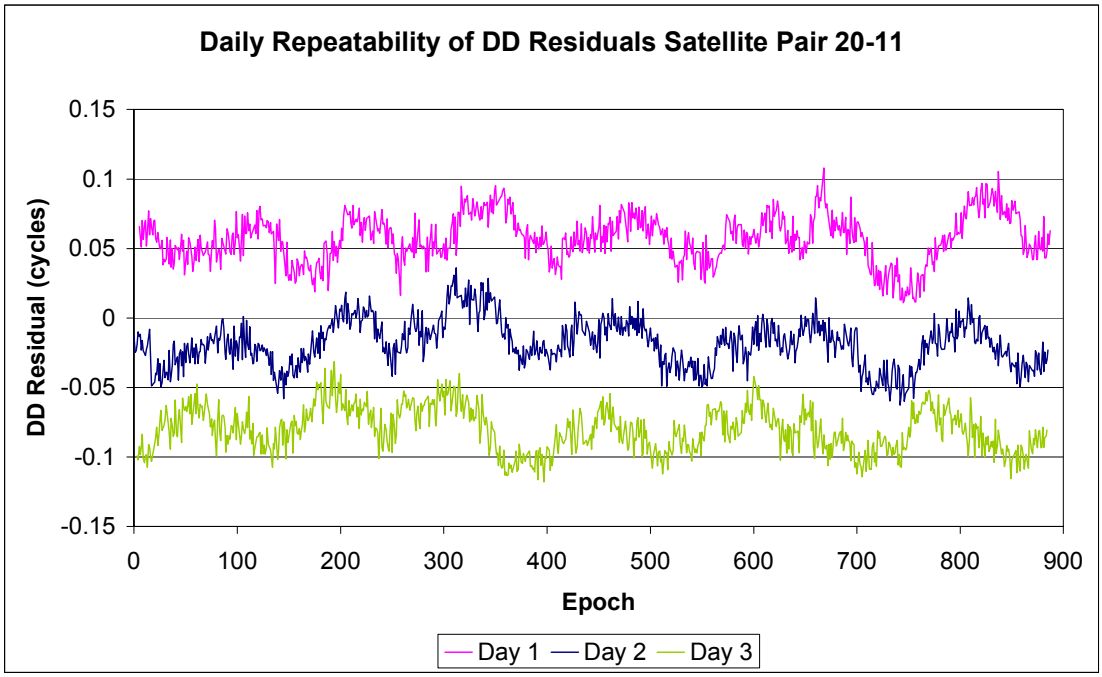

Figure 5.17 Daily repeatability for satellite pair 20-11, GPS week 1084, Station 3

Figure 5.17 illustrates the daily repeatability for satellite pair 20-11 at Station 3 over three days in GPS week 1084. Each successive day has been offset vertically for clarity. The multipath trends appear to repeat every day.

Data stacking techniques have been proposed in the literature to remove the effect of repeating signal multipath from GPS observations. An investigation into the assumptions surrounding the use of these techniques for deformation monitoring of steep slopes is presented in chapter 7.

5.3.8 Carrier-to-Noise Ratio Characteristics

The use of the Signal to Noise Ratio (SNR), and the Carrier-to-Noise Ratio (C/N0) has received much attention in the literature (Ward, 1996; Hartinger and Brunner, 1999; Brunner *et al*., 1999). It is suggested that the C/N0 ratio can be of use in determining the influence of signal distortion (for example diffraction and multipath) on the quality of the raw phase data observed. Unfortunately, research in this area is constrained by the lack of C/N0 values available to the user in most commercial GPS software. Furthermore, at the time of writing, the RINEX (receiver independent exchange) format definition does not incorporate provision for the C/N0 values. Instead, the SNR or C/N0 values must be scaled to an integer ranging between 0 and 9. It is only when the raw binary data are available, as is the case with the specialised software developed as part of this research, that the C/N0 parameters can be used directly.

Figure 5.18 illustrates a wire-mesh surface fitted to the C/N0 values observed throughout GPS week 1084 at one of the surface stations (Station 1). The C/N0 ratios observed at Station 1 are plotted in Figure 5.18 with respect to azimuth and elevation angle.

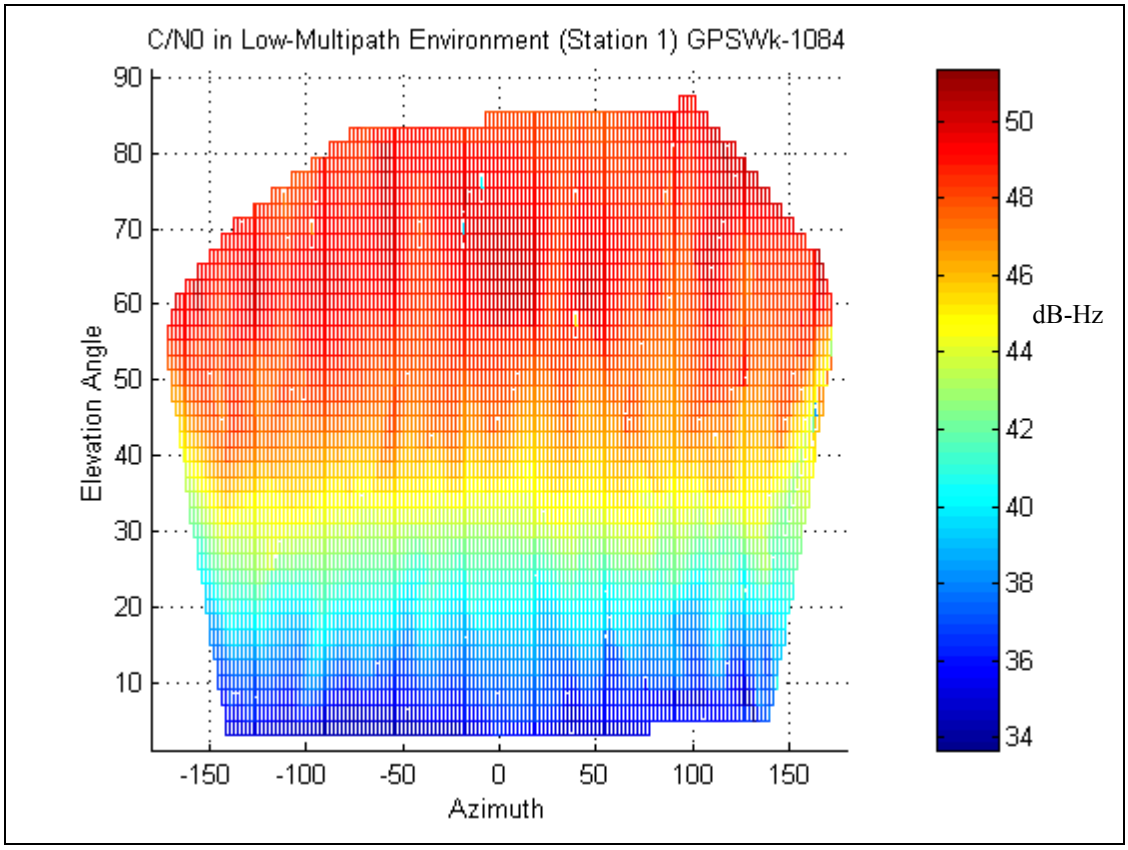

Figure 5.18 Carrier-to-Noise ratio observed at Station 1, GPS week 1084

The C/N0 ratios observed at Station 1 are plotted in Figure 5.18 with respect to azimuth and elevation angle. The horizontal banding effect seen in Figure 5.18 illustrates the presence of azimuthal symmetry that occurs when there are no sky obstructions. In this case the C/N0 values vary smoothly with respect to elevation angle. The gridding effects, and what appears to be missing data, are simply a function of the display quality of these images.

A skyplot for GPS week 1084 is illustrated in Figure 5.19, which shows the distribution of satellites at Station 1. Each point indicates the average location of a satellite for each session throughout GPS week 1084.

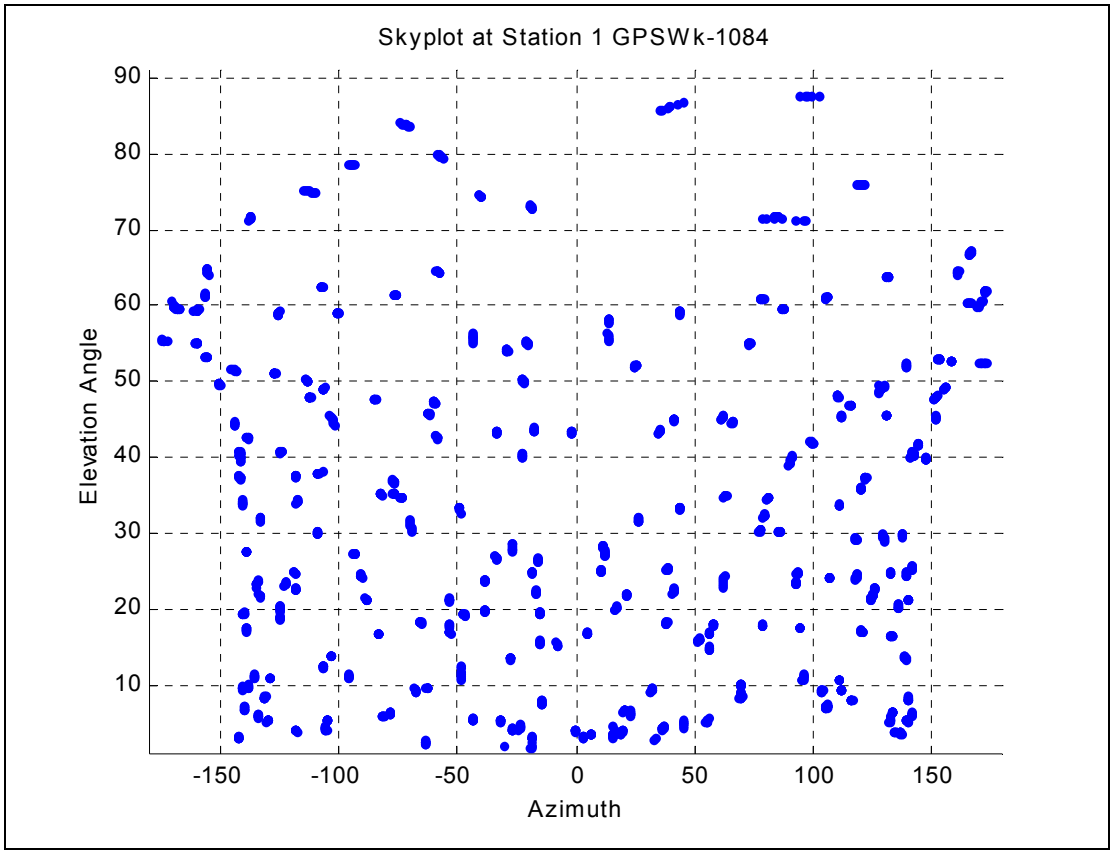

Figure 5.19 Skyplot at Station 1 illustrating average elevation and azimuth of satellites visible for each session during GPS week 1084

Figure 5.20 below shows a C/N0 plot for Station 3 next to the pit wall. The pit wall bounds the station almost completely to the East. The effect of the wall masking on the observed C/N0 values can be clearly seen in the eastern hemisphere.

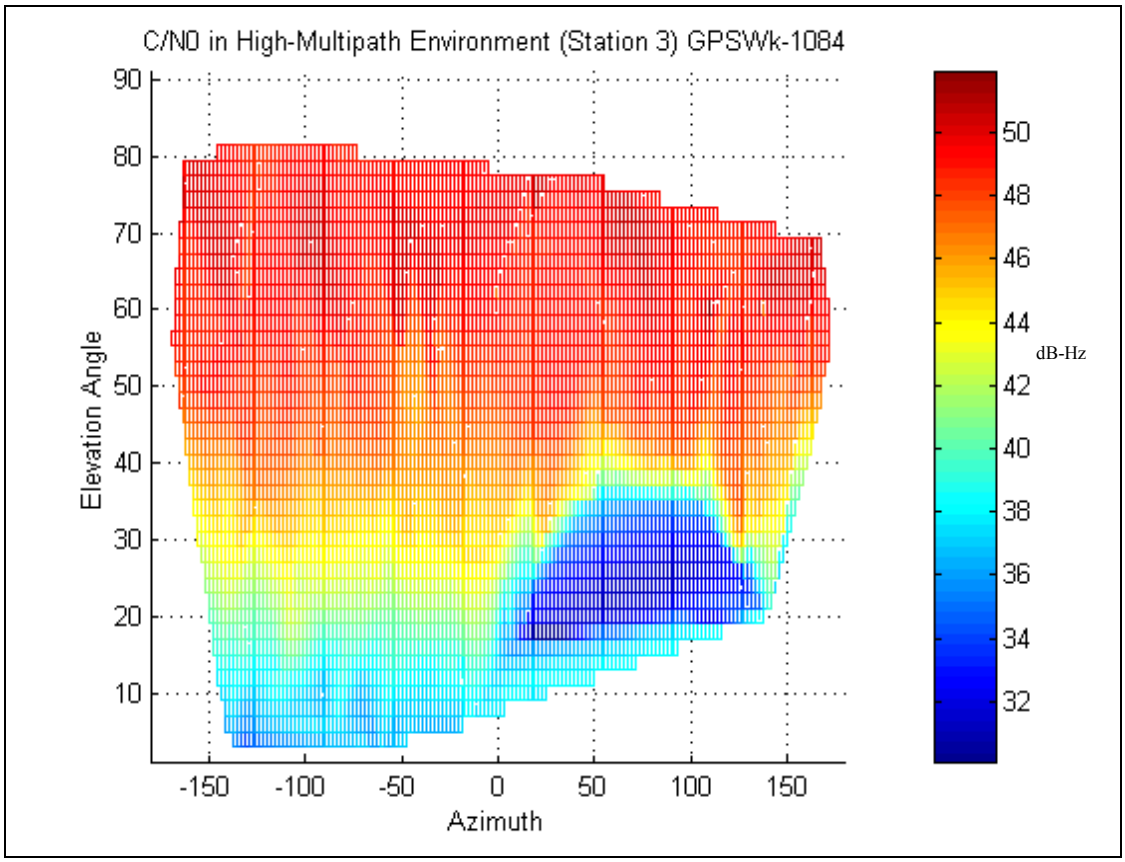

Figure 5.20 Carrier-to-Noise ratio observed at Station 3, GPS week 1084

The edge effects of the data near to the pit wall are of interest in Figure 5.20, indicating the effect of signal diffraction and multipath on the observed C/N0 values. With obstructed sky visibility, azimuthal symmetry can no longer be assumed in carrier-phase quality analysis.

The skyplot for GPS week 1084 at Station 3 is illustrated in Figure 5.21. The obscured sky visibility by the eastern pit wall can be clearly seen from 0° to approximately 150° in azimuth and from 0° to 40° in elevation angle.

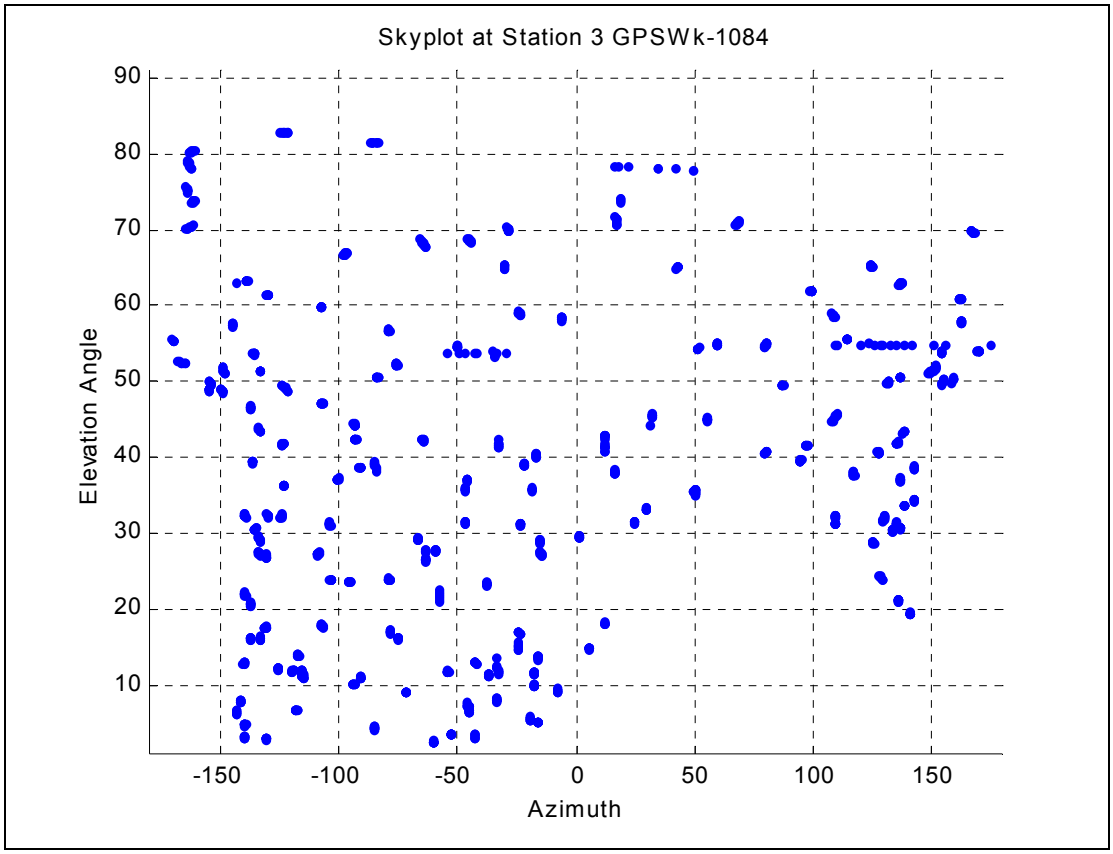

Figure 5.21 Skyplot at Station 3 illustrating average elevation and azimuth of satellites visible for each session during GPS week 1084

The results presented for Station 3 illustrate the effect of the nearby pit wall on the C/N0 and resulting sky visibility. These results support the suggestion that stochastic modelling techniques that assume azimuthal symmetry (such as the Sine and Han models) may not provide an optimal solution for weighting GPS observations under the multipath conditions experienced at Station 3 (see section 7.2.1).

5.4 Summary

The initial test results using the benchmark processing parameters presented in section 5.1 have been presented for approximately 16 weeks of near-continuous data collection at the WMC MKO open-pit mine in central Western Australia. The displacements measured ranged from between 32.6mm at Station 2 to 134.6mm at Station 3 over this period. This implies that between 2.0mm and approximately 8.5mm of motion per week were detected with GPS using the switched antenna array design.

Horizontal solution precision ranged from between ±4.0mm for surface stations to approximately ±6.7mm for the station experiencing significant satellite masking and severe multipath effects. These precision estimates were calculated with respect to a simple two-tailed moving average window data filter. Similar values for the precision of ellipsoidal height solutions range between ±8.4mm to ±13.7mm respectively.

Both the horizontal and height precision of the calculated deformation station locations are highly dependent on the number of reference stations used in the positioning campaign. An increase in horizontal precision of up to 48 percent was calculated for surface stations, with an associated increase of height precision of up to 50 percent when two reference stations were used in preference to one. Similar increases in horizontal and height precision of 54 percent and 52 percent respectively were computed for the sub-surface station (Station 3). Continuity of the multi-antenna GPS deformation monitoring system has also been shown to rely substantially on the number of reference stations used in the monitoring network.

The spectral signatures of the coordinate time-series have been presented to assist in characterising geometry-dependent effects of the GPS observations, where large spectral power values can be illustrated at a period of approximately 24 sidereal hours. Disparities have been illustrated between the expected and observed spectral response in the coordinate time-series. The problems experienced are possibly a result of the sampling process (and specifically the sampling interval) for monitoring points that experience deformation.

Automatic total station data have also been presented for a station near to Station 3. These results indicated that similar deformations may be extracted from both data sets. The respective qualities of the two monitoring methods differ however, with the pointing accuracy of the ATS system significantly reducing the quality of the 3D ATS-derived deformation positions.

Carrier-to-noise modelling based on data collected at two of the deformation stations has also been presented, indicating that the assumption of azimuthal symmetry for modelling the stochastic properties of GPS data in a multipath environment may not be valid.

Having established a benchmark processing strategy, it is now necessary to optimise the precision of the coordinate time-series. This is the subject of the following chapters.

6. OPTIMISATION OF PROCESSING PARAMETERS FOR GPS DEFORMATION MONITORING

This chapter investigates the effect of changing the benchmark processing parameters introduced in chapter 5 to optimise the deformation monitoring strategy. In some instances trade-offs will occur between the amount and type of data recorded and the precision level of the resulting coordinate time-series. The choice of processing parameters is of particular interest to the surveyor wishing to develop a monitoring system under similar conditions to those tested in this research. Reducing the data processing interval, for example, simulates the effect of reducing the data capture rate in the field. While this may seem a trivial issue, the associated communications requirement may be completely different if 10 second data are to be transmitted rather than 1 second data through the communications network.

This chapter includes the introduction of an automatic coordinate update process and a double difference outlier detection routine. Changes to the GPS data collection and processing options mentioned previously, such as the elevation masking angle, processing interval and session length are also evaluated to optimise the precision of the resulting coordinate time-series.

Before any improvements to the GPS solutions can be rigorously evaluated however, a reliable and repeatable method of detrending the time-series data must be established and validated. The normal practice of calculating dispersion estimates of a data set relies on the fact that the data are stationary in mean (Koch, 1999). The coordinate time-series presented in chapter 5 do not possess this quality and must be detrended before dispersion estimates can be calculated effectively. Unfortunately, the selection of an appropriate detrending process is a non-trivial task. If a detrending process is chosen that does not perform adequately, residual trends remaining within the coordinate time-series may bias any dispersion estimates that are calculated. In this case, it is then difficult to accurately determine if

improvements in the precision of the time-series are real, or only an apparent side-effect of a poor detrending process.

Various trend extraction techniques are investigated to determine an appropriate method that provides realistic precision estimates under the conditions examined within this research. The RMS of the differences between the raw coordinate solutions and the extracted trend is then used as an estimator to evaluate the precision of the time-series. In each case, data from the 168 sessions of GPS week 1084 are used to provide consistent data characteristics for each method that is evaluated. GPS week 1984 was chosen as the first week with complete data availability from all three GPS receivers. To further maintain data consistency, Station 0 and Station 3 are tested to represent surface station data and sub-surface station data respectively.

6.1 Simulation Tests to Estimate the Noise Level of Coordinate Time-series

To evaluate the effect of changing different processing parameters, it is necessary to establish and validate a technique that allows the dispersion of the data about the trend to be realistically estimated. The establishment of an appropriate detrending technique is primarily concerned with validating the resulting dispersion estimates rather than with the quality of the trend that is extracted (although this is evaluated also).

Simulation tests are presented to demonstrate the effectiveness of the MAW_2 technique presented in section 5.3.1 under the condition of nonstationarity of the mean of the time-series data and where the deforming displacements cannot necessarily be represented completely by predefined mathematical functions. The simulation tests also evaluate two other commonly used trend extraction techniques, those of linear and polynomial regression.

In order to evaluate the trend extraction routines implemented within this research, the simulation is represented by the following function:

$$y = f(x) + \varepsilon \tag{6.1}$$

where:

$f(x)$ is the time variant simulation function;

ε is a random noise term such that $\varepsilon \sim N(0, \sigma^2)$.

The time variant simulation functions are simple functions that are used as a known, or 'truth' term in the time-series analysis. These would represent a trend that exists in the data, such as surface deformation in GPS observations. The simulation then tests the performance of trend extraction routines with respect to this known simulation function. A pseudo-random noise generator is used to generate the noise term, based on a normal distribution, which is then scaled by a noise term multiplier.

The resulting trend (+ noise) was then estimated using:

- Linear regression;
- Polynomial regression (4^{th} order);
- MAW_2 of window length 40.

In this case, three values of σ are also tested (±5mm, ±10mm, and ±15mm). While the time component is arbitrary for simulation testing, the data have been constructed to represent a similar time-series to the GPS coordinate time-series from the monitoring trial at WMC MKO open-pit mine. In this case, each data sample would represent one GPS coordinate solution computed every sidereal hour over approximately 16 weeks.

The simulation function tested was comprised of multiple line segments constructed to broadly represent the deformation characteristics experienced in the easting component of Station 3, as was shown in chapter 5. The multi-line simulation function may be written as:

$$y(t) = ax(t) + b + \varepsilon \tag{6.2}$$

where:

a is the gradient of line between inflection points of deforming movements in easting component at Station 3;

b is an offset parameter defined by vector corresponding to inflection points of deforming movements in easting component at Station 3.

This function is illustrated graphically in Figure 6.1. The induced noise component in Figure 6.1 has a mean of zero and a standard deviation equal to ±5.0mm.

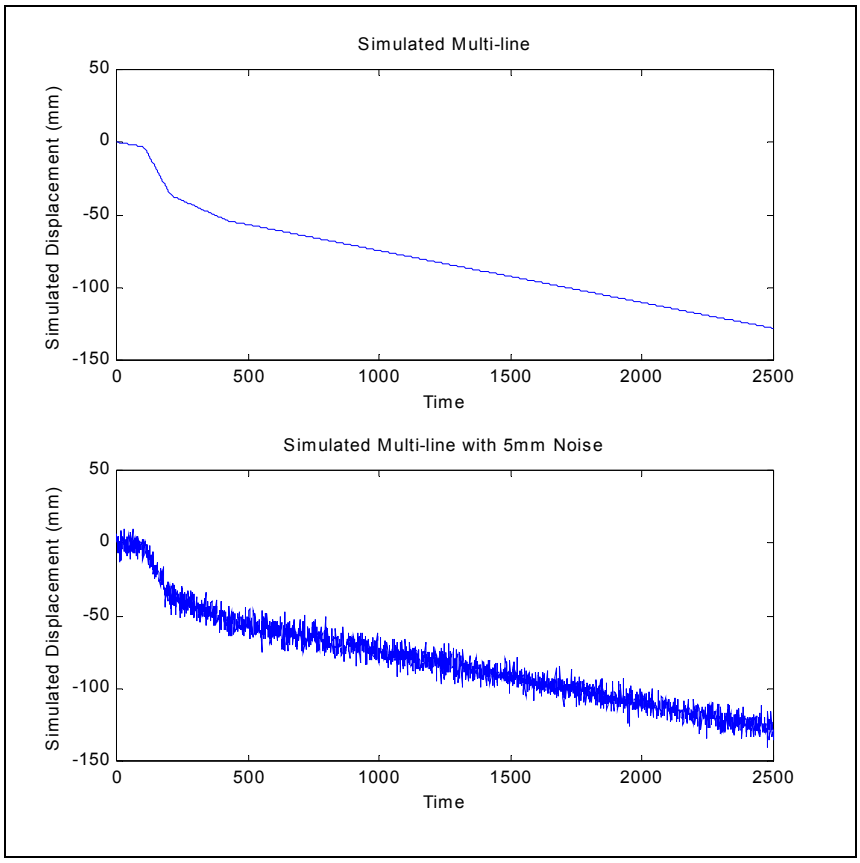

Figure 6.1 Simulated multi-line function with and without 5mm random noise

Using the data presented above, the following RMS estimates of the differences between the time-series data and the estimated trend were computed for the three different noise levels introduced into the system. Table 6.1 illustrates the computed RMS estimates for the different noise levels introduced into the simulation tests for each trend extraction technique.

Trend Extraction Method	Estimated Noise Level (mm)		
	(σ=±5mm)	(σ=±10mm)	(σ=±15mm)
Linear Regression	±9.28	±12.69	±16.90
Polynomial Regression	±5.64	±10.34	±15.23
MAW_2	±4.95	±9.89	±14.84

Table 6.1 Estimated noise levels using a multi-line simulation function

The linear regression technique models the dispersion characteristics poorly, with the greatest difference of approximately ±4.3mm occurring when ±5mm of noise is expected. The MAW_2 presents the best performance in this case, which can also be seen graphically in Figure 6.2.

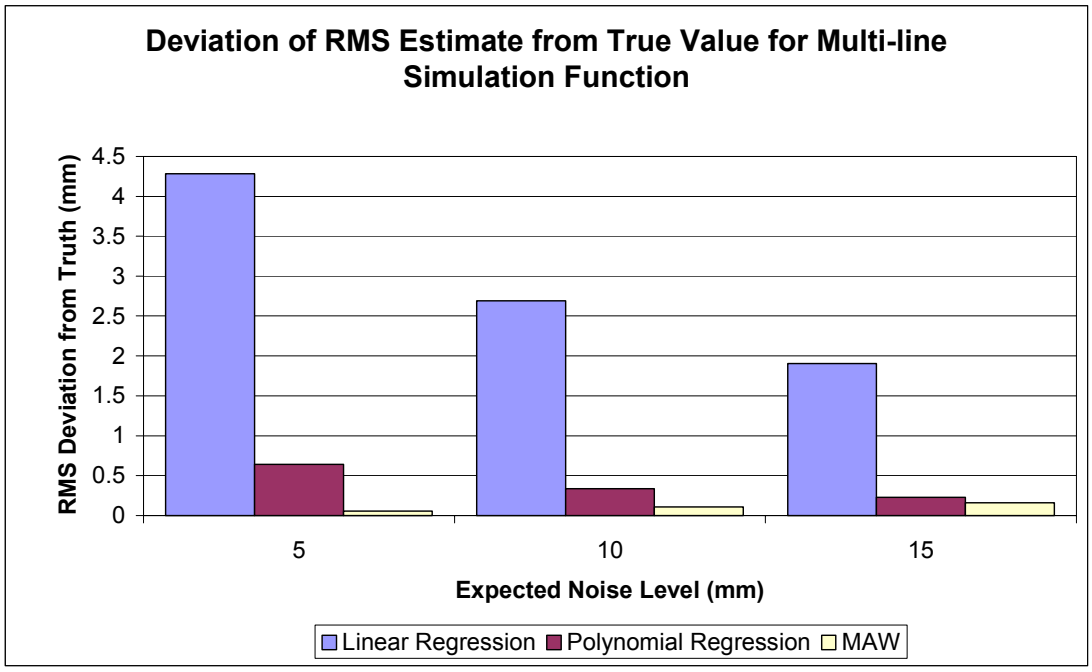

Figure 6.2 Deviation between the expected and estimated noise level for the multi-line simulation function

The graphical results of Figure 6.2 illustrate the precision with which each trend extraction technique can model the noise characteristics within the data. The best technique appears to be the MAW_2, where the maximum deviation in RMS from the expected value is approximately 0.15mm. Values for the linear and polynomial regression techniques are 4.3mm and 0.64mm respectively.

To evaluate the closeness of fit of the extracted trend, the maximum absolute differences are tabulated for the multi-line simulation function.

Trend Extraction Method	**Maximum Difference (mm)**		
	(σ=±5mm)	**(σ=±10mm)**	**(σ=±15mm)**
Linear Regression	28.72	28.55	28.38
Polynomial Regression	10.76	10.65	10.55
MAW_2	1.98	3.96	5.94

Table 6.2 Maximum differences between simulated and extracted trends for multi-line simulation function

Table 6.2 shows that a maximum deviation of nearly 30mm exists when a linear regression technique is used to detrend the time-series presented above. The simulation conducted shows that the polynomial regression technique will struggle to adequately represent deforming trends such as this. The MAW_2, however, continues to appropriately model the underlying trend, whilst also providing reasonable estimates of the variability within the data.

While these results are not unexpected, they do quantify the precision with which dispersion estimators may be calculated, given the motion detected within this research. It is also interesting that while linear regression techniques cannot be expected to appropriately model non-linear trends, as is the case here, some authors use this technique to detrend data prior to calculating variance estimates (for example King *et al*., 1995; Zhang *et al.*, 1997). The choice to use linear extraction techniques may be related to data density in these cases.

6.1.1 Selection of Moving Average Window Length

Having investigated three methods that can be used to extract the trend in the coordinate time-series of a deforming station, it would appear that without *a priori* knowledge of the characteristics of the deformation, it is most appropriate to use the MAW_2 process illustrated above. Appropriate choice of the length of the MAW also

needs to be addressed. In general, a MAW should be chosen such that the window length allows sufficient smoothing of the time-series data, whilst not removing the deformation signal. Should the length chosen be too short, the data will not be adequately smoothed. This will make interpretation much more difficult, particularly if the time-series is to be used to extract velocity estimates from the smoothed data. If the window length is too long, abrupt changes in the deformation signal may be averaged out, or removed completely from the smoothed signal. This is of particular importance when an abrupt change in the positional and velocity characteristics of the station could signify impending slope failure.

To quantify the relationship between trend extraction capability, the multi-line simulation function was tested for different MAW lengths.

Figure 6.3 illustrates the absolute mean differences between the simulated trend, and the trend extracted via the MAW_2 with a window length of between 10 and 60 sessions. Different levels of noise that were added to the simulation function (±5, ±10 and ±15mm) are also plotted.

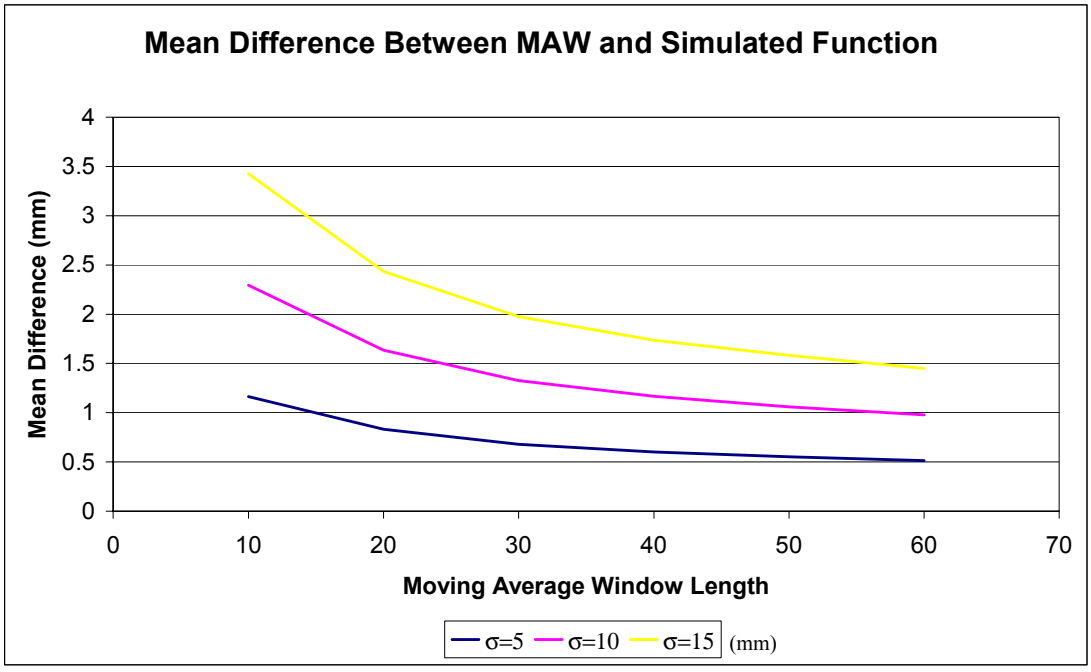

Figure 6.3 Difference between moving average window and simulated function for varying window lengths

Figure 6.3 illustrates the mean absolute difference between the true trend (simulated) and the MAW_2 trend extracted using window lengths ranging from 10 to 60 sessions. A maximum window length of 60 sessions was chosen as an upper bound considering the deformation characteristics represented within the open-pit wall at MKO. The trends extracted using shorter window lengths are more affected by variations in the data than for the trends extracted using longer window lengths. This results in a trend that is more variable and does not follow the smooth simulation function. As the window length and hence the averaging interval increases, small variations in the data have less of an impact on the estimated trend. This results in a trend that more closely follows the simulation function.

A MAW_2 with a window length of 40 sessions, as used in chapter 5, appears to be a reasonable window length when the first-differences (representing a discrete numerical differentiation) are taken sequentially between the data presented in Figure 6.3. These first-differences are illustrated in Figure 6.4.

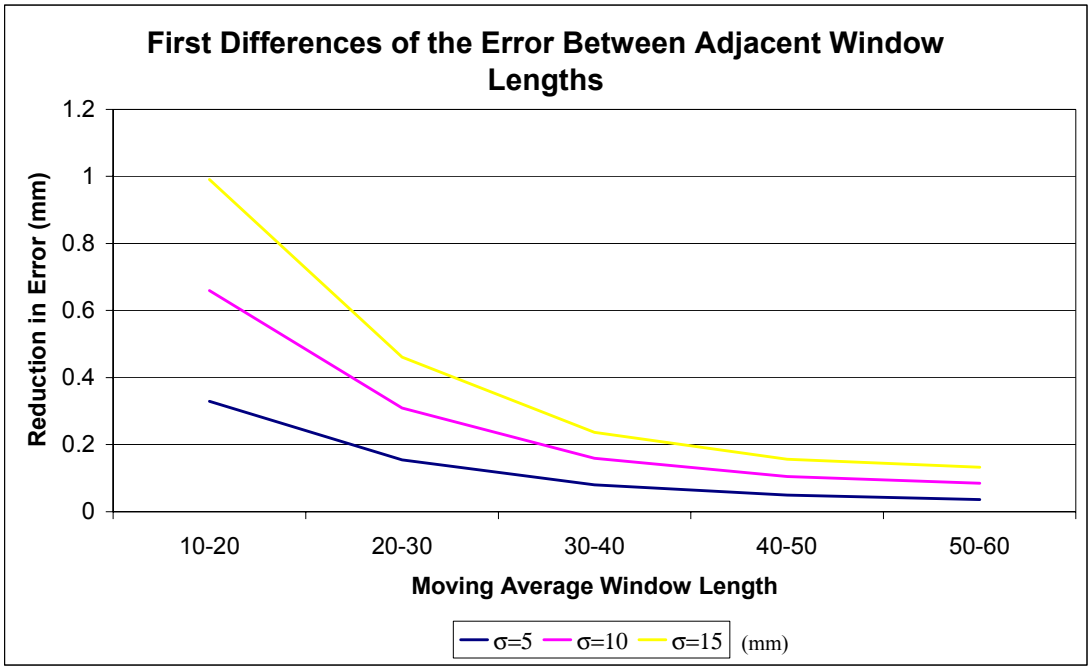

Figure 6.4 First differences of the error between adjacent window lengths

The first-differences of the error between adjacent MAW_2 window lengths indicate the increase or decrease in the ability of the MAW_2 to extract the simulated function as the window length is increased. These first-differences indicate that a

'diminishing return' exists as the window length is increased, and that there does not appear to be substantial benefit of increasing the window length beyond 40 sessions.

Aside from the mathematical aspects involved in the selection of moving average window lengths, the geotechnical characteristics of the deforming structure should also be considered. While increasing the window length will improve the trend extraction capabilities of a smoothly deforming structure, it will also reduce the ability to detect sudden changes in the state of the deformation. As such, a window length of 40 sessions, which equates to an averaging period of approximately ±20 hours would probably be the longest acceptable window length given the dynamics expected and experienced in the pit wall at Station 3 (Sarunic, 2000). Other monitoring situations would require the application of different window lengths based on the individual characteristics experienced in different projects.

One possible solution that may remove the problem of choosing an appropriate window length would be the use of multiple MAW filters of differing lengths, all of which could be used in the geotechnical interpretation process. Moving average filters of different window lengths could also be used to trigger different levels of alarm. This concept is illustrated in Figure 6.5.

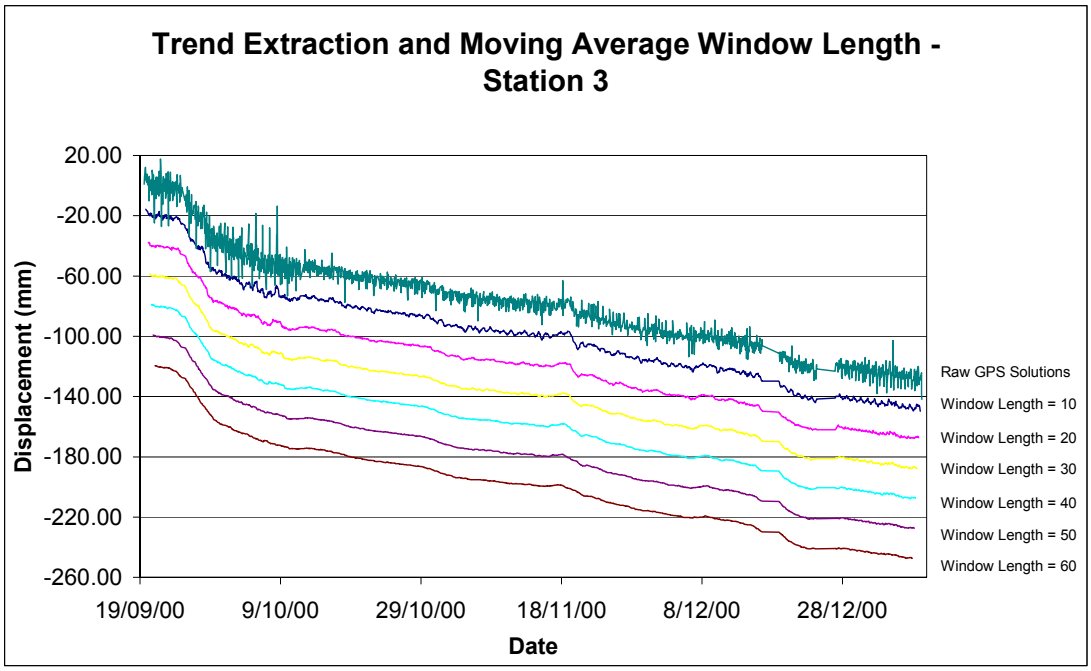

Figure 6.5 Trend extraction at Station 3 with different moving average window lengths

Window lengths ranging from 10 to 60 sessions for the easting coordinate time-series for Station 3 are illustrated in Figure 6.5. For clarity, each successive trend has been offset by 20mm. As the window length increases, the extracted trend becomes smoother, however the point of note is that a smoother trend will give a poorer ability to detect small changes in the state of the deformation.

6.1.2 Notes on the use of Moving Average Windows

Simple MAWs have been implemented and tested to provide a filtering procedure that can be used to extract the deformation within coordinate time-series. The simple MAW, however, is just one of a family of filters that may be used. More complex MAWs can be implemented whereby data are assigned less weight as the distance from the central value increases. Weighting can include linear decay functions or exponential decay functions. While these more complex MAWs are only marginally more difficult to compute, their biggest drawback is the need to have some *a priori* knowledge of the decay characteristics of the correlation within the coordinate time-series. This would require information regarding the behaviour of the dynamics of

the movement, together with knowledge of any auto-correlation that exists within the coordinate time-series.

Other techniques, such as Kalman filtering and semi-parametric modelling (Green and Silverman, 1994), can also be used to extract the associated deforming movements. However, these techniques require an increased computational complexity and are not considered further in this research.

6.2 Automatic Coordinate Update

As detailed previously in section 5.3.4, regular updating of the initial approximate coordinates is required to ensure that the integer rounding technique operates correctly.

An automatic coordinate update routine has been implemented to minimise the effect of imprecise initial coordinate information in the deforming environment. The automatic update function uses historical data of the coordinate time-series, and performs the following tasks:

- Check data for monotonic time-series;
- Smooth data based on a MAW;
- Linearly interpolate time-series data to user selected intervals;
- Plot data for user inspection if required.

Either a one- or two-tailed MAW can be selected, depending on user requirements. In this case, a simple two-tailed MAW with a window length of 40 sessions was used for post-processing operations. The smoothed data are output into daily solutions, although other output intervals could be selected, based on the dynamics of the deforming environment.

Figure 6.6 illustrates the easting coordinate component as updated daily, and plotted against the MAW_2 trend for Station 3 over the period of maximum station velocity from 22 to 30 September 2000.

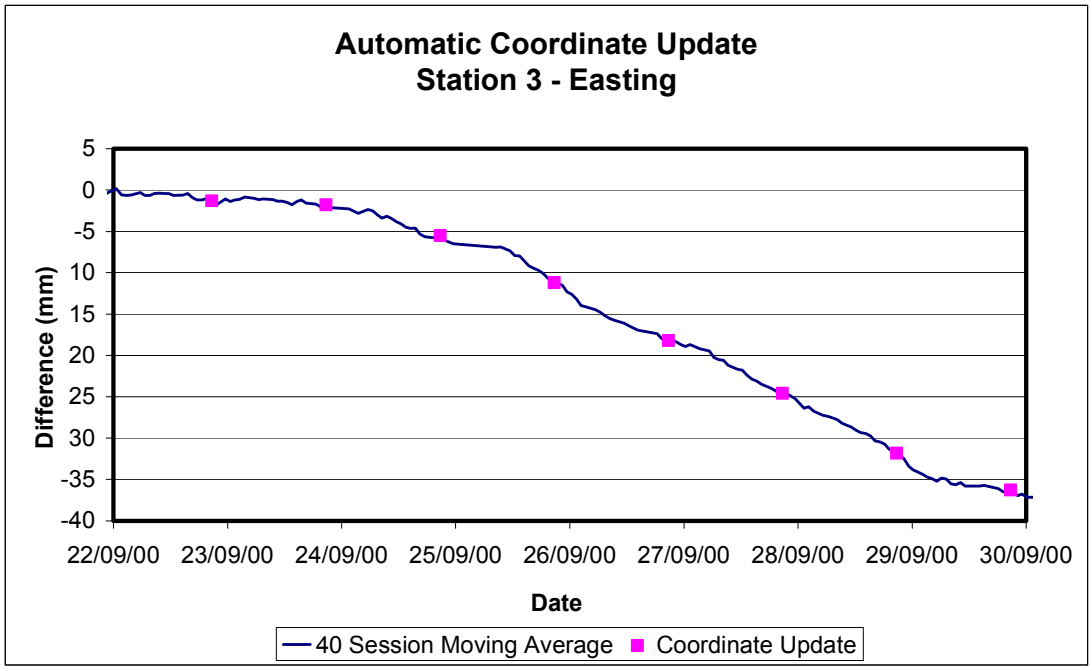

Figure 6.6 Update of the easting coordinate component for Station 3 during the period of maximum velocity

The maximum deviation between the updated easting coodinate and that obtained from the MAW for Station 3 occurs between 29 and 30 September 2000 as illustrated in Figure 6.6. This deviation reaches a maximum of approximately 3.0mm (when rounded to the nearest daily interval).

The interpolated output from the coordinate update function is used as an input to the *Multibas* processing software. A further linear interpolation is performed within *Multibas* to compute the initial approximate coordinate at the beginning of each processing session. In the case above, this would further reduce the approximation error to a maximum of 1.5mm. This gives sufficient resolution for the successful application of the integer rounding technique introduced in section 3.5.

Given the rate of motion observed at the four stations installed at WMC MKO (<8mm per day), daily updates provide a sufficient level of precision to ensure correct integer ambiguity resolution is maintained. Slopes experiencing higher rates of motion may require more frequent updates to the *a priori* coordinates to ensure that the ambiguity rounding technique can perform adequately.

6.3 Double Difference Outlier Detection

Empirical tests were conducted on the test data to develop a simple outlier detection and removal technique. The outlier detection (data snooping) process as implemented here is based on a simple data rejection routine, whereby observations are deleted if the DDOmC values fall outside the user-selected rejection limits.

To illustrate, data are presented from Station 3 for GPS weeks 1081 and 1084 to determine the percentage of observations falling outside set noise limits. These 2 weeks of data were chosen to represent processing with both one and two reference stations operating within the monitoring network. In fact, the operating environment at Station 3 offers a 'worst case' scenario in terms of the signal multipath and diffraction effects of all points monitored. It would be expected that poorer quality observations would be recorded at this location than at the other monitoring stations.

As any evaluation of the DDOmC parameters will be directly related to the *a priori* coordinate estimates, the automatic coordinate update routines presented in section 6.2 were implemented prior to testing.

Figure 6.7 illustrates the percentage of DDOmC observations that fall within the test bounds of ±0.10, ±0.15, ±0.20, ±0.25, ±0.30 and ±0.35 cycles. Over 10 million double difference observations were used from GPS weeks 1081 and 1084 at Station 3 to calculate these figures, although many of these observations will be correlated to some extent.

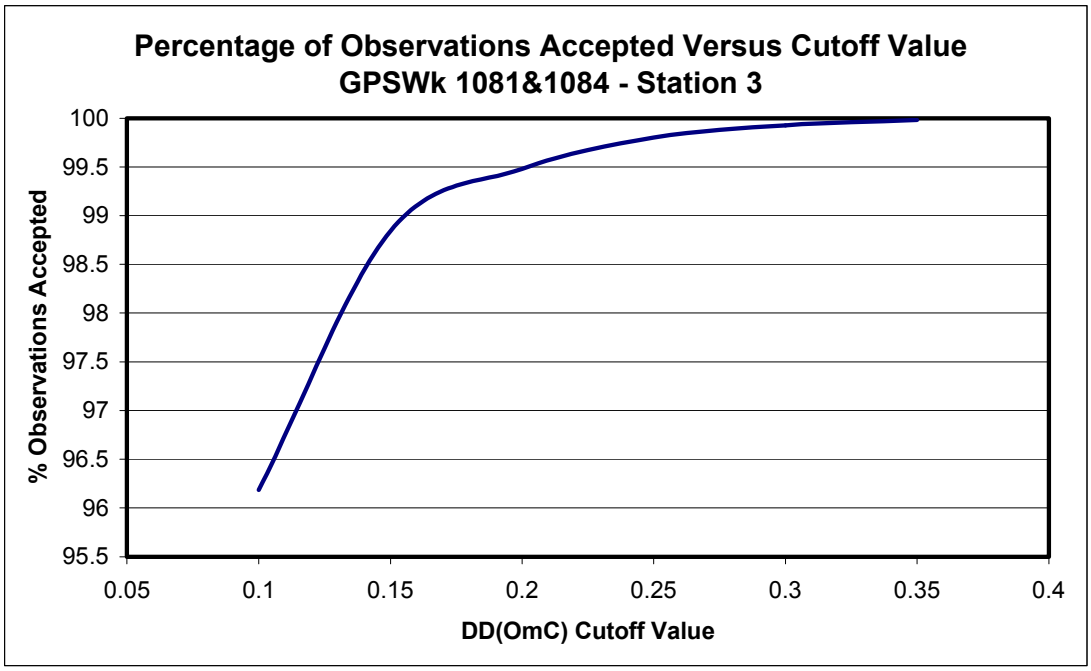

Figure 6.7 Double difference outlier detection statistics

From Figure 6.7, it can be seen that 96.19 percent of the DDOmC observations recorded have a magnitude of less than ±0.1 cycles. This rises to 99.98 percent having a magnitude of less than ±0.35 cycles.

One common method of detecting outliers is to use the *z*-score, or standardised data values as an indicator for outlier detection (Anderson *et al*., 1991). In this case, a *z*-score for a particular observation of less than –3, or greater than +3, is often used to signify a data outlier. Under the assumption that the data are normally distributed and uncorrelated, this would result in a rejection of 0.3 percent of the data (99.7 percent would not be regarded as outliers). Using this approach, any DDOmC observation that has a magnitude of greater than ±0.35 cycles would be considered an outlier. This is a somewhat relaxed limit, however, considering the level of data redundancy experienced within each processing session, and the expected high level of time correlation between double difference observations.

As such, it is recommended that a limit of ±0.2 cycles be used to detect outliers. This results in a rejection cut-off at approximately 99.5 percent, with a corresponding *z*-score of ±2.80. The ambiguity validation procedure applied in subsequent sections

will refer to this double difference cut-off level as part of the data processing parameters.

6.4 Dependence of Solution Quality on Elevation Masking Angle

Typically, an elevation masking angle of 15° is used to reduce the effect of unmodelled tropospheric delay errors on the positioning solution. Unfortunately, in situations where the sky is predominantly restricted by surrounding structures, the loss of satellite geometry from excluding low elevation observations may result in poorer solutions than if the observations were included in the positioning model. This may be an even more critical issue when short observation lengths are used to increase productivity. This section provides an analysis of the effect of the increased geometrical strength that is obtained when elevation masks are decreased below 15°.

Table 6.3 indicates the processing parameters used for the following tests. The parameters under consideration have been highlighted in bold type.

Processing Parameter	**Values Used**
Processing Interval	1 second
Session Length	~15 minutes
Elevation Cut-off	**5, 10, 15 degrees**
Tropospheric Model	Saastamoinen
Double Difference Outlier Detection	0.2 cycles
Coordinate Update	Automatic
Stochastic Model	Math

Table 6.3 Processing parameters for elevation angle dependence tests

Figure 6.8 illustrates the RMS differences between the raw coordinate solutions and a MAW_2 with a window length of 40 sessions at Station 0 for GPS week 1084. These results represent data from approximately 168 observations (one coordinate solution per hour for one week). It should be remembered that Station 0 offers an unobstructed sky view for GPS satellites. Elevation masking angles of 5°, 10° and 15° are presented.

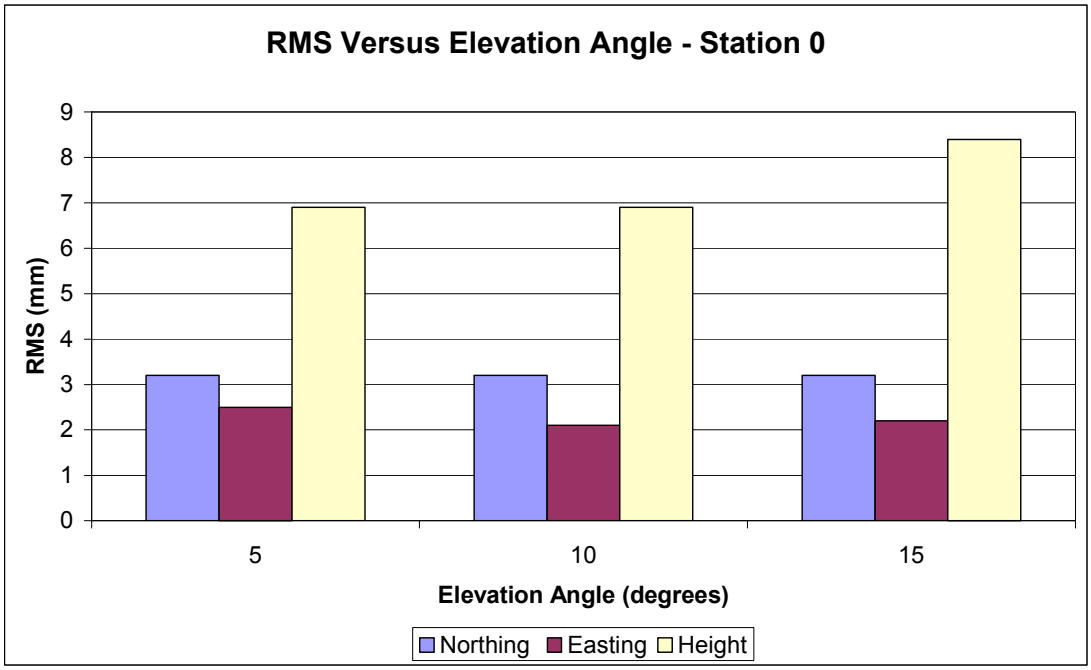

Figure 6.8 Comparative evaluation of variance versus elevation angle – Station 0

It can be seen that an improvement in the noise level in the height component is experienced when the elevation-masking angle is reduced from 15° down to 10° (from ±8.4mm to ±6.9mm). There is no apparent reduction when this is further reduced down to 5° degrees. The RMS values for the horizontal components are all very similar (±3.9mm, ±3.9mm and ±4.0mm for 5°, 10°, and 15° elevation masking angles respectively), showing no apparent difference in coordinate precision when the elevation angle mask is changed.

Possibly of more interest is the fact that there does not appear to be an increase in the noise level of the observations when the elevation masking angle is lowered to 5° as may be expected due to increased atmospheric effects.

Figure 6.9 illustrates the results for the precision level obtained at Station 3 over GPS week 1084. The horizontal precision appears to be relatively consistent. However, the vertical precision appears to be rather variable.

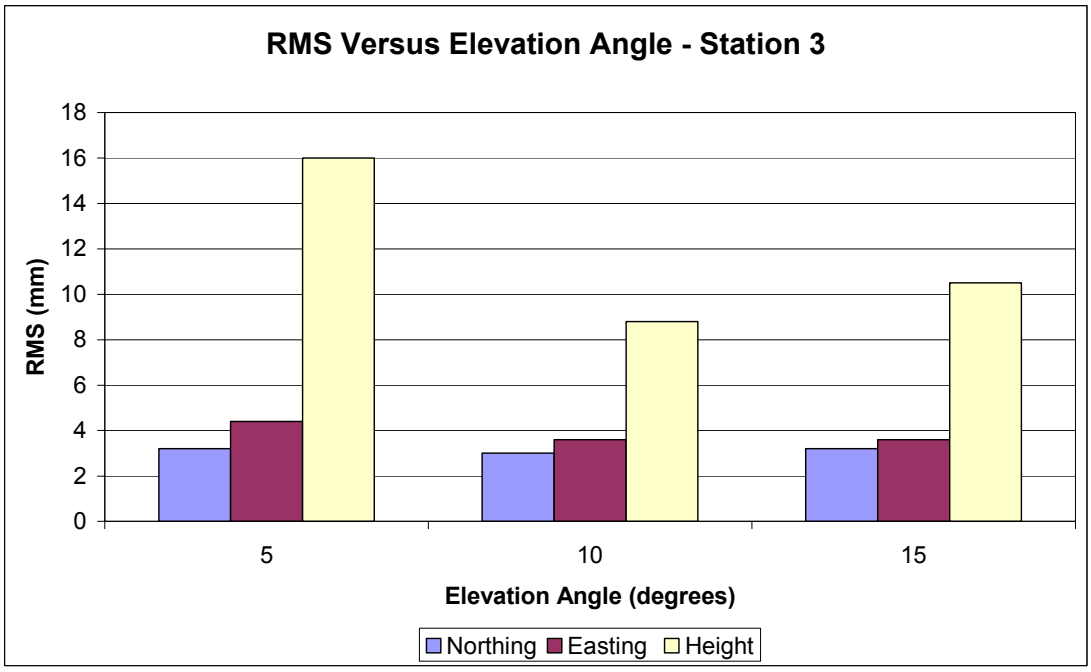

Figure 6.9 Comparative evaluation of variance versus elevation angle – Station 3

The horizontal RMS is ±5.4mm, ±4.7mm and ±4.8mm for 5°, 10° and 15° elevation masking angles respectively. It appears that the height component is most dependent on the elevation angle used, with RMS values of the differences reducing from ±16.0mm for an elevation-masking angle of 15° down to ±8.8mm for a masking angle of 10°. The noise in the coordinate solutions then increases again to ±10.5mm for an elevation-masking angle of 5°.

The results in the horizontal component also see a reduction in RMS values from ±5.4mm to ±4.7mm for a 15° and 10° elevation-masking angle respectively. Again, a rise in the RMS value is experienced (up to ±4.8mm) when the masking angle is further reduced to 5°.

It is suggested that the reduced noise level between 15° and 10° elevation angle results from the increased geometry and number of the observations that are included in the positioning model. The added contribution of these observations seems to outweigh the increased noise that would be expected on observations at lower elevations. When the elevation-masking angle is further reduced to 5°, it is possible that the residual atmospheric and multipath noise begins to outweigh any geometrical

strength that may be gained from the inclusion of extra observations. This is especially evident at Station 3 where the site is subjected to sky masking from the nearby mine wall.

Following the results presented in Figure 6.8 and Figure 6.9, an elevation-masking angle of 10° is used in subsequent sections. This elevation-masking angle seems to provide the best level of precision for positioning in both the open environment (minimal sky masking) and in environments that experience significant masking effects such as at Station 3.

6.5 Dependence of Solution Quality on Session Length

This section investigates the trade-off in solution quality that occurs with reducing the station occupation time for GPS-based deformation monitoring. Data were processed from Station 0 and Station 3 for GPS week 1084. This results in approximately 168 solutions for each station. The data were processed with session lengths of 1 second, 30 seconds, 2 minutes, 5 minutes, 10 minutes and approximately 15 minutes (that is, with all of the data collected), as indicated in Table 6.4.

Processing Parameter	**Values Used**
Processing Interval	1 second
Session Length	**1 second, 30 seconds, 2, 5, 10, ~15 minutes**
Elevation Cut-off	10 degrees
Tropospheric Model	Saastamoinen
Double Difference Outlier Detection	0.2 cycles
Coordinate Update	Automatic
Stochastic Model	Math

Table 6.4 Processing parameters for session length dependence tests

Figure 6.10 illustrates the RMS differences between the raw solutions and the 40 session MAW_2 for processing session lengths ranging from 1 second through to

approximately 15 minutes. These results represent the selection of shorter data collection times that could be adopted in the monitoring strategy.

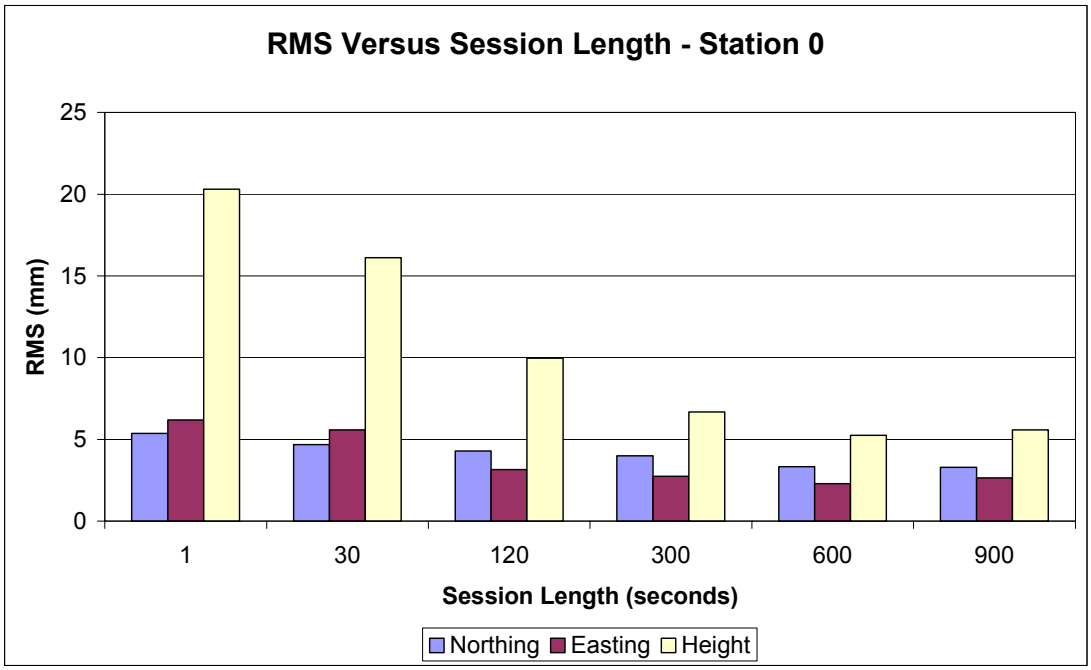

Figure 6.10 Comparative evaluation of variance versus session length – Station 0

As can be seen from Figure 6.10 the noise level decreases in all three coordinate components (northing, easting, and height) when the session length is increased from 1 second through to 10 minutes.

A small but unexpected increase in the precision level also occurs between session lengths of 10 and 15 minutes in the easting and height components with the horizontal RMS level increasing from ±4.0mm to ±4.2mm and the height RMS increasing from ±5.2mm to ±5.6mm. The northing component remains constant in this case. This is not expected to be significant.

Considering the differences from a session length of 1 second, to a session length of 10 minutes, a reduction in RMS in the height component of approximately 74 percent is computed. The corresponding decrease in the horizontal RMS is approximately 50 percent.

Similar results are presented for GPS week 1084, at Station 3. These results, presented in Figure 6.11 below, indicate that the RMS value decreases from approximately ±18.3mm in the horizontal and ±18.5mm in height components for a 1-second session, to approximately ±5.0mm and ±9.9mm in the horizontal height components respectively for the 15-minute session length. This represents a 72 percent reduction in the horizontal noise level, and an associated reduction of the height noise level of approximately 46 percent.

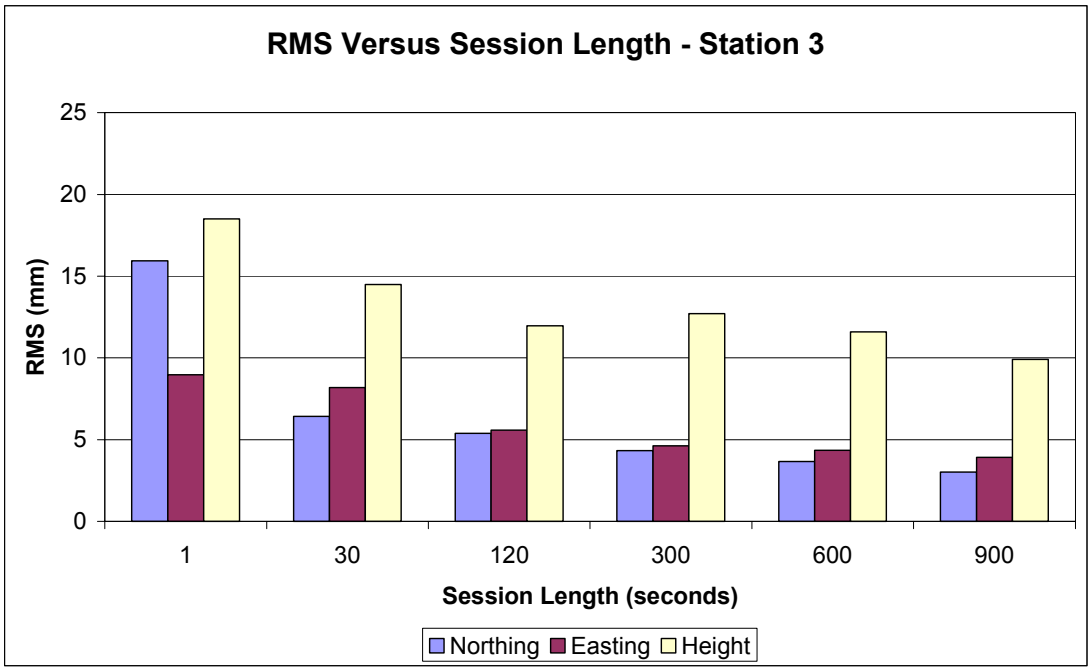

Figure 6.11 Comparative evaluation of variance versus session length – Station 3

It is commonly understood that increasing the occupation time when using GPS-based positioning techniques makes use of the changes in satellite geometry that allows more precise coordinate solutions to be attained. This has been confirmed here, especially in the case of the reduced sky visibility that is experienced at Station 3. One exception is noted, at Station 0 for an occupation length of 15 minutes. However the increase experienced is not considered significant.

Under periods of restricted sky visibility, and hence poorer satellite geometry, the greatest improvement in solution quality is experienced in the occupation length between 30 seconds and 2 minutes. A reduction of 68 percent in horizontal RMS and 60 percent in height RMS results from this increase in observation length.

In some situations, for example where many points are to be monitored, reducing the session length to between two and five minutes could provide a reasonable trade-off between coordinate solution quality and shorter occupation time.

6.6 Dependence of Solution Quality on Processing Interval

Finding the optimal data capture rate is an important issue when GPS systems are to be used for the purpose of monitoring deforming movements. To evaluate the impact of changing the data capture rate, the processing interval used to compute the coordinate solution can be altered to represent a change in the receiver set-up parameters implemented on-site.

While many GPS observations are temporally correlated and possibly redundant at high data capture rates, having extra data redundancy allows for more stringent quality control procedures to be implemented, in terms of outlier detection and removal. There is a trade-off, however, because recording and storing these extra data take up GPS receiver time, radio-modem bandwidth and data processing and storage/archival facilities. When the deformation system is designed for real-time operation, the most important of these factors are the radio-modem bandwidth and processing facilities.

To evaluate the effect of the processing interval on the coordinate solution, the following processing parameters were selected (Table 6.5):

Processing Parameter	**Values Used**
Processing Interval	**1, 2, 5, 10, 15, 30, 60 seconds**
Session Length	15 minutes
Elevation Cut-off	10 degrees
Tropospheric Model	Saastamoinen
Double Difference Outlier Detection	0.2 cycles
Coordinate Update	Automatic
Stochastic Model	Math

Table 6.5 Processing parameters for processing interval dependence tests

Data from GPS week 1084 were processed at different intervals to evaluate the effect described above. All RMS estimates have been computed as previously, with respect to a 40 session MAW_2 extracted from the data. Figure 7.12 illustrates the RMS of the difference between the raw data and a 40 session MAW_2 for Station 0.

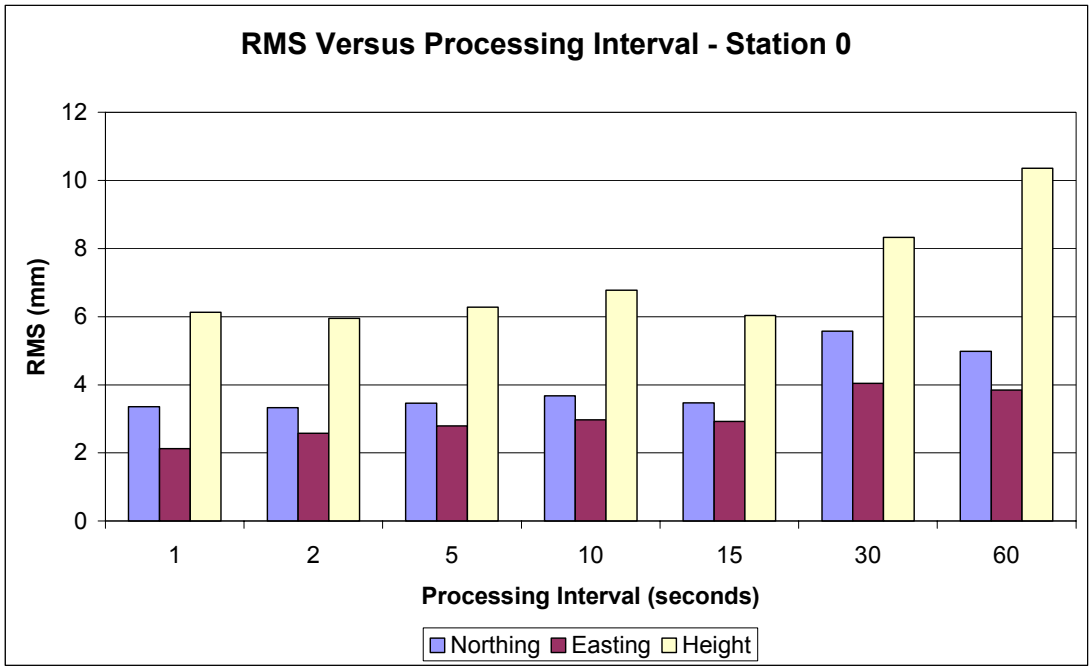

Figure 6.12 Comparative evaluation of variance versus processing interval – Station 0

Figure 6.12 illustrates the RMS estimates for processing intervals ranging from 1 second through to 60 seconds. The horizontal RMS is reduced by approximately

±2.3mm, or by 37 percent, when the processing interval is reduced from 60 seconds down to 1 second. The corresponding improvement in the height component is ±4.2mm, or by approximately 40 percent. The relative difference is not large when considering the RMS values between a 1-second processing interval and that of a 15-second processing interval. The corresponding reduction in RMS is in the sub-millimetre level for both the horizontal and height components.

Statistics are also presented for Station 3 in Figure 6.13 over the same observation period. Here, all data are in better agreement than the data presented for Station 0 above. The maximum difference between the RMS differences calculated is approximately 8 percent in the horizontal and 5 percent in height.

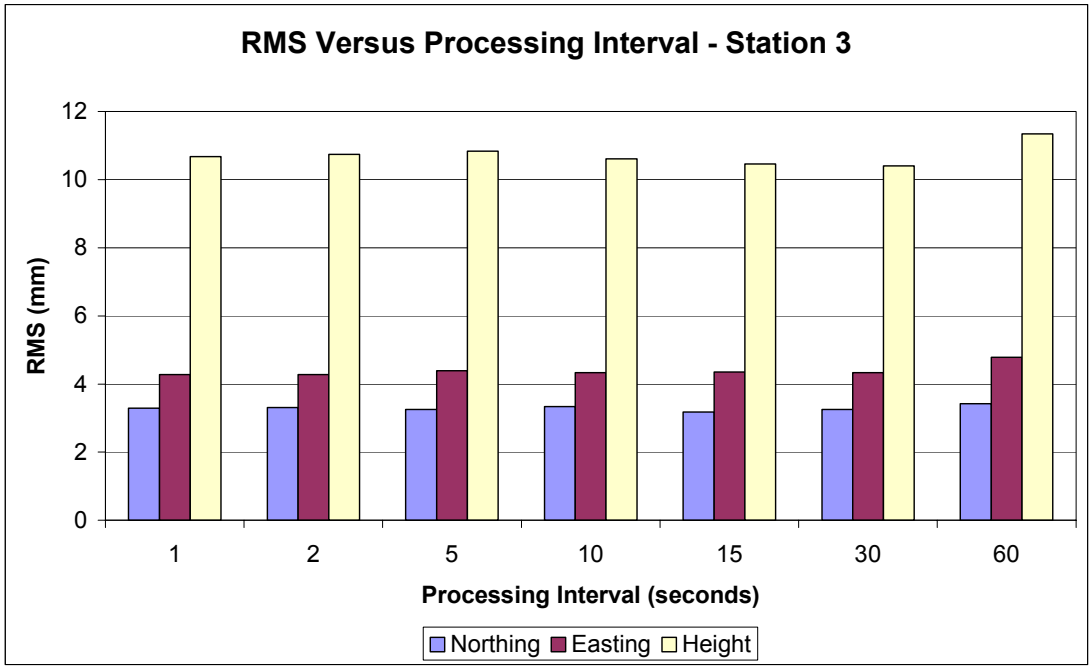

Figure 6.13 Comparative evaluation of variance versus processing interval – Station 3

It can be seen from Figure 6.13, that no significant differences occur at Station 3 when the processing interval is reduced from 60 seconds to 1 second. All data represent similar levels of noise. It is suggested that the consistency of the noise level is dominated by the geometry of the available observations in the positioning solution.

The test results presented above suggest that data collection or processing intervals between 1-second and 15-seconds result in similar levels of coordinate precision for both surface and sub-surface positioning. While coordinate precision should be considered when selecting an appropriate data collection interval, the amount of data captured is also important. Higher data capture rates require that more data be transmitted over the radio communication network. The time taken to process a GPS solution also depends on the amount of data collected. The selection of an optimal data collection interval should consider these issues and will be dependent on the hardware configuration of the monitoring system. This would need to be judged on a case-by-case basis.

6.7 Temporal Resolution of Coordinate Time-series in Detecting Deformation

The temporal resolution or frequency of the solution samples has a direct impact on the ability of the trend extraction process to determine deforming trends within the ground mass. As the sampling frequency is often related to the availability of equipment and personnel, continuous or quasi-continuous systems such as the one presented in this research, offer enhanced levels of trend extraction capabilities. This is particularly important when the noise level of the resulting coordinate time-series is large enough to restrict the confidence of making structural- and safety-based decisions with only a limited time-series of the data. This becomes evident when the GPS-based quasi-continuous coordinate time-series are down-sampled to represent an observation frequency that uses, for example, daily and weekly observations rather than hourly. This could simulate the results that may be obtained by episodic monitoring (not considering centering and set-up errors).

Figure 6.14 shows the raw hourly GPS observations plotted against the 40 session MAW for the easting time-series at Station 3 between 19 September and 22 November 2000. Trends of the deformation were also generated to represent daily (solid purple line) and weekly observations (solid red line with nodes at data points) by randomly selecting daily and weekly observations from the more dense hourly data set. In the case of the random selection of data points, the observations were binned into appropriate classes (daily and weekly), from which one observation was chosen at random.

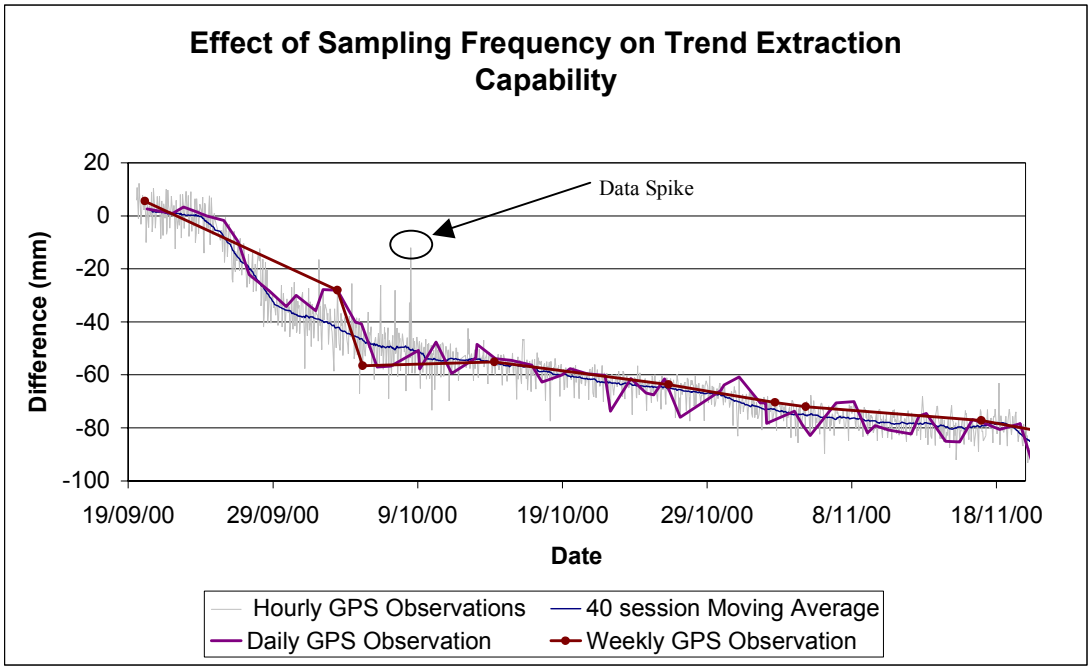

Figure 6.14 Random daily and weekly sampling versus hourly sampling campaigns

As can be seen from these results, the daily- and weekly-based trends do not always follow the trend extracted from the hourly observations. In fact the daily trend seems to be rather sporadic and appears to be easily corrupted by data spikes (coordinate solutions that deviate from the trend substantially). The trend extracted from the weekly observations appears to be less affected by data spikes but does not seem to closely represent the trend obtained from solutions every hour during the period of maximum velocity (between approximately 24 September and 9 October 2000).

Both of these trends also appear to suggest a large shift in the position of Station 3 around 4 October 2000. This movement is attributed to a number of data spikes that exist in the time-series data at this time.

It is interesting to note that in the absence of either an independent data set or a more dense time-series, decisions regarding the safety of the wall would be based on the data available. If daily or weekly solutions were all that were available, there would be very little chance of distinguishing between actual wall movement and data

outliers within the coordinate time-series. It is only with the addition of more data that individual outliers are detectable from the underlying surface movements.

Figure 6.15 illustrates another effect of down-sampling the easting coordinate time-series at Station 3 between 19 September 2000 and 22 November 2000. The raw time-series are plotted together with the 40 session MAW_2 detrended time-series and daily points that have been extracted from the raw time-series data.

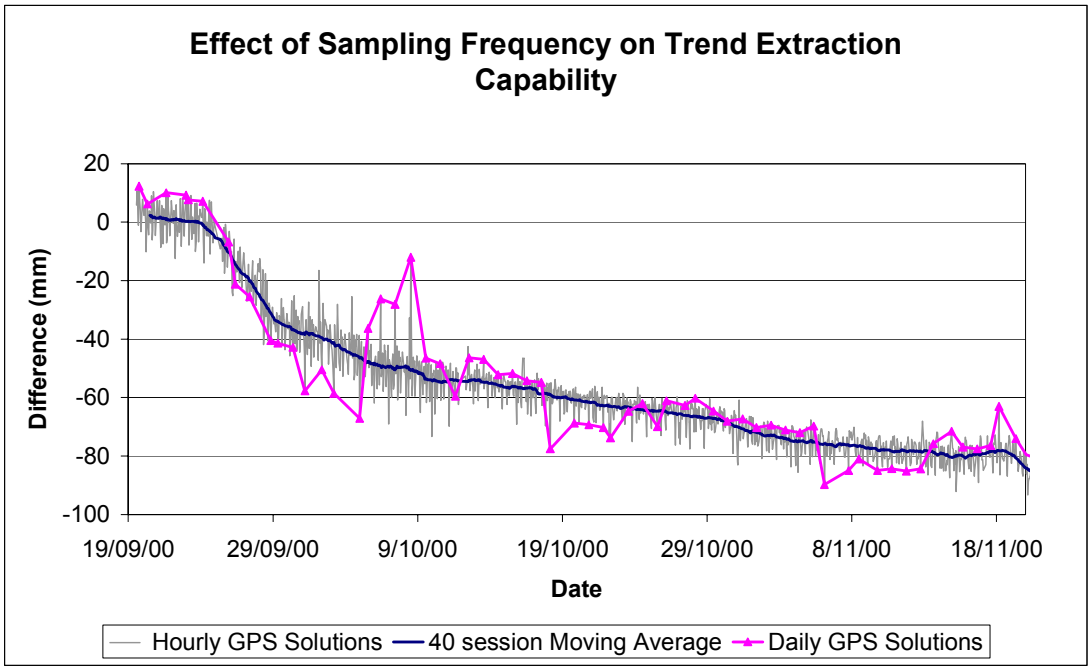

Figure 6.15 Effect of the sampling frequency on the ability to extract the deforming displacements.

The daily observation campaign here has been selected to represent one of the 'worst case' scenarios where most of the solutions selected are in fact spikes themselves. The point to note, however, is that again this is only visible to the user when the denser time-series can be viewed at the same time. The surveyor undertaking a daily observation regime would be unaware of this, and would not be able to separate spikes from the deformation signal. It is only when the temporal density of the solutions is increased substantially, that the two are separable.

Incidentally, many of the spikes discussed above are separated by one sidereal day. The effect of repeating satellite geometry on the coordinate time-series has already

been discussed in chapter 5. It should be remembered, however, that in a production mode of operation for episodic monitoring practices (if based on a daily observation scheme) the surveyor may collect GPS data at a similar time each day. This would usually be completed without any forethought (under conditions of a full satellite constellation) as to the similar satellite geometry that may bias or contaminate the resulting GPS time-series. Furthermore, velocity estimates would become even more unreliable, as can be seen when the gradients are visually inspected in Figure 6.15. In the case presented here, the time-series would represent spurious wall velocities that change quite dramatically in magnitude over the length of the time-series. These do not represent the dynamics of the system adequately, and would result in reduced confidence when making decisions regarding the safety of the pit wall.

6.8 Summary

Simulation results have indicated that the simple MAW filter can provide accurate estimates of the precision of time-series data. While some knowledge of the expected dynamics is required for determination of an appropriate window length, there is no requirement that the time-series conform to any mathematical representation, as is the case with linear and polynomial regression techniques.

The MAW technique can also be implemented using differing window lengths to assist in the accurate mapping of the dynamics of the time-series data. More complex MAWs are also available that may offer enhanced trend extraction capabilities. However, these may require that the decay of the correlation between observations is also considered.

This chapter has also introduced an automatic updating routine for the initial approximate coordinates, and has investigated a simple method to detect outliers within the double difference observations. Finally, the effect of changing the processing characteristics of the data collected has been examined to optimise the precision of the coordinate time-series that can be obtained in a quasi-continuous monitoring mode for high precision deformation monitoring applications. These parameters included the elevation masking angle, the session length, and the data processing interval.

An elevation-masking angle of 10° has been found to provide a reasonable compromise between satellite geometry and noise introduced by residual atmospheric delay. Session lengths between 2 and 15 minutes provide similar levels of coordinate precision. The data processing interval, signifying the data capture rate in the field should, on average, be selected between 1 and 15 seconds. More data captured requires a higher data throughput for the radio-modems and in practice, the choice of processing interval may be closely related to the design of the communications network.

The temporal resolution of the resulting coordinate time-series may be the most important factor in extracting the trend of deformation. As the sampling frequency is reduced, from hourly to daily and weekly for example, the resulting deformation estimate becomes more erratic and subject to distortion by data spikes. In the 'worst case' scenario, a poorly sampled time-series may give completely false indications of the dynamics of the slope being monitored.

The results presented in this chapter have illustrated the benefits achievable by a simple optimisation of the GPS data processing options. If a dedicated GPS monitoring system is designed with these issues in mind, the precision of the coordinate time-series can be optimised. Further enhancements to the data processing strategy, such as the use of data stacking techniques and stochastic modelling to increase coordinate precision, are presented in the next chapter.

7. ADVANCED TECHNIQUES FOR GPS DEFORMATION MONITORING

This chapter investigates some of the techniques for advanced GPS positioning that can be applied to slope deformation monitoring. The suitability of the assumptions used for data stacking techniques are evaluated with respect to using the correlated nature of the repeating multipath signature that exists in double difference GPS observations. Both observable stacking and coordinate solution stacking techniques are investigated. The issue of selecting an appropriate stochastic model is also discussed, which is of particular interest when positioning under strong multipath conditions. The three stochastic models introduced in chapter 3 are tested in an effort to further optimise the GPS solutions for deformation monitoring. A new stochastic model, called the SENR (Systematic Error-to-Noise Ratio), is also introduced. This model operates by weighting observations based on an estimation of the level of systematic error within the double difference data.

7.1 Stacking Approaches to Mitigate Recurring Multipath Trends

Data stacking approaches have been proposed in the literature to reduce the effect of multipath-induced systematic errors for high precision positioning applications, particularly in the case of deformation monitoring. For more information regarding the use of these techniques, the reader is referred to Alber *et al*. (2000), Bock *et al*. (2000), Braun *et al*. (2001), Brunner *et al*. (2000), Ding *et al*. (1999), Grenrich and Bock (1992), Ma *et al.* (2001), Radovanovic (2000), and Wübbena *et al*. (2001).

There are generally two types of stacking approaches available for the small-scale monitoring application tested in this thesis. The first technique uses observable (or residual) stacking, where least squares observations (or residuals) are correlated with respect to the sidereal day to reduce the impact of multipath delay on the positioning results. These techniques have been investigated, for example, by Ma *et al.* (2001), Ding *et al*. (1999), Radovanovic (2000), and Wübbena *et al*. (2001). The second technique uses stacking of the coordinate solutions to reduce the effects of

unmodelled systematic error (for example Bock *et al.*, 2000; Alber *et al.*, 2000; Braun *et al.*, 2001).

Both of these techniques rely on the high level of correlation that is expected between successive days of GPS data that is a result of the repeating satellite geometries, and subsequently the repeating multipath signatures that should be present in the GPS data. It will be shown that this is not necessarily the case with GPS double difference observations, even for the relatively short baselines used within this research. In some instances, the double difference observables appear to decorrelate on a day-to-day basis, which reduces the effectiveness of these data stacking techniques.

7.1.1 Observable Stacking Procedures for Multipath Mitigation

The observable (or residual) stacking procedures can be used in either of two ways. The first uses the correlation between the GPS observables to give a triple-difference type of solution across sidereal days, whereby the contribution of the correlated multipath signatures to the coordinate solution is expected to be removed. The second type of observable stacking procedure uses the multipath signature to estimate the deformation movements between sidereal days. The first method of observable stacking is of interest in this research, that is, the use of stacking procedures to improve the precision of the resulting coordinate time-series.

Some of the work presented in the literature uses the least squares residual parameters for multipath mitigation stacking (for example Ma *et al.,* 2001; Ding *et al.,* 1999), while other work uses the raw observations (for example Radovanovic, 2000). In this research, the observable stacking method is used in preference to the residual stacking method due to the possible corruption of residual parameters by other systematic error sources. For example, in a least squares solution double difference residuals of one satellite pair, may be biased by systematic errors that exist in other double difference observations.

Both the observable and residual stacking techniques rely on the assumption that a high level of correlation between successive sidereal days in the double difference

phase data time-series will primarily result from a repeating multipath signature. Results presented in this section indicate that this is not necessarily a valid assumption to impose on positioning solutions for steep slope monitoring applications, as the double difference observable decorrelates as a result of other unmodelled error sources or motion between epochs of data.

To illustrate this effect, data from Station 3, where signal multipath effects are evident, are plotted in Figure 7.1 for 14 successive days of DDOmC values for GPS weeks 1085 and 1086. The data have been stacked with respect to the theoretical length of the sidereal day. Elevation angles for the satellite pair 25-17 were approximately 13° and 66° respectively.

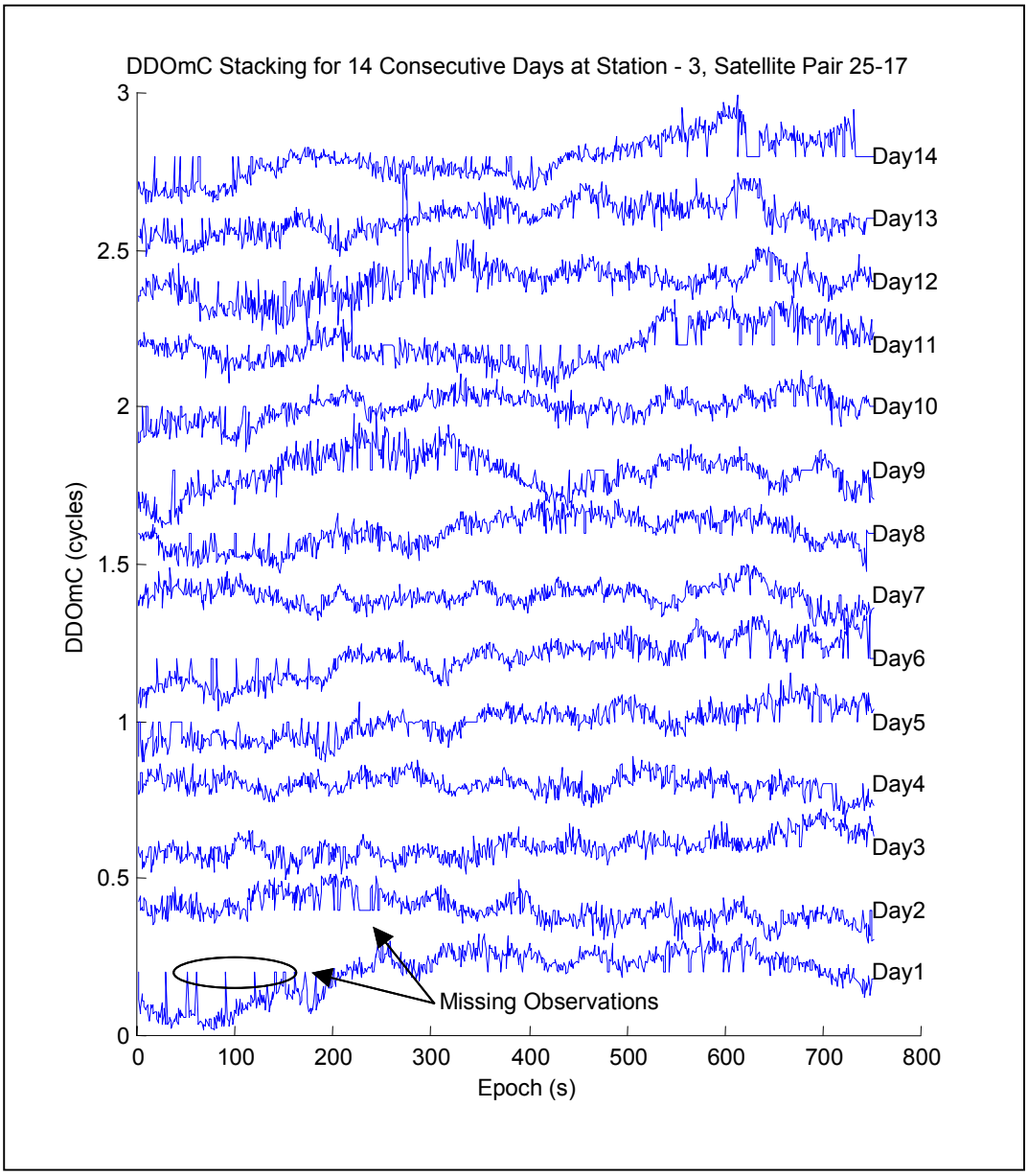

Figure 7.1 Daily stacking of DDOmC values for 14 successive days – Station 3

RMS differences (about the mean) for this data range from ±0.033 cycles to ±0.079 cycles with the average RMS being ±0.056 cycles.

Various spikes within the data are observed, for example between 0 and 100 seconds for day 1. These spikes represent missing observations which are assigned a zero term in the matrix/vector form (implemented in Matlab). While missing observations are not desirable in this type of correlation analysis, empirical tests have indicated that the correlation coefficient computed is not significantly affected (at the ~0.01 cycle level).

Some repeating multipath signatures can be seen in the data presented in Figure 7.1. It is more instructive to evaluate the correlation coefficients that can be computed between the time-series data. Table 7.1 illustrates the correlation coefficients for the complete 14-day data set.

Day	**1**	**2**	**3**	**4**	**5**	**6**	**7**	**8**	**9**	**10**	**11**	**12**	**13**	**14**
1	1.00	0.27	0.53	0.25	0.64	0.67	0.26	0.69	0.47	0.58	0.56	0.61	0.64	0.51
2		1.00	0.35	0.22	0.32	0.35	0.19	0.38	0.32	0.22	0.38	0.21	0.33	0.35
3			1.00	0.19	0.57	0.49	0.39	0.45	0.26	0.39	0.46	0.36	0.51	0.47
4				1.00	0.19	0.21	0.22	0.21	0.27	0.24	0.26	0.19	0.18	0.20
5					1.00	0.74	0.18	0.57	0.33	0.55	0.38	0.46	0.60	0.53
6						1.00	0.18	0.60	0.25	0.51	0.46	0.48	0.58	0.64
7							1.00	0.28	0.30	0.20	0.22	0.25	0.27	0.24
8								1.00	0.34	0.45	0.53	0.49	0.66	0.46
9									1.00	0.47	0.59	0.43	0.24	0.44
10										1.00	0.48	0.46	0.41	0.41
11											1.00	0.52	0.50	0.66
12												1.00	0.50	0.39
13													1.00	0.45
14														1.00

Table 7.1 Correlation coefficients calculated between 14 successive days of DDOmC data for satellite pair 25-17

The maximum correlation coefficient occurs between days 5 and 6 where a correlation coefficient of 0.74 is recorded. The lowest correlation coefficient is computed as 0.18 which incidentally occurs between the next two successive days (days 6-7). The average correlation coefficient for the off-diagonal elements presented in Table 7.1 is computed as 0.40 with a standard deviation of 0.15. Again, the relatively low correlation coefficients indicate that the observations are not as highly correlated as would be expected. This does not support the use of observable stacking techniques to reduce residual systematic error within the double difference data observed at the WMC MKO open-pit mine site. Decorrelation of the observables appears to be a result of errors other than signal multipath that do not necessarily repeat on a daily basis.

The effect of motion of the antenna location on the double difference observations presented above should also be considered. Approximately 12.2mm of motion were

detected over the two weeks of data presented. This motion may contaminate the double difference observations and reduce the resulting correlation coefficients. Residual atmospheric error may also contribute to the decorrelation effect on the double difference observations. Surface roughness may also impact on the apparent systematic error, however it may be difficult to separate these effects from signal multipath.

The results presented for Station 3 indicate that the systematic error components that are expected to repeat every sidereal day (for example signal multipath, diffraction and antenna phase centre variations) decorrelate due to the presence of other non-repeating errors and motion of the antenna location itself. To further investigate this finding, similar data are presented in Figure 7.2 over the same 14 day period for Station 0 that is expected to have minimal multipath effects (see section 4.3.2). Here, less multipath and motion is expected than at Station 3.

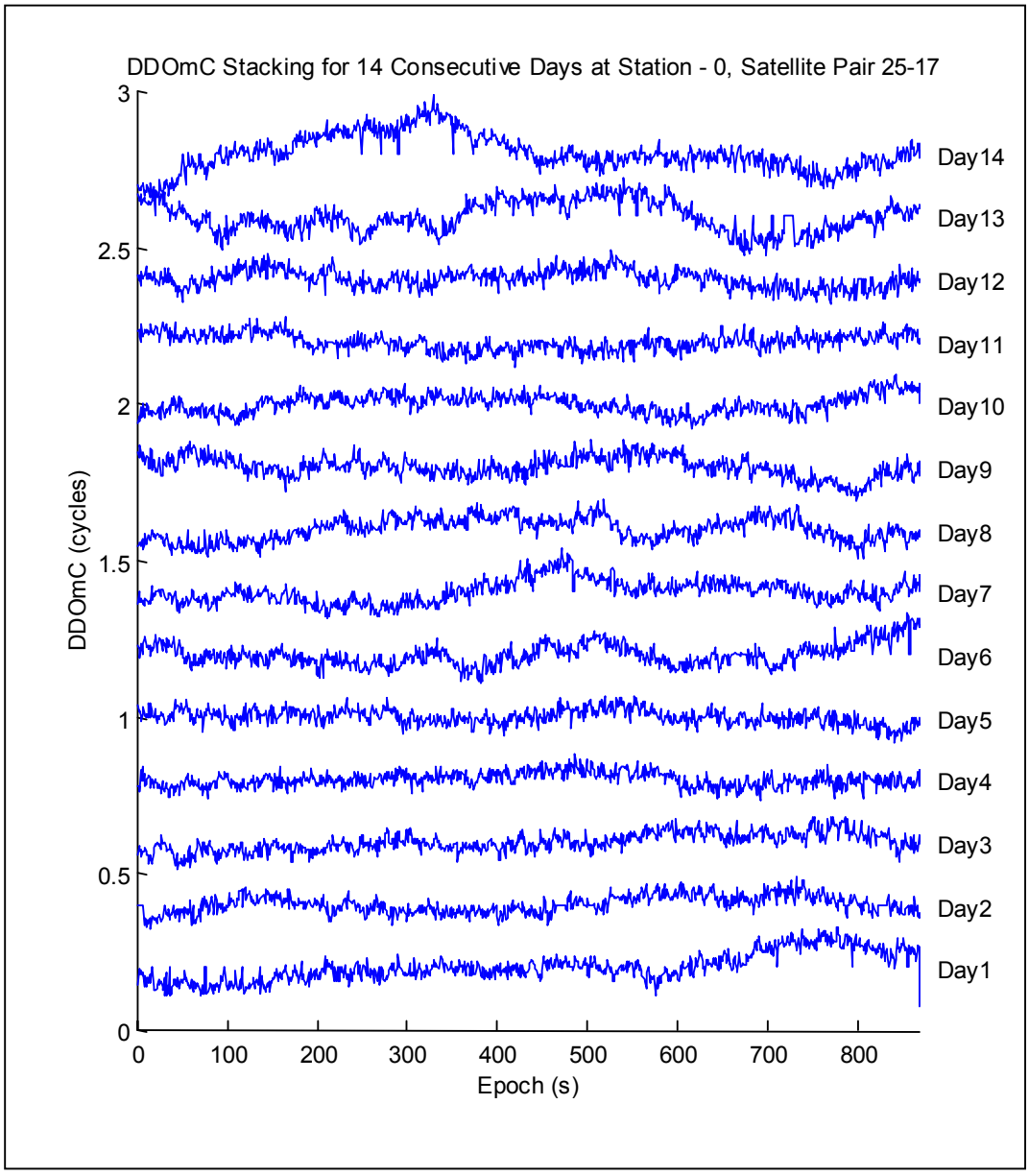

Figure 7.2 Daily stacking of DDOmC values for 14 successive days – Station 0

The noise level of the observations presented in Figure 7.2 for Station 0 is generally lower than for the observations at Station 3. The RMS values range from ±0.024 to ±0.060 cycles with a mean RMS value of ±0.036 cycles. It can also be seen that the DDOmC values observed at Station 0 experience less systematic error than at Station 3. This is evident, for example, in the data presented for days 3 to 5 and day 11. Other data, however, appears to be subject to systematic error, as can be seen during days 13 and 14.

By evaluating the correlation coefficients between data at Station 0, it can also be seen that there does not appear to be a strong relationship between the DDOmC data. This is illustrated in Table 7.2.

Day	1	2	3	4	5	6	7	8	9	10	11	12	13	14
1	1.00	0.41	0.56	0.39	0.26	0.44	0.45	0.32	0.28	0.28	0.32	0.27	0.42	0.46
2		1.00	0.45	0.35	0.22	0.25	0.48	0.45	0.35	0.33	0.26	0.23	0.48	0.49
3			1.00	0.29	0.17	0.39	0.46	0.35	0.24	0.25	0.26	0.22	0.33	0.39
4				1.00	0.22	0.25	0.31	0.39	0.36	0.34	0.31	0.29	0.50	0.42
5					1.00	0.26	0.28	0.21	0.37	0.27	0.30	0.36	0.31	0.23
6						1.00	0.41	0.36	0.24	0.30	0.22	0.35	0.25	0.33
7							1.00	0.52	0.26	0.42	0.33	0.25	0.40	0.52
8								1.00	0.29	0.32	0.30	0.25	0.42	0.57
9									1.00	0.33	0.39	0.42	0.55	0.34
10										1.00	0.30	0.33	0.43	0.35
11											1.00	0.38	0.39	0.43
12												1.00	0.37	0.35
13													1.00	0.54
14														1.00

Table 7.2 Correlation coefficients calculated between 14 successive days of DDOmC data

The mean of the off-diagonal correlation coefficients over the 14 day period presented in Table 7.2 is 0.35 with an associated standard deviation of 0.091. The mean value is similar to that recorded for the time-series data at Station 3 (0.4), while the standard deviation indicates less variability. In these results, the lower correlation coefficients, on average, for this station are to be expected, considering that there are less systematic errors present within the data observed at this point.

Of particular interest are the perturbations that are present within the time-series, for example during the data collected on days 13 and 14 in Figure 7.2. These perturbations may be the limiting factor in the use of observable stacking techniques for deformation monitoring as presented in this thesis. It has already been shown that in the presence of significant multipath reflectors, the DDOmC values decorrelate in the presence of other unmodelled errors. These errors are also present in the case of an environment that has minimal multipath inducing reflectors (at Station 0). This station also has less motion over the 14 days tested than at Station 3. In this case, approximately 4mm of deformation was detected over these 14 days. If

these types of perturbations are mistaken for multipath signatures that repeat daily, the precision of the resulting coordinate solutions may be biased.

With the presence of minimal multipath and motion, the DDOmC observations would be expected to be representative of random noise. This is not the case for the data presented, where other systematic errors still remain within the data. The remaining dominant error sources (after signal multipath) are likely to be residual atmospheric errors (section 3.3.2). There may also be a smaller contribution of thermal noise for the hardware and antenna cable components. Errors such as these that are present in data that has little multipath error and minimal motion (at Station 0), will also exist in multipath affected observations as is the case presented at Station 3 above. In this case, the associated systematic error effects may reduce the effectiveness of observation stacking techniques in the mining environment.

7.1.2 Coordinate Solution Stacking of Time-series for Multipath Mitigation

The second stacking technique involves the use of the processed coordinate solution time-series in a stacking process to reduce the impact of signal multipath on solution quality. The method presented by Bock *et al*. (2000), stacks instantaneous solutions (one solution computed every second). A similar approach has been implemented here, by stacking the 15-minute solutions for 50 days of data at Station 3 (that is 1200 GPS solutions in total). In this case, the 15-minute solutions are expected to capture similar satellite geometry (and hence signal multipath) each successive sidereal day. These results are presented in Figure 7.3.

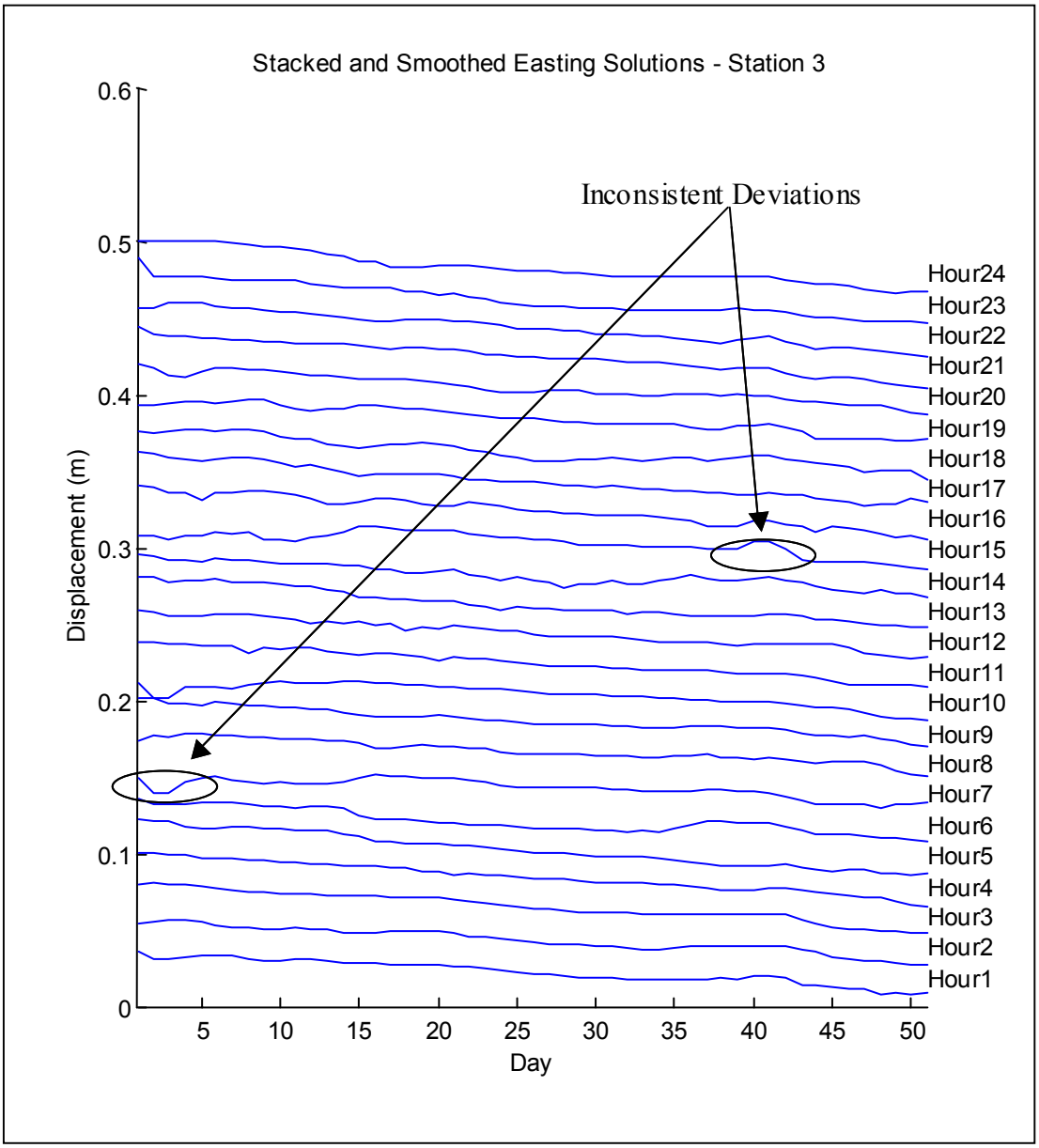

Figure 7.3 Stacked and smoothed coordinate solutions for easting component – Station 3

Figure 7.3 illustrates the stacked coordinate solutions at Station 3 for a 50-day period commencing on 9 October 2000. The time-series have been stacked on an hourly basis and were smoothed using a MAW_2 of window length of 2 days. This is a similar approach to that adopted in Bock *et al*. (2000).

Each line represents the coordinate time-series separated by approximately 1 hour, that is, one 15-minute solution from each hour. It would be expected that in the presence of only multipath and geometric-dependant error sources, each line should display the time-series in a relatively smooth manner (as the multipath/geometrical

contribution to the noise level is consistent within each line). Under this condition, deformation trends that are not related to multipath or geometry should be displayed as a vertical feature across all of the time-series. This does not, however, appear to be evident in the data presented in Figure 7.3, where some of the deviations that appear are not consistent in each hourly sample. An example of this may be the deviations highlighted in Figure 7.3. In these cases, if the deviation illustrated in the time-series were real, they would be evident in each of the stacked time-series. This inseparability between noise and real deformation in this case increases the uncertainty of using coordinate time-series stacking techniques.

Another method of coordinate stacking could involve the daily averaging of coordinate solutions. In this case, data from each sidereal day are binned and averaged. This method, illustrated in Figure 7.4, also allows for the computation of dispersion estimates (standard deviation or RMS error) for each day that can then be represented by error bars.

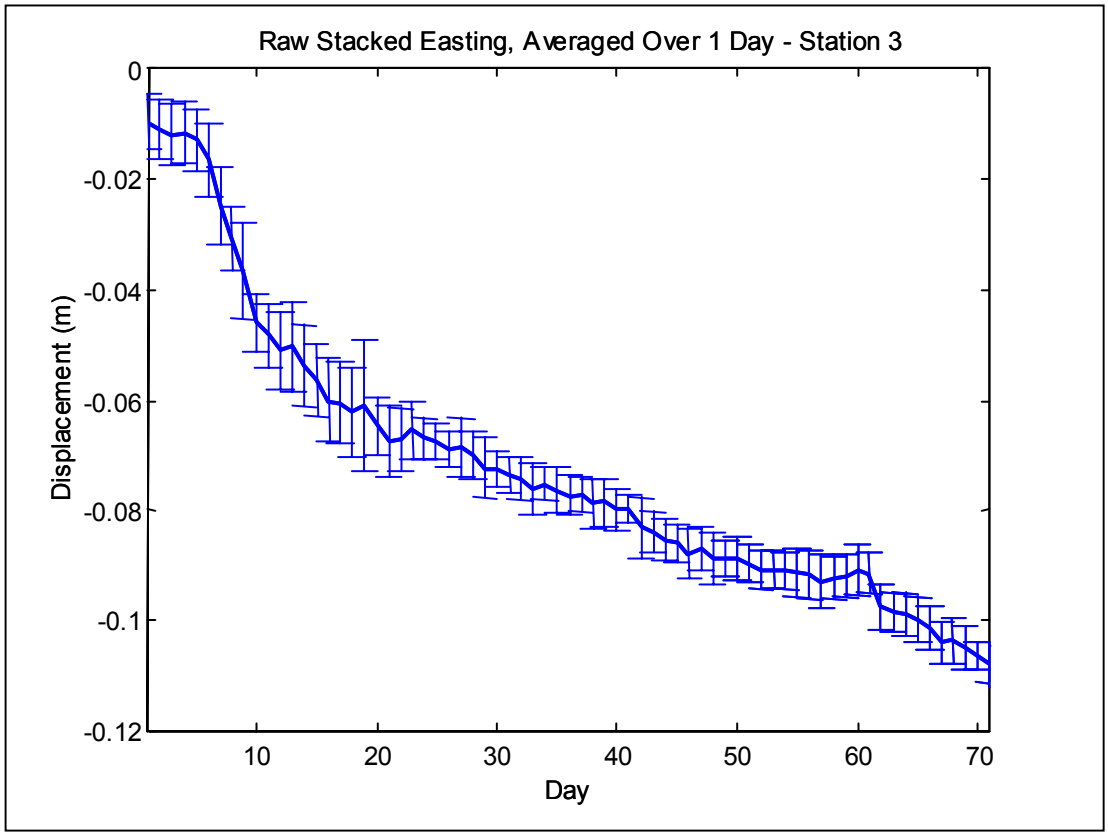

Figure 7.4 Mean daily solution of stacked easting component at Station 3

It can be seen from Figure 7.4 that when plotted in this manner, the daily solution offers a reasonably smooth time-series representation of the data set, whilst also giving a running indication of the precision of the coordinate solutions. One other advantage of plotting the coordinate time-series in this way is that the (sidereal) daily bins of coordinate solutions should capture the same satellite geometry and multipath signatures every day. This should result in a more consistent computation of the dispersion estimates for each daily solution.

It should be noted, however, that in periods of high velocity, as is experienced in some parts of this time-series set, the precision indicator may be biased by the deformation signal itself. For example, if the wall position changes significantly throughout the day, the computed variance or dispersion estimate will increase artificially (because the dispersion estimate assumes stationarity of the mean).

7.1.3 Remarks on Stacking Techniques for Multipath Mitigation

The underlying assumption for much of the work presented in the literature on data stacking techniques is that the multipath signature is well correlated on a daily (sidereal) basis. While this may be a largely valid assumption, there may be other issues that require consideration when operating under the conditions tested within this research. It should, therefore, be considered that:

- Other systematic errors are often inseparable from the multipath delay term, for example, residual tropospheric and ionospheric delay, and antenna phase centre variations;
- Other systematic error terms that are inseparable may decorrelate on a daily basis, even on short baselines of a few kilometres in length;
- Systematic errors may be mis-classified as multipath delay error. This may further reduce the effectiveness of stacking procedures resulting in poorer quality solutions than if stacking were not used;
- Multipath reflectors are often very complex and may vary due to changes in the surface reflectance/absorption characteristics of the obstruction under consideration.

The work presented by Ding *et al*. (1999), Ma *et al*. (2001) and Wübbena *et al*. (2001) for example, does not consider other systematic errors that may bias the results. Furthermore, the results presented are based on known simple, smooth reflecting surfaces used to induce signal multipath, in this case (Ding *et al*, 1999 and Ma *et al*, 2001), a small planar board was placed very close to the GPS antenna (see Figure 7.5).

Figure 7.5 Multipath reflectors used by Ma *et al*. (2001)

In the work conducted by Wübbena *et al*. (2001), the multipath was induced by establishing the GPS antenna close to a smooth concrete building, as shown in Figure 7.6.

Figure 7.6 Multipath reflectors used by Wübbena *et al*. (2001)

For an illustration of the multipath reflectors at Station 3 used in this research, the reader is referred to Figure 4.19.

The baseline lengths are also restricted to the order of a few tens of metres in much of the aforementioned work (for example Ding *et al*., 1999; Ma *et al*., 2001; Radovanovic, 2000), where the residual tropospheric and ionospheric delay error will be negligible, even for single frequency positioning. In the work presented in this thesis, the baseline lengths were relatively short (in the order 2-3km), however a considerable height difference existed between the reference station REF and the monitoring point Station 3. This height difference was approximately 90m. Considering this, and the fact that Station 3 was also located within the open-pit, the effect of complex atmospheric effects on decorrelation of the stacked results cannot be ruled out completely.

From the data collected in an open-pit mining environment, it has been shown that the combined systematic errors remaining within both the raw observations and the coordinate solutions reduces the effectiveness of coordinate stacking techniques.

The issue of the variability of multipath reflector characteristics also requires further attention, in terms of the level of decorrelation between multipath delay errors with changing surface and environmental characteristics, such as the effect of rainfall, dust and snow on the reflecting surface on the multipath signature.

For the data presented in this research, the surface reflector at Station 3 is predominantly the nearby mine wall. It is suggested that the irregularities existing within the wall face (the exposed rock) may also contribute to decorrelation of the multipath signature on successive days, especially when considering that the repeatability of the GPS wavefront could vary with atmospheric changes and small differences in the repeat position of the satellite on successive days.

7.2 Choice of Stochastic Model in GPS Processing for High Precision Deformation Monitoring

Much work has been undertaken in the field of GPS research to appropriately model the stochastic properties of GPS data. Present methods include stochastic modelling that consider factors such as noise dependence based on satellite elevation angle (Han, 1997), carrier-to-noise ratios (Brunner *et al*., 1999), and minimum norm quadratic unbiased estimators (MINQUE) (Wang, 1999).

In this research, three of the simpler stochastic models (in terms of implementation complexity) have been implemented and tested against the correlation-only model (Math), which only considers the mathematical correlations between the double difference carrier phase observations. These three models have been introduced as the Sine, Han, and SIGMA-Δ models in chapter 3. While the MINQUE technique offers a promising approach to stochastic modelling for GPS observations, in its original form it is numerically intensive and impractical for systems designed to operate in real-time. Recently published work on the use of the MINQUE technique by Satirapod (2002) significantly improves the efficiency of the MINQUE algorithm. Unfortunately, time considerations did not allow the inclusion of this work in this research.

A new stochastic modelling process developed by the author is introduced, based on using the Systematic Error to Noise Ratio (SENR), which uses the noise level within the raw double difference carrier phase data themselves to weight double difference observations.

7.2.1 Implementation and Evaluation of the SIGMA-Δ Stochastic Model

The carrier-to-noise based SIGMA-Δ model (Brunner *et al*., 1999), introduced in section 3.4.2.4, has been implemented and tested in an effort to find a stochastic model that appropriately models the noise characteristics of GPS observations.

7.2.1.1 Generation of the SIGMA-Δ Template

The SIGMA-Δ template provides a reference level of the maximum C/N0 values recorded for a particular antenna and receiver configuration. The L1 and L2 C/N0 data from three weeks of continuous data at all three stations were used to generate the SIGMA-Δ template. This resulted in 20,058,324 observations for both the L1 and L2 frequencies for the generation of the template model. The generation of the template model is dependent on the GPS receiver and antenna configuration. Given that the same antennas and receivers are used at every station throughout this research, only one template model was created.

The final template comprises the highest C/N0 value for each elevation angle, with the elevation angles binned into 0.2° classes. The template generated for the Leica CRS1000 receiver and AT504 antenna is illustrated in Figure 7.7.

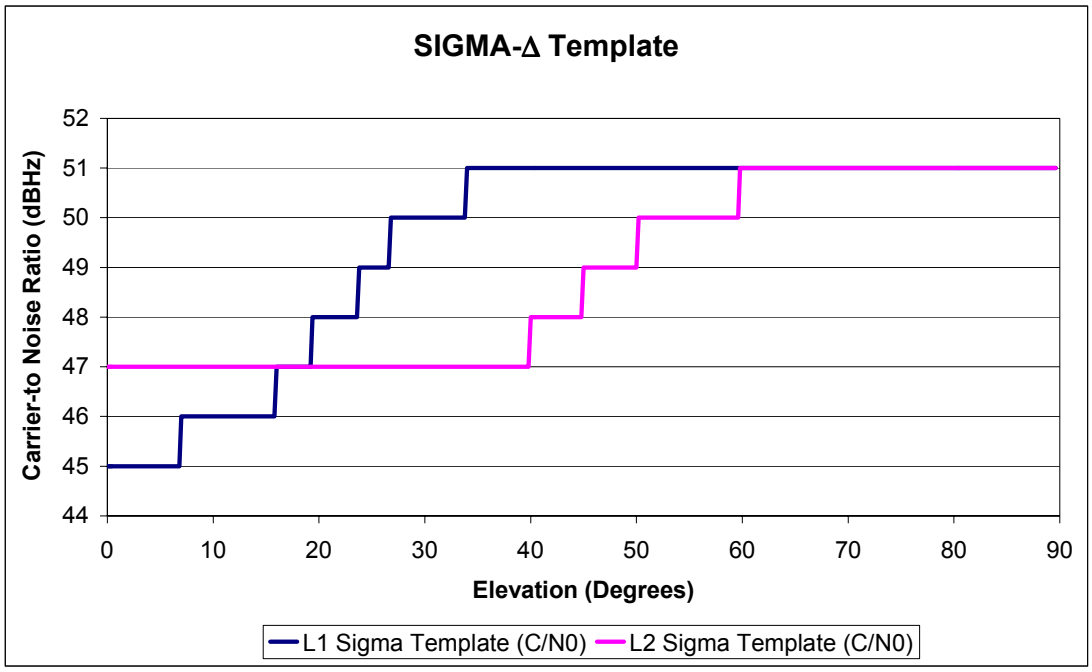

Figure 7.7 SIGMA-Δ template illustrating C/N0 versus elevation angle

It can be seen from Figure 7.7 that the C/N0 ratio for GPS observations in the L1-band varies between 45dBHz and 51dBHz. The highest C/N0 value for L1 is obtained for all elevation angles greater than 34°. The L2 template shows that the

lowest C/N0 ratio of 47dBHz is measured between 0° and approximately 40°, with a maximum value of 51dBHz being measured from approximately 60° in elevation.

The calculation of the SIGMA-Δ template for each 0.2° increment in elevation angle involves the adoption of the highest C/N0 ratio up to and including the elevation angle under consideration. In this way, the maximum C/N0 ratio will always be recorded for each elevation increment, even in the absence of data being available within every elevation bin. It is also possible to fit a curve to the template to remove the step-like appearance of the upper bound (Wieser, 2002). This, however, would result in a generalisation of the template function and is not implemented in the following tests.

7.2.1.2 Testing of the SIGMA-Δ Stochastic Model

The performance of the SIGMA-Δ stochastic model has been somewhat untested in the available literature, particularly with respect to its use with large data sets. In this case, the SIGMA-Δ model has been tested using the reference baseline between REF and BASE using the data collected during GPS week 1084. This particular data set was used due to the relative stability of the monuments over the period in question. With no apparent deformation between these two stations, precision estimates can then be computed directly, without the need for using the MAW filter presented in previous sections. This baseline also represents favourable conditions where there are minimal sky obstructions and lower levels of expected multipath than would be experienced next to the pit wall. The processing parameters used for this test are presented in Table 7.3.

Processing Parameter	**Values Used**
Processing Interval	1 second
Session Length	~15 minutes
Elevation Cut-off	10 degrees
Tropospheric Model	Saastamoinen
Double Difference Outlier Detection	None
Coordinate Update	Automatic
Stochastic Model	**SIGMA-Δ**

Table 7.3 Processing parameters for SIGMA-Δ stochastic model tests

Figure 7.8 below illustrates the RMS values about the mean derived from processing the reference baseline between REF and BASE for GPS week 1084 (representing 168 solutions) for the Math only model and three implementations of the SIGMA-Δ model (see Equation 3.10 in section 3.4.2.4).

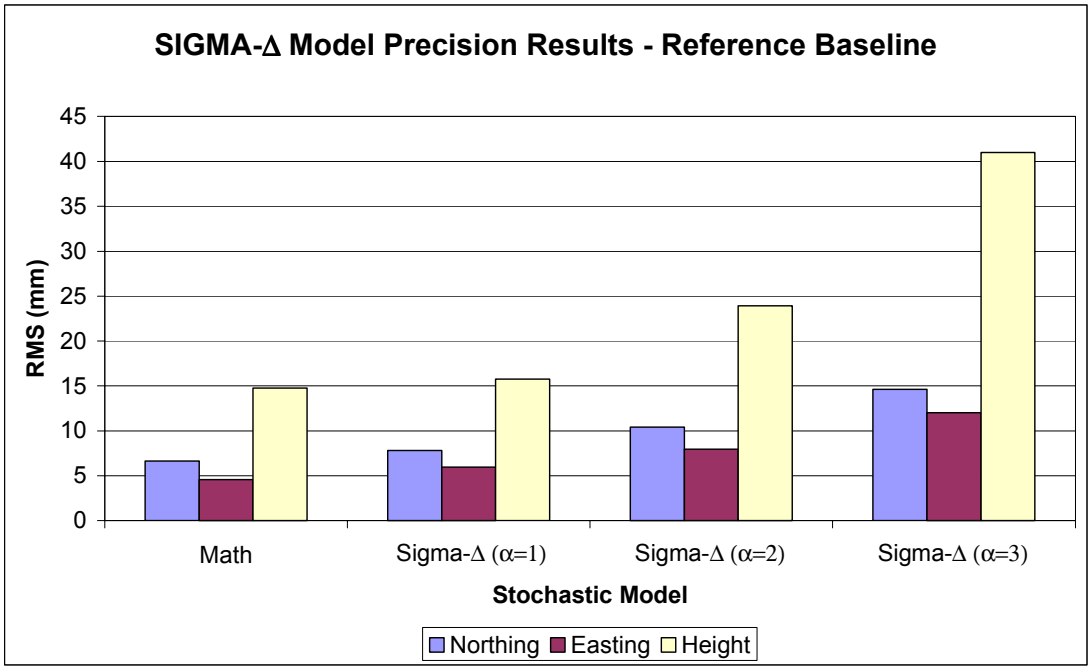

Figure 7.8 RMS values of the SIGMA-Δ model for the reference baseline

As the alpha term defines the decay of the SIGMA-Δ model, three different alpha terms have been tested in Figure 7.8 (α=1, 2, and 3). The work presented by Brunner *et al*. (1999) uses α=2. For the data tested, this results in RMS values of ±13.2mm in

the horizontal component and ±23.9mm in height for the data presented. This is higher than with the Math model which results in RMS values of ±8.0mm and ±14.8mm for the horizontal and height components respectively.

The best results from the SIGMA-Δ model are experienced when an alpha value of 1 is used. This results in RMS values of ±9.8mm in the horizontal component and ±15.8mm in height.

To evaluate the use of the SIGMA-Δ stochastic model under conditions of increased signal multipath and diffraction, Figure 7.9 illustrates the precision of the results when using the Math stochastic model and the SIGMA-Δ model at Station 3 for GPS week 1084. An alpha value of 1 was used following the results presented above.

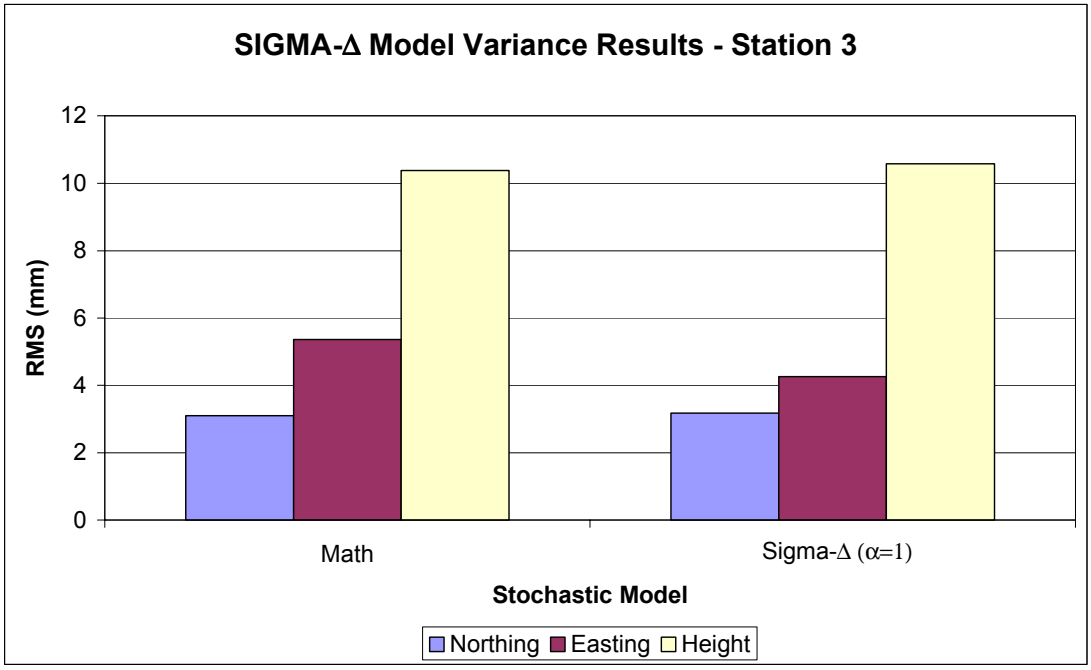

Figure 7.9 RMS values of the SIGMA-Δ model – Station 3

The RMS of the difference between the MAW_2 and the raw position solutions for the SIGMA-Δ model with α=1 are computed as ±5.31mm and ±10.57mm in the horizontal and height components respectively. Similar observations for the Math model result in RMS values of ±6.19mm and ±10.38mm for the horizontal and

height components respectively. Of interest here is that the height component is not improved when the SIGMA-Δ model is compared against the Math model.

These results indicate that in certain situations, the SIGMA-Δ model does not substantially improve the precision of the positioning results and may not be the preferred stochastic model for high precision positioning under high levels of multipath. This supports the findings of Wieser and Brunner (2000) who also indicate similar deficiencies in the SIGMA-Δ stochastic model under high levels of signal multipath. As such, this stochastic model will not be considered further in following analyses.

7.2.2 Background of the SENR Ratio

The origin of the SENR is derived from the development of the Multipath-to-Noise Ratio (MNR) first presented by Schaal and Netto (2000). The MNR was used as an indicator to quantify the level of signal multipath in GPS observations based on the generation of the MNR from the double difference residual information. In this work, the RMS values of the double difference residual series were used to quantify the MNR for each satellite pair. Effectively, a moving average window was applied to the double difference residuals to extract the multipath trend. After removal of this multipath trend from the double difference residual parameters, the resulting ratio between the RMS of the double difference residuals, and the RMS of the multipath-free double difference residuals is denoted as the MNR.

In the work conducted by Schaal and Netto (2000), one MNR value was computed for each satellite pair and used to quantify the effect of multipath on the final solution. This research did not, however, consider the use of this information as a way to describe the influence of the multipath signature on the stochastic properties of the variables.

The systematic error-to-noise ratio, or SENR, takes this concept forward by developing the MNR into a stochastic modelling strategy. Also, the MNR was used with reference to the level of signal multipath noise within the double difference

residuals. This is only partly true, however, as the resulting trends that can be observed within double difference residuals can be comprised of other systematic error terms. These include residual tropospheric and ionospheric delay errors, plus antenna phase centre variations that have not been appropriately described in a deterministic sense.

7.2.3 Generation of the SENR Stochastic Model

Rather than using the SENR generated from the double difference residual parameters, which may be contaminated by other errors that propagate into the final solution, the SENR stochastic modelling process proposed uses the SENR calculated from the raw DDOmC vector in the least squares estimation process. By using this approach, the MNR model can be applied in-line (within the accumulated least squares process) to model the relative noise components of each double difference observation.

The SENR may be represented by the following formula:

$$SENR = \frac{s+n}{n} \tag{7.1}$$

where:

s is the systematic error component;
n is the noise component.

If there are no remaining systematic errors, $s \to 0$, and SENR $\to 1$.

The computation of the SENR stochastic model may now be represented by the following formula:

$$\sigma_{AB}^{jk} = \frac{\sqrt{\frac{\sum_{1}^{n}(x_i)^2}{n}}}{\sqrt{\frac{\sum_{1}^{n}\left(x_i - \sum_{i-w_l}^{i}\frac{x_i}{w_l}\right)^2}{n}}} \tag{7.2}$$

where:

σ_{AB}^{jk}	is the observation standard deviation for the station pair *AB* and satellite pair *jk*;
i	is the current epoch;
x_i	is the DDOmC observation at epoch *i*;
w_l	is the length of moving average filter;
n	is the number of samples to current epoch *i*.

The length of the averaging window should be chosen to adequately describe the lower frequency variations that commonly exist within the DDOmCs under conditions of unmodelled systematic error (namely multipath error for the short baselines used in this research). In this case a MAW_1 with window length of 1 minute is used to capture the systematic error remaining within the observations. For lower data capture rates (for example 30 or 60 seconds), the systematic error may not be described well when using a MAW with length of one minute.

The term σ_{AB}^{jk} represents the standard deviation of the double difference observation. One problem with the implementation of this model is that the SENR is computed at the double difference stage, while the correlation matrix is concerned with a direct mapping of the zero-phase (zero difference) to double-difference phase observations. Other models such as the Sine, Han and SIGMA-Δ operate on the zero-difference observable. As the contribution of the multipath noise is not separable between base and non-base satellites and stations, it is slightly more difficult to directly implement the SENR stochastic model at the double difference stage.

The solution to this problem can be found by considering single differences in matrix-vector form for two stations *A* and *B*, and four satellites *j, k*, *l* and *m* (following Hofmann-Wellenhof *et al*., 1997):

$$\underline{SD} = \underline{C}_{SD}\,\underline{\Phi} \tag{7.3}$$

where:

$\underline{SD}$ is the vector of single difference phase observations;
$\underline{C}_{SD}$ is the zero difference to single difference mapping operator matrix;
$\underline{\Phi}$ is the vector of zero difference phase observations,

such that:

$$\underline{SD} = \begin{bmatrix} \Phi_{AB}^{j} \\ \Phi_{AB}^{k} \\ \Phi_{AB}^{l} \\ \Phi_{AB}^{m} \end{bmatrix} \tag{7.4}$$

$$\underline{C}_{SD} = \begin{bmatrix} -1 & 1 & 0 & 0 & 0 & 0 & 0 & 0 \\ 0 & 0 & -1 & 1 & 0 & 0 & 0 & 0 \\ 0 & 0 & 0 & 0 & -1 & 1 & 0 & 0 \\ 0 & 0 & 0 & 0 & 0 & 0 & -1 & 1 \end{bmatrix} \tag{7.5}$$

$$\underline{\Phi} = \begin{bmatrix} \Phi_{A}^{j} \\ \Phi_{B}^{j} \\ \Phi_{A}^{k} \\ \Phi_{B}^{k} \\ \Phi_{A}^{l} \\ \Phi_{B}^{l} \\ \Phi_{A}^{m} \\ \Phi_{B}^{m} \end{bmatrix} \tag{7.6}$$

Then the law of propagation of variance applied to Equation 7.3 leads to:

$$\mathrm{cov}\left(\underline{SD}\right) = \underline{C}_{SD}\,\mathrm{cov}\left(\underline{\Phi}\right)\underline{C}_{SD}^{T} \tag{7.7}$$

Introducing the matrix-vector form of double differences now such that:

$$\underline{DD} = \underline{C}_{DD}\,\underline{SD} \tag{7.8}$$

where:

$\underline{DD}$ is the vector of double difference phase observations;
$\underline{C}_{DD}$ is the single difference to double difference mapping operator matrix,

such that:

$$\underline{DD} = \begin{bmatrix} \Phi_{AB}^{jk} \\ \Phi_{AB}^{jl} \\ \Phi_{AB}^{jm} \end{bmatrix} \tag{7.9}$$

$$\underline{C}_{DD} = \begin{bmatrix} -1 & 1 & 0 & 0 \\ -1 & 0 & 1 & 0 \\ -1 & 0 & 0 & 1 \end{bmatrix} \tag{7.10}$$

Applying the law of propagation of variance to Equation 7.8 leads to:

$$\mathrm{cov}(DD) = \underline{C}_{DD}\, \mathrm{cov}(\underline{SD})\underline{C}_{DD}^{T} \tag{7.11}$$

and substituting Equation 7.7 into Equation 7.11 leads to:

$$\mathrm{cov}(DD) = \underline{C}_{DD}\underline{C}_{SD}\, \mathrm{cov}(\underline{\Phi})\underline{C}_{SD}^{T}\underline{C}_{DD}^{T} \tag{7.12}$$

and finally by letting:

$$\underline{C} = \underline{C}_{DD}\underline{C}_{SD} \tag{7.13}$$

the covariance of double differences becomes:

$$\mathrm{cov}(DD) = \underline{C}\, \mathrm{cov}(\underline{\Phi})\underline{C}^{T} \tag{7.14}$$

where:

$$\underline{C} = \begin{bmatrix} 1 & -1 & 0 & 0 & -1 & 1 & 0 & 0 \\ 1 & 0 & -1 & 0 & -1 & 0 & 1 & 0 \\ 1 & 0 & 0 & -1 & -1 & 0 & 0 & 1 \end{bmatrix} \tag{7.15}$$

is the pure phase to double difference operator matrix.

Finally, the double difference weight matrix may be formed:

$$P_{DD} = \left(\underline{C}\,\mathrm{cov}(\Phi)\underline{C}^{T}\right)^{-1} \tag{7.16}$$

where:

P_{DD} is the double difference weight matrix;

This leaves the double difference weight matrix that may be constructed by the covariance matrix of zero difference phase observations and a zero- to double-difference operator matrix.

To implement the SENR, the covariance matrix considering the zero difference (or pure phase observations) is formed using Equation 7.17:

$$\mathrm{cov}(\boldsymbol{\Phi}) = diag\left[1 \quad 1 \quad 1 \quad 1 \quad 1 \quad \sigma_{AB}^{jk\,2} \quad \sigma_{AB}^{jl\,2} \quad \sigma_{AB}^{jm\,2}\right] \tag{7.17}$$

where *A* and j represent the base station and base satellite respectively.

Note that in Equation 7.17, the pure phase variances of the base station observations are given unit weight (terms 1-4 in Equation 7.17), as is the base satellite phase observation at the non-base station (term 5 in Equation 7.17). This is an acceptable implementation, because the SENR represents a ratio with respect to a double difference observable unaffected by multipath (that is, SENR=1.0).

It is also immediately apparent that the SENR model does not fully populate the variance-covariance matrix of observations. This is a classical problem in GPS data processing with few models completely describing the stochastic properties of the data.

Figure 7.10 illustrates the DDOmC observed from satellite pair 19-24 during GPS week 1084, session 64 at Station 3. The elevation angle for the base satellite is approximately 80° and approximately 15° for the non-base satellite. By visual inspection, it can be seen that the satellite observations are significantly affected by unmodelled systematic error (most likely signal multipath). This is evident from the cyclical type trends (with a magnitude approaching 0.1 cycles) that are evident in the top graph. The middle graph illustrates the MAW_1 that is used in the SENR technique to de-trend the systematic errors within the data. Finally, the lower plot illustrates the noise level that remains after de-trending the systematic components of the data. The de-trending process is not used to remove the systematic errors in the data. It is only used for the calculation of the SENR, that is, the ratio of the noise level before and after de-trending.

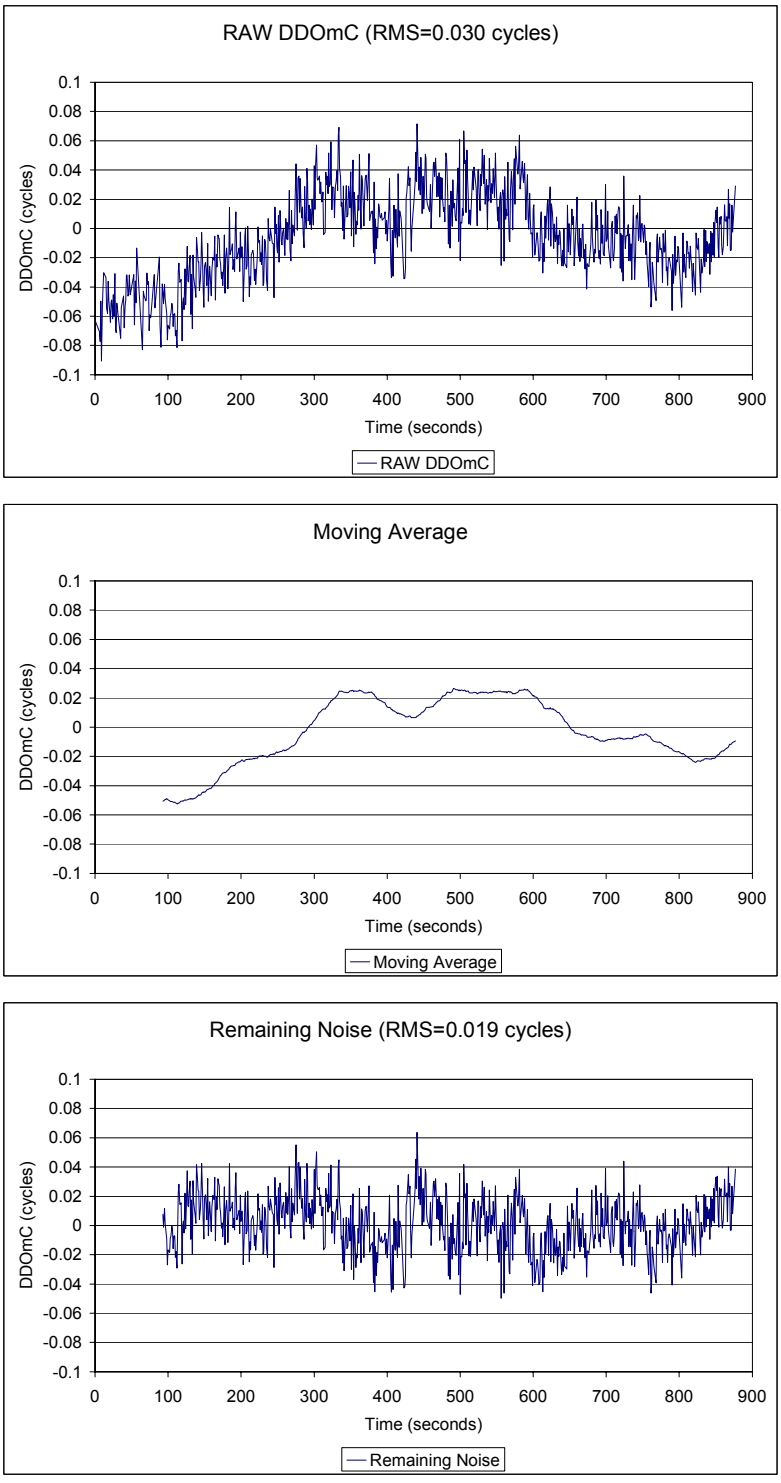

Figure 7.10 DDOmC in representing high multipath environment

The RMS of the raw DDOmC is calculated as 0.030 cycles, with the RMS after de-trending being 0.019 cycles. This results in a SENR of 1.55. When inverted, this would result in the observation being down-weighted by a factor of 0.645.

Figure 7.11 illustrates similar plots for double difference satellite observations not subject to high levels of systematic error.

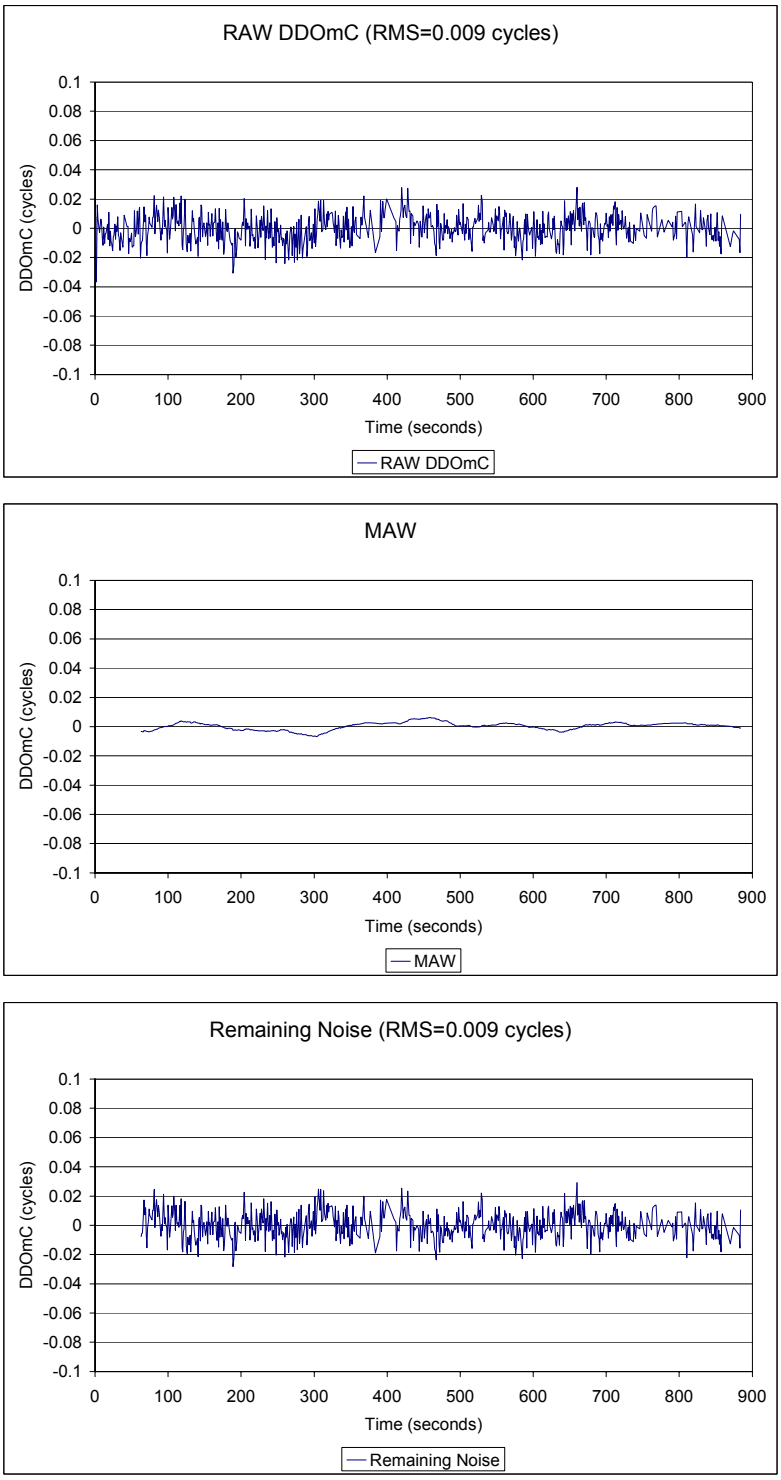

Figure 7.11 DDOmC in representing low multipath environment

Figure 7.11 illustrates similar plots for a satellite pair 19-27 for GPS week 1084, session 64 at Station 2. This station has unrestricted sky visibility with no multipath inducing obstructions at the deformation site. The elevation of the base satellite is approximately 85°, and the non-base satellite approximately 60°. The overall noise level is lower for this satellite pair than at Station 3. In this case, the SENR is computed as 1.015. Again, when inverted, this would result in the observation being down-weighted by a factor of 0.985, which is close to unity.

Data presented in Figure 7.10 and Figure 7.11 have illustrated some of the simpler cases experienced in GPS positioning. In the first case, the high multipath environment at Station 3, together with a low elevation non-base satellite, results in systematic error existing within the DDOmC parameters. In the second case, the low multipath environment at Station 2, combined with higher elevations for both the base and non-base satellites result in less systematic error delay. In both of these cases, elevation-based weighting models, such as the Sine and Han models would down-weight the lower elevation satellites in an effort to account for the increased noise expected from the remaining systematic error. The double difference standard deviations for the Sine and Han stochastic models, together with the weighting of the SENR model computed for this data, are shown in Table 7.4.

Stochastic Model	**Double Difference Observation Weights**	
	Satellite Pair	
	19-24	*19-27*
Sine	±5.65mm	±2.11mm
Han	±11.58mm	±6.02mm
SENR (ratio)	0.645 (1/1.550)	0.985 (1/1.015)

Table 7.4 Double difference weighting using various stochastic models

For each stochastic model, the observations between satellite pair 19-24 would be down-weighted with respect to the observations between satellite pair 19-27 in the least-squares estimation process. This seems appropriate, given the data characteristics of the DDOmCs presented in Figure 7.10 and Figure 7.11.

There are cases, however, where these elevation dependent models will not appropriately estimate the noise level of higher elevation satellites. Such an instance might be when a higher elevation satellite measurement is subjected to multipath, ionospheric delay and/or signal diffraction. In these cases, the elevation-only models will not appropriately model the remaining systematic errors.

An example of this situation is presented in Figure 7.12 illustrating satellite pair 19-27 for GPS week 1084, session 64.

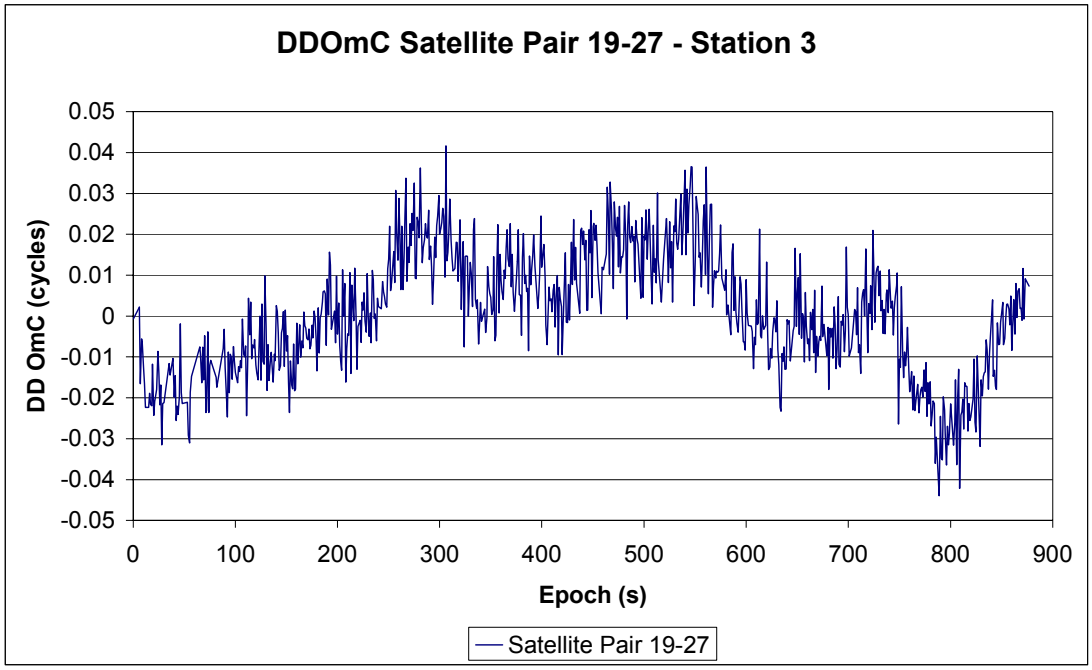

Figure 7.12 DDOmC for a high elevation satellite with systematic error

Figure 7.12 illustrates the DDOmC observations for satellite pair 19-27 at Station 3 for GPS week 1084, session 64. The base satellite has an elevation angle of approximately 80°, with a non-base satellite elevation of approximately 65°.

As discussed in section 3.4.2, both elevation dependent models have very little decay in the noise estimated for GPS observations above approximately 20° in elevation. Neither of these models accounts for the increased double difference noise that is experienced as a result of residual systematic error on the high elevation satellites illustrated above. Table 7.5 shows the various weighting values that can be calculated for the Sine, Han, and SENR stochastic models for the above data.

Stochastic Model	**Double Difference Observation Weights**
	Satellite Pair 19-27
Sine	±2.11mm
Han	±6.02mm
SENR (ratio)	0.714 (1/1.400)

Table 7.5 Double difference weighting for a high elevation satellite with systematic error

The observation weights that are calculated for this satellite pair by the Sine and Han stochastic models are the same as those calculated for the data presented previously for Station 2 in Figure 7.11 (which appears to be largely free from systematic error). It can be clearly seen that the systematic error present within the data from Station 3 for the same satellites with similar elevation angles should result in a lower weight being assigned to these double difference observations. From the three stochastic models presented, only the SENR considers this by reducing the associated observation weight (by 0.714 in this case).

One of the main advantages of the SENR stochastic model is that observation weights depend on the actual data that are recorded, rather than only on the associated elevation angle of each satellite. This may be one of the biggest advantages of this form of stochastic modelling technique.

7.2.4 Performance Evaluation of Stochastic Models

Similar testing procedures to those described in previous sections (sections 6.2-6.4 for example) have been implemented to evaluate the performance of the stochastic models under review. These models include the Han elevation model, the Sine elevation model and the SENR stochastic model. All are tested with respect to the Math model that only considers the mathematical correlations of the double difference observations.

Data from the 168 sessions of GPS week 1084 were processed for Station 0 and Station 3. The processing options are listed in Table 7.6 below.

Processing Parameter	**Values Used**
Processing Interval	1 second
Session Length	~15 minutes
Elevation Cut-off	10 degrees
Tropospheric Model	Saastamoinen
Double Difference Outlier Detection	0.2 cycles
Coordinate Update	Automatic
Stochastic Model	**Math, Han, Sine, SENR**

Table 7.6 Processing parameters for stochastic model performance evaluations

Comparative results for the evaluation of the four stochastic models are presented in Figure 7.13 for data collected during GPS week 1084 at Station 0.

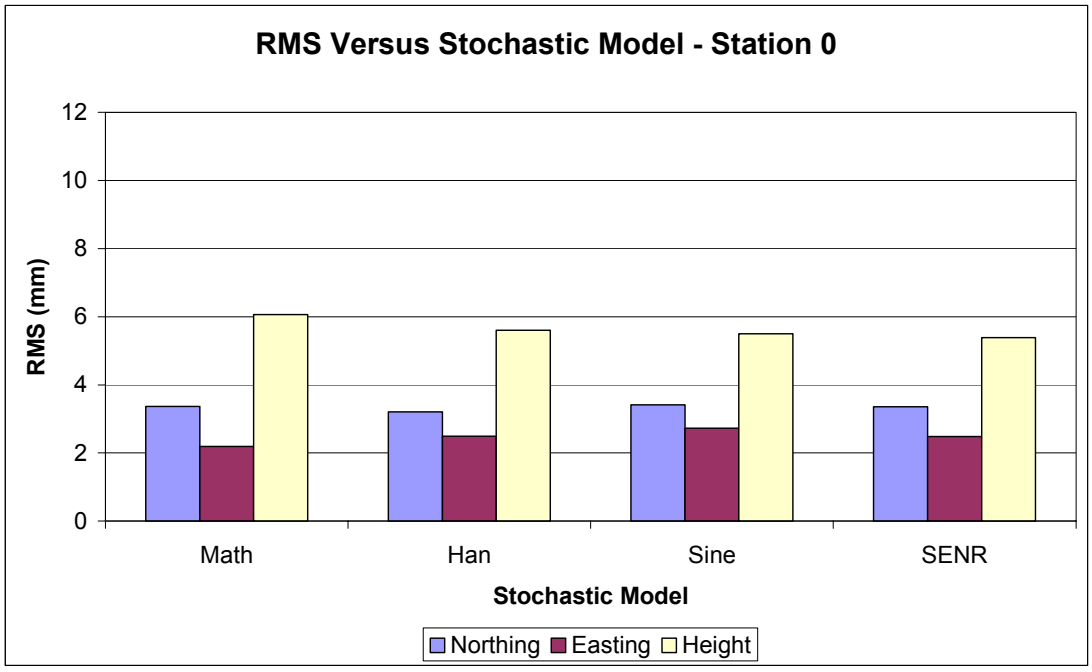

Figure 7.13 Comparative evaluation of RMS versus stochastic model – Station 0

From Figure 7.13, it can be seen that there is little difference between the Han, Sine and SENR stochastic models and the correlation-only mathematical model. In fact,

each of these models increases the noise level in the horizontal component. The horizontal noise level is computed as ±4.0mm for the Math model, ±4.0mm for the Han model, ±4.4mm for the Sine model and ±4.2mm for the SENR model. The RMS values in the height component are improved when the three models are implemented with respect to the Math model. The greatest improvement occurs with the use of the SENR stochastic model, where the RMS estimates are reduced from ±6.1mm to ±5.4mm in the height component. This corresponds to an improvement of approximately 11 percent in the height component when the SENR stochastic model is used.

Figure 7.14 shows similar results for tests applied at Station 3, which has reduced sky visibility and increased systematic error effects.

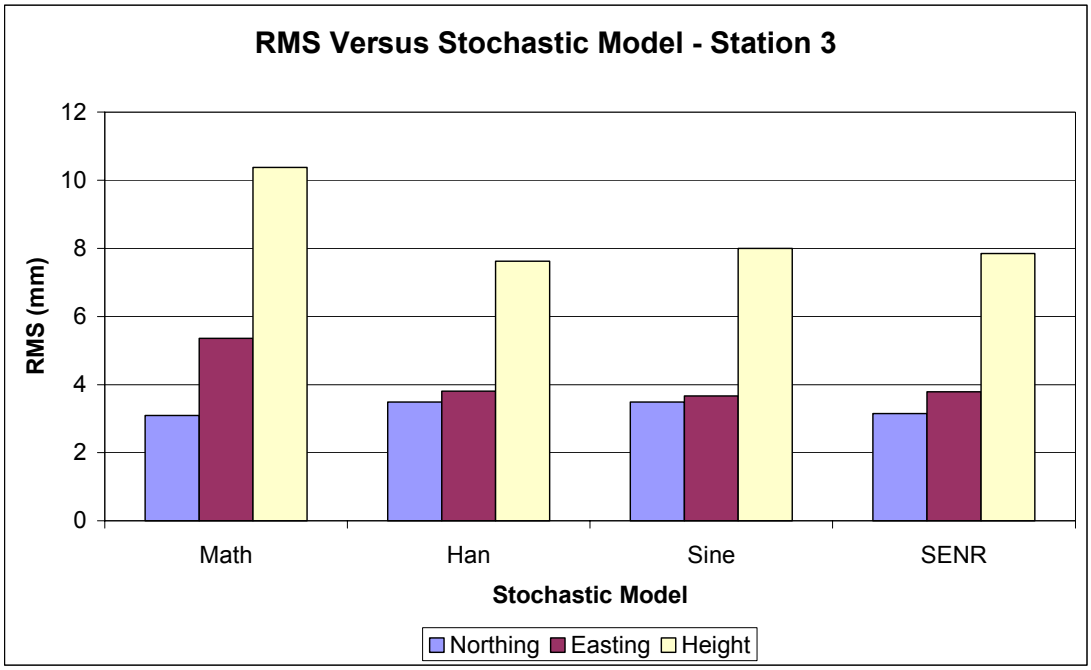

Figure 7.14 Comparative evaluation of RMS versus stochastic model – Station 3

Results from Station 3 illustrate that the difference in RMS recorded using the three stochastic models of Han, Sine, and SENR all result in an improvement in both the horizontal and height components. The maximum improvement in the horizontal component is obtained when the SENR model is used, which results in a 19.5 percent reduction in the RMS between the raw positional solutions and the MAW_2 used to

de-trend the data. In the height component a maximum improvement is obtained with the Han elevation weighting model. The implementation of this model results in a reduction of approximately 25 percent of the RMS values.

Also of interest is the improvement recorded in the easting component between the three models tested (Han, Sine, and SENR) and the Math only model when the sky visibility is restricted, as is the case at Station 3. The RMS in the easting component between the raw solutions and the MAW_2 is reduced by approximately 27 percent on average for the three models tested. The northing component, on the other hand, indicates an increase in the average RMS level of the three models of approximately 10 percent.

It has been shown that the implementation of even simple stochastic models can have a positive impact on the precision of coordinate solutions obtained in the deforming environment. The SENR offers a simple way to implement the stochastic modelling process that uses the noise level within the double difference data themselves to weight the observations.

7.3 GPS Quality Indicators

From a GPS deformation monitoring system perspective, it would be desirable to present the user with a quality indicator that could be used to assess the precision of each GPS-derived coordinate within the time-series. Two common internal quality indicators available from the least squares positioning process include the unscaled *a posteriori* unit variance factor and the standard errors from the covariance matrix. In GPS positioning, these parameters are overly optimistic due to the presence of correlation within the data. While the magnitude of these quality indicators may not realistically represent the precision of the resulting coordinate solution, it may be useful to evaluate the relative improvement (if any) that results from the selection of the stochastic models presented in the previous section. In particular, it is of interest to evaluate whether the internal quality indicators become more realistic with the use of an improved stochastic model. To evaluate this, the correlation coefficient (hereafter denoted as r) was computed between the difference between the raw data and the MAW_2 trend, and the internal quality indicators from the GPS processing for

each point in the time-series. Again, GPS week 1084 was used to evaluate any correlation that may exist between the two forms of quality indicators. Figure 7.15 illustrates the correlation coefficient between the precision of each coordinate value for GPS week 1084 (the difference between the data and trend extracted using a 40 session MAW_2) and the internal standard deviation estimated from the GPS positioning software (*Multibas*).

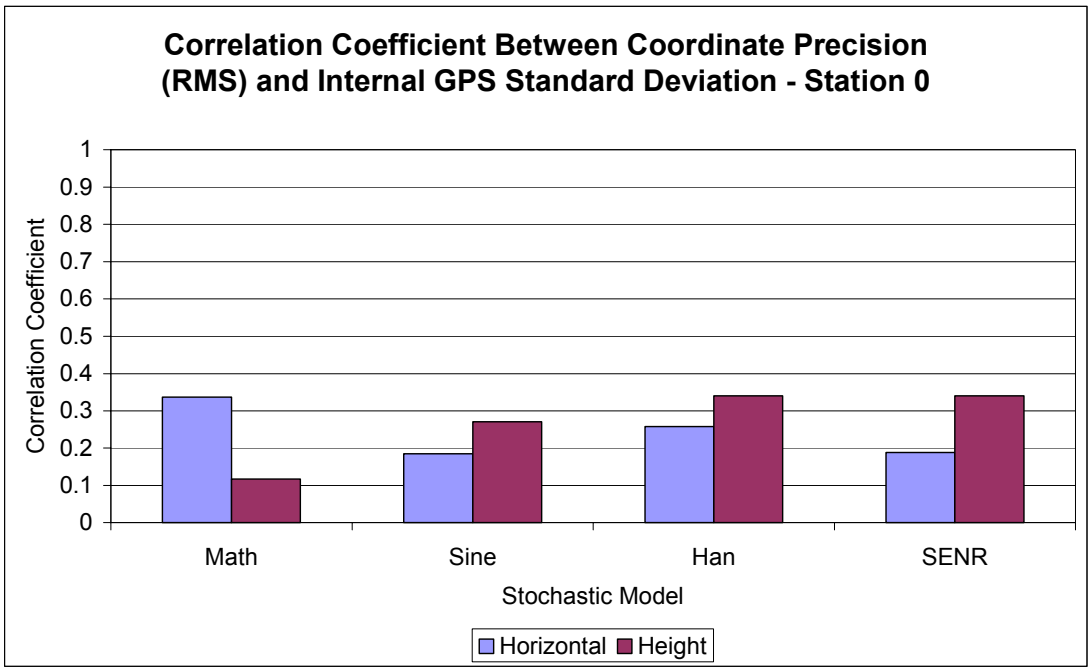

Figure 7.15 Correlation coefficient between coordinate precision and internal GPS standard deviation – Station 0

It can be seen that in all cases, a relatively low correlation exists between the coordinate precision values computed and the precision estimates from the GPS processing software. The Math stochastic model provides the most correlated estimates for the horizontal component (r = 0.34), while the Sine stochastic model provides the least correlated estimates (r = 0.18). In the height component, the use of the Han and SENR stochastic models result in the highest correlation coefficients with r = 0.34. The use of the Math stochastic model provides the poorest correlation between coordinate precision and internal GPS standard deviation with r = 0.18.

Similar correlation coefficients have been computed for Station 3 from data throughout GPS week 1084. These results, illustrated in Figure 7.16, show that a

higher correlation exists between the coordinate precision and the standard errors computed within the GPS processing software when a high level of systematic error (namely multipath) exists within the data.

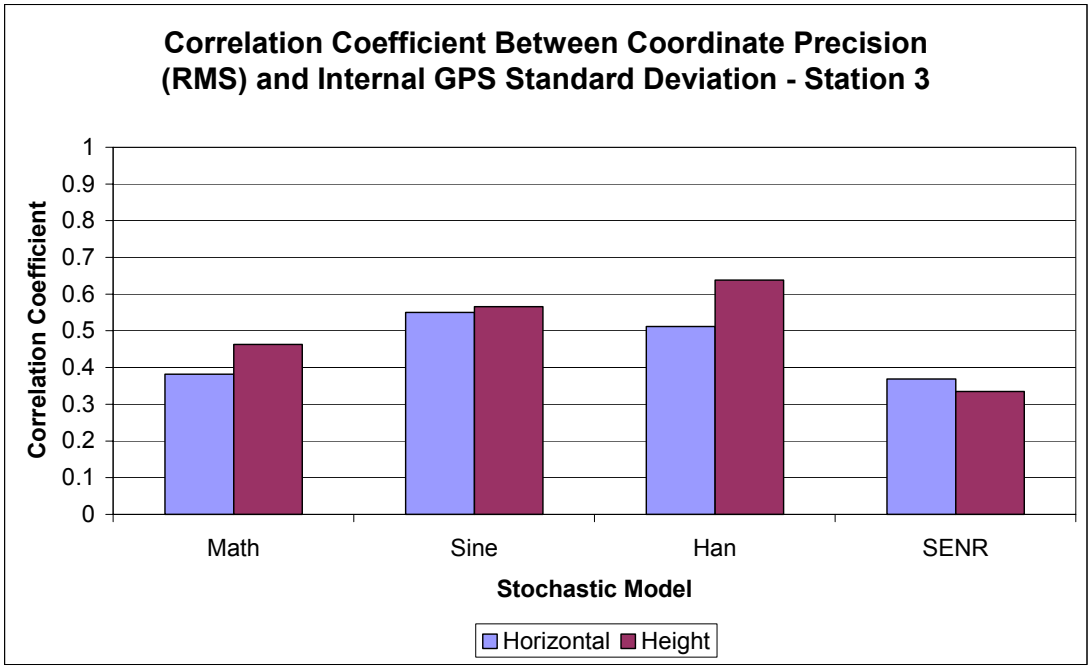

Figure 7.16 Correlation coefficient between coordinate precision and internal GPS standard deviation – Station 3

Under the conditions observed at Station 3, where the dominant error source is likely to be signal multipath, the correlation coefficient between the computed coordinate precision and the standard errors from the GPS processing software are most correlated for the horizontal component when the Sine model is used (r = 0.55). The highest level of correlation is experienced when the Han stochastic model is used (r = 0.64). The lowest correlations in both the horizontal and horizontal component result from the SENR stochastic model, where r = 0.37, and r = 0.34 respectively.

Similar correlation coefficients can be calculated between the coordinate precision estimates and the *a posteriori* standard deviation at Station 0 for GPS week 1084. In this case, the *a posteriori* standard deviation is computed by taking the square root of the unscaled unit variance. The *a posteriori* standard deviation is used in preference to the *a posteriori* unit variance for parameter consistency in the correlation computation process.

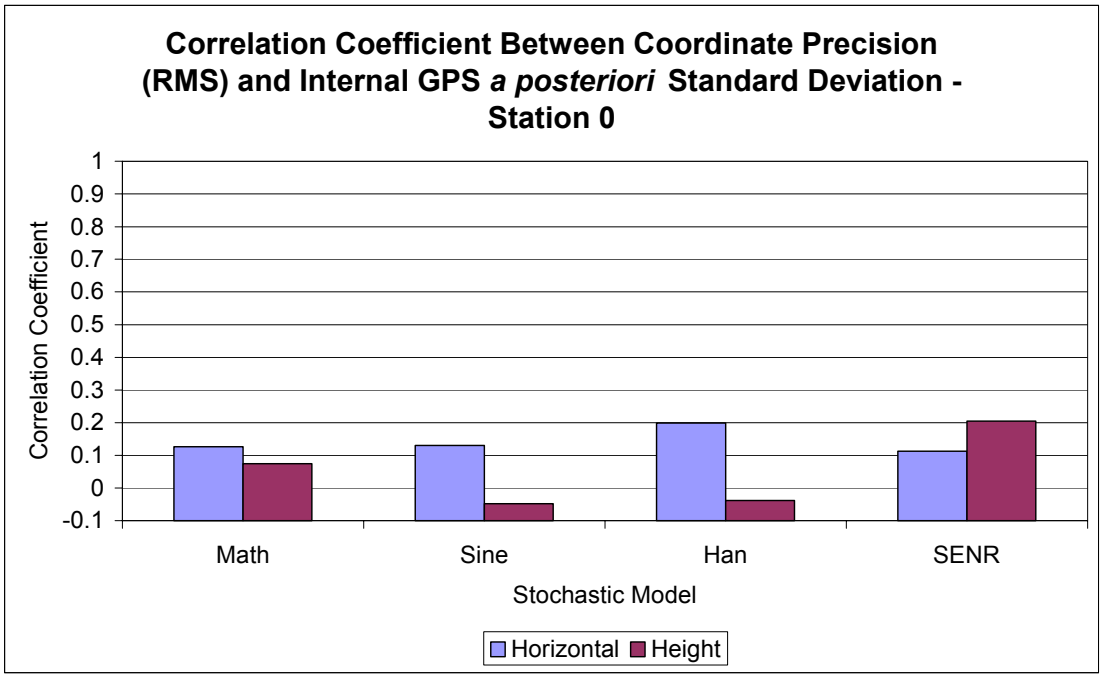

Figure 7.17 Correlation coefficient between coordinate precision and internal GPS *a posteriori* standard deviation – Station 0

The correlation coefficient calculated between the coordinate precision as computed by the RMS differences and the *a posteriori* standard deviations also indicate that a relatively poor correlation exists between the two data sets.

These results support similar findings presented by Barnes and Cross (1998) who indicate that the standard errors and the unit variance (*a posteriori* standard deviation squared in this case) do not correlate well with true precision estimates.

The correlation coefficients between coordinate precision and the *a posteriori* standard deviation computed at Station 3 are represented in Figure 7.18. These results also suggest that a higher level of correlation is apparent under the conditions of increased sky masking and signal multipath at Station 3.

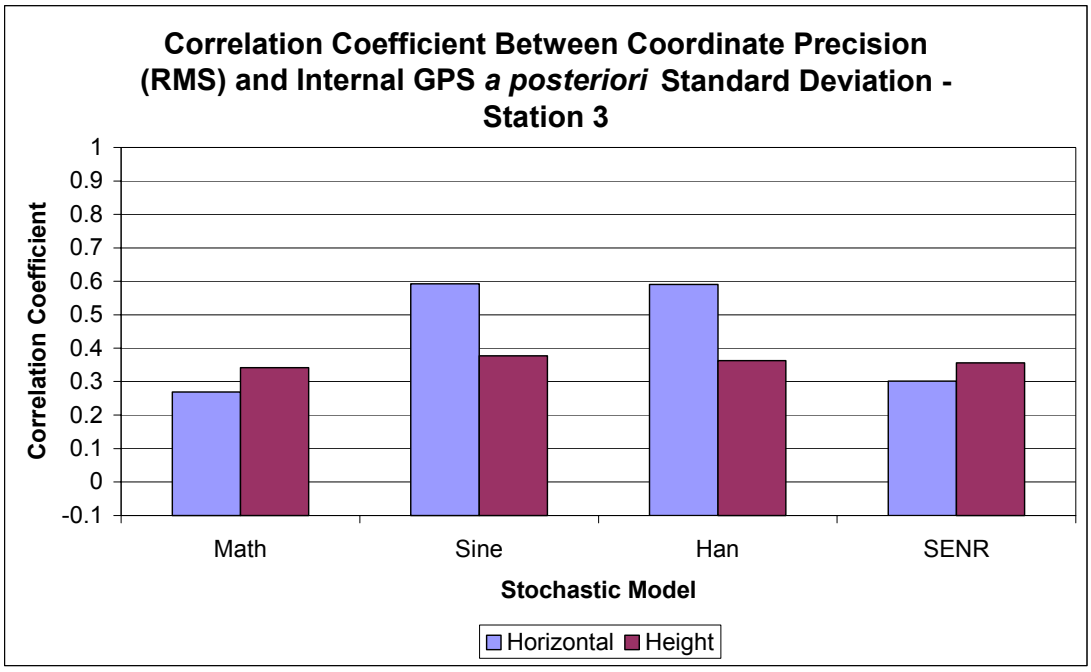

Figure 7.18 Correlation coefficient between coordinate precision and internal GPS standard deviation – Station 3

The Sine and Han stochastic models produce the greatest correlations in the horizontal component (r = 0.59 in both cases). Similar correlation coefficients for the height component are calculated for all stochastic models tested (where r varies between 0.34-0.38).

The least squares precision indicators obtained from the GPS processing software are more correlated with the coordinate precision estimates computed from the time-series of the data at Station 3 than under the conditions tested at Station 0. This is particularly evident with the use of the Sine and Han stochastic models (for the horizontal component at least) which implies that these two models better approximate errors within the data. It should be remembered, however, that the stochastic models tested are diagonal in nature and that more realistic estimates may be possible by fully populating the covariance matrix.

The results presented above indicate that, typically, only a low correlation exists between the internal GPS quality indicators and the resulting GPS coordinate precision. In this case, the internal quality indicators may not provide realistic

estimates of the actual precision of the resulting coordinates. The use of these indicators as a quality measure should be used with caution.

7.4 Summary

This chapter has investigated the effect of changing the processing characteristics of the data collected to optimise the precision of the coordinate time-series that can be obtained in a quasi-continuous monitoring mode for high precision deformation monitoring applications.

Stacking techniques have been investigated, highlighting some deficiencies in the fundamental assumptions used in previous research in this field. While these assumptions have been imposed to simplify the problem of multipath mitigation, they do not necessarily hold true under all positioning circumstances. More research is needed to find an appropriate way of mitigating the remaining systematic error sources within GPS data for high-precision positioning applications.

The SIGMA-Δ, Sine and Han stochastic models were also tested for one surface station (Station 0) and the sub-surface station (Station 3). These tests indicate that the SIGMA-Δ model does not substantially improve the precision of the coordinate time-series, while improvements are possible with the use of the elevation dependent stochastic models denoted as Sine and Han.

A new stochastic modelling procedure, using the systematic error-to-noise ratio (SENR) has been proposed, based on the level of systematic error that remains within the double difference data. While this model comprises only a small portion of this research, it offers a promising alternative to the current stochastic modelling procedures in use. Moreover, it has been illustrated that the correct choice of stochastic model can have a positive impact on the precision of the coordinate solutions that are obtained.

Finally, the quality indicators of the GPS standard error estimates and the *a posteriori* standard deviations were evaluated with respect to the precision of the resulting GPS coordinates. The correlation coefficients between these quality

indicators and the resulting coordinate precision indicated that these quality indicators do not provide a reasonable estimate of the actual precision of the GPS coordinates. These quality indicators should, therefore, be used with caution for high precision deformation monitoring of steep slopes such as these tested in this research.

8. CONCLUSIONS AND RECOMMENDATIONS

8.1 Summary

The monitoring of steep slopes is an important issue for many geotechnical engineering operations. Very few single-system monitoring methods can provide 3D information about the dynamics of deforming movements within a steep slope environment. The use of GPS offers one method that can provide accurate and precise positional and velocity information of discrete points on the slope surface. Unfortunately, establishing CORS networks can be expensive due to high hardware costs. Episodic monitoring techniques can provide a cheaper alternative but have the disadvantage of a lower temporal resolution of the resulting coordinate time-series.

In an effort to bridge the gap between these two types of GPS monitoring systems, a dedicated multi-antenna monitoring method has been proposed in this thesis. This method has the advantage of reducing the amount of GPS equipment required to monitor multiple points, while offering the dense coordinate time-series required to adequately model the deforming movements at each point.

A prototype of the system was designed and installed in an open-pit nickel mine at Mount Keith in central Western Australia. The system was installed after cut-back operations were performed on the face of the mine wall. Normally, a relaxation response of the wall is expected to result from the unloading of the face mass. Deforming movements were detected using the multi-antenna monitoring system by the placement of antennas at 4 monitoring points. The maximum 3D displacement of the GPS antenna on one section of the wall was recorded as approximately 135mm over a 16-week observation period. Interestingly, after these field trials ended, access ramps below this section of the wall were closed for fear of impending wall failure. Unloading options were then examined by the geotechnical engineers to reduce the build-up of stresses within the wall mass.

To determine an optimal processing strategy for high precision GPS deformation monitoring, simple factors such as the choice of elevation masking angle, data collection and processing interval, and observation span length have all been evaluated. The stochastic modelling of the GPS observations was also investigated based on both elevation and carrier-to-noise power density ratio techniques. The assumptions supporting data stacking techniques were evaluated to determine if they could be used to improve the coordinate precision of GPS observations in high multipath environments. Both observable and coordinate stacking solutions were investigated to this end. A new stochastic modelling procedure was also formulated which weighted observations based on the level of systematic error remaining within the GPS double difference observations. Finally, the correlation between two common GPS quality indicators and the precision of the respective coordinate solutions has been investigated.

8.2 Specific Outcomes

This research has investigated the use of a multi-antenna GPS positioning method to monitor deforming movements on steep slopes. The work conducted provides a comprehensive framework of GPS slope deformation monitoring, particularly for the open-pit mining environment. Some of the specific outcomes of this research are listed below.

8.2.1 Design and Implementation of a Multi-Antenna Array GPS Monitoring System

Historically, the prohibitive cost of employing CORS has been the need to establish one complete GPS system (including GPS receiver, antenna, communications system, antenna cables, and a power supply) at each monitoring location. It has been shown in this research that by switching between a number of GPS antennas, it is possible to monitor multiple locations with a single GPS receiver and associated peripheral hardware. This research involved the design and development of one such prototype system through the construction of all the hardware, software, and communications components necessary to conduct quasi-continuous monitoring at multiple stations.

Western Mining Corporation's Mount Keith nickel mine in central Western Australia hosted the system at which two reference stations (REF and BASE) and four monitoring stations were established (0, 1, 2, and 3). Of these, Stations 0, 1, and 2 were situated at ground level, and Station 3 was situated approximately 45m below the surface and approximately 4m away from the pit wall.

8.2.2 Initial Test Results

Initial test results were generated through the introduction of a set of benchmark processing parameters. Using a simple moving average window to filter the time-series of these coordinate solutions, the maximum displacement (of Station 3) was calculated as 134.6mm.

From the initial test results, the following can also be concluded:

- Horizontal solution precision approached ±4.0mm for surface stations and ±6.7mm for stations experiencing significant satellite masking and severe multipath delay errors;
- Ellipsoidal height solution precision ranged from ±8.4mm under favourable visibility and multipath conditions through to ±13.7mm under poorer conditions;
- Increasing the number of GPS reference stations (from one to two) improved the geometrical strength of the GPS network solution which resulted in an average improvement in the noise level of the coordinate time-series of approximately 47 percent in the horizontal component and 48 percent in height for surface stations (section 5.3.2). Similar improvements of approximately 54 percent and 52 percent in the horizontal and height components were calculated for the station located next to the pit wall;
- The operational stability and reliability of the multi-antenna array monitoring system developed can provide continuous positioning capabilities without the need for high levels of user intervention (section 5.3.9). Data gaps occurred from procedural problems of data backup and power problems on-site. While

these are not considered major problems, they must be addressed to ensure that system reliability is maintained;

- The long antenna cables used in this research (up to 340m) appeared to work effectively, with no loss of system efficiency.

8.2.3 Optimisation of Processing Parameters for GPS Deformation Monitoring

In an effort to improve the positioning results generated, the following conclusions and comments can be made:

- Simulation tests were developed (section 6.1) to test the dispersion estimates of various detrending methods. In conditions where there is no *a priori* information regarding the dynamics of the deformation (and hence the resulting coordinate time-series), the simple moving average window can be used as an effective data filter;
- For the use of GPS positioning techniques where integer rounding of the double difference observations is used in an epoch-by-epoch manner, automatic coordinate updates are required for the initial parameter estimations within the least squares positioning process (section 6.2). Again, simple moving average window filters combined with linear interpolation can be used to extract precise approximates of the initial coordinates;
- A simple double difference observation rejection strategy (section 6.3) can be implemented to remove single GPS observations that have an unacceptable level of noise. The bound for this technique was chosen as ±0.2 cycles, provided that the initial approximate parameters (coordinates) are of sufficiently high precision;
- Under conditions of reduced satellite visibility, GPS observations below approximately 10° elevation provide more noise than is gained by the increased satellite geometry from the extra observations included (section 6.4);
- Reducing the sampling frequency of the monitoring campaign can substantially reduce the trend extraction capability of the system. This may lead to a reduction in the confidence of the results and possibly obstruct the

decision making process regarding safety considerations of catastrophic wall failure (section 6.7).

8.2.4 Advanced Techniques for GPS Deformation Monitoring

Advanced techniques for monitoring using GPS have involved the investigation of data stacking and improved stochastic modelling techniques. From this, the following conclusions may be drawn:

- Stacking techniques that rely completely on the presence of correlated multipath signatures within the double difference observations may not adequately consider the decorrelation effects from other error sources (section 7.1);
- For the positioning scenarios tested, the SIGMA-Δ model does not appear to provide significant improvements to the precision of the positioning results obtained (section 7.2.1);
- Elevation angle stochastic models and the Systematic Error to Noise Ratio (SENR) stochastic model can provide improved precision of the coordinate time-series (section 7.2.2 to 7.2.4). Reductions to the noise level of the coordinate time-series of approximately 20 percent in the horizontal and 25 percent in height components respectively have been demonstrated;
- A high level of correlation does not always exist between internal quality indicators and coordinate precision (section 7.3). Without further testing, the use of the internal least squares quality indicators as a precision estimator should be used with caution. These results may rely on an adequate definition of the stochastic model used in the GPS positioning process.

8.3 Recommendations and Future Work

There are many areas within GPS deformation monitoring that may benefit from continued research. Based on the findings of this research, the following recommendations for future work are proposed.

The research conducted within this thesis has used equipment that represents the state of the art in GPS hardware technology. The use of cheaper hardware components could be used to further reduce the cost of installing a dedicated system such as the one presented in this thesis. Meteorological sensors at each monitoring location (for example, within the XA controller used for data communications) could also assist in improving coordinate precision by allowing differential atmospheric effects to be monitored.

Stochastic modelling of observations is a continuing research topic for high precision GPS positioning. The SENR stochastic modelling process introduced in this thesis offers an interesting approach to this problem by utilising the information about the characteristics of the data from the raw observations. This is particularly useful when positioning in conditions that experience signal distortion such as multipath and diffraction. This process appears to be an intuitive approach to the problem of correctly estimating the noise characteristics of GPS observations. However, there is still much work to be completed in this area to further optimise the stochastic modelling process for GPS observations in general.

Data stacking is another emerging data analysis technique that may enhance the precision achievable of GPS deformation monitoring systems. The findings of this research suggest that the assumptions on which these techniques are based may not be completely realistic for slope deformation monitoring in the mining environment. It is recommended that these techniques be used with caution, until further research can validate their use in similar environments. This may require a complete investigation into each of the contributing error sources in GPS positioning.

The unexpected spectrum of the coordinate time-series generated in this research requires further investigation to determine if other data sets collected under similar circumstances would exhibit similar problems.

Realistic quality indicators are also a necessary component of any automated monitoring system. The generation of realistic quality estimators from the internal least squares statistics can assist the user in making safety-based decisions concerning the stability of the steep slope under consideration. Further investigation

into this issue should consider the appropriateness of the stochastic model, such as a fully populated variance-covariance matrix, together with the temporal correlations that are present within the GPS data.

Augmented GPS systems under development may provide enhanced deformation monitoring capabilities to further improve the accuracy and precision of monitoring results attainable in areas similar to those tested within this research. Such systems include Wide Area Augmentation Systems (WAAS), Galileo, and the use of ground-based GPS transmitters (pseudolites). Research into these augmentation systems will enhance the robustness of the deformation monitoring system, while also improving the error detection and mitigation capabilities of the deformation monitoring system.

Further investigation into the application of statistical testing methods in the presence of unmodelled systematic error for GPS coordinate time-series is required to ensure that the quality indicators used to evaluate GPS solution precision are both realistic and robust. The presence of unmodelled error, particularly when the errors cover a broad frequency spectrum, reduces the confidence of standard statistical testing methods, by which comparative evaluations of system performance are normally made. A detailed evaluation into advanced methods for evaluating precision and accuracy estimators under the conditions experienced in this research would make a substantial contribution to geodetic community.

REFERENCES

Alber, C., Ware, R.H., Rocken, C. and Braun, J.J. (2000) Obtaining Single Path Delays from GPS Double Differences, *Geophysical Research Letters*, Vol, 27, No. 7, pp. 2661-2664.

Allnut, J.E. (1989) *Satellite-to-Ground Radiowave Propagation*, Peter Peregrinus Ltd., London, UK, 421 pp.

Anderson, D., Sweeney, D. and Williams, T. (1991) *Introduction to statistics: Concepts and Applications* (2nd Edition), West Publishing, New York, USA, 714 pp.

Angeli, M.G., Gasparetto, P., Pasuto, A. and Silvano, S. (1989) Examples of Landslide Instrumentation, *Proceedings of the 12th International Conference on Soil Mechanics and Foundation Engineering*, Rio de Janeiro, Brazil, pp. 1531–1534.

Angeli, M.G., Gasparetto, P., Silvano, S. and Tonetti, G. (1988) An Automatic Recording System to Detect the Critical Stability of Slopes, *Proceedings of the 5th International Symposium on Landslides*, Lau-sanne, Switzerland, pp. 375–378.

AUSLIG (2001) *Australian Surveying and Land Information Group Online GPS Processing Service*, http://www.auslig.gov.au/geodesy/sgc/wwwgps/wwwgps.htm

Baltsavias, E.P. (1999) Airborne Laser Scanning: Basic Relations and Formulas, *ISPRS Journal of Photogrammetry and Remote Sensing*, Vol. 54, No. 2 – 3, pp. 199–214.

Barnes, J.B. and Cross, P.A. (1998) Processing Models for Very High Accuracy GPS Positioning, *Journal of Navigation*, Vol. 51, No. 2, pp. 180-193.

Behr, J.A., Hudnut, K.W. and King, N.E. (1998) Monitoring Structural Deformation at Pacoima Sam, California Using Continuous GPS, *Proceedings of the 11th International Technical Meeting of the Satellite Division of the Institute of Navigation ION-98*, Nashville, Tennessee, USA, September 15-18, pp. 59-68.

Beutler, G., Gurtner, W., Bauersima, I. and Rothacher, M. (1986) Efficient Computation of the Inverse of the Covariance Matrix of Simultaneous GPS Carrier Phase Difference Observations, *Manuscripta Geodetica*, Vol. 11, pp. 249-255.

Black, H.D. (1978) An Easily Implemented Algorithm for the Tropospheric Range Correction, *Journal of Geophysical Research*, Vol. 84, No. B4, pp. 1825-1828.

Blewitt, G. (1998) GPS Data Processing Methodology, in: *GPS for Geodesy*, Kleusberg A. and Teunissen P.J.G. (ed.), Springer-Verlag, Berlin, Germany, pp. 231-270.

Bock, Y., Abbot, R.I., Councelman, C.C., Gourevitchm, S.A. and King, R.W. (1986) Interferometric Analysis of GPS Phase Observations, *Manuscripta Geodetica*, Vol. 11, pp. 282-288.

Bock, Y., de Jong, P. de Honcik, D., Bevis, M., Bock, L. and Wilson, S. (2001) Epoch-By-Epoch™ Positioning Applied to Dam Deformation Monitoring at Diamond Valley Lake, Southern California*, Proceedings of the 10th FIG International Symposium on Deformation Measurements*, Orange, California, USA, March 19-22, pp. 78-87.

Bock, Y., Nikolaidis, R.M., de Jonge, P. and Bevis, M. (2000) Instantaneous Geodetic Positioning at Medium Distances with the Global Positioning System, *Journal of Geophysical Research*, Vol. 105, No. B12, pp. 28223-28255.

Bonnard, C. and Steinmann, G. (1990) Continuous measurement of landslide measurements, *Geotechnical Instrumentation in practice: Purpose, performance and* interpretation, Institution of Civil Engineers, Thomas Telford, London, UK, pp. 177-189.

Braun, J., Rocken, C. and Ware, R. (2001) Validation of Line-of-Sight Water Vapour Measurements with GPS, *Radio Science*, Vol. 36, No. 3, pp. 459-472.

Brigham, E. O. (1974) *The Fast Fourier Transform*, Prentice-Hall Inc., New Jersey, USA, 252 pp.

Brown, A. (2000) Multipath Rejection Through Spatial Processing, *Proceedings of the 13th International Technical Meeting of the Satellite Division of the Institute of Navigation ION GPS-2000*, Salt Lake City, Utah, USA, September 19-22, pp. 2330-2337.

Brunner, F.K., Hartinger, H. and Ritcher, B. (2000) Continuous Monitoring of Landslides using GPS: A Progress Report, in: *Proceedings of the Geophysical Aspects of Mass Movements*, *Bauer, S.J. and Weber, F.K.* (ed.), Austrian Academy of Sciences, Vienna, Austria, pp. 75-88.

Brunner, F.K., Hartinger, H. and Troyer, L. (1999) GPS Signal Diffraction Modelling: the SIGMA-Δ model, *Journal of Geodesy*, Vol. 73, pp. 259-267.

Chen, Y., Ding, X., Huang, D., and Zhu, J. (2000) A Multi-Antenna GPS System for Local Area Deformation Monitoring, *Earth, Planets and Space*, Vol. 52, No. 10, pp. 873-876.

Corominas, J., Moya, J., Lloret, A., Gili, J.A., Angeli, M.G., Pasuto, A. and Silvano, S. (2000) Measurement of Landslide Displacements using a Wire Extensometer, *Engineering Geology*, Vol. 55, No.3, pp. 149-166.

Cross, P.A. (1994) Advanced Least Squares Applied to Position Fixing, *Working Paper No. 6*, North East London Polytechnic, London, UK, 205 pp.

Cross, P.A., Hawksbee, D.J. and Nicolai, R. (1994) Quality Measures for Differential GPS Positioning, *The Hydrographic Journal*, No. 72, pp. 17-22.

Dai, L., Zhang, J., Rizos, C., Han, S. and Wang, J. (2000) GPS and Pseudolite Integration for Deformation Monitoring Applications, *Proceedings of the 13th International Technical Meeting of the Satellite Division of the Institute of Navigation ION GPS-2000*, Salt lake City, USA, September 19-22, pp. 1-7.

de Heus, H. (1997) Subsidence Monitoring with GPS in the Netherlands, *Proceedings of the International Symposium on: Current Crustal Movement and Hazard Reduction*, Wuhan, China, November, Seismological Press, Beijng, China, pp. 184-195.

de Jonge, P.J. and Tiberius, C.C.J.M (1996) The LAMBDA Method for Integer Ambiguity Estimation: Implementation Aspects LGR Series No. 12, Delft Geodetic Computing Centre, 49 pp.

Ding, X., Chen, Y., Huang, D., Zhu, J., Taskiri, M. and Stewart, M. (2000) Slope Monitoring using GPS – a Multi-Antenna Approach, *GPS World*, Vol. 11, No. 3, pp. 52-55.

Ding, X., Chen, Y., Zhu, J. and Huang, D. (1999) Surface Deformation Detection Using GPS Multipath Signals, *Proceedings of the 12th International Technical Meeting of the Satellite Division of the Institute of Navigation ION GPS-99*, Nashville, Tennessee, September 14-17, pp. 53-62.

Department of Minerals and Energy (2000) *External Information System (Exis) database*, Western Australia, http://www.dme.wa.gov.au/prodserv/remote/exis.html

Duffy, M.A., Hill, C., Whitaker, C., Chrzanowski, A., Lutes, J. and Bastin, G. (2001) An Automated and Integrated Monitoring Program for Diamond Valley Lake in California, *Proceedings of the 10th FIG International Symposium on Deformation Measurements*, Orange, California, USA, March 19-22, pp. K1-K23.

Dunnicliff, J. (1988) *Geotechnical Instrumentation for Monitoring Field Performance*, John Wiley, New York, USA, ISBN 0471005460, 608 pp.

El-Filky, G.S., Kato, K. and Oware, E.N. (1999) Crustal Deformation and Interplate Coupling in the Shikoku District, Japan, as seen from Continuous GPS Observation, *Techniphysics*, Vol. 314, pp. 387-399.

Featherstone, W., Forward, T.A., Penna, N. T., Stewart, M. P., Tsakiri, M., McCarthy, R., Houghton, H. and Xanthis, G. (2001) Establishment of GNSS Testing and Validation Facilities in Perth, Western Australia, *Proceedings of*

the 5th International Symposium on Satellite Navigation Technology and Applications, Canberra, Australia, July 24-27, 2001, paper No. 10, 10 pp.

Fenton, P., Falkenberg, B., Ford, T., Ng, K. and van Dierendonck, A.J. (1991) Novatel's GPS Receiver: The High Performance OEM Sensor of the Future, *Proceedings of the 3rd International Technical Meeting of the Satellite Division of the Institute of Navigation ION GPS-91*, Albuquerque, New Mexico, September 9-13, pp. 49-58.

Garin, L., van Diggelen, F. and Rousseau, J. (1996) Strobe & Edge Correlator Multipath Mitigation for Code, *Proceedings of the 9th International Technical Meeting of the Satellite Division of the Institute of Navigation ION GPS-96*, Kansas City, USA, September 17-20, pp. 657-664.

Garin, L. and Rousseau, J. (1997) Enhanced Strobe Correlator Multipath Rejection for Code and Carrier, *Proceedings of the 10th International Technical Meeting of the Satellite Division of the Institute of Navigation ION GPS-97,* September 16-19, Kansas City, USA, pp. 559-568.

Ge, L., Chen. H.-Y., Han, S. and Rizos, C. (2000) Adaptive Filtering of Continuous GPS Results, *Journal of* Geodesy, Volume *74,* No. 7/8, pp. 0572-0580.

Gelb, A. (ed.) (1996) *Applied Optimal Estimation*, MIT Press, Cambridge, UK, 374 pp.

Gerdan, G. P. (1995) A comparison of Four Methods of Weighting Double Difference Pseudorange Measurements, *Trans Tasman Surveyor*, Vol. 1, No. 1, pp. 60-66.

Giani, G.P. (1992) *Rock Slope Stability Analysis*, A.A. Balkema, Rotterdam, Netherlands, ISBN 90 5410 122 9, 361 pp.

Gili, J.A., Corominas, J. and Rius, J. (2000) Using Global Positioning System Techniques in Landslide Monitoring, *Engineering Geology*, Vol 55, pp. 167-192.

Goad, C.C. and Goodman, L. (1974) *A modified Hopfield Tropospheric Refraction Correction Model,* Paper presented at the American Geophysical Union Fall Annual Meeting, San Francisco, California, USA, December 12-17, 28 pp.

Green, P.J. and Silverman, B.W. (1994) *Nonparametric Regression and Generalized Linear Models*, Chapman & Hall, London, UK, 182 pp.

Grenrich, J.F. and Bock, Y. (1992) Rapid Resolution of Crustal Motion at Short Ranges with the Global Positioning System, *Journal of Geophysical Research*, Vol. 97, No. B3, pp. 3261-3269.

Han, S. (1997) Quality-Control Issues Relating to Instantaneous Ambiguity Resolution for Real-Time GPS Kinematic Positioning, *Journal of Geodesy*, Vol. 71, No. 6, pp. 351-361.

Han, S. and Rizos, C. (2000) GPS Multipath Mitigation using FIR filters, *Survey Review*, Vol. 35, pp. 487-498.

Hand, D. (2000) Report into the Inquest into the Deaths Arising from the Thredbo Landslide, *Coroners Report*, NSW Attorney Generals Department, 29th June, 205 pp.

Hartinger, H. and Brunner, F.K. (1999) Variances of GPS Phase Observations: the SIGMA-ε Model, *GPS Solutions*, Vol. 2, No. 4, pp. 35-43.

Hartinger, H. and Wieser, A. (2000) The SIGMA-Models for GPS Phase Observations, *Contributions to the work of IAG SSG 1.182 Multipath mitigation*, 7 pp.

Hofmann-Wellenhof, B., Lichtenegger, H. and Collins, J. (1997) *GPS Theory and Practice* (4th Revised Edition), Springer-Verlag, New York, USA, 389 pp.

Hudnut, K.W., Bock, Y., Galetzka, J.E., Webb, F.H. and Young, W.H. (2001) The Southern California Integrated GPS Network (SCIGN), *Proceedings of 10th International Symposium on Deformation Measurements*, Orange, USA, March 19-22, pp. 129-148.

Jia, M., Tsakiri, M. and Stewart, M. (2000) Mitigating Multipath Errors using Semi-Parametric Models for High Precision Static Positioning, *International Association of Geodesy Symposia, Geodesy Beyond 2000 - The Challenges of the First Decade*, Vol. 121, pp. 393-398.

Jin, X. (1996) Theory of Carrier Adjusted DGPS Positioning Approach and some Experimental Results, *PhD Dissertation*, Delft University, Delft University Press, Netherlands, 162 pp.

Julg, T. (1996) Evaluation of Multipath Error and Signal Propagation in a Complex Scenario for GPS Multipath Identification, *Proceedings on the IEEE Symposium on Spread Spectrum Techniques and Applications*, Vol. 2, pp. 872-876.

King, N.E., Svarc, J.L., Fogleman, E.B., Gross, W.K., Clark, K.W., Hamilton, G.D., Stiffler, C.H. and Sutton, J.M. (1995) Continuous GPS Observations across the Hayward Fault, California, 1991-1994, *Journal of Geophysical Research*, Vol. 100, No. B10, pp. 20271–20283.

Koch, K-R. (1999) *Parameter Estimation and Hypothesis Testing in Linear Models, 2nd Edition*, Springer-Verlag, Berlin, Germany, ISBN 3-540-65257-4, 333 pp.

Koivula, H., Ollikainen, M. and Poutanen, M. (1998) Use of the Finnish Permanent GPS Network (FINNNET) in Regional GPS Campaigns, *Advances in Positioning and Reference Frames*, Vol. 118, IAG Scientific Assembly, Rio de Janeiro, Springer-Verlag, Berlin, Germany, pp. 137-142.

Langley, R. (1997) GPS Receiver System Noise, *GPS World*, Vol. 8, pp. 40-45.

LawLink, (2001) *Aerial view of Thredbo landslide*, NSW Attorney Generals Department, Australia, http://www.lawlink.nsw.gov.au/lc.nsf/pages/thredbo_view

Leica (1999) Leica CRS1000 Reference Station GPS Receiver, *Installation, Operation and Maintenance Manual, Rev-B P/N 10916*, Leica Geosystems Incorporated, California, USA, 86 pp.

Leick, A. (1995) *GPS Satellite Surveying* (2nd Edition), John Wiley and Sons, N.Y., 560 pp.

Ma, E., Chen, Y. and Ding, Z. (2001) Monitoring of Slope Stability by using Global Positioning System (GPS), *Proceedings of the International Symposium on Kinematic Systems in Geodesy, Geomatics and Navigation - KIS2001*, Alberta, Canada, June 5-8, pp. 298-310.

Macquarie University (2001) *Stevenson Screens*, http://atmos.es.mq.edu.au/~aws2/hardware/stevenson.html

Marini, J.W. (1972) Correction of Satellite Tracking Data for an Arbitrary Tropospheric Profile, *Radio Science*, Vol. 7, No. 2, pp. 223-231.

Mikhail, E.M. (1976) *Observations and Least Squares*, Dun-Donnely Publisher, New York, USA, 498 pp.

Niell, A.E. (1996) Global Mapping Functions for the Atmospheric Delay at Radio Wavelengths, *Journal of Geophysical Research*, Vol. 101, No. B2, pp. 3227-3246.

Ohkura, H. (1998) Application of SAR Data to Monitoring Earth Surface Changes and Displacement, *Advances in Space Research*, Vol. 21, No. 3, pp. 485-492.

Oppenheim A.V. and Willsky, A.S. (1997) *Signals and Systems* (2nd Edition), Prentice-Hall International, New Jersey, USA, 957 pp.

Parkinson, B.W. (1996) GPS Error Analysis, in: *Global Positioning System: Theory and Applications* (Vol. I), Parkinson, B.W. and Spilker, J.J. (ed.), American Institute of Astronautics, Washington, D.C., USA, pp 469-484.

Petrovski, I., Kawaguchi, S., Torimoto, M., Chachin, T. and Okano, K. (2000) LAMOS-BOSHAI™: Landslide Monitoring System Based On High-speed Sequential Analysis for Inclination, *Proceedings of the 13th International Technical Meeting of the Satellite Division of the Institute of Navigation ION GPS-2000*, Salt Lake City, Utah, USA, September 19-22, pp. 84-94.

Radovanovic, R.S. (2000) High Precision Deformation Monitoring by Multipath Mitigation via Day-To-Day Correlation Analysis, *Proceedings of the 13th International Technical Meeting of the Satellite Division of the Institute of*

Navigation ION GPS-2000, Salt Lake City, Utah, USA, September 19-22, pp. 35-44.

Ray, J.K. (1999) Use of Multiple Antennas to Mitigate Carrier Phase Multipath in Reference Stations, *Proceedings of the 12th International Technical Meeting of the Satellite Division of the Institute of Navigation ION GPS-99*, Nashville, Tennessee, USA, September 14-17, pp. 269-279.

Ray, J.K. (2000) Mitigation of GPS Code and Carrier Phase Multipath Effects using a Multi-Antenna System, *PhD Dissertation*, University of Calgary, Canada, 260 pp.

Reeves, B., Noon, D., Stickley, G. and Longstaff, D. (1997) Monitoring Rock Slope Deformation by Radar Interferometry, *Proceedings of the Workshop on Applications of Radioscience*, the Australian Academy of Science, Barossa Valley, Australia, September 21-23, pp. 119-123.

Remondi, B.W. (1984) Using the Global Positioning System (GPS) Phase Observable for Relative Geodesy: Modelling, Processing, and Results, *PhD Thesis*, University of Texas at Austin, Centre for Space Research, 360 pp.

Radio Frequency Innovations (1998) RFI-9256 Wireless Data – Operation Manual, RF Innovations Pty., Ltd., Document Number 9256V210, 81 pp.

Rizos, C. (1997) *Principles and Practice of GPS Surveying*, Monograph 17, School of Geomatic Engineering, University of New South Wales, Australia, 555 pp.

Rizos, C., Han, S., Ge, L., Chen, H., Hatanaka, Y. and Abe, K. (2000) Low-cost Densification of Permanent GPS Networks for Natural Hazard Mitigation: First Tests on GSI's GEONET network, *Earth, Planets and Space*, Vol. 52, No. 10, pp. 867-871.

Saastamoinen, J. (1973) Contributions to the Theory of Atmospheric Refraction, *Bulletin Géodésique*, No. 105, pp. 279-298.

Sarunic, W. (2000) *Personal Communication*, Engineering Geologist, *(Formerly at)* Mining Department, Western Mining Corporation Mount Keith Operations.

Satirapod, C. (2002) Improving the GPS Data Processing Algorithms for Precise Static Relative Positioning, *PhD Dissertation*, University of New South Wales, Australia, 126 pp.

Schaal, R. E. and Netto, N. P. (2000) Quantifying Multipath using MNR Ratios, *GPS Solutions*, Vol. 3, No.3, pp. 44-48.

Selby, M.J. (1987) Rock Slopes, In: *Slope Stability*, Anderson and Richards (ed.), John Wiley and Sons, New York, USA, pp. 475-504.

Sippel, K. (2001) Modern Monitoring System Software Development, *Proceedings of the 10th FIG International Symposium on Deformation Measurements*, Orange, California, USA, March 19-22, pp. 88-100.

Sjöberg, J. (1999) Analysis of Large Scale Rock Slopes, *Doctoral Thesis*, Lulea University of Technology, 788 pp.

Srinivasan, C. Arora, S.K., and Benady, S. (1999) Precursory Monitoring of Impending Rockbursts from Microseismic Emissions at Deeper Levels, *International Journal of Rock Mechanics and Mining Sciences*, Vol. 36, pp. 941-948.

Stewart, M. and Tsakiri, M. (2001) The Status of the Global Positioning System for Dam Surface Monitoring, *Proceedings of the Institute of Civil Engineers – Geotechnical Engineering*, Vol. 149, No. 4, pp. 249-252.

Stewart M.P., Tsakiri, M. and Duckrell, R. (1999) Dam Deformation Monitoring with Episodic GPS, *Proceedings of 6th South East Asian Surveyors Congress*, Fremantle, Western Australia, November, pp. 477-485.

Teunissen, P.J.G. (1993) Least-Squares Estimation of the Integer GPS Ambiguities, *Invited Lecture*, Section IV, Theory and Methodology, IAG General Meeting, Beijing, China, August, 16 pp.

Teunissen, P.J.G. (1995) The Least Squares Ambiguity Decorrelation Adjustment: A Method for Fast GPS Integer Ambiguity Estimation, *Journal of Geodesy*, Vol, 70, pp. 65-82.

Teunissen, P.J.G. (1998) Success Probability of Integer GPS Ambiguity Rounding and Bootstrapping, *Journal of Geodesy*, Vol. 72, pp. 606-612.

Teunissen, P.J.G. (2000) Probabilistic Properties of GNSS Integer Ambiguity Estimation, *Earth Planets Science, Vol*. 52*,* pp. 801-805.

Teunissen, P.J.G, de Jonge, P.J. and Tiberius, C.C.J.M (1997) The Performance of the LAMBDA Method for Fast GPS Ambiguity Resolution*, Navigation*, Vol. 44, No. 3, pp. 373-383.

Tiberius, C.C.J.M. and de Jonge, P.J. (1995) Fast Positioning using the LAMBDA Technique, *Proceedings of DSNS-95*, Bergen, Norway, paper No. 30, 8 pp.

Turner, A.K. and Schuster, R.L. (ed.) (1996) Landslides Investigation and Mitigation, *Special Report 247, Transport Research Board, National Research Council,* National Academy Press, Washington, D.C., USA, 673 pp.

Wang, J. (1999) Modelling and Quality Control for Precise GPS and GLONASS Satellite Positioning, *PhD. Dissertation*, School of Spatial Sciences, Curtin University of Technology, Perth, Western Australia, 171 pp.

Wanninger L. and May, M. (2000) Carrier Phase Multipath Calibration of GPS Reference Stations, *Proceedings of the 13th International Technical Meeting of the Satellite Division of the Institute of Navigation ION GPS-2000*, Salt Lake City, Utah, USA, September 19-22, pp. 132-144.

Ward, P. (1996) Satellite Signal Acquisition and Tracking, In: *Understanding GPS: principles and applications*, Kaplan E. D. (ed.), Artech House, Boston, USA, pp. 119-208.

Wells, D.E., Beck, N., Deilikaraoglou, A., Kleusberg, A., Krakiwsky, E.J., Lachapelle, G., Langley, R.B., Nakiboglu, M., Swarz, K.P., Tranqilla, J.M., and Vanicek, P. (1997) *Guide to GPS Positioning*, Canadian GPS Associates, Frederiction, N.B,. Canada.

Western Mining Corporation (2000a) Leinster-Mount Keith Nickel Operation, *Internal Report*, Western Mining Corporation, 20 pp.

Western Mining Corporation (2000b) WMC Nickel, *Internal Report*, Western Mining Corporation, 16 pp.

Western Mining Corporation (2000c) Mt Keith Nickel Operations Business Briefing, *Internal Report*, Western Mining Corporation, November 2000, 23 pp.

Wieser, A. (2002) *Personal Communication*, Technical University of Graz, Austria.

Wieser, A. and Brunner, F. K. (2000) An Extended Weight Model for GPS Phase Observations, *Earth, Planets and Space*, Vol. 52, pp. 777-782.

Windsor, C.R. (1993) Measuring Stress and Deformation in Rock Masses, *Proceedings of the Australian Conference on Geotechnical Instrumentation and Monitoring in Open Pit and Underground Mining*, Kalgoorlie, Western Australia, June 21-23, pp. 33-52.

Windsor, C.R., and Worotnicki, G. (1986) Monitoring Reinforced Rock Mass Performance, *Proceedings of the International Conference on Large Rock Caverns*, Helsinki, Vol 2, pp. 1087-1097.

Wübbena, G., Bagge, A., Bettcher, G., Schmitz, M. and Andree, P. (2001) Permanent Object Monitoring with GPS with 1 Millimeter Accuracy, *Proceedings of the 14th International Technical Meeting of the Satellite Division of the Institute of Navigation ION GPS-2001*, Salt Lake City, Utah, USA, September, *in press*.

Zhang, J., Bock, Y., Johnson, H., Fang, P., Williams, S., Genrich, J., Wdowinski, S. and Behr, J. (1997) Southern California Permanent GPS Geodetic Array: Error Analysis of Daily Position Estimates and Site Velocities, *Journal of Geophysical Research*, Vol. 102, No. B8, pp. 18035–18055.

APPENDIX 1

SPECIFICATIONS FOR THE RADIAL COAXIAL SWITCH

COAXIAL SWITCHES

N - TNC - BNC

COAXIAL SPnT up to 12.4 GHz – RAMSES Concept

GENERAL SPECIFICATIONS - RF PERFORMANCES

Connectors		N - BNC - TNC						
Number of positions		3 to 6			7 to 10		11 and 12	
Frequency range	*GHz*	DC - 12.4			DC - 8		DC - 8	
		DC- 3	3 - 8	8 -12.4	DC- 3	3 - 8	DC- 3	3 - 8
V.S.W.R. (max)		1.20	1.35	1.50	1.30	1.50	1.35	1.70
Insertion Loss (max)	*dB*	.20	.35	.50	.30	.50	.50	1.00
Isolation (min)	*dB*	80	70	60	80	70	70	60

GENERAL SPECIFICATIONS - ADDITIONAL SPECIFICATIONS

Operating mode		Normally open or Latching			
		Normally open		Latching	
Actuator voltage (nominal)	*Vdc*	12	28	12	28
Operating current at 23°C	*mA*	250	102	See table below	
Average power		See Power Rating Chart page 9			
Peak power	*kW*	1.5 (1 µs, 1 ‰)			
TTL INPUT	*High level* *Low level*	2.2 to 5.5 V (TTL option) / 3.5 to 5.5 V (BCD option) 0 to 0.8 V (TTL option) / 0 to 1.5 V (BCD option)			
Indicator rating		1 W - 30 V - 100 mA			
Switching time (max)	*ms*	15 (for automatic reset models, SP3T to SP6T: 40 ms, SP7T to SP12T: 50 ms)			
Life	SP3 to 6T	R573 serie	5 10^6 cycles per way		
		R574 serie	2 10^6 cycles per way		
	SP7 to 12T	2 10^6 cycles per way			
Connectors		N, TNC, BNC			
Actuator terminals		Solder pins or DSUB			
Operating temperature range	°C	-40, +85			
Storage temperature range	°C	-55, +85			
Impedance	Ω	50			
For terminated models		50 Ω termination ±5% 1 Watt per termination 3 W total power handling per switch			
Switching sequence		Break Before Make			

Operating current at 23°C (mA) SPnT LATCHING				
	12 V		28 V	
	manual reset	automatic reset	manual reset	automatic reset
SP 3 to 4 T	320 x n	640	125 x n	250
SP 5 to 8 T	320 x n	960	125 x n	375
SP 9 to 12 T	320 x n	1280	125 x n	500

n = number of ways